A STUDY OF THE REACTION BETWEEN HYDROGEN SULPHIDE AND ZINC OXIDE

Catriona H. Lawrie

Ph.D Thesis
University of Edinburgh
1990

ABSTRACT

Experiments were conducted to study the absorption reaction of hydrogen sulphide with zinc oxide forming zinc sulphide and water. The reaction is of commercial importance for the removal of hydrogen sulphide from reactor feed streams and from natural gas. Most of the experiments were performed on a commercial ICI zinc oxide-based absorbent prepared by calcination of basic zinc carbonate but a number of experiments were also performed on samples of basic zinc carbonate or of zinc oxide prepared by different treatments.

The reactions were carried out in a shallow bed flow reactor containing 0.2-0.6g of absorbent at a pressure just above atmospheric and at temperatures in the range 0 to 45°C. Feed gases containing 0.06-0.7% v/v hydrogen sulphide and 0-0.5% v/v water in nitrogen were used. On-line gaseous analysis was performed using a Thermal Conductivity Detector with complementary information provided by sulphur analysis and electron microprobe analysis of the discharged partially sulphided absorbent.

The specific reaction rate was observed to be very high initially but to decline to a much slower pseudo-steady state (pss) rate. The pattern of this decline was found to be a function of particle size, with larger particles exhibiting slower, diffusion-limited rates in the initial period but higher pss rates than smaller particles. This latter result was attributed to an enhanced water concentration in the centre of larger particles. Microprobe analysis indicated uniform sulphiding at about 20% absorbent conversion whereas at low conversions an outer sulphided shell surrounds a central unreacted core.

The conversion of the absorbent at pss (in the range 9-23%) was observed to increase with increasing partial pressures of water and of hydrogen sulphide in the feed. A marked dependence of the pss rate upon water partial pressure and a decrease in the rate with increasing temperature were observed and interpreted as indicative of an autocatalytic reaction. The role of water in facilitating solid rearrangement is consistent with the results of interrupted experiments which showed enhanced water adsorption and reaction rate after isolation. The pss rate was found to be insensitive to hydrogen sulphide concentration in the range studied.

There appears to be an optimal calcination temperature of the absorbent precursor although this may not correspond with the temperature yielding maximal specific surface area. The effects of some impurities in the commercial absorbent were also investigated.

ACKNOWLEDGEMENTS

This work has been possible only due to the efforts of many people, whose help I am delighted to be able to acknowledge. Above all, I am grateful to my supervisor, Dr Mike Davidson, who has throughout my work been inspiring in his enthusiasm and committment. He has devoted many hours to the glass-blowing of various reactors, water bubblers and the associated connections, to the filling of 'mixture' cylinders, to zinc analysis, infra-red work and the tedious preparation of a 'sodium-free' zinc oxide, and to the search for enlightening references. Besides all of which, we have had many fascinating discussions - more often than not on Saturday mornings.

I spent a fortnight in the ICI research laboratories at Billingham where as well as preparing samples and using their 'breakthrough' apparatus with Jill Turner's help, I also gained a valuable background to the project work. For this I am grateful to my Industrial Supervisor Dr Pat Denny, whose experience in the development of zinc oxide absorbents and whose engaging attitude to the work made for a very enjoyable experience.

One of the periods of most intensive work on the project was a fortnight around the end of May 1988 when in determining once and for all whether the Perkin Elmer Flame Photometric Detector could be adapted for the duty required, I was almost persuaded by Martin Speck's superb example to seek a career as a Service Engineer for analytical instruments.

For the speed and expertise with which changes to equipment were made I am indebted to Davie Ketchin in particular, also to Bobby Hogg and Arthur Donachie whose accompanying comic double act would rapidly dispel the

gloom brought on by an unsuccessful morning. I am grateful also to Sam Leddy, Kenny Fee, Rab Kilgour and Matthew Rea for their frequent and dependable help at short notice.

I wish to thank Drs Peter Hill, Stuart Kearns and John Craven in the Department of Geology for their interest and assiduity in discussing with and advising me on the optimal preparation and analysis of zinc oxide samples and for allowing me time on both the electron and ion microprobes despite very heavy usage of both instruments. I am grateful also to Mike Saunders in the Geology Department for the use of his Flame Photometer for sodium analysis, to Jim Goodall in the Department of Electrical Engineering for his analysis of a number of samples on the Scanning Electron Microscope, and to Khalid Sohail in the Chemical Engineering Department for his extreme patience in demonstrating to me the use of the thermal microbalance.

I have also received advice from time to time from other members of staff of the Chemical Engineering Department to all of whom I am grateful.

Financially, I am obliged to the Royal Society of Edinburgh, to the Department of Chemical Engineering and to the Faculty of Science for supporting successively my years as a postgraduate.

Finally, I must apologise to my present boss, Dr Dave Cresswell, for inevitably giving less of my attention to my current job because of the distraction of writing up my thesis.

Last but by no means least I wish to thank Ewan McQueen for giving me a number of chemistry tutorials and for being a reliable drinking partner, Maurice Prendergast for his daily enquiries about the progress of my thesis

when I thought I had escaped such interest by moving to Runcorn, and my sister, Madeleine, for listening on numerous occasions to various technical and practical problems and consistently giving sound advice.

CONTENTS

NOTATION

CHAPTER 1

$A_{(g)}$	gaseous reactant
$B_{(g)}$	gaseous product
S	solid reactant
S'	solid product

CHAPTER 2

a	activity of diffusant
A	electron affinity of anion
A_g	grain surface area
c	concentration of diffusant
c_i	concentration of component i
c_b	Madelung constant
D	diffusion coefficient of intrinsic point defects
D^0	pre-exponential factor in equation (20)
D_i	diffusion coefficient of component i
$\tilde{D}$	chemical diffusion coefficient
D'	self-diffusion coefficient
e_0	electronic charge
E_{bM}	energy of cation-derived conduction band
E_{bX}	energy of anion-derived valence band
E_F	energy of Fermi level
E_a	energy level of adsorbed species
E_{bg}	energy of band gap
$f(E_a)$	probability of occupation of an adsorbed species energy level E_a
F	Faraday constant
G	Gibb's free energy
I	ionisation potential of cation
j_i	diffusive flux of component i
k	Boltzmann constant
K_{FZn}	equilibrium constant for Frenkel disorder in zinc sublattice
K_S	equilibrium constant for Schottky disorder
m	grain shape factor, defined by equation (64)
n_i	number of particles of component i
p	partial pressure
p_0	vapour pressure at given temperature
P	system pressure
Q	activation energy for diffusion
r_{MX}	shortest cation-anion distance in lattice
r_g	grain characteristic dimension
R	universal gas constant
R_Γ	ratio of the number of particles in a distorted region to the number of particles in the rest of the crystal
T	temperature
u_i	electrochemical mobility of component i

V_b bulk Madelung potential
V_{bM} Madelung potential for cation M
V_{bX} Madelung potential for anion X
V_g grain volume
x scalar of distance
z valence of ion
z_i valence of ions of type i

γ activity coefficient
Γ_D jump frequency of particles in the region around dislocations and grain boundaries in a crystal
Γ_L jump frequency of particles in the region of a crystal containing point defects
δ fractional excess of zinc in zinc oxide
μ_i chemical potential of particles of type i
η_i electrochemical potential of particles of type i
ρ_D density of dislocations
σ_i conductivity of particles of type i
ϕ_e electrical potential
ϕ_∞ work function

$[V_O^{\cdot}]$ concentration of singly ionised oxygen vacancies
$[Zn_i^{\cdot}]$ concentration of singly ionised zinc interstitials
$[V_{Zn}']$ concentration of singly ionised zinc vacancies

Notation introduced in model of Ishida and Wen
D_{eA} diffusivity in product layer
D_{eA}' diffusivity in zone of unreacted and partially reacted solid

Notation introduced in model of Mantri et al.
c_A concentration of A
c_{Ag} concentration of gaseous reactant in bulk gas
c_S solid concentration
c_{S0} initial concentration of solid reactant
D_p product layer diffusivity (defined exactly as D_{eA})
D_r diffusivity in reacting zone
k_g film mass transfer coefficient
k_v kinetic rate constant
r_0 radius of pellet
r_1 radius of interface between reacting and reacted zones
r_2 radius of unreacted core

Notation introduced in grain model of Szekely et al.
c_{As} surface concentration of gaseous reactant A at external surface of pellet
c_{Cs} surface concentration of gaseous product C at external surface of pellet
c_C concentration of gaseous product
D_e effective diffusivity

K_E equilibrium constant
r_c radius of unreacted core
r_0 grain radius
R_0 pellet radius

ε porosity of solid reactant
υ_A local chemical rate
ρ_S molar density of solid reactant

Notation introduced in Ramachandran & Smith's modified grain model

ε_p porosity of product layer
M_r, M_p molecular weights of solid reactant and product

γ ratio of molar volumes of solid product to solid reactant
ρ_r, ρ_p densities of solid reactant and product

Notation introduced in Georgakis et al.'s modified grain model

ϕ Thiele modulus

Notation introduced in model of Garza-garza and Dudukovic

ε_0 initial porosity of solid reactant
ω nett increase in solid volume at complete conversion per unit initial voids

Notation introduced in single pore model of Ramachandran and Smith

c concentration of gaseous reactant
c_0 concentration of gaseous reactant at mouth of pore
l pore length
r initial radius of pore
x distance along pore

δ total thickness of product layer
δ_1 thickness of the part of the product layer from the initial position of the pore wall to its position at any subsequent time.
δ_2 thickness of the part of the product layer from the initial position of the pore wall to the position of the reaction interface.
$\eta(x)$ local conversion
λ radius of solid concentric with pore

Notation introduced in model of Bhatia and Perlmutter

D_p effective diffusivity in product layer
$f(r)$ pore size distribution
L_0 initial total length of pore system
M molecular weight of solid reactant
R_0 initial particle radius

S_0	initial total surface area of pore system
x	solid conversion
β	Biot number, defined by equation (63)
ε_0	initial porosity
ρ	mass of solid reactant per unit volume of solid phase
σ	particle size parameter, defined by equation (62)
τ_x	time required to achieve a conversion x
ψ	structure parameter, defined by equation (61)

CHAPTER 3

c_{Ai}	concentration of gaseous reactant A in the reactor feed
d	interplanar spacing of crystal
F	F-value of a given linear regression
n_F	number of feed analyses
n_P	number of product analyses
p	partial pressure
p_s	vapour pressure at temperature T
Q	gas flowrate
r	random variable (rv) representing the difference between corresponding feed and product analyses
$\bar{r}$	mean difference between feed and product analyses
r_p	pore radius
$-r_A$	reaction rate
R	universal gas constant
$s(\bar{r})$	standard deviation of $\bar{r}$
t_1, t_2	times delimiting the pseudo-steady state (pss) period
$\bar{t}_p$	average of end-point times of pss interval
T	temperature
V_m	liquid molar volume
$Var(r)$	variance of r
W	weight of absorbent
x	fractional conversion
y_F	rv representing feed analyses
y_P	rv representing product analyses
$\tilde{y}_F$	estimated feed signal at $t=\bar{t}_p$
$\tilde{y}_P$	estimated product signal at $t=\bar{t}_p$
α, β	constant and coefficient of general straight line equation
α_F, β_F	constant and coefficient in line fitted to feed data
α_P, β_P	constant and coefficient in line fitted to product data
θ	contact angle between liquid and solid
θ_i	angle of incidence of X-rays on a crystal
λ	wavelength of X-rays generated from a sample in the electron microprobe
σ^2	mean square of deviations from regression line

σ_s surface tension

CHAPTER 4

D_e effective diffusivity
k_v kinetic rate constant
L length parameter
m defined by equation (88)

ϕ Thiele modulus
η effectiveness factor

CHAPTER 5

c_{A0} initial concentration of gaseous reactant
k_1 rate constant of non-autocatalytic reaction
k_2 rate constant of autocatalytic reaction
$\bar{x}$ fractional conversion of reactant particle

β dimensionless constant, defined by equation (98)
η effectiveness factor

APPENDIX A

m_{abs} number of grams of absorbent sample
N Avogadro's number
q process gas flowrate
(-r) rate of replacement of surface oxygens by sulphurs
S_{abs} specific surface area of absorbent sample
t_{min} minimal time for replacement of all surface oxygens
x %hydrogen sulphide content of gas

ρ_s surface site density

APPENDIX B

n number of analyses
x GC area analysis for hydrogen sulphide or water
y % hydrogen sulphide or water in feed stream

α proportionality constant, defined by equation (101)

APPENDIX D

f_{calib}	GC calibration factor for hydrogen sulphide

APPENDIX E

a	radius of granule
c	concentration of H_2S at centre of sphere
c_0	surface concentration of H_2S
c_1	initial uniform concentration of H_2S through sphere
c_B	concentration of gas diffusing into sphere
D	combined diffusivity, defined by equation (109)
D^e	effective diffusivity, defined by equation (110)
D_{AB}	binary diffusivity of gases A and B
D_K	Knudsen diffusivity
D_M	molecular diffusivity
f(r)	function defined by boundary conditions on equation (107)
r	radius of arbitrary 'shell' of sphere
Δr	thickness of 'shell'
t	time
v	variable defined equal to $c_B r$
ϵ	particle porosity
τ_p	pore tortuosity

APPENDIX F

a	$(=x_0)$, lower limit of the integration interval
A_i	area of i^{th} trapezoid
b	$(=x_n)$, upper limit of the integration interval
f(x)	function of x to be integrated
f_i	$f(x_i)$
h	width of trapezoid
J	definite integral, defined by equation (111)
J^*	piecewise linear approximation to J
K	defined by equation (115)
M_2	largest value of the second derivative of the function f(x) in the integration interval
M_2^*	smallest value of the second derivative of the function f(x) in the integration interval
n	number of trapezoids in integration interval
$s^2(A_i)$	sample variance of the area A_i
t_i	time corresponding to the upper limit of the i^{th} trapezoid
x_i	value of the variable x corresponding to the upper limit of the i^{th} trapezoid
y_{Pi}	actual product signal at $t=t_i$
$\tilde{y}_{Fi}$	estimated feed signal at $t=t_i$

ε	difference between the definite integral and its approximation, ie. the error

LIST OF TABLES

LIST OF FIGURES

LIST OF PLATES

CHAPTER 1

INTRODUCTION

1.1 The Quantitative Analysis of Gas-Solid Noncatalytic Reactions

Gas-solid noncatalytic reactions are widely used to effect important industrial processes. Amongst these, the extraction of metals from their ores, the combustion of solid fuels, the gasification of coal, the oxidation of carbon in decoking reactions and the absorption from flue gases of sulphur dioxide by limestone are but a few examples. Strong similarities exist between the processes involved in gas-solid reactions and those involved in heterogeneous catalysis. The former class of reactions are in general more complex because of the progressive consumption of the solid reactant with time. Thus, gas-solid reactions are inherently of a transient nature.

Although dependent upon the general form of the reaction - whether it yields only solid or only gaseous products or both solid and gaseous products - and upon the reactor contacting pattern, gas-solid reactions are generally composed of a number of elementary steps which take place sequentially with respect to a particular gaseous molecule. These are

1. the mass transfer of the gaseous reactant from the bulk gas phase to the external surface of the reactant particle,
2. the diffusion of the gaseous reactant through the pores of the solid product (if a solid product is formed) and/or of the partially reacted solid,
3. the adsorption of the gaseous reactant on the solid surfaces, and
4. the chemical reaction of the adsorbed reactant with the solid.

In fact, processes 2 and 3 may occur repetitively if the gaseous molecule adsorbs initially on an inactive area

of the surface. The molecule may then desorb and be further transported by gaseous diffusion before readsorbing, or may move over the solid surface by surface diffusion. Where a gaseous product is formed the following additional steps must also be considered:

1. the desorption of the gaseous product from the solid,
2. the pore diffusion of the gaseous product towards the external surface of the particle, and
3. the mass transfer of the gaseous product from the external surface of the particle into the bulk gas stream.

Solid state diffusion may also take place and is likely to make a significant contribution to the overall rate of reaction where the solid product is non-porous. It is frequently found to be the case that one of these elementary steps in the mass transfer and reaction sequence proceeds at a much slower rate than the rest. This allows the reaction rate expression to be substantially simplified on the basis of this Rate Determining Step (RDS). Thus, for example, where the purpose of an experimental study is to determine reaction kinetics, it is essential first to ensure that under the operating conditions of the study the RDS is the rate of the surface reaction. Consideration of the transient nature of gas-solid reactions suggests at once the likelihood that the process which represents the RDS may change with time, and, as for catalytic reactions, where temperature and/or concentration gradients exist in the reactor, or where the solid reactant particles are of non-uniform size, the RDS may vary from one particle to another.

Gas-solid reactions may be classified according to the nature of their products thus,

Type 1: $A_{(g)} + S \rightleftharpoons S'$

Type 2: $A_{(g)} + S \rightleftharpoons B_{(g)}$

Type 3: $A_{(g)} + S \rightleftharpoons S' + B_{(g)}$

It is clear that the techniques which may be used to study the progress of gas-solid reactions are influenced by the phases of the reaction products. Thus, gravimetry is a widely used and valuable technique not only for the study of decomposition reactions but also for gas-solid reactions of the first two types, where the sample weight respectively increases and decreases with time.[1] While thermogravimetric analysis (TGA) may yield detailed information on reaction kinetics, this is subject to the use of meticulous experimental technique and an awareness of the specific sources of experimental variation. Wiedemann and Bayer[2] have discussed factors relating to the properties of the solid sample or to the experimental conditions which profoundly affect the results of the thermogravimetry. Amongst these, the need to correct for the effect of buoyancy of both the crucible and the sample as a function of temperature is essential. The effect of the heating rate is also important with much greater resolution being possible at lower heating rates. The packing of the sample in the crucible also affects the weight loss curve through its influence on the rates of heat and mass transfer. The sample weight and volume should be as small as possible to minimise the effects of temperature inhomogeneity and retention of gaseous products. It is evident that the gas atmosphere is of great importance in affecting the rate of a given reaction, and that the position of the sample within the furnace should be such that gas flow is unimpeded and temperature gradients are minimised. Finally, properties relating to the sample itself are of significance. The shape and size of the particles which make up the sample and their extent of crystallinity will determine the packing density and surface

area/weight ratio of the sample, and thereby its effective thermal conductivity and rate of reaction. The degree of homogeneity of a sample during the course of a reaction is a measure of how closely the system approaches ideality. The decomposition of hydrozincite was cited by Wiedemann and Bayer as an example of the difficulty of achieving such homogeneity. Clearly, in the absence of a homogeneous system, the interpretation of rate data is very difficult and differential analysis inapplicable.

In spite of these difficulties, a number of workers[3,4] have used thermogravimetry to study the reaction of hydrogen sulphide with zinc oxide. Such a reaction, being of type 3, has the additional complexity that in order to interpret the weight change curve, either the product gas must be assumed to desorb instantaneously or else gas analysis must be performed, making the gravimetric analysis redundant. The present work suggests that the assumption of instantaneous desorption of the product gas, water, is not valid under ambient temperature conditions. In general, adsorption/desorption effects must be allowed for and a combined TGA/FTIR system is ideal for this purpose but impractical where a very high degree of accuracy is required in order to analyse very small changes in conversion.

Given that a carrier gas is likely to be required for the detector, gaseous analysis has the particular advantage for the first reaction that continuous analysis is feasible. In general, however, only discrete gaseous analysis will be possible for reactions of types 2 and 3. The requirement for gas chromatography limits the applicability of the analysis to those reactions which are sufficiently slow to allow a reasonable number of analyses to be made, although a

higher frequency of analyses can be obtained using capillary rather than packed columns. Note that this problem may also arise in heterogeneous catalytic reactions which have a transient nature due, for example, to excessive and rapid fouling. In such cases a pulse reactor may be valuable for studying the transient phase.

Finally, sectioning of the solid particles and analysis by any of a number of techniques including electron microprobe analysis and radio-isotope tracing may provide useful complementary information to the method of on-line analysis used to study reactions of types 1 and 3. Quantitative analysis by these methods may, however, be greatly hindered if either the solid reactant or product is porous. The hardness of the solid is also likely to be important because of its effect on the quality of surface that can be prepared. The utility of the technique will therefore be determined not only by the spatial resolution and analytical accuracy of the instrument used but also by the physical properties of the solid itself.

An important decision to be made in the design of experiments to determine kinetic parameters is the form of the analysis, whether integral or differential. These two analytical methods are distinguished by their respective assumptions concerning the experimental data. The use of integral analysis implies that the concentration changes in the reactor are sufficient to affect the rate significantly. It is therefore necessary to account for the changing rate by integrating the assumed rate expression or expressions between the limits of the inlet and outlet concentrations of one of the reactants or products. Conversely, the use of differential analysis implies that the changes in the reactant and product

concentrations are very small and that there is therefore little error introduced by calculating a mean rate by a simple mass balance. This rate then corresponds to particular known concentrations of the reactants. The advantage of differential analysis is that no assumption need be made about the form of the rate expression in order to compute experimental rates. Instead, experiments are performed over a range of reactant concentrations and temperatures and the form and parameters of the rate expression, and the Arrhenius parameters are then found from appropriate plots of the experimental data. The major problem with differential analysis is the requirement to achieve low conversion, consistent with the assumptions of the analysis, and simultaneously to achieve a very high degree of accuracy on the analysis of concentration so as to have an acceptable level of accuracy on the calculated rate.

The effective definition of differential analysis for gas-solid reactions is rather more restrictive than it is for catalytic reactions. In the latter case, for a given concentration of the reactant gas (or gases), a very low conversion can be achieved by reducing the quantity of catalyst used or by increasing the gas flowrate. For a gas-solid reaction, however, differential analysis requires that the conversion of both gaseous and solid reactants be low. Even when the conversion of the solid reactant is low, however, the fractional conversion of solid reactant on its surfaces may be significant, and if the effect of this upon the rate is substantial then the conditions for the applicability of differential analysis are not met. For the system under study, the absorption of hydrogen sulphide by zinc oxide, it was found that for certain partial pressures of hydrogen sulphide over unsulphided zinc oxide differential analysis was not possible. The very high rate of the surface reaction gave substantial

conversions of both reactants. Two possible adjustments to the system which might make differential analysis feasible are the use of much lower partial pressures of hydrogen sulphide and the use of partially sulphided zinc oxide. A range of partial pressures of hydrogen sulphide has been used of which the lower limit was determined by the sensitivity of the detector used, and the upper limit by the maximal partial pressures of interest in industrial absorber systems. Within this range, the conditions for differential analysis could not be fulfilled using unsulphided zinc oxide. The use of partially sulphided zinc oxide permits the application of differential analysis but the reaction considered under these circumstances is that of the bulk solid as opposed to the surface reaction. Experiments have been performed,[5] however, which suggest the feasibility of differential analysis of the surface reaction of methane thiol with zinc oxide where the gaseous reactant is present in a diluent at the level of about 10ppm and is analysed using a Flame Ionisation Detector (FID).

1.2 The Zinc Oxide/Hydrogen Sulphide Reaction - ICI Experimental Program

An absorbent composed substantially of zinc oxide, is used to remove hydrogen sulphide from gas streams over a wide range of temperatures and partial pressures. The thermodynamics of the reaction to form zinc sulphide and water,

$$ZnO_{(s)} + H_2S_{(g)} \rightleftharpoons ZnS_{(s)} + H_2O_{(g)} \qquad (1)$$

are such that hydrogen sulphide can be reduced to very low levels in the process stream. This is of great importance in some applications such as catalyst protection where even very low levels of hydrogen sulphide would be sufficient to poison the active sites

of the catalyst. The other principal advantage of zinc oxide as a sorbent for hydrogen sulphide relates to off-shore uses where the size and weight of a packed bed of zinc oxide granules compare favourably with those of a conventional amine absorber and regeneration system.

ICI manufactures zinc oxide based granular absorbents. Two different absorbents are made which are designed specifically for low and high temperature applications,[6] and a large number of experiments have been performed on these absorbents at ICI under the direction of P.J.Denny. These have taken the form of breakthrough tests with the experiment being run until breakthrough of hydrogen sulphide is detected by the blackening of lead acetate solution. Such experiments allow the comparison of different absorbents and may suggest correlations between sulphur absorption capacity and any of a number of physical parameters of the absorbent (eg. specific surface area, porosity, pore size distribution, particle size, method of preparation etc.).[7] The effect of the reaction temperature may also be investigated.

The bed itself has a volume of 60ml, which is subdivided into 6 sections of 10ml by means of wire gauzes. The bed is contained within a glass tube to which the gases are fed in downflow from a gas manifold system. The reactor outlet gas, although free of hydrogen sulphide for most of the duration of the experiment, passes through a 'dump bed' containing excess absorbent. Gas flowrates of $42lhr^{-1}$ ($700mlmin^{-1}$) are used, corresponding to space velocities of $700hr^{-1}$. Information about the axial variation of the absorbent sulphur content through the bed is obtained as follows. At the end of an experimental run, the bed is flushed with nitrogen after which the sections of the bed are removed and the granules 'riffled' to obtain a representative sample of

.6-.7g from each section. These are then analysed for sulphur. The distribution of sulphur within a granule is found by one of two techniques. The use of radioactive sulphur, ^{35}S, to label the hydrogen sulphide allows the sulphur distribution through the granule to be analysed by exposing photographic film to the granule cross-section for about a week. Alternatively, the sulphur distribution may be determined without the use of labelled hydrogen sulphide by electron microprobe analysis. Such methods are very important in providing qualitative information on the relative rates of pore diffusion and of the chemical reaction.

The analyses of sulphur distribution in individual granules revealed that the less efficient absorbents tended to have the sulphur concentrated in the outer shell of the granule or pellet[7] suggesting that pore diffusional resistance was rate limiting, and indeed that pore blockage might be occurring and restricting the efficiency of usage of the pellet. The more efficient absorbents had sulpur distributed throughout the interior of the granules. Even in these cases, however, for granules taken from the bed outlet which had been exposed only to very low levels of hydrogen sulphide and had low sulphur contents, a significant zoning effect was nevertheless apparent with the sulphur being concentrated in an outer shell.

The gas streams used in these experiments contained 0.5-5% hydrogen sulphide in methane. It was observed from the results of the sulphur analyses for the six sections of the bed that the profile of the sulphur content through the bed showed a maximum in the third or fourth section, with the sulphur content upstream being marginally lower while the sulphur content downstream dropped off very rapidly. In order to investigate whether this maximum arose due to a beneficial effect on

the reaction rate of the water produced in the reaction, experiments were performed using a range of water partial pressures. For experiments performed at room temperature, the use of a water-saturated gas stream increased the breakthrough time and gave sulphur profiles through the bed such that the sulphur content decreased monotonically towards the bed outlet. Moreover, the beneficial effect of water in the gas stream was more marked where the concentration of hydrogen sulphide in the feed was lower. (The use of a water-saturated feed increased the value of the maximal sulphur analysis from 3.2 to 6.7, from 9.4 to 16.4 and from 11.0 to 13.9 %S w/w for streams containing 0.5, 1.0 and 5.0 % hydrogen sulphide respectively.)

The effect of increasing the reaction temperature was also to increase the sulphur pick-up by the bed with maximal sulphur contents of 23.0 and 26.5 %sulphur w/w achieved at 70 and 150°C respectively (with the use of direct steam injection into the feed gas) compared with a theoretical maximum of 32.9 %sulphur for pure zinc sulphide.

Clearly, the measured maximal sulphur contents in such runs may depend not only upon the partial pressures of hydrogen sulphide and of water in the feed and upon the reaction temperature, but also upon the effective residence time in the bed which is a function of diffusivity, bed length, bed voidage, particle diameter and fluid velocity. For this reason, a number of runs were continued well beyond breakthrough to discover to what level the maximal sulphur content in the bed would rise. The highest measured sulphur content for a reaction performed at room temperature was 24.6% sulphur for a water-saturated feed stream containing 5% hydrogen sulphide. Taking into account the non-reacting impurities present in the absorbent, this represents a

solid conversion of about 96%.

1.3 Objectives of the Present Experimental Program

The experiments performed at ICI demonstrate the favourable effect on reaction rate of the presence of water in the feed stream, and of increasing the reaction temperature in the range examined ie. 20, 70, 150 and 250°C. They are also very useful as a guide to predicting the lifetime (breakthrough time) of a full-scale absorption bed. Such experiments are not ideal, however, as a means of understanding the reaction mechanisms nor for determining local reaction rates and their rate of decay with time. To obtain this kind of information, the use of an experimental system which permits of differential analysis is much more attractive. The integral problem requires the solution of equations which contain time constants differing by orders of magnitude viz. those for the chemical reaction, pore diffusion and for the bed breakthrough time. Such a mathematical system is computationally exceedingly difficult to solve. It has therefore been a primary objective of the present work to design and run an experimental system, the results of which might be analysed differentially with a satisfactory degree of accuracy. It was envisaged that such a system would involve frequent and repetitive gas analysis and would therefore require to be computer controlled.

Further objectives of the program were to study the rate effects revealed by the ICI work, to verify these and to determine the rate limiting steps of the reaction under the conditions of interest. It was also proposed to measure local rates in an attempt to elucidate the likely reaction mechanism. The reaction temperatures of interest are around ambient and down to 0°C. The laboratory rig is operated at atmospheric pressure and

with higher concentrations of hydrogen sulphide in the feed gas than would be encountered in an industrial system. In this respect it is similar to the ICI experimental set-up in that the tests are 'accelerated' sulphiding experiments although the partial pressures of hydrogen sulphide may be similar to those found industrially (ie. 0.5% hydrogen sulphide at about 1 bar in the laboratory experiment gives a hydrogen sulphide partial pressure of 0.005 bar, corresponding to 50ppm in 100 bar for an industrial gas feed to an absorption unit.)

REFERENCES

[1] Wendlandt W.W.
"Thermal Methods of Analysis"
John Wiley & Sons, London (1974)

[2] Wiedemann H.G., Bayer G.,
"Trends and Applications of Thermogravimetry"
Topics in Current Chemistry, 77, 67-140 (1978)
Springer-Verlag

[3] Westmoreland P.R., Gibson J.B., Harrison D.P.
"Comparative kinetics of high-temperature reaction between H_2S and selected metal oxides"
Environ. Sci. Tech. 11, 488-491 (1977)

[4] Gibson J.B., Harrison D.P.
"The reaction between hydrogen sulphide and spherical pellets of zinc oxide"
Ind. Eng. Process Des. Dev. 19, 231-237 (1980)

[5] Davidson M., Stevenson S.
Undergraduate dissertation
University of Edinburgh (1989)

[6] Carnell P.J.H., in
"Catalyst Handbook", ch.4
ed. Twigg M.V.
Wolfe Scientific (1988)

[7] Carnell P.J.H., Denny P.J.
"Techniques for investigating sulphur removal by zinc oxide absorbents"
AIChE Ammonia Safety Symp. (1984)

CHAPTER 2

LITERATURE SURVEY

Introduction

Zinc oxide is an n-type semiconductor and an important component in a number of catalysts. Its properties have therefore been extensively studied. This chapter reviews the available literature which may prove pertinent to the study of the absorption reaction of hydrogen sulphide with zinc oxide.

The chemistry of zinc oxide is the subject of section 2.1. It describes the crystal structure of zinc oxide and details what is understood of the defect structure. Mechanisms for diffusion are then discussed in terms of the defect structure. Finally, some comments are made on the various methods of preparation of zinc oxide, and the effects of these on the properties of the zinc oxide produced. Section 2.2 concerns adsorption on zinc oxide and how it bears on the hydrogen sulphide-zinc oxide reaction. The section begins with a description of the surface electronic states. This is followed by a review of the adsorption of water and of carbon dioxide on zinc oxide with comments on the different activities of the different crystal faces of zinc oxide. Where possible, mention is made in both sections 2.1 and 2.2 of the effect of impurities in modifying the behaviour of the pure material. The third section (2.3) discusses the modelling of gas-solid non-catalytic reactions and the final section (2.4) reviews the existing information on the hydrogen sulphide-zinc oxide reaction.

2.1 The Chemistry of Zinc Oxide

2.1.1 Crystal structure

Zinc oxide crystallizes in the hexagonal wurtzite lattice (Figure 2.1) with lattice constants a=3.250Å and c=5.207Å.[1] The Zn-O distances are 1.99Å parallel to the c-axis and 1.97Å in the other three directions. In terms of the ionic radii of oxygen and zinc, 1.40Å and 0.74Å respectively, the lattice may be envisaged as a structure of oxygen atoms in hexagonal close-packing with zinc atoms occupying half of the tetrahedral spaces in the oxygen lattice (Figure 2.2). Crystals naturally expose crystal planes having low Miller indices.[1] These planes have a relatively high packing density with consequent energetic stability. In zinc oxide, the crystal planes of particular interest are the polar (0001) and (000$\bar{1}$) faces and the prism (10$\bar{1}$0) face. Ideally, the prism faces are stoichiometric, exposing equal numbers of zinc and oxygen atoms while the polar (0001) and (000$\bar{1}$) faces expose only Zn and only O atoms respectively. Studies of the three surfaces using Low Energy Electron Diffraction (LEED) indicate that the respective surface structures very closely resemble those expected of a truncated bulk solid.[2] The differing activities of the different crystal planes are considered in section 2.2 in relation to adsorption studies on zinc oxide.

Zinc oxide crystals are white at room temperature, indeed zinc oxide is used as a white pigment. However,

---

[1]For hexagonal crystal systems of which wurtzite is an example, it is convenient to use 4 crystallographic axes to define the planes of a crystal, these being 3 diads at 120° and a hexad axis normal to the plane formed by the diad axes. The notation for specifying crystal planes in a hexagonal system is a modification of Miller's axes suggested by Bravais.

Figure 2.1: Schematic diagram of the hexagonal wurtzite structure of zinc oxide (atom spacings in Angstroms)

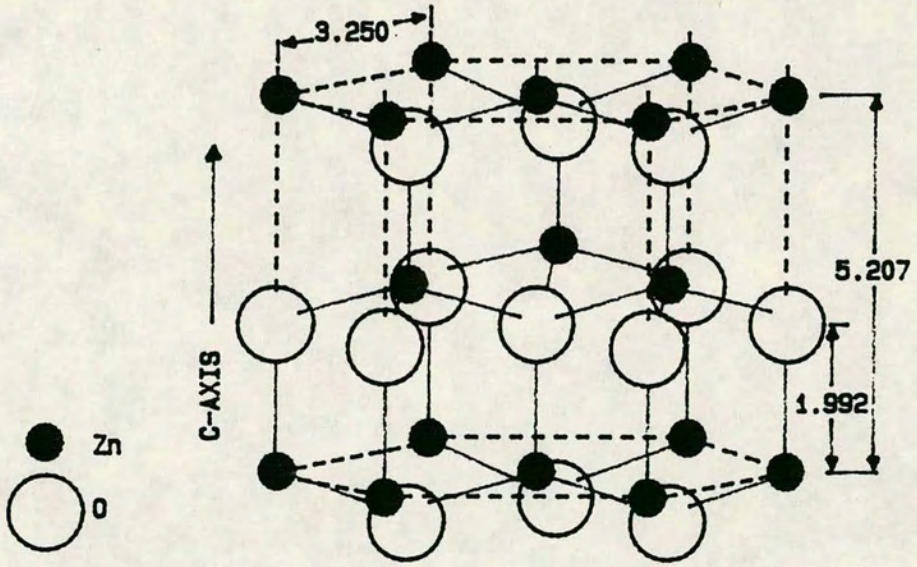

Figure 2.2: Close packing of oxygen atoms- in zinc oxide the zinc occupies half the tetrahedral holes in the oxygen sublattice.

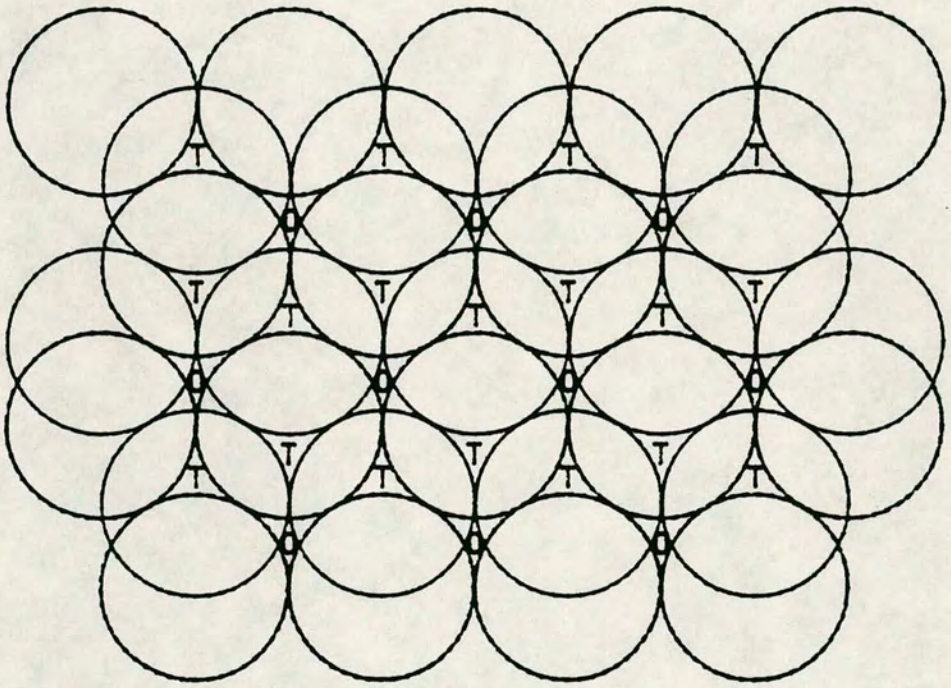

T **tetrahedral hole**

O **octahedral hole**

zinc oxide appears yellow upon heating to over 500°C [3] although the colour is lost again on cooling. Many oxides in solid solution give zinc oxide a yellow colour, as does mechanical strain of the crystal although in the latter case whiteness can be restored by annealing. There is evidence also that the ion Zn_2^{2+} is yellow in colour.[4]

2.1.2 Defect structure

Just as an understanding of adsorption on a molecular level is a prerequisite for the elucidation of heterogeneous catalysis, so the characterisation of the crystal defect structure - which is an important source of the chemical reactivity of solids - is essential to the understanding of the reactivity of solids.

Crystal defects are usefully categorised according to their dimension and field of effect.[5] Thus point defects are atomic defects which may be vacancies in the crystal lattice, interstitial or misplaced atoms or substitutional defects caused by doping with a foreign material (see Figure 2.3). Their field of effect is usually limited to their immediate neighbourhood. Dislocations may be regarded as 1-dimensional defects. They are of two types, edge and screw dislocations, defined according to whether the lattice displacement occurs respectively perpendicular or parallel to the dislocation line (Figure 2.4) The crystal lattice is distorted in the vicinity of a dislocation, and this distortion may extend over many atomic separations, ending at a surface or at the edge of the distortion field of another dislocation. Two dimensional defects occur in the form of surfaces, grain boundaries and stacking faults. Surfaces are very important to the chemical reactivity of solids and are associated with energetic states distinct from those of the bulk

Figure 2.3: Illustration of point defect types.

Figure 2.4: Types of dislocation.

(a) Edge dislocation

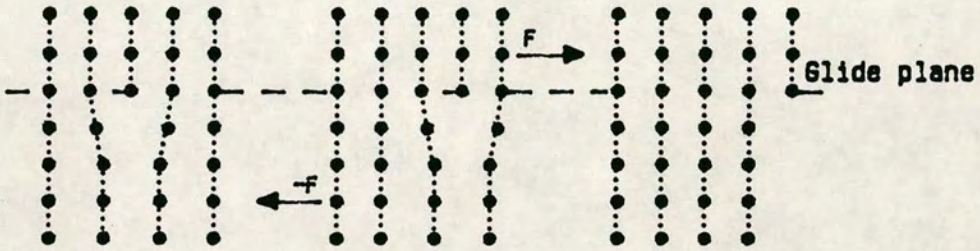

(b) Screw dislocation

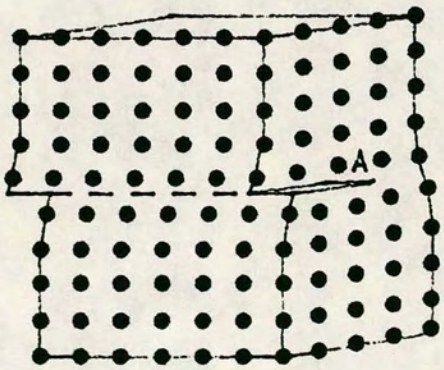

(section 2.2.1). When species chemisorb on a high surface area semiconductor, the entire solid is likely to lie within the potential field which is created by the adsorption process. Grain boundaries result in similarly extensive regions of distortion of electrical potential. They are formed where two crystals grow towards each other in a partly coherent boundary resulting in a series of edge dislocations as illustrated in Figure 2.5. Stacking faults are imperfections in the crystal packing structure. Thus a crystal lattice having hexagonal close-packing, the stacking sequence of which may be represented by ..ABABAB.. where alternate layers of atoms lie identically on top of one another (Figure 2.2), may contain a number of planes stacked as in a face-centred cubic crystal giving a sequence such as ..ABABCAB.. . Finally, three dimensional defects may be present in a crystal in the form of inclusions of foreign material, precipitates or pores.

Of these defects, only point defects may be in thermodynamic equilibrium - their concentration determined by pressure, temperature and crystal composition. At low temperatures, however, the attainment of thermodynamic equilibrium is likely to be kinetically hindered. The presence and extent of the higher dimensional defects in a crystal are determined by the method of preparation. This is considered in section 2.1.4. The present section reviews what is known concerning the point defects in zinc oxide.

Zinc oxide generally exists as n-type conducting zinc oxide,[6] that is, it is nonstoichiometric and contains excess zinc which acts as a donor. This n-type zinc oxide may be represented by $Zn_{1+\delta}O$. A zinc excess could exist in the crystal as a result of the presence of either zinc interstitials or oxygen vacancies in the

Figure 2.5: Schematic diagram of a low angle grain boundary.

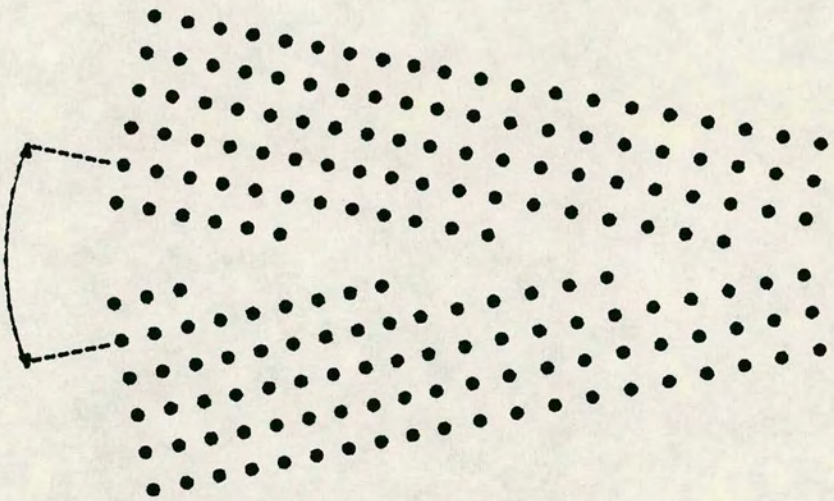

lattice. Neumann[6] discusses the likelihood of either defect type being the majority defect type in terms of the ionicity of zinc oxide. In an ionic crystal where the cationic and anionic radii are nearly equal, the thermally created point defects are likely to be of Schottky type, that is pairwise vacancies of cations and anions. If the cations and anions are of very different size, however, the point defects are likely to be of Frenkel type occuring as interstitials and vacancies of the smaller ion. The much smaller ionic radius of zinc compared to that of oxygen, 0.74Å and 1.40Å respectively, would appear to be evidence for Frenkel disorder in the zinc sublattice. However, the tetrahedral bonding in zinc oxide is suggestive of a more covalent type of bonding. Moreover, the sum of the covalent radii - 1.31Å for zinc and 0.66Å for oxygen - corresponds very well with the observed zinc-oxygen bond lengths in zinc oxide of 1.97Å and 1.99Å. Consideration of the covalent radii, however, suggests the likelihood of Frenkel disorder in the oxygen sublattice. Neumann[6] concludes that as theoretical considerations yield an ionicity for zinc oxide of 50-60%, the ionic and covalent radii give no information regarding the disorder type.

Various methods are used to determine the extent of non-stoichiometry of zinc oxide ie. the value of δ.[7] Such investigations are fraught with difficulty, however, because of the problem of measuring an equilibrium value of δ. This can arise because of either the slow kinetics of lattice defect reactions or because of the use of different conditions for pretreating the zinc oxide sample and for performing the measurement of the stoichiometric deviation, so that defect loss may occur before the measurement can be performed. Reasonable agreement between a number of analytical methods has been found.

Experimental evidence for the nature of the majority defect type is contradictory. X-ray diffraction at the octahedral interstitial position in the oxygen sublattice[8] together with the observed increase in the lattice constants with increasing zinc content[9] appear to provide strong evidence for zinc interstitials as the majority defect type. However, electron paramagnetic resonance (EPR) studies have been interpreted in terms of oxygen vacancies and interstitials while different researchers have discussed conductivity measurements in terms of oxygen vacancies or zinc interstitials. Hagemark[10] considers the possibility of zinc excess being due to oxygen vacancies in the surface layer and zinc interstitials in the bulk lattice. This proposition arises from his observation of conductivity dependence on zinc pressure (p_{Zn}) at high p_{Zn} but not at intermediate zinc pressures, which behaviour he attributes to the native donor, interstitial zinc (because of its higher mobility than that of oxygen vacancies) and to 'frozen-in' oxygen vacancies respectively.

It has already been stated that excess zinc acts as a donor in n-type zinc oxide. Formulation of the equations describing defect equilibria indicate the equivalence of zinc interstitials and oxygen vacancies in this respect. The notation used in the following equations is that of Kröger[11] and is summarised in Table 2.1.

The non-stoichiometry of zinc oxide may be considered as arising from the dissolution of zinc in zinc oxide forming the donor, D,

$$Zn_{(g)} \rightleftharpoons D \qquad (2)$$

Conductivity measurements indicate that in the temperature range 27-727°C, donors are singly

Table 2.1: Nomenclature for point defects
(after Kroger[11] and Neumann[6])

Symbol	Defect	Effective charge
D	Donor	0
$D^{\cdot}$	Singly ionized donor	+1
Zn_{Zn}	Zinc ion in a zinc lattice site	0
O_O	Oxygen ion in an oxygen lattice site	0
$Zn_i^{\cdot}$	Zinc ion (singly ionized) in an interstitial position	+1
O_i'	Oxygen ion (singly ionized) in an interstitial position	-1
V_{Zn}'	Singly ionized vacancy in the zinc sublattice	-1
$V_O^{\cdot}$	Singly ionized vacancy in the oxygen sublattice	+1
e'	Electron in the conduction band	-1
$h^{\cdot}$	Hole in the valence band	+1
$Zn_{(g)}$	Gaseous zinc atom	0
$O_{2(g)}$	Gaseous oxygen molecule	0

ionized.[12] Thus equation (2) may be re-written as

$$Zn_{(g)} \rightleftharpoons Zn_i^{\cdot} + e' \qquad (3)$$

if the zinc excess is present as interstitial zinc, or as

$$Zn_{(g)} \rightleftharpoons Zn_{Zn} + V_O^{\cdot} + e' \qquad (4)$$

if the zinc excess is due to oxygen vacancies. The non-stoichiometry may also be understood as arising from the partial vaporisation of oxygen. Thus, for ionised donors, the corresponding equations are

$$Zn_{Zn} + O_O \rightleftharpoons Zn_i^{\cdot} + \tfrac{1}{2}O_{2(g)} + e' \qquad (5)$$

$$Zn_{Zn} + O_O \rightleftharpoons Zn_{Zn} + V_O^{\cdot} + \tfrac{1}{2}O_{2(g)} + e' \qquad (6)$$

In a similar way, it is possible to formulate equations describing the creation of ionised acceptors in the form of zinc vacancies or oxygen interstitials due to the dissolution of oxygen in zinc oxide or to the partial vaporisation of zinc. These equations are further linked by the vapour pressure equilibrium of zinc oxide,

$$Zn_{Zn} + O_O \rightleftharpoons Zn_{(g)} + \tfrac{1}{2}O_{2(g)} \qquad (7)$$

The disorder type of the crystal depends on the relative values of the equilibrium constants for the formation of Schottky and Frenkel defects for which the equations are

$$0 \rightleftharpoons V_{Zn}' + V_O^{\cdot} \qquad (8)$$

$$0 \rightleftharpoons Zn_i^{\cdot} + V_{Zn}' \qquad (9)$$

$$0 \rightleftharpoons O_i' + V_O^{\cdot} \qquad (10)$$

where '0' represents the non-defected state. It would appear that both n-type and p-type conducting zinc oxide might exist depending on the pressure of oxygen and zinc and the attainment of equilibrium. However, p-type zinc oxide has not been observed.[6] The much faster diffusion rate of zinc than that of oxygen over a wide temperature range[12,13] provides evidence that the equilibrium constant for Frenkel disorder in the zinc sublattice

(equation (9)) is much greater than the equilibrium constant for Schottky disorder (equation (8)).

The doping of zinc oxide with other oxides, or its contamination with other metal ions due to the method of preparation (section 2.1.4), results in modification of the crystal defect structure. The effect of addition to n-type zinc oxide of the oxide of a monovalent metal such as lithium, which is typically used for doping, or sodium, which may be present as a result of a preparation method involving precipitation, may be represented as

$$Li_2O + D^{\cdot} + e' \rightleftharpoons 2Li_{Zn}' + O_O + V_O^{\cdot} + D^{\cdot} \qquad (11)$$

or

$$Li_2O + Zn_{Zn} + D^{\cdot} + e' \rightleftharpoons 2Li_{Zn}' + O_O + Zn_i^{\cdot} + D^{\cdot} \qquad (12)$$

Such addition evidently leads to a decrease in conductivity as is experimentally observed. An initial increase in conductivity with lithium doping has been observed in a system under zinc pressure[14] and this has been interpreted in terms of the temporary presence of lithium in interstitial sites. Mackrodt et al.[15] predict on the basis of molecular orbital calculations that doping with either lithium or sodium leads to lattice substitution compensated by anion vacancies and holes, and they cite evidence for sodium for the interaction of Na_{Zn}' with holes. They have also considered defects involving H^+ and conclude that free H^+ is not present in the zinc oxide lattice but exists as OH^- groups and that these interact appreciably with Na_{Zn}'. The addition of copper which forms a monovalent ion also causes a decrease in carrier density.[12] Conversely, the addition to n-type zinc oxide of a trivalent metal such as aluminium leads to an increase in conductivity -

$$Al_2O_3 + Zn_i^{\cdot} \rightleftharpoons 2Al_{Zn}^{\cdot} + 3O_O + Zn_{Zn} + e' \qquad (13)$$

or

$$Al_2O_3 + V_O^{\cdot} \rightleftharpoons 2Al_{Zn}^{\cdot} + 3O_O + e' \qquad (14)$$

2.1.3 Mechanisms for diffusion

In systems of electrically charged particles, diffusion occurs as a result of a gradient in electrochemical potential. The electrochemical potential, η_i, of particles of type i is defined as

$$\eta_i = (\partial G/\partial n_i)_{P,T,nj} = \mu_i + z_i F\phi \qquad (15)$$

where μ_i is the corresponding chemical potential, z_i is the valence of ions of type i, F is the Faraday constant (the product of Avogadro's number and the electronic charge, e_0) and ϕ is the electrical potential. Fick's 1st law may therefore be expressed as

$$j_i = - (D_i c_i/RT)\, \partial\eta_i/\partial x \qquad (16)$$

where D_i is the diffusion coefficient of component i. The modified Nernst- Einstein relation expresses the diffusion coefficient in terms of the mobility of the charged particle or the electrochemical mobility, u_i. This is defined as the average drift velocity per unit electric field strength. Thus,

$$D_i = RTu_i/z_iF = kTu_i/z_ie_0 \qquad (17)$$

Equivalently, the diffusive flux, j_i, may be expressed as a function of the conductivity, σ_i, of particles of type i,

$$j_i = -\sigma_i/(z_iF)^2\, \partial\eta_i/\partial x \qquad (18)$$

and it follows that the diffusion coefficient, D_i, may be derived from conductivity measurements according to

$$D_i = \sigma_i RT/[c_i(z_iF)^2] \qquad (19)$$

As well as point defects, polycrystalline zinc oxide contains dislocations and low and high angle boundaries and exposes a significant surface area. As the mobility

of zinc and of oxygen varies widely within these different defect regions of the lattice, the possible diffusion mechanisms and experimentally observed diffusivities of the different disorder types are considered separately.

Studies to determine the diffusion coefficient, D, of intrinsic point defect migration should be carried out on single crystals because polycrystalline materials are necessarily ill-defined in terms of their defect structure, and experimental data from them is therefore very difficult to interpret.[16]

The temperature dependence of the diffusion coefficient is of the form

$$D = D^0 \exp(-Q/kT) \qquad (20)$$

The activation energy for diffusion, Q, is the sum of the energies of formation and migration of the defect. Neumann[16] has derived expressions for the energies of formation of the zinc and oxygen diffusing species for both stoichiometric and n-type zinc oxide. He considers in turn the cases of Schottky disorder and of Frenkel disorder in the zinc sublattice as being the predominant disorder type. Thus, for example, in stoichiometric zinc oxide, if the equilibrium constant for Frenkel disorder in the zinc sublattice greatly exceeds the equilibrium constant for Schottky disorder,

$$K_{FZn} \gg K_S \qquad (21)$$

the defect concentrations should satisfy

$$[V_O{\cdot}] \ll [Zn_i{\cdot}] \simeq [V_{Zn}{'}] \qquad (22)$$

Oxygen is assumed to diffuse via a vacancy mechanism because of the absence of experimental evidence for p-type zinc oxide and for the existence of oxygen interstitials. Zinc, however, should diffuse via zinc interstitials because although the concentration of zinc

interstitials and zinc vacancies are approximately equal, studies of diffusion in metals have shown vacancy diffusion to be a much slower process.[16]

A number of studies have been performed on zinc oxide single crystals in order to determine the diffusion coefficients for oxygen and zinc. The temperature range over which measurements have been made is 900 to 1300°C. Most of the investigations have been carried out on crystals which are not at equilibrium with respect to the defect concentration because of the different conditions of pretreatment and measurement. More importantly, no determinations of dislocation densities have been made so that the measured diffusivities are likely to include contributions from these high mobility routes.[16,17] Methods of both tracer diffusion using ^{65}Zn and ^{18}O and chemical diffusion - where the diffusivity is measured under conditions of a gradient in the diffusant concentration - have been used. The diffusion coefficients derived from these two experimental methods are related as follows -

$$\tilde{D} = D'[\partial(\ln a)/\partial(\ln c)] = D'\{1 + [\partial(\ln \gamma)/\partial(\ln c)]\} \quad (23)$$

where $\tilde{D}$ and D' are the chemical and self-diffusion coefficients respectively, the latter being obtained by the tracer method, and a and c are respectively the activity and concentration of the diffusant, related by the activity coefficient, γ,

$$a = \gamma c \quad (24)$$

The chemical diffusion coefficients are several orders of magnitude larger than the self-diffusion coefficients. Heiland and Mollwo[18] have attempted to compare data obtained by the two methods by assuming that only interstitial zinc acts as a donor, and using the measured conductivity to calculate the mole fraction of interstitial zinc. However, the agreement between

data from the two methods is still rather poor and they conclude that the assumption of interstitial zinc as the only donor is in error, with ionised oxygen vacancies also likely to be present. The activation energies, Q, determined from the tracer experiments are in reasonable agreement indicating a value of Q of 3.0 to 3.3eV (ie. 289 to 338kJmol^{-1}).

Crystals having the wurtzite structure should show anisotropic vacancy diffusion.[16,17] The observed diffusivity is isotropic, however, and this appears to provide evidence for an interstitial mechanism. Neumann also considers the possibility of an interstitialcy mechanism whereby an interstitial zinc moves into an occupied zinc site forcing the zinc present in the site out into an interstitial site.[5]

The available data on oxygen diffusion shows great scatter,[16,19] however, Neumann concludes that the migrating defects can only be singly ionised oxygen vacancies ($V_O^{\cdot}$) and, moreover, that the dominating defects in zinc oxide are zinc interstitials.

In general, isolated dislocations, subgrain and grain boundaries provide high mobility routes for atom migration relative to the process of lattice (or volume) diffusion which proceeds via point defects.[2] Such higher dimensional defects are known therefore as short circuit paths.[19] The relative importance of these short circuit

---

[2]In considering mechanisms for diffusion of ions in the bulk of a crystallite of zinc oxide, it is useful to bear in mind the relative importance of surface and bulk transport processes as indicated by the specific surface area of the material. Thus for a specific surface area of x m^2g^{-1}, the percentage of zinc oxide which is exposed on the crystallite surfaces is 0.067x. In zinc oxide samples having specific surface areas of 10 and 100m^2g^{-1}, for example, the percentage of surface zinc oxide is therefore 0.67 and 6.7% respectively.

paths in contributing to the observed diffusivity in polycrystalline zinc oxide may be expressed in terms of the mean jump frequencies of particles in the lattice and in the defect regions.[5] Thus if Γ_L is the jump frequency of particles in the lattice containing point defects, and Γ_D is the jump frequency of particles in the distorted regions of dislocations or grain boundaries, then the magnitude of diffusion in the distorted regions is comparable with the volume diffusion when the ratio, R_Γ, of the number of particles in the distorted region to the number of particles in the rest of the crystal is given by

$$R_\Gamma \simeq \Gamma_L/\Gamma_D \qquad (25)$$

More explicitly, the relative magnitudes of the two contributions to the overall diffusion depend on the density of dislocations, ρ_D, defined as the number of points where dislocation lines cross the crystal surface per cm^2 of surface, and the mean linear grain dimension.[20]

An edge dislocation can migrate along its glide plane under the action of a shear force as illustrated in Figure 2.4. Movement of the dislocation can also occur perpendicular to the glide plane by the addition or subtraction of atoms from the half-plane which causes the dislocation. This movement is known as climb and occurs by means of the addition of interstitial atoms or the creation of vacancies in the bulk lattice (downward climb), or by the generation of interstitials and the 'condensation' of vacancies on the half-plane.[5,11] The movement of an edge dislocation can in this way facilitate the achievement of equilibrium between point defects. Screw dislocations are the other limiting type of the general dislocation line, where displacement occurs both perpendicular and parallel to the dislocation line. These are known to have a higher

activation energy for diffusion along the dislocation than do edge dislocations.[17] It is interesting to consider how these two types of dislocation manifest themselves at a surface. While an edge dislocation appears as what is virtually a point defect at the surface as the centre of a small stressed region, a screw dislocation is manifested as a 2-dimensional defect (see Figure 2.4(b)). In crystallisation screw dislocations therefore tend to act as nuclei for rapid growth onto a surface as atoms adding onto the line of the surface disturbance make an additional bond compared to those adding onto the undefected surface. Moreover, the stronger bonding away from the end of the disturbance (indicated on Figure 2.4(b) by the letter 'A'), which is understandable in simple geometric terms, results in spiralling growth about that end.

Two particular transport phenomena involving dislocations are of interest. The first is where the diffusion of a foreign ion causes stress fields due to changes in the lattice constant. In this case the diffusion of the foreign ions may itself cause dislocations to form and these may be carried along with the diffusion front giving unpredictable diffusivities. Secondly, annealing of a crystal containing dislocations may lead to their ordering as a low angle grain boundary. Diffusion in these is known to be anisotropic[5,17] being much greater in directions parallel to the dislocation core than perpendicular to it. In tracer experiments of zinc diffusion in polycrystalline zinc oxide using ^{65}Zn, Roberts[21] found the predominant diffusional mechanism to be grain boundary diffusion for temperatures up to 1400°C. If the activation energies and pre-exponential factors which have been reported[13,18,19,21] for the diffusion of oxygen and zinc in zinc oxide either by volume diffusion mechanisms or by short circuit paths at temperatures in

the range 900 to 1400°C may be considered valid at ambient temperature, these correspond to a wide range of values of the diffusivity with a maximum value of about $10^{-24}cm^2s^{-1}$.

The effects of higher dimensional defects are likely to be relatively much more important at lower temperatures because their various activation energies are lower than that of volume diffusion.[5] Thus, fine-grained crystalline material with a high dislocation density should show structure-sensitive diffusivity at lower temperatures, while at temperatures approaching the crystal melting point lattice diffusion will predominate.

The presence of three-dimensional defects in a solid in the form of pores is of great importance in increasing the chemical reactivity as it provides easy access for reactive gases to the bulk of a solid particle. The importance of porosity and of the pore structure is considered in sections 2.3 and 2.4.

2.1.4 Effect of the method of preparation on the properties of zinc oxide

The chemical and physical properties of any zinc oxide sample are highly dependent upon its method of preparation. The method used may be a major source of contamination of the zinc oxide by foreign ions and in many cases will be the single most important factor in determining the degree of non-stoichiometry and the nature of the defect structure of the solid. Furthermore, it will determine the specific surface area of the resulting material and its pore volume and pore structure. Any of these parameters may control the catalytic activity or absorption capacity of zinc oxide. This section reviews the literature on the effect of the method of preparation on the properties of zinc oxide.

Gour et al.[22] have studied the effect of the precipitating agent used in the preparation of zinc oxide on its physical parameters. The precipitating agents used - sodium carbonate, ammonium oxalate, ammonia solution, ammonium carbonate and ammonium bicarbonate - were mixed thoroughly with zinc nitrate solution at controlled temperature and pH. The resulting slurries were treated identically, being filtered, washed and dried at 110°C prior to decomposition at 400°C. The zinc oxide samples thus obtained were milled to the desired size range, made into a paste with the addition of alkali and water, and subsequently dried and sieved. The extents of non-stoichiometry of the zinc oxide samples prepared in this way were determined iodometrically [7] and found to vary in the range 4.5 to 6.6 ppm excess zinc.[3] The different samples also exposed different surface areas and varied in total pore volume, in the distribution of pore size and in the mean grain size. The decomposition of carbonates and oxalates was found to yield samples with higher surface areas and lower grain sizes than the decomposition of hydroxides and bicarbonates. No direct correlation between surface area and pore volume was apparent, however, and this was attributed to the differences in pore size distribution amongst the samples. The zinc oxide samples were also tested for their sulphur absorption capacity which was correlated with the degree of non-stoichiometry (section 2.4.3).

Plyasova et al.[23] determined the effect of the

---

[3]Note, however, that a zinc excess of 5ppm in 25ml of a 1.0M zinc solution represents 1.25×10^{-7}moles. Iodometric determination of this excess would require, for example, about 0.01ml of a 0.01M iodine solution. Given the volumes involved, some doubt must exist as to the accuracy with which such small differences in non-stoichiometry can be determined.

decomposition temperature on the extent of decomposition of zinc hydrocarbonate, and on the structure of the zinc oxide thus produced. By analysis of the radial distribution of atoms, they interpreted the interatomic distances observed as indicating the presence of zinc atoms in some of the octahedral spaces of the oxygen sublattice. The fractional occupation was found to be higher for a decomposition temperature of 300°C compared to that for a decomposition temperature of 1000°C. Increasing the temperature to 1000°C in the experiment with the lower decomposition temperature resulted in liberation of more water and carbon dioxide. Plyasova et al. concluded that decomposition is incomplete at 300°C and that the presence of remaining CO_3^{2-} and OH^- groups distorts the zinc oxide structure and is the cause of the distribution of some of the zinc atoms in interstitial (octahedral) sites.

The decomposition temperature of the zinc oxide precursor is also important in determining the surface area of zinc oxide, which is found to go through a maximum with increasing temperature of decomposition of the basic zinc carbonates, which may be written as $ZnCO_3.2ZnO.4H_2O$[24] and $ZnCO_3.3Zn(OH)_2.H_2O$.[25] The calculated pore structure is also a function of decomposition temperature.[24]

Not only may the extent of surface area of zinc oxide be important in determining its activity, but the distribution of exposed crystal faces may also be highly influential (section 2.2.2). Fubini et el.[26] have performed adsorption calorimetric measurements on two zinc oxide samples prepared by combustion of zinc metal and thermal decomposition of smithsonite ($ZnCO_3$). The former has a lower specific surface area (10 m^2g^{-1} compared with 37 m^2g^{-1} for the zinc oxide prepared by thermal decomposition) but a greater fraction of this

surface area is to be found on the polar (0001) and (000$\bar{1}$) faces.

2.2 Adsorption on zinc oxide

2.2.1 Surface electronic states

The surfaces of crystals represent discontinuities in the periodic lattice potential and give rise to electronic surface states distinct from the electronic states of the bulk lattice. These surface states may cause changes in the lattice defect structure, and, when modified by adsorption, generate electric fields which may extend over 100 to 1000Å[29,30] into the crystallites of a semiconductor such as zinc oxide. These effects are likely to be particularly significant for high surface area polycrystalline zinc oxide, where the extent of the electric field is comparable in magnitude to the crystallite dimensions.

The electron configurations of the zinc and oxygen atoms are expressed as:

Zn $1s^2 2s^2 2p^6 3s^2 3p^6 4s^2 3d^{10}$
O $1s^2 2s^2 2p^4$

The inner electrons of both atoms in the zinc oxide lattice are located in orbitals around their respective nuclei - these are the K, L, M shells, the energy differences between which result in the generation of characteristic X-rays upon electron bombardment (section 3.5.1). Only the outer or valence electrons are available for chemical bonding which may be ionic or covalent or some hybrid of the two (section 2.1.2,[6]). Quantum mechanical theory predicts that in a crystal the atomic orbitals of these electrons overlap giving rise to energy bands. Each such orbital of the original atoms of which the lattice is composed gives rise to an energy band in the crystal where the number of energy levels

within the band is equal to the number of that kind of atom in the crystal. Thus the bands may effectively be considered as continua.[27] The Madelung potential method for the determination of electronic energy levels and band gaps is based on the classical theory of electronic states in an ionic lattice. The bulk Madelung potential, V_b, is the energy required to remove an ion from the bulk of the crystal, it being assumed that for a crystal of type MX, the Madelung potentials for an anion(X) and a cation(M) are equal, ie.-

$$V_{bX} = V_{bM} = V_b \qquad (26)$$

and where V_b is given by,

$$V_b = c_b(Ze_0/r_{MX}) \qquad (27)$$

Z is the valence of the ion and may be fractional if the crystal bonding is not purely ionic, e_0 is the electronic charge and r_{MX} is the shortest cation-anion distance. The Madelung constant, c_b, is a measure of the interaction of an ion with all the other ions in the crystal and is dependent on the geometry of the lattice structure. The validity of equation (26) follows from the definition of c_b. The energies of the cation-derived conduction band and the anion-derived valence band which the bonding electrons form may thus be represented as[28]:

$$E_{bM} = V_b - I \qquad (28)$$

$$E_{bX} = -V_b - A \qquad (29)$$

where I and A are the ionisation potential of the cation and the electron affinity of the anion respectively. The band gap, E_{bg}, is given by

$$E_{bg} = E_{bM} - E_{bX} = 2V_b - (I-A) \qquad (30)$$

This expression is only approximate because in real crystals the conduction and valence bands are not discrete levels but energy bands of finite width. The band width increases with decreasing interatomic

distance corresponding to increasing delocalisation of the valence electrons, and a transition from semiconductor-type behaviour to a more metallic behaviour.[11]

There is evidence that the extent of filling of the 3d orbitals in transition metal oxides is influential in determining both the chemical bonding and activity of such oxides.[29] Where the d-states are partially filled, as in Cr_2O_3, MnO, FeO, CoO and NiO, the electrons in these d-states are relatively delocalised. In zinc oxide, however, the 3d state is fully occupied and its energy is as a consequence substantially reduced. The 3d orbitals do not therefore take part in chemical bonding and their energy is about 8eV below the edge of the valence band which derives largely from the O 2p orbital.[29] The conduction band, however, has substantially Zn 4s character and the band gap which separates the valence and conduction bands is about 3.1eV.[6] While in cobalt oxide and nickel oxide the effect of Ligand Field Stabilisation Energy[4] (LFSE) is to make a co-ordination number of 6 more stable than one of 4 thus giving rise to an octahedral structure, for zinc oxide there is no gain of LFSE because of the full d-state and a co-ordination number of 4 is favoured resulting in a tetrahedral structure. It may well be that the activity of zinc oxide towards hydrogen sulphide is attributable at least in part to the low co-ordination of the zinc.

Surface states are of two kinds - intrinsic and extrinsic. The intrinsic states may be attributed to the termination of the periodic potential of the lattice. Because the surface Madelung constant is smaller than the Madelung constant in the bulk - surface ions having reduced coordination relative to ions in the bulk lattice - it follows that the surface band gap is also

smaller than the bulk band gap (equation (30)). The resulting respectively cation- and anion-derived conduction and valence bands at the surface should lie just within the band gap, E_{bg}, of the bulk states. These surface states are sometimes known as the zinc and oxygen dangling bonds, the former being the empty, acceptor-like conduction level, and the latter the filled, donor-like valence level.[28]

It can be very difficult to distinguish experimentally the intrinsic and extrinsic surface states. The latter appear due to the adsorption of foreign molecules or to the presence of surface defects. It is the difficulty of preparing completely clean and undamaged surfaces therefore which leads to controversial interpretations of observed electronic states.[28]

Adsorption of gaseous molecules onto a surface may be classified as either physisorption or chemisorption. Physisorption involves only a weak interaction between adsorbate and adsorbent whereas chemisorption is generally described as involving charge transfer between the adsorbed species and the solid surface. Chemisorption may be described in terms of the redistribution of charge within the adsorbate-adsorbent system on the basis of the band model for the electronic state of the adsorbent. The extent of chemisorption and the direction of charge transfer are governed by the energetic levels of the orbitals of the adsorbed species relative to the Fermi level of the solid.[30] The Fermi level, E_F, is the highest occupied energy level of the system at absolute zero. At higher temperatures, however, some states below the Fermi level will be vacant and some states above it will be filled, the occupation probabilities being given by Fermi-Dirac statistics.[27] The probability, $f(E_a)$, of occupation of a given energy level, E_a, of the adsorbed species is

given by

$$f(E_a) = (1 + \exp[(E_a-E_F)/kT])^{-1} \quad (31)$$

As has been mentioned already at the beginning of this section, adsorption on zinc oxide generates electric fields in the solid which extend into the bulk of the crystallites. Thus, the adsorption of oxygen on zinc oxide, for example, results in a depletion layer in the zinc oxide due to charge transfer to the adsorbate. This is termed the space charge layer (SCL). The relationship between adsorption and the generated SCL is interactive in the sense that the SCL induces bending of the electronic bands. For an adsorptive gas such as oxygen which acts as an acceptor, the effect of the band bending is to raise the energy of the bands towards the surface to above the Fermi level, and thereby to limit further adsorption.[29] The energy required to remove an electron from the Fermi level to the vacuum level which corresponds to infinite separation from the lattice is given by the work function, ϕ_∞. Chemisorption of an acceptor gas, such as oxygen, lowers the effective Fermi level by increasing the energy required to remove an electron from the Fermi level by an amount equivalent to the potential created in the SCL.[27] Thus the work function increases with increasing adsorption and conversely decreases with increasing adsorption of a donor gas. It is therefore a useful experimental measure of the extent of adsorption. Figure 2.6 illustrates the charge distribution, electron energy levels and electron concentrations as a function of distance into a zinc oxide crystal perpendicular to the surface for the cases of chemisorption of an acceptor and of a donor gas.

Figure 2.6: Schematic diagrams of the electronic condition of a zinc oxide surface after transient exposure to (a) an acceptor gas eg. oxygen, or (b) a donor gas eg. hydrogen.

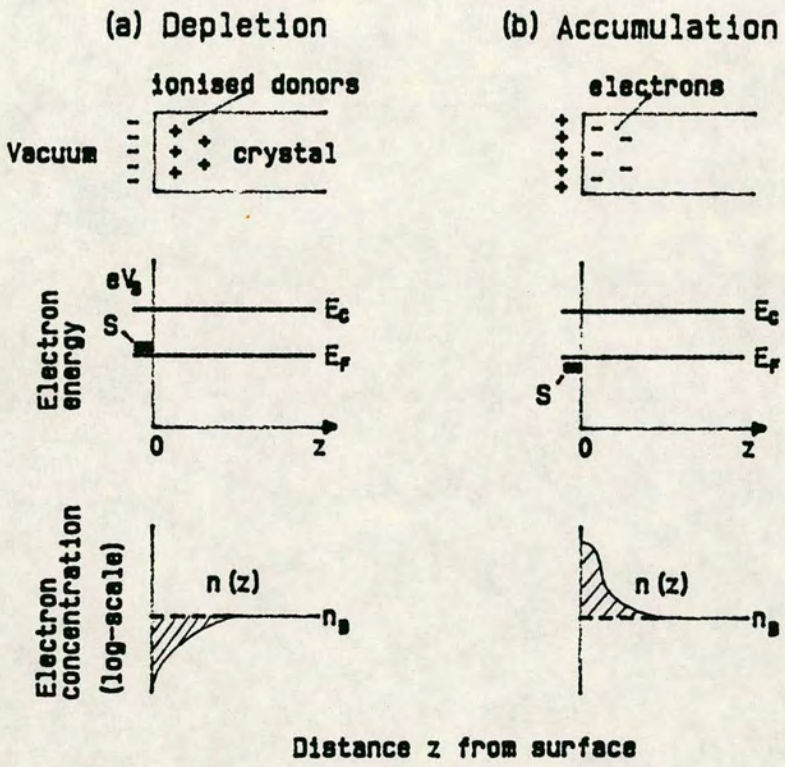

2.2.2 Structural Differences amongst the Crystal Faces of Zinc Oxide

The different structures of the three natural faces of zinc oxide - the polar Zn(0001) and O(000$\bar{1}$) surfaces and the non-polar (10$\bar{1}$0) surfaces (Figure 2.1) - are considered briefly in this section, with regard to their respective reactivities.

Zinc ions on the Zn(0001) surface are coordinatively unsaturated, being bonded to only three lattice oxygens. Similarly, oxygen ions on the O(000$\bar{1}$) surface are bonded to only three lattice zincs, whereas both zinc and oxygen ions are tetrahedrally coordinated in the bulk structure. On the nonpolar, prism (10$\bar{1}$0) face, both cations and anions are unsaturated, being bonded to only two lattice oxygen and zinc ions respectively. Thus the reactivity of the three faces for adsorption of a foreign molecule may vary widely depending on the molecule's requirement of an anion, cation or anion-cation pair for bonding.[31] For ionic adsorbates or those possessing a significant dipole moment, the different faces also provide very different sites, there being no net dipole moment on the nonpolar surfaces, but respectively outwardly-directed and inwardly-directed dipoles on the Zn(0001) and O(000$\bar{1}$) faces. The different sizes of the anion and cation modify the reactivities of the polar faces because of the effective shielding of the zinc ions by the larger oxygen ions on the O(000$\bar{1}$) face, the reverse effect being much less significant because of the smaller size of the cation. Finally, the presence of steps on the polar surfaces exposing the nonpolar (10$\bar{1}$0) face is known.[31,32]

The relative positions of zinc and oxygen ions on the three surfaces may also be important for determining the extent of adsorbate interactions as has been considered

by Atherton et al.[33] with respect to hydrogen bonding of hydroxyls.

In zinc oxide samples containing impurities, depending on the physical size and nature of the impurity, and the method of its introduction into the sample, it may be preferentially concentrated on the crystal surfaces and distributed unequally between the polar and prism faces. Thus, potassium ions, for example, are considered to be concentrated preferentially on the polar faces[34] and have been shown to be held particularly strongly on the oxygen polar face .[35]

Finally, the distribution of exposed faces on a zinc oxide sample may also affect the rate of reaction of zinc oxide if the dominating diffusional process is anisotropic.

2.2.3 Water adsorption on zinc oxide

The nature of the interactions between water and zinc oxide surfaces has variously been studied using infrared (IR)-absorption, calorimetric, volumetric, thermogravimetric and conductivity techniques.[30,36] The work reviewed here has been performed on zinc oxide powders and pellets. Although Zwicker and Jacobi[37] have made thermal desorption studies of the adsorption states of water on single crystal zinc oxide surfaces, their work is confined to water adsorption at sub-ambient temperatures and consequently to states of molecularly adsorbed water. They observed six different adsorption states on each of the Zn(0001) and O(000$\bar{1}$) polar faces and on the nonpolar (10$\bar{1}$0) face, with strongest bonding to the Zn sites. Higher temperature studies of adsorption on single crystals would provide valuable and unequivocal information on the interactions of water with the different zinc oxide crystal faces.

Atherton et al.[33] found that commercially available zinc oxide prepared by combustion of metallic zinc contained both carbonate and hydroxylic surface species after storage under ambient conditions. The carbonate species were removed by treatment with oxygen and water vapour at 400°C. The IR spectrum of the hydroxylated surface contained four strong absorption bands - two narrow bands at 3670 cm^{-1} and 3620 cm^{-1}, and two broad bands at 3555 cm^{-1} and 3440 cm^{-1}. These were identified as correspoding to OH species by means of deuterium oxide (D_2O) exchange experiments. The absence of an absorption band at around 1600 cm^{-1} - corresponding to the deformation vibration of molecular water[38] - was cited as evidence for the absence of molecularly adsorbed water on the surface. The hydroxyl-carrying surface was progressively dehydroxylated by outgassing at increasing temperatures in the range 47-452°C in order to study the effect on the IR spectrum. This lead to a gradual reduction in intensity of the two broad bands with some decrease also observed in the band located at 3670 wavenumbers. The band at 3555 cm^{-1} was observed to disappear abruptly at about 352°C which was interpreted[33] as indicating the condensation of adjacent surface hydroxyls on attainment of a critical mobility, most probably on the $(10\bar{1}1)$ and $(10\bar{1}\bar{1})$ faces, where the atomic spacing on the face should permit weak hydrogen bonding. The other broad band at 3440 cm^{-1} was attributed to hydrogen bonded hydroxyls on the $(10\bar{1}0)$ face and the two narrow bands at 3670 cm^{-1} and 3620 cm^{-1} to the fundamental O-H stretching frequency of hydroxyls on the (0001) and $(000\bar{1})$ faces respectively. The interatomic distances on these faces were judged likely to prohibit hydrogen bonding. A repetition of this work on a modern instrument equipped with reflectance IR would be interesting. In particular, the use of labelled species to differentiate between bulk and surface

structures could be extended (see section 2.2.4).

Mattmann et al.[39] have also studied the adsorption of water on zinc oxide by means of thermogravimetry and IR-absorption spectroscopy. They found absorption bands at 3670 cm^{-1} and 3620 cm^{-1} which, like Atherton et al., they attributed to hydroxyl groups located on the polar faces. They suggested, however, that the non-polar faces were inert to water chemisorption, associating the bands at 3560 cm^{-1} and 3450 cm^{-1} with water molecules physisorbed on chemisorbed hydroxyl groups. Desorption of water from surface hydroxyl groups was observed at temperatures up to 640°C.

Measurements of the heat of immersion of partially hydroxylated zinc oxide samples by Nagao et al. were used to calculate the differential heat of chemisorption of water on zinc oxide. Heat treatment of hydroxylated samples at 250°C and 450°C indicated loss of mainly physisorbed and of physisorbed and some chemisorbed water respectively.[40] The calculated differential heat of chemisorption showed a maximum at a hydroxyl coverage of about 0.8 of a monolayer.[41] It was suggested that this maximum arises because of cooperative adsorption of water due to hydrogen bonding on the $(10\bar{1}0)$ face, leading to a so-called closed hydrogen-bonded structure. Such a structure was thought likely to provide a rather weak attractive potential to approaching water molecules .[41] It was therefore cited as an explanation for the 2-dimensional condensation of water on hydroxylated zinc oxide, which was observed [42] in adsorption isotherms at temperatures below the 2-dimensional critical temperature of 44.9°C, calculated using the Hill-de Boer model.[43] Nagao et al.[41] found that zinc oxide calcined prior to de-gassing and water treatment, showed a decreasing capacity for chemisorption on a unit area basis with increasing temperature of calcination in the

range 600-900°C, and an apparent increasing surface heterogeneity.[42]

Estimates of the coverage of hydroxyl groups on a fully hydroxylated surface by Mattmann et al.[39] and by Nagao[42] are in good agreement, being 8.4 and 7.5 $OH^-/100Å^2$ respectively. Mattmann has also estimated the water concentration in the first condensed layer of physisorbed water as 4-5 molecules/$100Å^2$, and has measured the build-up of surface water to a depth of 200 monolayers at a relative pressure, p/p_0, of 1.

Uematsu et al.[44] have studied the effects of annealing temperature and of grinding on the adsorption of water by zinc oxide. They found that the specific surface area decreased with increasing annealing temperature in the range 700-1000°C. This result complements the behaviour observed by Khalil and Kolboe[45] of a maximum in the surface area with annealing temperature in the range 100-530°C at about 300°C on zinc oxide similarly prepared. Uematsu et al. also found that the amount of water reversibly adsorbed per unit surface area at 500°C decreased drastically with increasing annealing temperature. The effect of grinding the zinc oxide was to decrease dramatically the observed quantity of reversibly adsorbed water with, initially, no change in surface area. After some time, however, the grinding produced a 6-fold increase in surface area with a marginal increase in the amount of reversibly adsorbed water per unit area of surface.

The effect of heat treatment of zinc oxide in the range 350-700°C on the adsorption of water has been further investigated[46] for both granular and needle-like zinc oxide samples. The former expose a sizeable proportion of polar faces while the latter expose predominantly prism faces.[3] Heat treatment was found to decrease the

surface area significantly, the decline being more substantial at higher temperatures. It also affected the desorption temperature of adsorbed water, decreasing the amount desorbed between 400-500°C and greatly increasing the amount desorbed at 80°C which is assumed to represent water adsorbed molecularly onto lattice zinc ions on the prism face. Electron micrographs of the heat treated specimens revealed a loss of definition of the edge regions, and this was interpreted as the stabilisation of high surface energy regions by formation of prism faces. Thus the increase of molecularly adsorbed water was accounted for. Following Mattmann et al.,[39] Ohkuma et al.[46] assume that chemisorbed hydroxyls are present only on the polar faces, attributing the 500°C desorption peak observed in the Differential Thermal Gravimetric Analysis (DTGA) to the desorption of hydroxyls from the (0001) and (000$\bar{1}$) faces. It was suggested that the spreading of the 500°C desorption peak to lower temperatures (400-500°C), which was observed with heat treatment of the granular zinc oxide, was related to a partial stabilisation of the polar faces.

Morishige et al.[47] have also used the technique of thermal gravimetric analysis together with IR-absorption spectroscopy to investigate the nature of adsorbed water on zinc oxide. As the peak maxima in the thermal desorption spectra (TDS) occur at the same temperatures for five different zinc oxide samples prepared by different methods, each peak is considered as originating from the desorption of adsorbed water on a particular crystal face of zinc oxide. In particular, a broad peak at 80°C is attributed to the desorption of strongly physisorbed water molecules, while a prominant peak at about 270°C is attributed to the desorption of hydroxyl groups. The effect of increasing outgassing temperature on the IR spectra is a pronounced decrease

in intensity of an absorption band at 3540 cm^{-1}. This is interpreted as corresponding to the peak at 270°C in the TDS, and it is proposed that the desorption is caused by 2-dimensional condensation from an inactive surface which they suggest to be the $(10\bar{1}0)$ face of zinc oxide. This interpretation is in contrast to that of Atherton et al.[33] who observed a similar behaviour of the 3555 cm^{-1} band, attributing it to the desorption of hydrogen-bonded surface hydroxyls on the $(10\bar{1}1)$ and $(10\bar{1}\bar{1})$ faces. No assignment was made to a second prominant peak at about 220°C in the TDS.

Bhattacharyya et al.[48] have studied the relation between water chemisorption and conductivity of zinc oxide. Non-stoichiometric n-type zinc oxide was produced by heat treatment in vacuo at 400°C of a zinc oxalate-derived zinc oxide. The n-type character of the zinc oxide was confirmed by the measured increase and decrease in conductivity of respectively gallium- and lithium-doped zinc oxides (section 2.1.2, equations (11)-(14)). The conductance of n-type material was observed to increase exponentially with temperature.

Adsorption of water at 215, 230 and 250°C was shown to be of the acceptor-type (section 2.2.1), causing a reduction in conductivity. At 230 and 250°C water adsorption was followed, after a brief period, by hydrogen evolution. The quantity of hydrogen evolved was greatest on gallium-doped zinc oxide. It was concluded that dissociative chemisorption occurred with the formation of hydrogen ions, and that hydrogen was evolved by means of the capture by hydrogen ions of the electrons which give rise to conductivity. Thus, the chemisorption and hydrogen evolution are the cause of the observed reduction in the material's conductivity. These observations were interpreted as a reaction with doubly ionised interstitial zinc[48] but could be

described in terms of either interstitial zinc or oxygen vacancies, either donor being singly ionised at this temperature.[12] Bhattacharyya et al. propose that the observation of surface hydroxyl groups on zinc oxide exposed to water vapour at 400°C[33] suggests that the zinc oxide used by Atherton et al. was stoichiometric.

Sengupta et al.[49] have also studied water chemisorption on n-type zinc oxide at 150 and 250°C by means of conductivity measurements. They propose that the n-type activity of their zinc oxide sample arises from the decomposition of surface carbonate leaving superficial oxygen atoms on the surface which are removed by de-gassing at 250°C, thereby creating highly non-stoichiometric zinc oxide. Prolonged de-gassing at elevated temperature, however, is thought to lead to precipitation of excess zinc causing the observed slow decrease in conductivity. Both acceptor-type and donor-type adsorption of water were observed, the former being more apparent at the lower temperature. Thus, the acceptor-type adsorption was judged to have a lower activation energy. It was proposed that acceptor and donor adsorption occurred on $Zn^{+}O^{-}$ and $Zn^{+}O^{2-}$ adsorption centres respectively. Hydrogen pre-treatment of the sample lead to a reduction in both kinds of adsorption which was explained in terms of the removal of both O^{2-} and O^{-} ions from the surface with increasing non-stoichiometry of the zinc oxide.

While an unambiguous interpretation of the adsorbed states of water on zinc oxide is still not possible, it is clear that high temperature treatment of zinc oxide can lead to loss of surface area through sintering; this loss of surface area is likely to be accompanied by a change in the distribution of exposed crystal faces and also in the available sites for water adsorption.

The presence of surface carbonate on zinc oxide samples has been widely reported.[33,39,44,46,47,49] As surface carbonate is likely to be present on any zinc oxide-based absorbent, the adsorption of carbon dioxide on zinc oxide is considered in the following section.

2.2.4 Adsorption of carbon dioxide on zinc oxide

The adsorption of carbon dioxide has been studied on single crystal surfaces and on powders, and also in connection with the adsorption and decomposition reactions of other molecules.

The adsorption of carbon dioxide on nonpolar surfaces[50] appears to have a very low activation energy and to be fully reversible between 25 and 200°C. The adsorption is of the acceptor type, giving a decrease in conductivity and an increase in the surface potential. Reports are contradictory as to whether non-stoichiometry affects the adsorption.[30] Akhter et al.[31] observed no carbon dioxide in the Thermal Desorption Spectra (TDS) after exposure of the O(000$\bar{1}$) face to carbon dioxide at ambient temperatures, and assumed that if adsorption occurs on this face, it is very weak - the molecules being desorbed during evacuation. In an IR study, Saussey et al.[32] assigned bands in the spectra to linear species and bidentate carbonates at edge sites formed by the (0001) and (10$\bar{1}$0) faces, and to a number of other species. They have also considered the effect of adsorbed carbon dioxide in increasing the Lewis acidity of zinc oxide and thereby altering the surface interactions with a number of other probe molecules.[51] Bowker et al. assume that carbon dioxide is much more strongly held on the polar than on the prism faces of polycrystalline zinc oxide[52] and attribute the low coverage of the species to the adsorption site being some kind of surface defect.[53]

Atherton et al.[33] compared the extent of adsorption of carbon dioxide on the partially hydroxylated and fully hydroxylated surfaces of polycrystalline zinc oxide. They found the chemisorption of carbon dioxide at ambient temperature to be much more significant on the partially hydroxylated surface, leading to formation of carbonate ions. Exposure of these surfaces to an excess of water vapour at ambient temperature, however, was seen to displace the carbonate very readily. Although ^{14}C was not used to determine whether the carbonate initially present in the sample was located exclusively on the crystal surfaces, it seems possible that this was the case, given the relative ease with which the carbonate was subsequently removed. In the dosing experiments with carbon dioxide, there is no evidence for the formation of bulk carbonate. The distinction between surface and bulk carbonate present in zinc oxide may be of some importance with respect to its activity as an absorbent for hydrogen sulphide.[4]

2.3 The modelling of gas-solid non-catalytic reactions

2.3.1 Introduction

The understanding and modelling of single particle reacting systems is crucial to the efficient design of, and interpretation of data from, multi-particle systems. This section therefore provides a review of the range of models which have been developed to describe single-particle gas-solid reactions. Such reactions

---

[4]In this laboratory, stoichiometric carbonation of a slurry of zinc hydroxide to hydrozincite has been performed. Calcinations of both hydrozincite and zinc oxide - the latter having been stored open to the atmosphere and thus exposed to a certain partial pressure of carbon dioxide - indicate the extreme difficulty of completely removing all traces of carbonate. Plyasova et al.[23] have studied this problem quantitatively.

encompass a broad range of reacting systems including those where significant differences in porosity exist between reactant and product solids, where sintering or pore closure may be important or where complete gasification occurs with no solid product being produced. A number of mathematical models have been developed which account for various of these effects and their success in describing experimental data for any particular reaction system is likely to depend on the appropriateness of the underlying assumptions of the model. A review of the principal models is given here with respect to a reaction which may be expressed as:

$$A_{(g)} + B_{(s)} \rightleftharpoons C_{(g)} + D_{(s)} \qquad (32)$$

which describes the stoichiometry of the reaction between hydrogen sulphide and zinc oxide. As zinc sulphide has a larger molar volume than zinc oxide, models which account for structural changes with progress of the reaction are of particular interest. All of the models discussed below refer to the formation of some kind of solid product layer. With respect to the sulphiding of zinc oxide, the fact that both oxide and sulphide exist in the wurtzite structure - although the sulphide also forms as sphalerite which is the more stable structure in the temperature range of interest (section 2.4.1) - may well facilitate the bulk reaction. It is likely also to affect the range of composition of a zinc oxide/zinc sulphide binary solid solution. Little information is available on this subject, however, solid solutions of composition $ZnS_{0.85}O_{0.15}$ have been observed.[54]

The reaction of a single solid particle may be considered as consisting of a number of basic steps, as detailed in section 1.1, namely:

1. gas phase mass transfer of the gaseous reactant, A, from the bulk of the gas stream to the external

surface of the particle, and of the gaseous product, C, in the opposite direction
2. diffusion of gas A through the pores of the solid matrix to the internal surfaces of the solid reactant, B, and pore diffusion of the gas C from the internal surfaces outwards
3. adsorption on the solid surface of gas A and desorption of C
4. chemical reaction at the solid surface

Where significant quantities of heat are either generated or consumed by the chemical reaction, heat transfer may also be important.

This sequence of steps describes the gas-solid contacting solely in terms of the mobility of the gaseous molecules. For many gas-solid reactions this is likely to be valid, however, in certain cases the much lower mobility of ions within the solid matrix may yet be essential for the contacting of the gaseous reactant with the unreacted solid B. The rate of the overall reaction is often dominated by a single step within this complex sequence, and in such cases a rather simple model may adequately describe the experimental data. One of the complicating features of gas-solid non-catalytic reactions, however, is that structural changes accompanying the continuous reaction of the solid may cause the controlling regime in a single particle to change with time.

Models for gas-solid reactions may be classified according to two broad categories[55] - distributed or structural models. Distributed models arise from consideration of diffusion and reaction processes in the particle as a whole, while structural models are based on concepts about either the solid or pore structure. Both types of model are described here. Although other particle geometries have been considered, the models are described and formulated here for a spherical particle henceforth referred to as a pellet.

2.3.2 Distributed models

The sharp interface model (SIM) - also known as the shrinking unreacted core model - is one of the simpler and more widely used of the distributed models. It is generally applicable to the reaction of a nonporous solid which reacts to give a porous solid product. It has also often been applied to the reaction of a porous solid when the rate of diffusion of the reactant gas through the pores is assumed to be much slower than the other steps in the overall reaction, in particular the rate of surface reaction. The rates of external mass transfer and of adsorption and desorption are generally fast although external mass transfer can become the rate-limiting process at very high reaction temperatures. The slow rate of pore diffusion means that reaction occurs at a sharp interface between the outer shell of completely reacted solid and the inner core of unreacted solid. Bowen and Cheng[56] have developed a modified SIM which allows for a reacting zone of finite width as oppose to a 'sharp interface'. Such a model is more appropriate in particular for the reaction of a porous solid. However, their assumption of a linear variation of the reactant gas concentration within the reacting zone limits the applicability of the model to situations where the width of the reacting zone is very narrow.[55]

The volume reaction model[57] which is applicable only to the reaction of a porous solid represents the opposite extreme of the set of distributed models. It arises from the assumption that the rate is predominantly controlled by the intrinsic (chemical) rate and that the reaction takes place simultaneously at all points in the pellet. The rate is likely to decrease towards the centre of the pellet due to the decreasing concentration of reactant gas which results from some degree of pore

diffusion resistance. Clearly the variation of rate with radial distance in the pellet will in this case depend partly on the intrinsic kinetics and reaction order with respect to the gaseous reactant. In the extreme case of pure chemical control, the concentration of reactant gas, and hence the rate, is constant through the pellet giving the homogeneous model.

Ishida and Wen[58] have described a 2-stage model which allows for the effect of structural change due to reaction by incorporating different effective diffusion coefficients for pore diffusion of the gaseous reactant A in the product layer, D_{eA}, and in the mixed zone of unreacted and partially reacted solid, D_{eA}'. Due to the higher concentration of the gaseous reactant A towards the outer surface of the pellet, the reaction rate increases in the radial direction. After some time the solid reactant at the pellet surface is completely reacted, and this indicates the end of the first stage. During the second stage of reaction two zones exist - the central zone of unreacted and partially reacted material and an outer shell of increasing width of pure product. These two stages of the model are shown in Figure 2.7(a) and (b). In the formulation of the model the effective diffusion coefficients, D_{eA}' and D_{eA}, are used for the first and second stages respectively. Ishida and Wen have shown that their model reduces to the volume reaction model if $D_{eA} = D_{eA}'$, and to the shrinking unreacted core model if $D_{eA}' \ll D_{eA}$.

Mantri et al.[55] have developed a generalised zone model of which the SIM and volume reaction model are special cases. They argue that their model is more general than that of Ishida and Wen as it allows for the existence of three zones - a central unreacted core and outer product layer separated by a zone of reacting solid. The three stages of the model are indicated in Figures 2.8 and 2.9

Figure 2.7: Concentration profiles through a reactant pellet according to the model of Ishida and Wen.

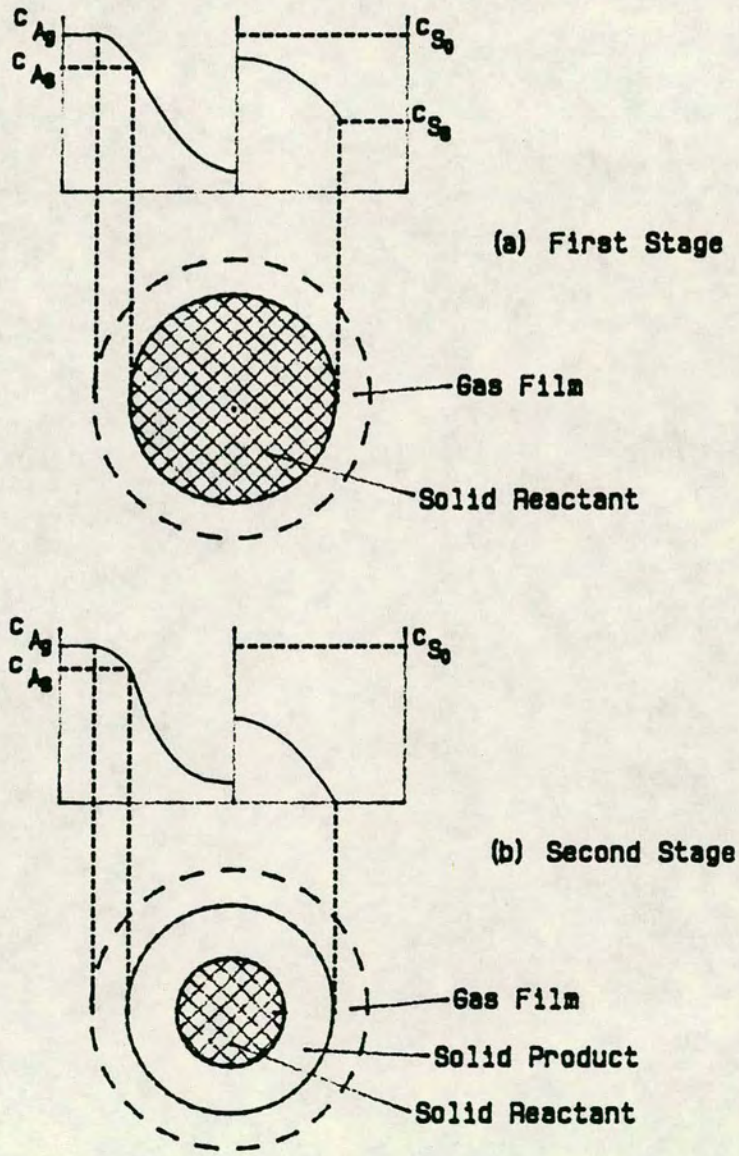

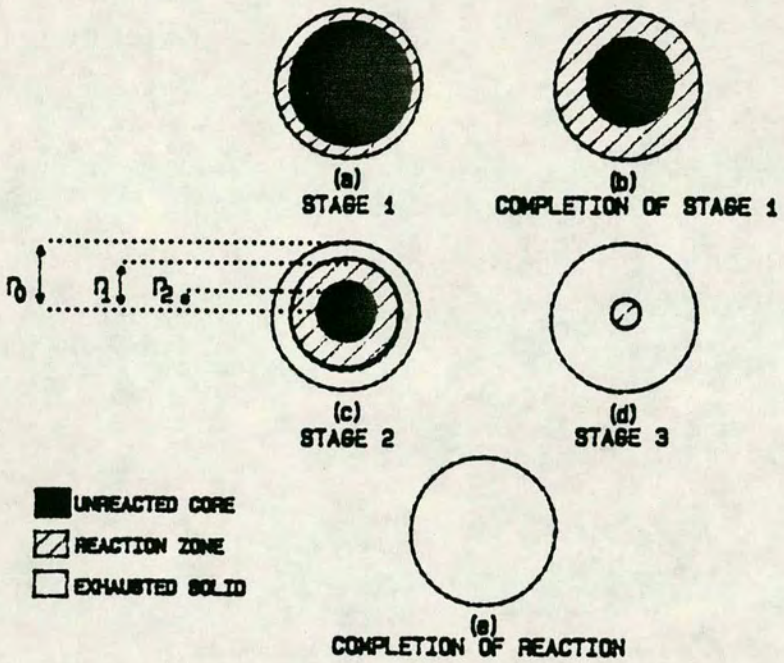

Figure 2.8: The stages of the generalised zone model of Mantri et al.

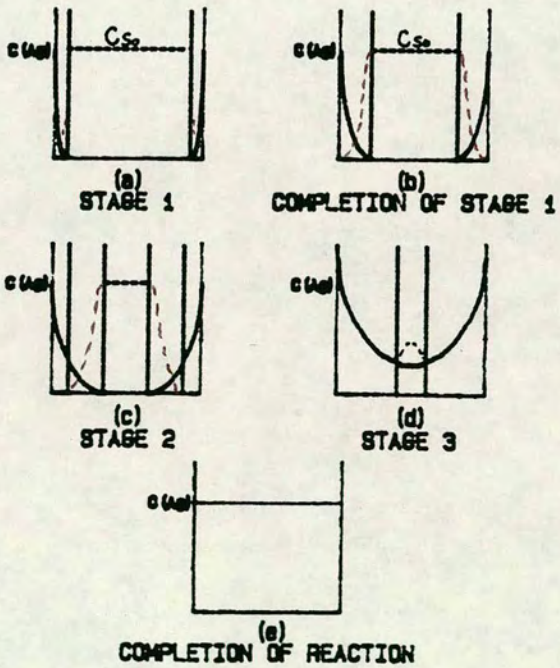

Figure 2.9: Concentration profiles corresponding to the respective stages of the generalised zone model.

which show the developing zone structure and the corresponding reactant concentration profiles. During the first stage reaction occurs at the external surface of the pellet, progressing inward with time and thereby creating a reacting zone of increasing width (Figure 2.8(a)). This zone reaches a maximum width when the solid reactant at the pellet external surface becomes exhausted (Figures 2.8(b) and 2.9(b)). All three zones exist during stage 2 which corresponds to the detachment from the external surface and inward migration of the reacting zone. Stage 3 begins when the core of unreacted solid disappears and further reaction causes shrinkage of the reacting zone until the reaction is complete (Figure 2.9(d) & (e)). The model equations have been formulated on the basis of an intrinsic rate which is first order in the concentration of the gaseous reactant and independent of the concentration of the solid reactant. As the latter assumption is widely made in gas-solid model formulation, Mantri et al. carried out a test on the zinc sulphide oxidation system to confirm its validity. The test consisted of comparing the rates of oxidation of two pellets of identical diameter, length and porosity under reaction conditions adjusted to allow observation of the intrinsic chemical rate. The first pellet was made from zinc sulphide powder and the second from a 4:1 mixture of zinc sulphide and zinc oxide powders. At a reaction temperature of 600°C and with an air flowrate sufficient to give negligible film diffusion resistance, the oxidation rates (expressed per unit external surface area) observed for the two pellets were indistinguishable over a period of 80 minutes. The rates were initially constant for about 20 minutes then fell gradually. Mantri et al. concluded that the reaction was indeed zero order with respect to the solid reactant.

The mass balance equations for the model may therefore be written for the three zones as:

Zone 1

$$(D_p/r^2)\ \partial\left[r^2\ \partial c_A/\partial r\right]/\partial r = 0 \qquad r_1 \leqq r \leqq r_0 \qquad (33)$$

Zone 2

$$(D_r/r^2)\ \partial\left[r^2\ \partial c_A/\partial r\right]/\partial r - k_v c_A = 0 \qquad r_2 \leqq r \leqq r_1 \qquad (34)$$

$$\partial c_S/\partial t - k_v c_A = 0 \qquad r_2 \leqq r \leqq r_1 \qquad (35)$$

Zone 3

$$c_A = 0 \qquad 0 \leqq r \leqq r_2 \qquad (36)$$

The following boundary and initial conditions apply:

$$D_p(\partial c_A/\partial r) = k_g(c_{Ag}-c_A) \qquad \text{at } r=r_0 \qquad (37)$$

$$c_A = c_{A1} \qquad \text{at } r=r_1 \qquad (38)$$

$$D_p(\partial c_A/\partial r) = D_r(\partial c_A/\partial r) \qquad \text{at } r=r_1 \qquad (39)$$

$$c_S = c_{S0} \qquad \text{at } t=0 \qquad (40)$$

where C_A and C_S are the concentrations of gaseous and solid reactant respectively at a position r in the particle; C_{S0} is the initial solid reactant concentration and C_{Ag} the gaseous reactant concentration in the bulk fluid; D_p and D_r are the effective diffusion coefficients in the product and reacting layers respectively; k_v is the fluid volume-based kinetic rate constant and k_g is the gas film mass transfer coefficient. The radii r_0, r_1 and r_2 are indicated in Figure 2.8(c). Solution of these equations yields expressions for concentration profiles during each of the reaction stages.[59] Mantri et al. observe that for certain values of the physical properties of the system, the reacting zone would extend from the external surface, or from the product interface, into the pellet centre. In such a case, stage 2 of the model ceases to exist and the generalised

zone model corresponds to that of Ishida and Wen.[58]

2.3.3 Structural models

Structural models are of two basic conceptual types - those based on assumptions about the solid structure of a pellet and those based on assumptions about its pore structure. The former group are called grain models or particle-pellet models because they envisage the particle as an agglomeration of individual grains or particles (Figure 2.10(a)). Such a description would appear to be a plausible basis for a model as pellets and granules are frequently made by the compaction of powders. Szekely et al.[60] have formulated a generalised grain model for isothermal systems of porous solids with simultaneous pore diffusion and first order chemical reaction. The individual grains are assumed to be nonporous and to react therefore according to the SIM. It is further assumed that there is no change with reaction in grain or pellet size, and that the diffusional resistance of the product layer surrounding a grain may be considered negligible due to the diffusional path length through the product layer being very much shorter than that through the pellet. For the general gas-solid reaction,

$$A_{(g)} + bB_{(s)} \rightleftharpoons cC_{(g)} + dD_{(s)} \qquad (41)$$

where the coefficients b, c and d give the stoichiometry of the reaction, the model equations may be written as follows. Mass balances on the gaseous reactant and product yield,

$$D_e \nabla^2 c_A - \upsilon_A = 0 \qquad (42)$$

$$D_e \nabla^2 c_C + \upsilon_A = 0 \qquad (43)$$

where υ_A is the local rate of consumption of the gaseous reactant A. For a reaction which is first order in the gaseous reactant, the local rate of reaction at the

Figure 2.10: Schematic representation of the grain model of Szekely et al.

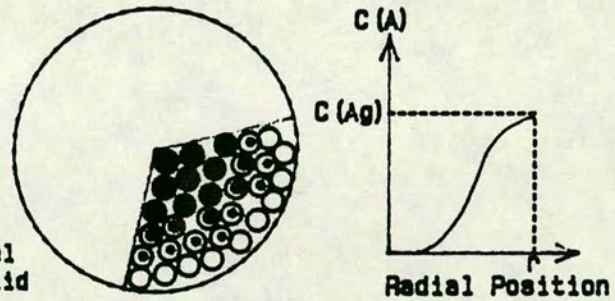

(a)
Representation of the grain model for the reaction of a porous solid wih a gas.

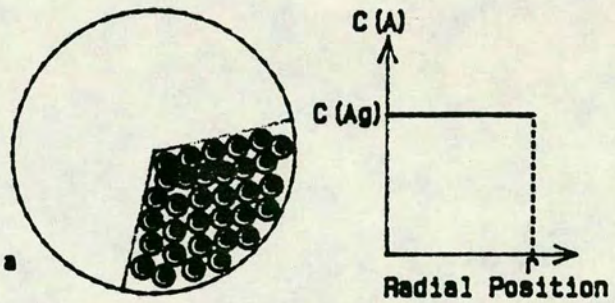

(b)
The grain model for the case of a solid undergoing reaction under conditions of chemical control.

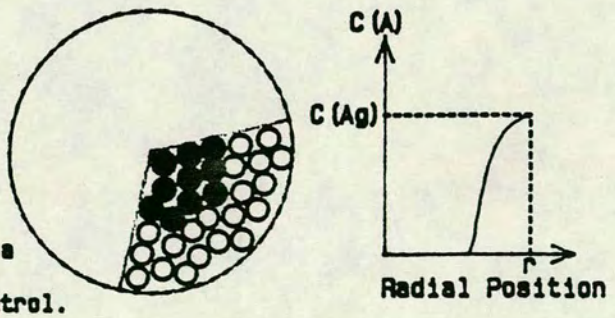

(c)
The grain model for the case of a solid undergoing reaction under conditions of pore diffusion control.

solid surface is given by

$$-\rho_s(\partial r_c/\partial t) = bk_v(c_A - c_C/K_E) \quad (44)$$

where ρ_s is the molar density of the solid reactant, r_c is the radius of the retreating reaction front in the spherical grain, k_v is the reaction rate constant and K_E the equilibrium constant. The local reaction rate, υ_A, may be expressed as

$$\upsilon_A = (1-\varepsilon)k_v(A_g/V_g)(c_A - c_C/K_E) \quad (45)$$

The initial and boundary conditions are:

$$r_c = r_0 \qquad \text{at } t=0 \quad (46)$$

where r_0 is the grain radius,

$$c_A = c_{As} \qquad \text{at } R=R_0,\ t\geq 0 \quad (47)$$

$$c_C = c_{Cs} \qquad \text{at } R=R_0,\ t\geq 0 \quad (48)$$

where c_{As} and c_{Cs} are the concentrations of A and C respectively at the pellet external surface and R_0 is the pellet radius. Finally,

$$\partial c_C/\partial R = \partial c_A/\partial R = 0 \qquad \text{at } R=0,\ t\geq 0 \quad (49)$$

Szekely et al. observe that if the product forms a nonporous layer around the reacting grain then reaction can only proceed via transport of the solid reactant by means of solid state diffusion. This is generally a slow process with a high activation energy. It has, however, been proposed as the rate controlling process in the partial reduction of wustite, a non-stoichiometric iron oxide. If the product layer is porous, however, then under conditions of chemical control, where the gaseous reactant concentration is uniform throughout the pellet (Figure 2.10(b)), the time required to achieve a particular conversion is proportional to the grain volume. Under conditions where pore diffusion is rate-controlling (Figure 2.10(c)) the time required for a given conversion is

proportional to the square of the characteristic pellet dimension, ie. the radius for a spherical pellet.[60]

Ramachandran and Smith[59] modified the grain model in order to account for porosity changes and the effects of sintering during the course of a reaction. For a reaction with the stoichiometry of equation (32), the ratio of molar volumes, γ, which determines whether the particle porosity increases or decreases with reaction, is given by

$$\gamma = \rho_r M_p / [\rho_p(1-\varepsilon_p)M_r] \qquad (50)$$

where ρ_r and ρ_p are the densities of the solid reactant and the solid product respectively; M_r and M_p are the solid reactant and product molecular weights and ε_p is the porosity of the product layer. If $\gamma=1$ no change occurs in the grain radius with reaction, however, if $\gamma>1$ or $\gamma<1$ the grain swells or shrinks respectively. Clearly such changes affect the macroporosity of the pellet and are likely to cause a change in the controlling regime with progress of the reaction. Sintering, which is thought to lead to a decrease in porosity due to the progressive removal of pore interconnections, thereby also increases the tortuosity factor of the pore network and can cause drastic reductions in the effective diffusivity. Sintering is likely, however, to be important only at reaction temperatures above the Tammann temperature which is approximately half the solid melting point.[59] For an isothermal reaction where sintering is not important, the model predicts that for $\gamma<1$ a given conversion will be achieved more rapidly than were there no change in molar volume ($\gamma=1$). Conversely, any given conversion is achieved more slowly if $\gamma>1$ and, depending on the initial porosity, pore closure may occur resulting in incomplete conversion.

Georgakis et al.[61] have also considered the effect of changes in the grain size. Where the molar volume increases with reaction ($\gamma>1$) they note that if the initial porosity is less than $(\gamma-1)/\gamma$ then pore closure will occur leading to incomplete conversion. For such a case, the final conversion will depend on the relative rates of pore diffusion and chemical reaction, that is upon the value of the Thiele modulus, ϕ, which is defined for a spherical particle of radius R_0 as

$$\phi = R_0/3 \sqrt{(k_v/D_e)} \qquad (51)$$

Thus for large values of ϕ, corresponding to diffusion-limited reaction, the conversion at the point of pore closure will be much less than for small values of ϕ, because in the former case, when pore closure occurs at the external surface of the pellet the core of the pellet will be virtually unreacted. Georgakis et al. have compared the conversion-time behaviour predicted by their model with experimental data[62] on the absorption of sulphur dioxide by limestone ($CaCO_3$).[5] Here, the reacting solid exhibits a substantial increase in molar volume ($\gamma\simeq3$). The model was found to provide a reasonable fit to the data.

Garza-garza and Dudukovic[64] have used the same model and considered the effects of the various model parameters on the reaction rate using the structural

---

[5]This data was obtained by Hartman and Coughlin using a differential reactor[63] and analysing gas samples for SO_2 by absorption in dilute H_2O_2 solution followed by titration of the sulphuric acid thus formed with 0.1N KOH solution. The sulphided solid samples were analysed for sulphate by dissolving the sample in distilled water containing an excess of cation-exchange resin. The sulphate was then determined by titration of the filtrate with 0.05N $Ba(ClO_4)_2$ solution in 80% isopropyl alcohol using a mixture of thorin and methylene blue as an indicator.

parameter ω, which is defined as the net increase in solid volume at complete conversion per unit initial volume of voids,

$$\omega = (\gamma-1)[(1-\varepsilon_0)/\varepsilon_0] \qquad (52)$$

They considered two cases: the first where pore blockage at the pellet surface does not occur because of grain shrinkage or because although $\gamma>1$, the initial porosity is sufficient to prevent pore closure ie. $\omega<1$; the second case corresponds to pore closure at the surface which occurs if $\omega\geq1$. Garza-garza and Dudukovic observe that pore closure will not cause the reaction to stop because the effective diffusivity is not zero but equal to the diffusivity in the product layer. They propose that the reaction may be modelled according to a modified shrinking unreacted core model with further reaction resulting in an increase in the pellet size.

Rajeswara Rao et al.[65] have used a non-isothermal grain model to describe their experimental results on the decomposition of calcium carbonate. Although it is not concerned with a reaction between a gaseous and a solid reactant, this work is of interest in demonstrating the success of the grain model in predicting the experimental results. The experimental system consisted of a pellet suspended in a thermobalance. Pairs of runs were performed under identical conditions in order to measure both the weight loss and the temperature change with time. The model parameters were determined by physical measurement: the porosity from the pellet dimensions and true density of the solids, grain size from electron microscopy and diffusivities from diffusion cell measurements on the solid reactant and on partially and completely reacted solid. The effective thermal conductivity and its variation with solid conversion was calculated.[65] Thus only the Arrhenius' parameters of the rate constant and the reaction order

with respect to carbon dioxide partial pressure were parameters to be fitted using the experimental rate data. The model satisfactorily predicted the conversion-time and temperature-time behaviour of the pellet.

In the selection of a model for a gas-solid non-catalytic reaction it is suggested that physical evidence of the solid structure - whether it has a distinct crystalline structure or has an amorphous appearance - should be the criterion for adopting either a grain model or a model based on assumptions about the pore structure.[64]

Ramachandran and Smith[66] developed a model for gas-solid non-catalytic reactions which involves structural changes based on the analysis of a single cylindrical pore (Figure 2.11). The solid pellet is conceptualised as consisting of a number of such cylindrical pores of finite length. A pore is of length l and of initial radius r and has associated with it an annulus of the solid reactant having an outer radius λ. The solid reactant surrounding the pore is assumed to be nonporous so that the pore space of the whole pellet consists only of macropores. Only axial variation of the concentration of the reactant gas A in the pore is considered and the model accounts only for radial diffusion within the product layer. As in the previously described models, isothermality is assumed, the external mass transfer resistance is assumed to be negligible, and the chemical reaction is considered to be irreversible and first order with respect to the gaseous reactant concentration and the interfacial surface of the solid reactant B. The model equations are thus as follows:

$$D_e\, \partial[(r-\delta_1)^2 \partial c/\partial x]/\partial x =$$

$$2c\left[[k_v(r+\delta_2)]^{-1} + (1/D_p)\ln[(r+\delta_2)/(r-\delta_1)]\right]^{-1} \qquad (53)$$

Figure 2.11: The single pore model of Ramachandran and Smith.

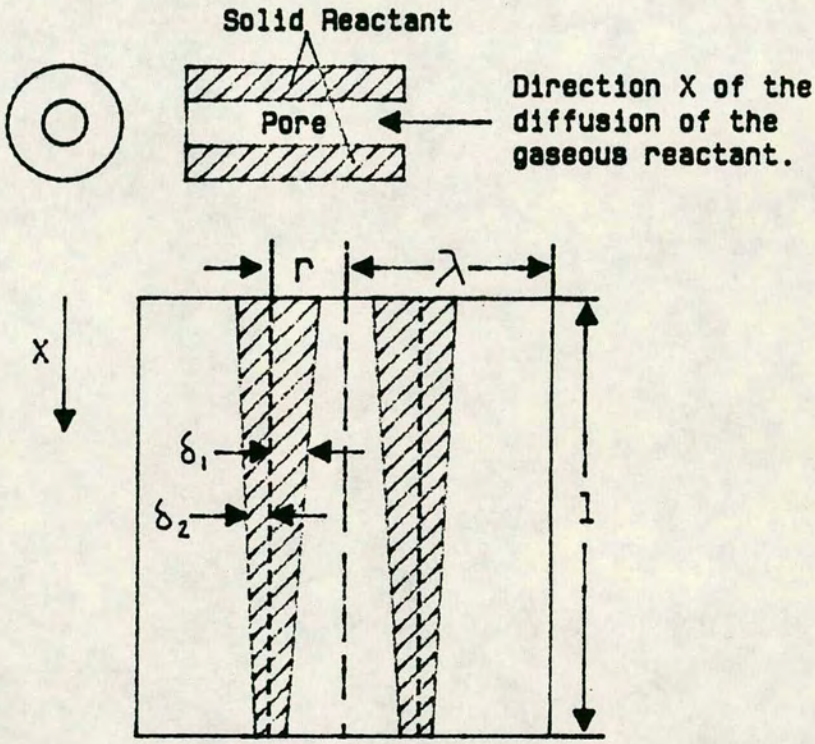

Equation (53) is a mass balance on the gaseous reactant A, where the LHS of the equation represents the net diffusive flux of the gaseous reactant into the pore and the diffusivity, D_e, includes contributions from both bulk and Knudsen diffusion. The RHS of the equation is an expression for the reaction rate per unit pore length and combines in series the product layer diffusional resistance (diffusivity D_p) and the chemical resistance.

Equation (54) is obtained by equating the rate of consumption of the gaseous reactant with the rate of formation of the solid product,

$$\partial\delta/\partial t = \left[M_p c/[\rho_p(1-\varepsilon_p)(r+\delta_2)]\right] \div \left[[k_v(r+\delta_2)]^{-1} + (1/D_p)\ln[(r+\delta_2)/(r-\delta_1)]\right] \quad (54)$$

and δ is the total thickness of the product layer.

$$\delta = \delta_1 + \delta_2 \quad (55)$$

The criterion of conservation of mass is given by equation (56) where γ is given by equation (50)

$$(r-\delta_1)^2 = (1-\gamma)(r+\delta_2)^2 + \gamma r^2 \quad (56)$$

The boundary and initial conditions are:

$$c = c_0 \quad \text{at } x=0 \quad (57)$$

$$\partial c/\partial x = 0 \quad \text{at } x=1 \quad (58)$$

$$\delta_1 = \delta_2 = 0 \quad \text{at } t=0 \quad (59)$$

The local conversion, $\eta(x)$, is given by

$$\eta(x) = 1 - [\lambda^2-(r+\delta_2)^2]/[\lambda^2-r^2] \quad (60)$$

and the average conversion for the pore is found by integration of equation (60) over the pore length. Equations are given for the determination of the model parameters (pore radius, r, pore length, l, the outer radius, λ, of the associated solid concentric with the

pore, the effective diffusivity, D_p, in the product layer, and the surface reaction rate constant, k_v) from measurements of pellet density, specific surface area, initial porosity and the porosity of the completely reacted solid and from initial rate data. The determination of the parameters depends upon the random pore model approximation[67] and upon calculation of the effectiveness factor, the latter being required in order to obtain the surface reaction rate constant from initial rate data.

Bhatia and Perlmutter have described a random pore model which accounts for the intersections of randomly orientated pores and for the continuous development of the reaction surface during the course of reaction.[68,69] The model equations are developed in terms of the pore size distribution, f(r), where f(r)dr is the total length of cylindrical pores per unit pellet volume having radii between r and (r+dr). From the pore size distribution, expressions are readily obtained for the total pore length, surface area and volume of the pore system. The model equations are written in terms of the structure parameter, ψ, and the particle size parameter, σ, defined as:

$$\psi = 4\pi L_0(1-\varepsilon_0)/S_0^2 \qquad (61)$$

$$\sigma = R_0 S_0/(1-\varepsilon_0) \qquad (62)$$

where L_0 and S_0 are the initial total length and surface area respectively of the intersecting pore system; ε_0 is the initial porosity and R_0 the initial particle radius. The physical significance of the parameters ψ and σ is apparent from the time, τ_x, required to achieve a given solid conversion, x, as a function of these parameters. In general τ_x increases with σ but becomes independent of σ at high values of the parameter where the extent of the pellet external surface becomes negligible in comparison with the internal surface area. At low values

of σ, corresponding to very small pellets, τ_x is independent of the internal structure, that is of ψ. Whereas at high σ, τ_x decreases substantially with increasing ψ. Bhatia and Perlmutter[70] have shown that ψ reflects the dispersion of the pore size distribution and that the reaction rate increases with increasing ψ, indicating the intrinsically lower reactivity of solids possessing a very narrow pore size distribution. For a bimodal pore size distribution they suggest that an optimal distribution of porosity between the macropores and micropores exists for maximal solid reactivity, and that this has implications for the preparation of pellets from microporous particles.

In the regime of kinetic control of the reaction, it is observed that for large σ, the changing surface area of the solid reactant shows a maximum with conversion for large ψ. This maximum is also observed in the reaction rate and is interpreted as arising from the opposing effects of the growth in the reaction surface area around individual pores and the loss of surface area through increasing intersections of the pore reaction surfaces. Figure 2.12 indicates the development of the reaction surface with time.

Bhatia and Perlmutter[69] have also considered the effects on the overall reaction rate and on the conversion of the three diffusional resistances: mass transfer in the gas film, intrapellet diffusion and product layer diffusion. Where there is no change in the molar volume with reaction ($\gamma=1$) the effect of increasing any of these resistances is of course to reduce the overall rate. However, if $\gamma>1$ and $\omega\geq 1$ (equation(52)) then for any given value of the Thiele modulus ϕ (equation(51)), increasing the product layer diffusional resistance although decreasing the overall rate has the effect of increasing the maximal

Figure 2.12: Development of the reaction surface in the model of Bhatia and Perlmutter.

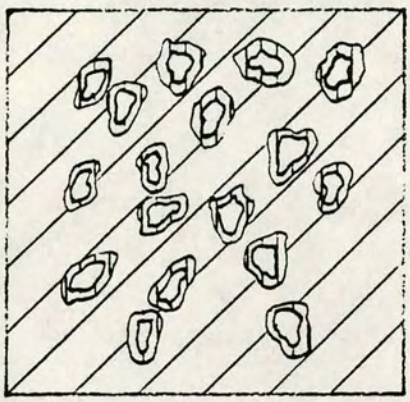

(a) Early stage of reaction: Product layer surrounds each pore.

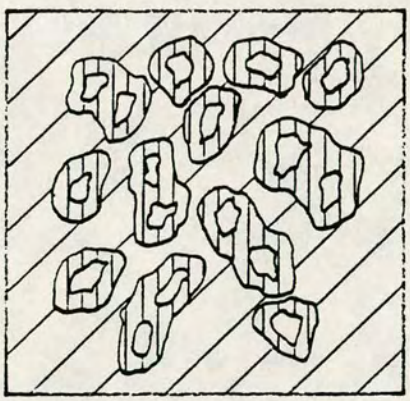

(b) Intermediate stage of reaction: Overlapping of reaction surfaces from adjacent pores.

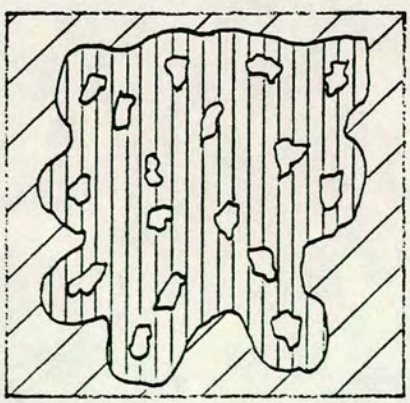

(c) Late stage of reaction: Fully developed product layer and single growing reaction surface.

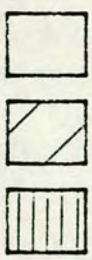

conversion. This occurs because the increasing importance of the product layer diffusivity modifies the effect of the intrapellet diffusivity resulting in a flatter concentration profile of the reactant gas through the pellet, thereby increasing the overall conversion achieved when pore closure at the external surface occurs.

In relation to experimental data on the absorption of sulphur dioxide by lime, Bhatia and Perlmutter[70] have investigated the effects of the reactant's initial surface area and porosity on the maximal conversion achieved. They observed that the maximal conversion rises sharply with increasing initial porosity for a constant initial surface area, but decreases significantly with increasing initial surface area for a constant initial porosity. These observations were interpreted as indicating the desirability in delaying pore plugging of a predominance of large pores, associated with high porosity, over a larger number of smaller pores, associated with high specific surface areas. The extent of surface area clearly also affects the rate: while an increasing surface area increases pore diffusional resistance, it decreases the resistance associated with the product layer diffusion. Thus a larger surface area will give initially a higher reaction rate. The effect of an increase in the pore structure parameter, ψ, and thus of an increase in the dispersion of the pore size distribution is a marginal decrease in the overall conversion. A balance thus exists between the effect of increasing ψ in increasing the reaction rate and its simultaneous effect in decreasing the overall conversion of the solid reactant.

In investigating the ability of the random pore model to describe experimental data for the sulphation of lime, all but one of the model parameters were determined from

independent physical measurements leaving only the Biot number, β, to be used as a fitting parameter. The Biot number is given by

$$\beta = 2k_v\rho(1-\varepsilon_0)/(MD_pS_0) \qquad (63)$$

where k_v is the kinetic rate constant, ρ is the mass of the solid reactant per unit volume of the solid phase, M is the molecular weight of the solid reactant and D_p is the effective diffusivity of the gaseous reactant in the product layer. The best fit value of β allowed the activation energy for the product layer diffusion mechanism to be estimated as 120 $kJmol^{-1}$. This very high value was taken as evidence that the process involved was in fact solid state diffusion through a nonporous layer of calcium sulphate. Bhatia and Perlmutter note that the product layer diffusive mechanism could, however, involve diffusion of the gaseous species through sub-microscopic cracks, the creation of which is activated.

Where the shape of the grains in the grain model is considered as one of the model parameters, rather than being implicitly assumed, the grain and random pore models are seen to rely on the same number of system parameters.[70] Reasonable correspondance between the models has been found for spherical grains and $\psi=1$ in the random pore model. The grain shape is expressed in terms of the grain shape factor, m, which is defined as

$$m = A_g r_g/V_g \qquad (64)$$

where A_g and V_g are the surface area and volume of the grain and r_g is its characteristic dimension, being the radius for a spherical or cylindrical grain and the thickness of a flat plate-like grain, these being the three shapes commonly assumed. The grains which make up porous pellets may frequently be of highly irregular shape. In such cases, determination of a grain shape

factor is very difficult and use of the random pore model to predict the solid reactivity may be more appropriate with interpretation of the structure parameter, ψ, in terms of the pore structure rather than the solid structure.

2.4 Studies of the reaction between hydrogen sulphide and zinc oxide

2.4.1 Structural changes due to reaction

Zinc sulphide exists in two forms: Wurtzite (α-ZnS) and Sphalerite (β-ZnS). Sphalerite is the chief ore of zinc, and the stable form of the sulphide below 1020°C, at which temperature it inverts to Wurtzite.[71] Also known as zinc blende, it has the cubic face-centred lattice structure of diamond (Figure 2.13) with lattice constant a=5.409Å. Wurtzite, however, has a hexagonal structure similar to that of zinc oxide (Figure 2.1) with lattice constants, a=3.811Å and c=6.234Å. The larger cell dimensions (compare section 2.1.1) result from the larger size of the anion. In view of the intermediate ionicities of both zinc oxide and zinc sulphide,[6,72] it is reasonable to consider both ionic and covalent radii when comparing the size of the sulphur and oxygen 'anions'. In either case, the radius of the sulphur anion is greater than that of the oxygen, being 1.84Å compared to 1.40Å for the ionic radii, and 1.04Å compared to 0.66Å for the covalent radii.[4] Analysis of samples of zinc oxide which have been sulphided for several hours has indicated the presence of α-ZnS only,[73] however, both Wurtzite and Sphalerite have been found in sulphided zinc oxide discharged from commercial plant, and it has been suggested that Wurtzite is formed first but then converts slowly to Sphalerite.[74]

It is evident that sulphiding of zinc oxide must cause

Figure 2.13: The structure of zinc blende.

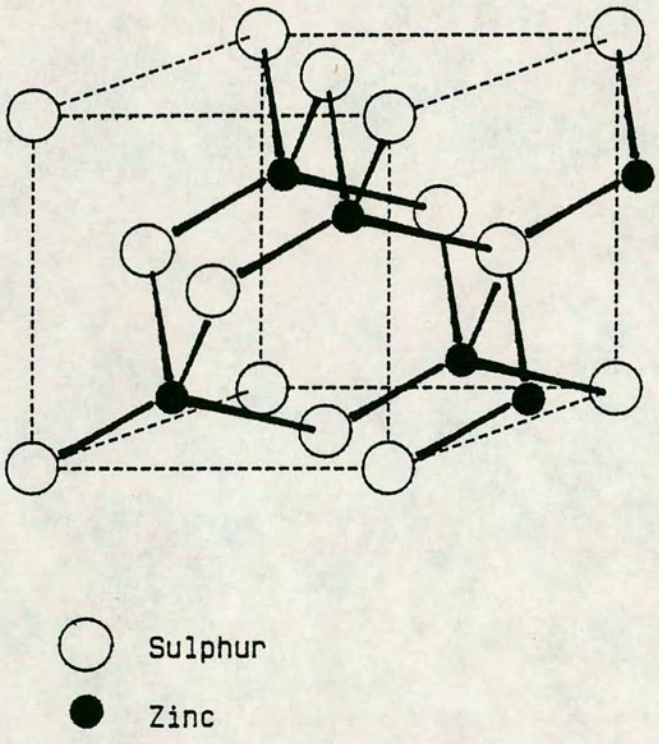

distortion of the lattice structure in order to accommodate the larger anion. Moreover, the volumetric increase of about 37% which is observed on conversion of zinc oxide crystallites to zinc sulphide with no corresponding increase in the particle volume[75] means that there is a reduction in porosity of the sulphided regions of the particle. Clearly, this indicates that the rates of pore diffusion of hydrogen sulphide and water are likely to change with progress of the reaction.

2.4.2 Reaction thermodynamics

The reaction between hydrogen sulphide and zinc oxide to form Sphalerite (the more stable form of zinc sulphide at the temperatures of interest),

$$H_2S_{(g)} + ZnO_{(s)} \rightleftharpoons ZnS_{(s)} + H_2O_{(g)} \qquad (65)$$

is exothermic at 25°C, with a heat of reaction, $\Delta H = -76.7 kJmol^{-1}$. The standard free energy change of the reaction, $\Delta G_{298}°$, is negative ($\Delta G_{298}° = -75.8 kJmol^{-1}$) so that the formation of zinc sulphide is strongly favoured thermodynamically. The equilibrium pressure of hydrogen sulphide over zinc oxide at various temperatures for particular pressures of water vapour is very important, as this determines the level to which the hydrogen sulphide partial pressure of a gas may be reduced in a given set of circumstances. As zinc oxide is frequently used upstream of catalytic beds which may rapidly be poisoned by small quantities of hydrogen sulphide, it is important that the equilibrium pressure of hydrogen sulphide under the operating conditions should be low. The dependence of the equilibrium partial pressure of hydrogen sulphide over zinc oxide on water partial pressure and temperature is indicated in Table 2.2.

Table 2.2: Variation of the concentration of H_2S (ppm) in equilibrium with zinc oxide as a function of temperature and the water vapour content of the gas

	Water content of gas/%			
Temperature °C	0.1	0.5	1	5
25	5.8×10^{-11}	2.9×10^{-10}	5.8×10^{-10}	2.9×10^{-9}
100	2.8×10^{-8}	1.4×10^{-7}	2.8×10^{-7}	1.4×10^{-6}
200	4.9×10^{-6}	2.5×10^{-5}	4.9×10^{-5}	2.5×10^{-4}
300	1.4×10^{-4}	6.9×10^{-4}	1.4×10^{-3}	6.9×10^{-3}
400	1.4×10^{-3}	7.1×10^{-3}	1.4×10^{-2}	7.1×10^{-2}

2.4.3 Investigations of the hydrogen sulphide/zinc oxide reaction

Most of the experiments performed to investigate the reaction between hydrogen sulphide and zinc oxide have been breakthrough tests. In such experiments, a packed bed of granules or pellets of zinc oxide or of a zinc oxide-based absorbent, is exposed to a flow of a hydrogen sulphide-containing gas. The experiment is stopped when 'breakthrough' or 'slippage' occurs, that is, when hydrogen sulphide is detected in the reactor outlet stream at a given concentration. Experiments have also been carried out to determine the sulphur capacity of absorbents, or, using a microbalance reactor, to measure initial rates of reaction,[76] and to study the reaction of a single pellet.[77] The range of experimental conditions studied varies widely, covering a temperature range of about 100-800°C and a hydrogen sulphide content of the feed gas from 10ppm to 100%. Very little information is available on the absorption reaction at ambient temperatures.[74] This section details these various experiments, indicating what conclusions have been drawn about the factors affecting the sulphur absorption capacity and the reaction rate. The following section summarises the observed absorption properties of zinc oxide in relation to other metal oxides.

Furmer et al.[78] found that pellets of an industrial zinc oxide-based absorbent exhibited a range of mechanical strengths which was well described by a Gaussian distribution. Two groups of pellets were therefore prepared on a laboratory press such that their mean mechanical strengths were equal to those of pellets at the two extremes of the distribution. Determinations of total pore volume and of the distribution of pore sizes revealed that pelleting produced a reduction in

pore volume relative to the starting material, and that pellets having a greater mechanical strength had a lower pore volume and a smaller modal pore radius. Thus the two sample groups of pellets had modal pore radii of 250 and 160Å and total pore volumes of 0.203 and 0.140cm^3gm^{-1} respectively corresponding to the lower and upper limits of the mechanical strength of the pellets prepared. Experiments were performed by exposing the pellets to a stream of 10% hydrogen sulphide - the balance being natural gas and nitrogen - or to pure hydrogen sulphide for periods of between 0.5 and 6.5 hours at 350°C. These experiments were not breakthrough tests - the concentration of hyrogen sulphide in the reactor outlet gas being substantial - but rather experiments to determine how the physical properties of the absorbent and the reaction conditions affect the maximum capacity of the absorbent for sulphur uptake.

Hydrogen sulphide gas labelled with the radioactive isotope ^{35}S was used. This allowed the subsequent analysis of the sulphur distribution in the pellets both by electron microprobe and by autoradiography, where an image of the distribution of radioactive material over a pellet section is obtained. This analysis revealed two distinct zones in the pellets - an outer, completely sulphided region and a central unreacted core, with the sulphur content falling from its level in the sulphided region to zero over a distance equivalent to only 5-8% of the pellet radius. The degree of penetration of the sulphided region into the pellet increased slightly with time. Porosity measurements on the sulphided pellets revealed a loss of pore volume and an increase in the modal pore radius. These data were interpreted as indicating a reaction rate limited by the rate of diffusion of hydrogen sulphide through the zinc sulphide.

Under these experimental conditions, the absorption is evidently well described by the sharp interface model (SIM). Furmer et al.[78] conclude that the reaction is chemically controlled very briefly while the reaction is localised at the external surfaces of the pellets, but that pore diffusion is subsequently the rate determining process. A further observation was made concerning the effect of the pellet porosity on the rate of sulphur uptake. While the pellets with lower porosity exhibited a much lower rate of uptake at 350°C, very little effect of porosity was observed at a reaction temperature of 150°C. This was attributed to the increased influence of the intrinsic reaction rate on the global rate at lower temperatures. At both temperatures, the rate of uptake was greater for the pure hydrogen sulphide feed than for the diluted feed.

Furmer et al.[74] have extended these experiments to investigate the absorption efficiency of a number of industrial and model absorbents, using nitrogen feeds with hydrogen sulphide concentrations down to 4%. These experiments confirmed the importance of the pore volume and pore size distribution in determining the rate of sulphur uptake and indicated that a low pore volume and inappropriate pore size distribution could result in a substantially reduced sulphur capacity. This was explained in terms of pore closure restricting or completely blocking access of hydrogen sulphide to unreacted zinc oxide. The effect of the absorbent's pore volume was found to be more significant at lower feed concentrations of hydrogen sulphide. Finally, the reduction in total sulphur capacity with decreasing reactor temperature was confirmed.

Carnell and Denny[75] performed 'accelerated' breakthrough tests with concentrations of hydrogen sulphide in the feed gas substantially greater than

those encountered in catalyst protection applications - .2% compared with 200ppm or less in commercial applications - in order to compare the effectiveness of several zinc oxide-based absorbents. The tests were carried out at 370°C and a pressure of 30 bar. Analysis of sulphur distribution in the discharged absorbent samples was by electron microprobe and radiography. It was found that the sulphided absorbents exhibited a reduction in both surface area and porosity compared to the unsulphided absorbents. However, redetermination of these properties on particles which had been split in half gave higher values for both, thus confirming that pores in the outer sulphided regions had become blocked preventing access of gas to the cores. Carnell and Denny also selected porosity as a reasonable indicator of likely absorbent performance, concluding that, as the size of zinc oxide crystallites must be inversely proportional to the specific surface area, the lack of correlation between sulphur pick-up and surface area was evidence against lattice diffusion being the rate-determining process.

Gour et al.[22] used five different precipitating agents to prepare zinc oxide samples which were then evaluated as to their potential as absorbents for hydrogen sulphide. A breakthrough test was used for this purpose, with a packed bed of the sample absorbent being exposed at 400°C to a flow of naphtha containing 33.2% hydrogen and 10.5ppm hydrogen sulphide by volume. The extent of sulphiding of the absorbent was calculated from the flowrate of hydrogen sulphide and the time to breakthrough - indicated by lead acetate paper. Measurements of specific surface area, porosity and pore size distribution were made before and after sulphiding, and the non-stoichiometry of the zinc oxide samples was determined. Table 2.3 presents the data of Gour et al. on the pore volume, surface area and excess zinc content

Table 2.3: Physical Properties and Sulphur Absorption Capacities of Various Zinc Oxide Samples – after Gour *et al.* [21]

Sample no.	Precipitating agent	Total pore volume cm^3gm^{-1}	Specific surface area m^2gm^{-1}	Excess zinc ppm	Sulphur absorption capacity %w/w
1	sodium carbonate	0.3844	31.6	5.49	28.53
2	ammonium oxalate	0.5356	24.7	5.83	28.99
3	ammonia solution	0.2566	2.9	4.50	20.61
4	ammonium carbonate	0.6479	21.7	6.58	32.75
5	ammonium bicarbonate	0.5043	11.7	4.62	28.44

of the zinc oxide samples together with the calculated sulphur contents at breakthrough. The sulphur contents are plotted as a function of each of these physical properties in Figures 2.14(a), (b) and (c). Gour et al. conclude that the degree of non-stoichiometry is the most important factor in determining sulphur uptake, and interpret this in terms of the role of interstitial zinc in facilitating the transport of ions in the lattice. They further propose that a reducing environment is likely to be favourable for sulphur absorption due to the diffusion of hydrogen into the zinc oxide lattice leading to reduction and the creation of further zinc interstitials and oxygen vacancies. It is, however, difficult to place any unambiguous interpretation on the data of Gour et al. because of the simultaneous changes in several physical properties between samples prepared using different precipitating agents. Moreover, no mention is made of the degree of contamination of the various samples by cations from the precipitation process, nor of the error associated with any of the measurements of the physical properties or with the calculated sulphur content of the sulphided samples. This last point is of interest because of the apparent almost complete conversion (>99%) of sample 4 (Table 2.3) which is suggestive of a very steep absorption front, and because of the very similar absorption performances observed for samples 1, 2 and 5.

Westmoreland et al.[76] studied the initial rate of reaction of hydrogen sulphide with zinc oxide in a thermobalance reactor between 300 and 800°C in order to exclude pore and lattice diffusion effects and to measure the intrinsic chemical rate. Although the assumption is not explicitly stated, it seems probable that they assumed negligible adsorption of water on the solid surfaces at these temperatures, thus attributing any weight gain solely to the sulphiding of the zinc

Figure 2.14: Correlation for variously prepared zinc oxide absorbents of sulphur pick-up with physical properties (after Gour et al.)

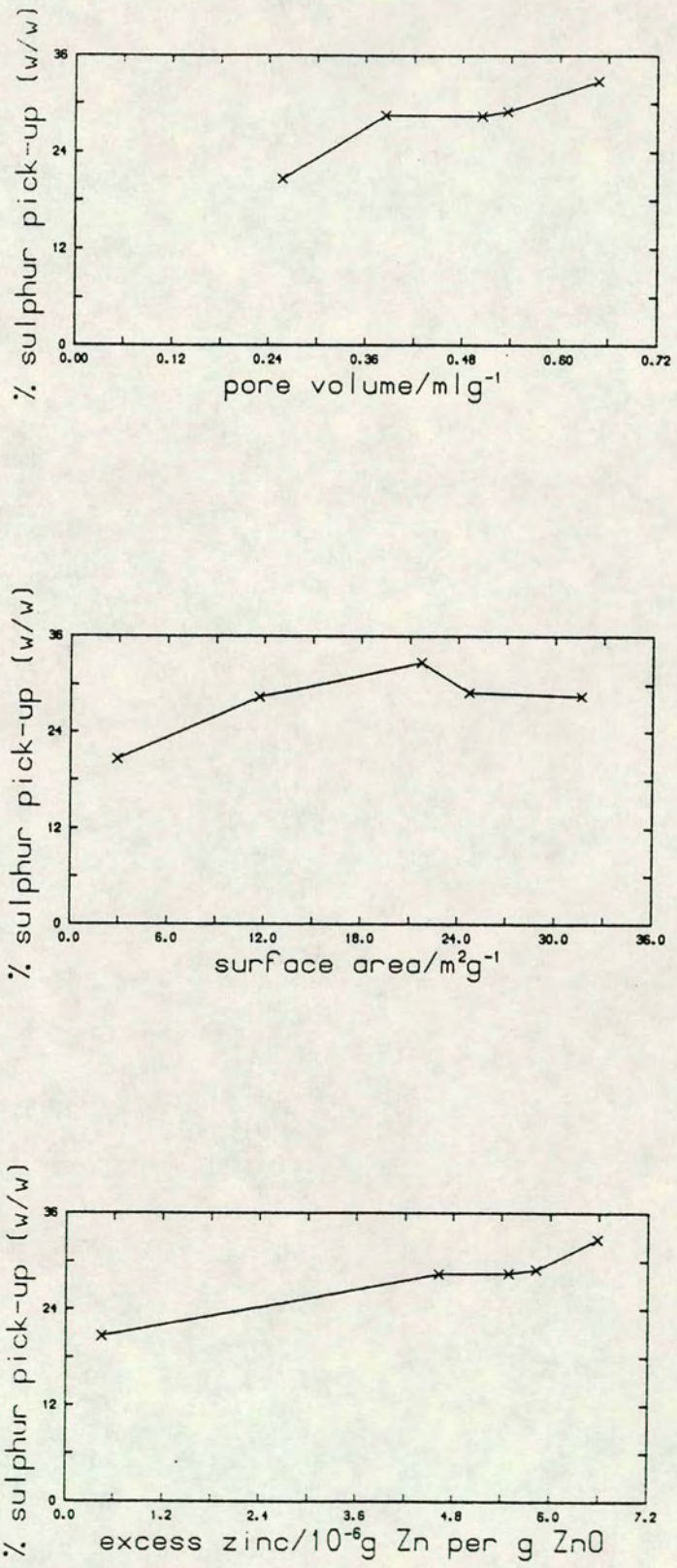

oxide sample. The experiments were performed at ambient pressure and with a hydrogen sulphide content in the feed of 1.9-7.0% by volume. Hydrogen was added to the feed in order to prevent hydrogen sulphide decomposition at high temperatures. Operation within a regime of chemical control was ensured by progressive reduction of the ratio of the absorbent sample size to flowrate until the measured rate became constant ie. independent of the value of the ratio. The initial reaction rate was found to be first order in the concentration of hydrogen sulphide, and the Arrhenius parameters of the rate constant were determined from its temperature dependence.

Single pellet reaction studies have been performed by Gibson and Harrison[77] and analysed in terms of the grain model for gas-solid noncatalytic reactions. The reaction was studied between 375 and 800°C in a microbalance reactor and the sulphur distribution in the pellet analysed by electron microprobe. All model parameters except the grain diffusivity were either measured directly or estimated from literature correlations. The choice of a high value for the grain diffusion coefficient such that grain diffusion resistance was negligible gave good agreement between the model and the experimental data in the temperature range 600-700°C. Here, microprobe analyses revealed distinct zones of oxide and sulphide, the latter forming a shell around the core of unreacted zinc oxide. This was taken as evidence for pore diffusional control of the rate in this temperature range. At higher temperatures a vapour phase reaction was observed, while at lower temperatures, 375-500°C, the observed saturation of the absorbent at sulphur levels less than the stoichiometric, also noted by Furmer et al.,[73,76] and the poorer fit of the grain model were interpreted as indicating a poor estimate in the model of a highly

temperature dependent parameter. With progress of the reaction, deviation of the experimental data from the behaviour predicted by the model increased. The deviation was therefore attributed to the grain diffusion term in the model, as grain diffusion resistance should become increasingly important with reaction progress due to the increased length of the diffusion path. Gibson and Harrison also noted that deviations from experimental results were likely to arise due to the simplistic assumption made in the basic grain model of constant physical properties. Clearly changes in the pore structure of the solid as a result of sulphiding do occur.

Except where initial rate studies were performed to measure the intrinsic rate of reaction of hydrogen sulphide with zinc oxide,[76] all of the reaction studies have been controlled by diffusional processes. At higher reaction temperatures pore diffusion is most likely to be rate-limiting as indicated by the analyses of sulphur distribution in sulphided absorbent pellets. Structural changes as a result of sulphur absorption, indicated by reduced porosity and specific surface area, have been widely observed. Solid state diffusion has also been proposed as the rate-determining step under certain experimental conditions.[22,75]

2.4.4 Comparison of the effectiveness of zinc oxide with other metal oxides for hydrogen sulphide absorption

Westmoreland and Harrison[79] have performed a thermodynamic analysis of the oxides of 28 elements- selected by means of preliminary screening of the Periodic Table - to evaluate their potential for high temperature desulphurisation of gases rich in carbon monoxide, hydrogen and nitrogen but containing small quantities of water vapour, carbon dioxide and hydrogen

sulphide. Their criteria for candidate metal oxides were expressed in terms of thermodynamically achievable fractional conversion and solid stability. On this basis they selected iron, zinc, molybdenum, manganese, vanadium, calcium, strontium, barium, cobalt, copper and tungsten as showing thermodynamic feasibility for the duty. These metal oxides show potential in different temperature ranges with vanadium, zinc, cobalt, molybdenum and copper looking most attractive in terms of equilibrium conversion at low temperatures.

Experimental comparisons of the sulphur capacities and rates of hydrogen sulphide uptake of a number of metal oxides have been made in the temperature range 350-800°C. Westmoreland et al.,[76] by means of initial rate studies, found the intrinsic rate of absorption to be first order in hydrogen sulphide for manganese(II) oxide, zinc oxide, calcium oxide and di-vanadium trioxide. However, the magnitudes of the rates varied significantly, decreasing in the order:

$$MnO \gg CaO \simeq ZnO \gg V_2O_3 \qquad (66)$$

Jalan[80] compared both the absorption and regeneration potentials of a number of absorbents by performing breakthrough runs at 650°C. The absorbent conversions achieved were uniformly low, which Jalan explained in terms of sintering and pore plugging due to the high reaction temperature and progressive sulphiding. Microprobe analyses showed the metal sulphide to be restricted to a thin outer shell on the absorbent granules. The chemical regenerability of sulphided zinc oxide was found to be good, with the use of a steam/air mixture facilitating regeneration at lower temperatures (650°C), however, the pore structure was found to be badly damaged by the high temperature treatment.

Yumura and Furimsky[81] considered the relative

effectiveness of iron oxide, calcium oxide and zinc oxide in the temperature range 600-800°C for the removal of hydrogen sulphide by absorption and decomposition. Iron oxide was shown to have the highest sulphur capacity per gram absorbent, however, zinc oxide showed the highest sulphur capacity per unit exposed surface area of the absorbent. The catalytic effects of calcium oxide and zinc sulphide for the decomposition reaction of hydrogen sulphide were noted.

Clearly the choice of a particular metal oxide for absorption of hydrogen sulphide is likely to depend upon a number of factors, and which of these is most important will depend on the application. Thus, Carnell[74] notes that although iron oxide is a relatively low cost absorbent, its equilibrium position with respect to hydrogen sulphide removal is significantly less attractive than that of zinc oxide. Iron sulphide is, moreover, pyrophoric.

REFERENCES

[1] West A.R.
"Solid state chemistry and its applications"
John Wiley & Sons, London (1984)

[2] Mark P., Chang S.C., Creighton W.R., Lee B.W.
Crit. Rev. Solid State Sci. 5(2), 189- (1975)
(cited in reference [28])

[3] Sneed M.C., Brasted R.C. (eds)
"Comprehensive Inorganic Chemistry", Vol.4
D. Van Nostrand Co., Inc., New Jersey (1955)

[4] Cotton F.A., Wilkinson G.
"Advanced Inorganic Chemistry"
Wiley-Interscience, New York (1988)

[5] Schmalzried H.
"Solid state reactions"
Academic Press, Inc., New York and London (1974)

[6] Neumann G.
"Non-stoichiometry and defect structure"
Curr. Top. Mater. Sci. 7, 153-168 (1981)

[7] Neumann G.
"The quantitative determination of excess zinc"
Curr. Top. Mater. Sci. 7, 199-211 (1981)

[8] Mohanty G.P., Azaroff L.V.
"Electron density distributions in ZnO crystals"
J. Chem. Phys. 35, 1268-1270 (1961)
(cited in reference [5])

[9] Cimino A., Mazzone G., Porta P.
"Lattice parameter study of defective zinc oxide.
I Zinc excess and distortions in pure ZnO"
Z. Phys. Chem. N.F. 41, 154-172 (1964)
(cited in reference [5])

[10] Hagemark K.I.
"Defect structure of Zn-doped ZnO"
J. Solid State Chem. 16, 293-299 (1976)

[11] Kröger F.A.
"The chemistry of imperfect crystals"
North-Holland, Amsterdam (1974)

[12] Littbarski R.
"Carrier concentration and mobility"
Curr. Top. Mater. Sci. 7, 212-225 (1981)

[13] Moore W.J., Williams E.L.
"Diffusion of zinc and oxygen in zinc oxide"
Disc. Faraday Soc. 28, 86-93 (1959)

[14] Lauder J.J.
J. Phys. Chem. Sol. 15, 324- (1960)
(cited in reference [15])

[15] Mackrodt W.C., Stewart R.F., Campbell J.C., Hillier I.H.
"The calculated defect structure of ZnO"
J. Phys., Colloq. (Orsay, Fr.) C6, 64-67 (1980)

[16] Neumann G.
"Diffusion and transport processes"
Curr. Top. Mater. Sci. 7, 279-303 (1981)

[17] Shaw D., in
"Atomic diffusion in semiconductors", ch.1
ed. Shaw D.
Plenum, New York (1973)

[18] Heiland G., Mollwo E.
Disc. Faraday Soc. 28, 123-125 (1959)

[19] Stevenson D.A., in
"Atomic diffusion in semiconductors", ch.7
ed. Shaw D.
Plenum, New York (1973)

[20] Harrison L.G.
"Influence of dislocations on diffusion kinetics in solids with particular reference to the alkali halides"
Trans. Faraday Soc. 57, 1191-1199 (1961)

[21] Roberts J.P.
Disc. Faraday Soc. 28, 123 (1959)

[22] Gour P.K., Upadhyay S.N., Pande S., Chatterjee R., Bhattacharyya N.B., Sen S.P.
"Effect of precipitating agents on activity and physical parameters of zinc oxide"
Proc. Symp. Sci. Catal. Its Appl. Ind.
Sindri, India (1979)

[23] Plyasova L.M., Yurieva T.M., Solovieva L.P., Ketchik S.V., Khadzhiev D.I., Minyukova T.P.
"Distribution peculiarities of zinc ions in oxides"
React. Kinet. Catal. Lett. 22(3-4), 315-318 (1983)

[24] Khalil A.M., Kolboe S.
"Surface characterisation of some selected zinc oxide samples IV: Zinc oxide prepared by the thermal decomposition of zinc basic carbonate"
Surf. Technol. 18, 249-262 (1983)

[25] Klissurski D., Uzunov I., Kumbilieva K.
"Preparation of highly dispersed zinc oxide by thermal decomposition of basic zinc carbonate"
Thermochim. Acta 93, 485-488 (1985)

[26] Fubini B., Bolis V., Giamello E.
"Description of surface structures by adsorption microcalorimetry"
Thermochim. Acta 85, 23-26 (1985)

[27] Clark A.
"The chemisorptive bond"
Academic Press, London (1974)

[28] Ernst L.
"Intrinsic surface states"
Curr. Top. Mater. Sci. 7, 322-330 (1981)

[29] Heiland G., Luth H., in
"The chemical physics of solid surfaces and heterogeneous catalysis",
Vol. 3(B), ch.4
ed. King D.A., Woodruff D.P.

[30] Bonasewicz P., Littbarski R., Grunze M.
"Adsorption Phenomena"
Curr. Top. Mater. Sci. 7, 371-409 (1981)

[31] Akhter S., Lui K., Kung H.H.
"Comparison of the chemical properties of the zinc-polar, the oxygen-polar, and the nonpolar surfaces of ZnO"
J. Phys. Chem. 89, 1958-1964 (1985)

[32] Saussey J., Lavalley J-C., Bovet C.
"Infrared study of CO_2 adsorption on ZnO"
J. Chem. Soc., Faraday Trans. I 78, 1457-1463 (1982)

[33] Atherton K., Newbold G., Hockey J.A.
"Infra-red spectroscopic studies of zinc oxide surfaces"
Disc. Faraday Soc. 52, 33-43 (1971)

[34] Chadwick D., O'Malley P.J.R.
"Propan-2-ol adsorption and decomposition on zinc oxide promoted by alkali metal"
J. Chem. Soc., Faraday Trans. I 83, 2227-2241 (1987)

[35] Hopkins B.J., Leysen R., Taylor P.A.
"Role of impurities in the stability of zinc oxide surfaces"
Surf. Sci. 48, 486-496 (1975)
(cited in reference [34])

[36] Thiel P.A., Madey T.E.
"The interaction of water with solid surfaces: fundamental aspects"
Surf. Sci. Rep. 7(6-8), 211-385 (1987)

[37] Zwicker G., Jacobi K.
"Site-specific interaction of H_2O with ZnO single-crystal surfaces studied by thermal desorption and UV photoelectron spectroscopy"
Surf. Sci. 131, 179-194 (1983)

[38] Peri J.B.
"A model for the surface of γ-alumina"
J. Phys. Chem. 69(1), 220-230 (1965)

[39] Mattmann G., Oswald H.R., Schweizer F.
"Physicosorption and chemisorption of water on zinc oxide surfaces"
Helvet. Chim. Acta 55(4), 1249-1266 (1972)
(abstract only)

[40] Nagao M., Morimoto T.
"Differential heat of adsorption and entropy of water adsorbed on zinc oxide surface"
J. Phys. Chem. 73(11), 3809-3814 (1969)

[41] Nagao M., Yunoki K., Muraishi H., Morimoto T.
"Differential heat of chemisorption.
1. Chemisorption of water on zinc oxide and titanium oxide"
J. Phys. Chem. 82(9), 1032-1035 (1978)

[42] Nagao M.
"On physisorption of water on zinc oxide surface"
J. Phys. Chem. 75(25), 3822-3827 (1971)

[43] Ross S., Olivier J.P.
"Physical adsorption"
Interscience (1964)

[44] Uematsu K., Ohkuma N., Mizutani N., Kato M.
"Adsorption of water vapour on ZnO: Effects of annealing and grinding"
J. Solid State Chem 25, 205-206 (1978)

[45] Khalil A.M., Kolboe S.
"Surface characterisation of some selected zinc oxide samples I: Analytical reagent (Merck) zinc oxide"
Surf. Technol. 17, 37-47 (1982)

[46] Ohkuma N., Uchida S., Mizutani N., Kato M.
"Changes in the adsorption state of water on the surface of zinc oxide microparticles due to heat treatment"
Nippon Kagaku Kaishi 12, 1736-1741 (1986)
(J. Chem. Soc. Japan)

[47] Morishige K., Kittaka S., Moriyasu T.
"Thermal desorption study of surface hydroxyls on ZnO"
J. C. S. Faraday I 76, 728-745 (1980)

[48] Bhattacharyya D.P., Dey A.K., Mukherjee P.N.
"Water chemisorption and electrical conductivity of zinc oxide"
J. Res. Inst. Catalysis, Hokkaido Univ., 24(3), 149-158 (1976)

[49] Sengupta G., Ahluwalia H.S., Banerjee S., Sen S.P.
"Chemisorption of water vapour on zinc oxide"
J. Colloid Interface Sci. 69(2), 217-224 (1979)

[50] Hotan W., Gopel W., Haul R.
"Interaction of CO_2 and CO with nonpolar zinc oxide surfaces"
Surf. Sci. 83, 162-180 (1979)

[51] Lavalley J-C., Saussey J., Bovet C.
"Infrared spectroscopic study of the CO_2 adsorption effect on the surface acidity of zinc oxide"
J. Molec. Struct. 80, 191-194 (1982)

[52] Bowker M., Houghton H., Waugh K.C., Giddings T., Green M.
"Crystal plane dependence of adsorption and reaction on zinc oxide"
J. Catal. 84, 252-255 (1983)

[53] Bowker M., Houghton H., Waugh K.C.
"Mechanism and kinetics of methanol synthesis on zinc oxide"
J. Chem. Soc., Faraday Trans. I 77, 3023-3036 (1981)

[54] Vinogradov E.A., Grachev V.L., Rzaev D.A.
"Optical properties of zinc sulphide films in the infrared spectral region"
Fiz. Tverd. Tela (Leningrad) 26(8), 2273-2277 (1984) (abstract)

[55] Mantri V.B., Gokarn A.N., Doraiswamy L.K.
"Analysis of gas-solid reactions: Formulation of a general model"
Chem. Eng. Sci. 31, 779-785 (1976)

[56] Bowen J.H., Cheng C.K.
"A diffuse interface model for fluid-solid reaction"
Chem. Eng. Sci. 24, 1829-1831 (1969)

[57] Doraiswamy L.K., Kulkarni B.D., in
"Chemical reaction and reactor engineering"
ed. Carberry J.J., Varma A.
Marcel Dekker, Inc., New York (1987)

[58] Ishida M., Wen C.Y.
"Comparison of kinetic and diffusional models for solid-gas reactions"
AIChE J. 14(2), 311-317 (1968)

[59] Ramachandran P.A., Smith J.M.
"Effect of sintering and porosity changes on rates of gas-solid reactions"
Chem. Eng. J. 14, 137-146 (1977)

[60] Szekely J., Evans J.W., Sohn H.Y.
"Gas-solid reactions"
Academic Press, Inc. (London) Ltd. (1976)

[61] Georgakis C., Chang C.W., Szekely J.
"A changing grain size model for gas-solid reactions"
Chem. Eng. Sci. 34, 1072,1075 (1979)

[62] Hartman M., Coughlin R.W.
"Reaction of sulphur dioxide with limestone and the grain model"
AIChE J. 22(3), 490-498 (1976)

[63] Hartman M., Coughlin R.W.
"Reaction of sulphur dioxide with limestone and the influence of pore structure"
Ind. Eng. Chem. Process Des. Dev. 13(3), 248-253 (1974)

[64] Garza-Garza O., Dudukovic M.P.
"A variable size grain model for gas-solid reactions with structural changes"
Chem. Eng. Sci. 24, 35-45 (1982)

[65] Rajeswara Rao T., Gunn D.J., Bowen J.H.
"Kinetics of calcium carbonate decomposition"
Chem. Eng. Res. Des. 67, 38-47 (1989)

[66] Ramachandran P.A., Smith J.M.
"A single-pore model for gas-solid noncatalytic reactions"
AIChE J. 23(3), 353-361 (1977)

[67] Wakao N., Smith J.M.
"Diffusion in catalyst pellets"
Chem. Eng. Sci. 17, 825-834 (1962)
(cited in reference [62])

[68] Bhatia S.K., Perlmutter D.D.
"A random pore model for fluid-solid reactions: I. Isothermal, kinetic control"
AIChE J. 26(3), 379-386 (1980)

[69] Bhatia S.K., Perlmutter D.D.
"A random pore model for fluid-solid reactions: II. Diffusion and transport effects"
AIChE J. 27(2), 247-254 (1981)

[70] Bhatia S.K., Perlmutter D.D.
"The effect of pore structure on fluid-solid reactions: Application to the SO_2-lime reaction"
AIChE J. 27(2), 226-234 (1981)

[71] Battey M.H.
"Mineralogy for students"
Longman, London (1981)

[72] Berry R.S., Rice S.A., Ross J.
"Physical Chemistry"
(1980)

[73] Furmer Yu.V., Beskov V.S., Brui O.I., Yudina V.V., Dantsig M.L.
"Kinetics of the chemisorption of hydrogen sulphide by zinc oxide adsorbents"
The Soviet Chem. Ind. 14(12), 1499-1507 (1982)
(Khim. Prom-St. (Moscow))

[74] Carnell P.J.H., in
"Catalyst handbook", ch.4
ed. Twigg M.V.
Wolfe Scientific (1988)

[75] Carnell P.J.H., Denny P.J.
"Techniques for investigating sulphur removal by zinc oxide absorbents"
AIChE Ammonia Safety Symp. (1984)

[76] Westmoreland P.R., Gibson J.B., Harrison D.P.
"Comparative kinetics of high-temperature reaction between H_2S and selected metal oxides"
Environ. Sci. Technol. 11, 488-491 (1977)

[77] Gibson J.B., Harrison D.P.
"The reaction between hydrogen sulphide and spherical pellets of zinc oxide"
Ind. Eng. Chem. Process Des. Dev. 19, 231-237 (1980)

[78] Furmer Yu.V., Kosorotov V.I., Brui O.I., Pronina R.N., Kolomin V.I.
"Desulphurisation of natural gas using absorbents based on zinc oxide"
The Soviet Chem. Ind. 11(3), 158-161 (1979)
(Khim. Prom-St. (Moscow))

[79] Westmoreland P.R., Harrison D.P.
"Evaluation of candidate solids for high-temperature desulphurisation of low-Btu gases"
Environ. Sci. Technol. 10(7), 659-661 (1976)

[80] Jalan V.
"High temperature desulphurisation of coal gases by regenerative sorption"
Int. Gas Res. Conf. 291-303 (1981)

[81] Yumura M., Furimsky E.
"Comparison of CaO, ZnO and Fe_2O_3 as H_2S adsorbents at high temperatures"
Ind. Eng. Chem. Process Des. Dev. 24, 1165-1168 (1985)

CHAPTER 3

EXPERIMENTAL APPARATUS AND PROCEDURES

This chapter describes the equipment used to measure rates of sulphiding, the operation of that equipment and the analysis of data collected from it. Details are also given of the methods employed to prepare the absorbent materials, and of the various techniques used to characterise the absorbent both before and after sulphiding.

3.1 Sulphiding equipment

The sulphiding equipment, illustrated in Figure 3.1, was used to measure the rate of reaction of hydrogen sulphide with the zinc oxide absorbent under a variety of conditions by employing the methods of differential analysis. A description of the equipment and its operation follows together with details of the collection and analysis of data. Equipment labels mentioned in the text refer to the appropriate Figure. The operating pressure in the reactor (R1) is a little above atmospheric in order to provide sufficient pressure head to flush the GC sample valve (GSV). This is achieved by means of the combined resistance to flow on the main line from the T-piece, immediately downstream of the reactor, of a capillary glass line and the needle valve NV1. With the gas supplies adjusted to give a total gas flowrate through the reactor of about $430 ml min^{-1}$, the needle valve NV1 is set so as to give a gas flowrate of $60-70 ml min^{-1}$ through the sample valve which conditions correspond to a gauge pressure of 20cm of oil on PI1 of Figure 3.1. The needle valve NV2 is adjusted so that when the bleed stream through the gas sample valve of the GC is diverted to waste via NV2 by means of the 2-way solenoid SV2 (in order to allow

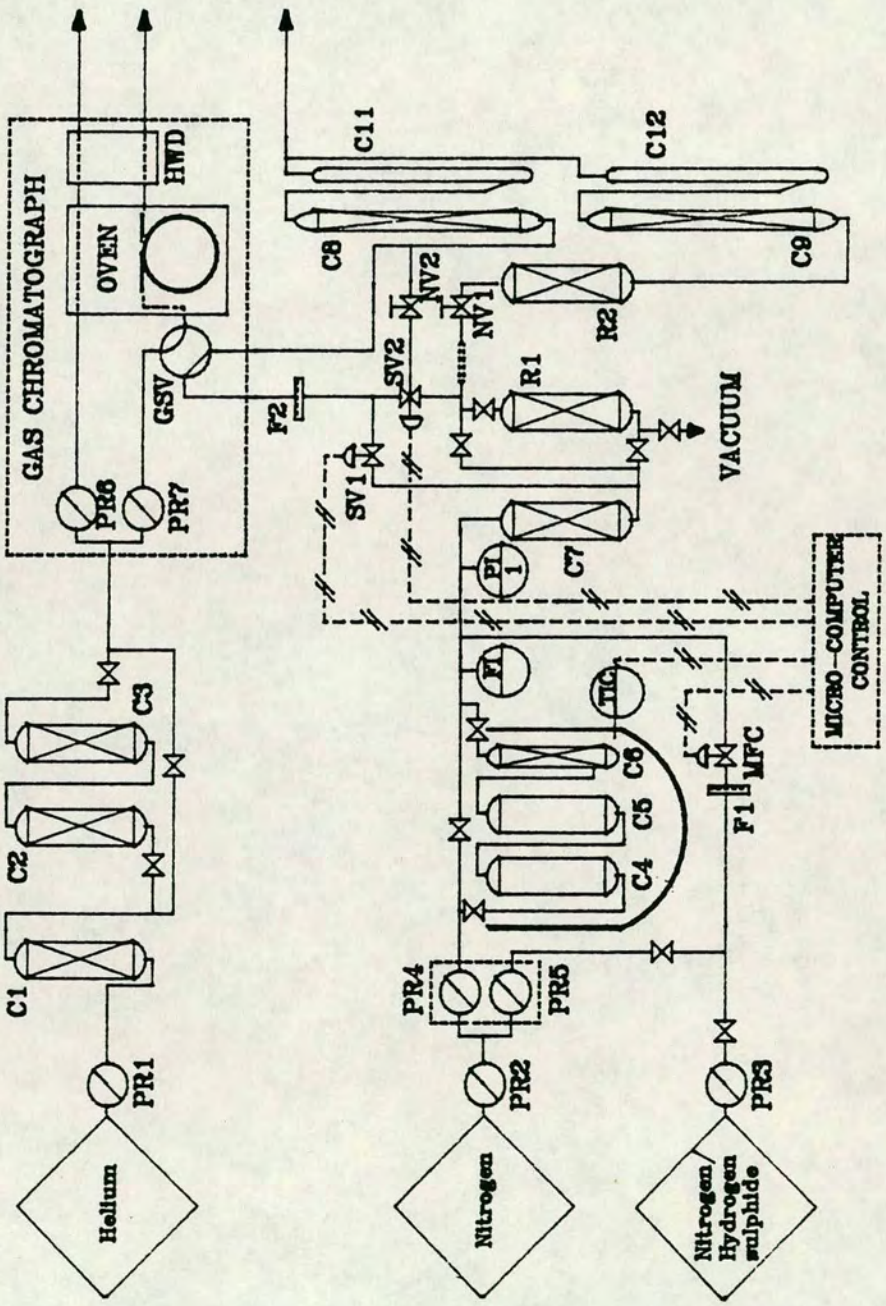

Figure 3.1: Sulphiding equipment.

pressure equilibration and sampling), the resistance to flow, and hence the total flowrate, is unchanged and is only minimally disturbed as the solenoid switches position.

3.1.1 Gas supplies

The gas supply system has been designed to be both simple and flexible. Thus the gas feed stream to the reactor is composed of two streams; one of hydrogen sulphide in nitrogen and the other a water-saturated nitrogen stream from the thermostatted water bubbler. (The water bubbler comprises two water-filled columns in series, C4 and C5, followed by a disentrainment section, C6.) Mixtures of hydrogen sulphide in nitrogen are made up periodically in quantities sufficient for a batch of 6-7 runs using the equipment shown in Figure 3.2. Control of the hydrogen sulphide and water contents of the feed stream is achieved by changing the gas composition of the mixture cylinder and the temperature of the bubbler bath respectively while leaving the gas flowrates unchanged. This method has been adopted in order to allow substantial changes in the feed gas composition to be made without the necessity to control the streams accurately over very wide ranges of flowrate. As close control of the composition of the mixture cylinder is not feasible, mixture compositions were chosen which differed substantially from each other.

A mass flow controller (MFC), protected by a sintered glass filter (F1), fixes the flowrate of the hydrogen sulphide-containing stream while the flowrate of the water-saturated stream is set by the nitrogen pressure head on a glass capillary. (The mercury manometer connected across the glass capillary immediately downstream of the bubbler has been calibrated to give

Figure 3.2: Equipment configurations for the transferral of (a) hydrogen sulphide and (b) nitrogen.

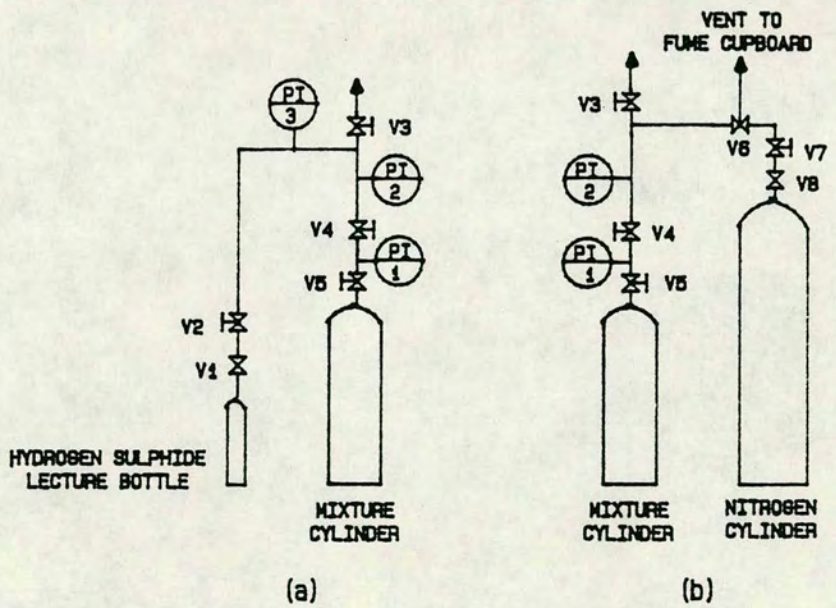

the gas flowrate and is shown therefore as a flow indicator, FI, in Figure 3.1.) The two streams mix in a short section (C7) packed with glass ballotini. When necessary, as during water equilibration of the absorbent sample (section 3.1.7) or in order to purge the lines of hydrogen sulphide, either gas flow may be replaced by a pure nitrogen stream.

3.1.2 Reactor

The reactor (R1) consists of a shallow bed of absorbent particles supported on graded glass ballotini, the ballotini immediately below the absorbent particles being of comparable size to the absorbent particles themselves. Thus the gas flow pattern is fully developed before the gas contacts the absorbent. A further section of ballotini above the absorbent bed ensures thorough mixing of the partially reacted gas. The reactor is 18mm in diameter and the absorbent bed typically 2-4mm in depth, corresponding to a weight of absorbent of 200-600mg. The majority of experimental runs have been performed on particles in the size range 300-710 microns. In these experiments wall channeling is likely to have been negligible. Channeling may have been significant, however, on those runs performed on whole absorbent granules.

The reactor may be isolated by means of two rotaflow valves. Removal of the plug of the downstream valve allows loading of the absorbent and ballotini and vacuum discharge of the same by means of a flexible connection to a vacuum pump. The design purpose of the permanent vacuum line to the reactor was to allow in situ surface area measurement (section 3.3). The physical positioning of the reactor has been arranged so as to allow space for a Dewar or thermostatted water bath for control of the reactor temperature while minimising the

distance between the reactor and the gas sample valve of the chromatograph.

A second reactor (R2) downstream of the first and of the T-piece, which directs a fraction of the total flow to the Gas Chromatograph, is used for the pre-sulphiding of samples.

3.1.3 Gas Analysis (Flame Photometric Detector)

In order to have the potential to study the surface reaction of hydrogen sulphide with zinc oxide on a timescale which permits a reasonable number of analyses (see Appendix A), it is necessary to be able to perform accurate analyses of gas streams which are very dilute in hydrogen sulphide, and thereby to delay saturation of the surface. A Perkin Elmer 8410 gas chromatograph fitted with a Flame Photometric Detector (FPD) was selected for this duty. In this detector the column effluent is mixed with hydrogen and burnt in air. Sulphur compounds present in the sample decompose in the detector flame producing S_2^* species which emit radiation at 394nm on transition to the ground state.[1]

The detector has a number of advantages; it is sulphur specific, has a very low detection limit (of a few ppm hydrogen sulphide) and yet it has a large range of attenuation of 1:4096 enabling analysis of fairly concentrated mixtures. The sulphur specificity indicates the potential of the detector for continuous analysis under certain conditions. It was envisaged that a number of different carrier gases might be used in the experimental work, amongst which helium, nitrogen and methane would be of particular interest. (Of these, the first two would allow investigation of the effect of the gaseous diffusivity, while the last would mimic more closely a major industrial application of the absorbent.) With either helium or nitrogen used as

carrier in both the reaction system and for the chromatograph, continuous analysis would be possible provided there were no interfering effect caused by the water produced in the reaction.[1] Quenching can be a problem where hydrocarbons elute coincidentally with the sulphur compound of interest. It was indeed observed that without a chromatographic column in place diminution of the sulphur signal occurred where methane was used as the carrier in the reaction system. This is attributed to the deactivation of the excited S_2^* species through collision with methane or, more probably, carbon dioxide molecules.[1] In this case therefore only discrete analysis is possible.

A chromatographic column packed with Phasesep 'Porapak QS' was purchased to perform the separation duty. At low levels of hydrogen sulphide, however, there appeared to be an initial 'conditioning' period for the column during which some hydrogen sulphide was retained on the column packing. Because of the detector ceiling on the absolute quantity of hydrogen sulphide which can be analysed, it proved necessary in order both to reduce the conditioning time of the column packing to a few minutes and to avoid overloading the detector, to install a splitter at the column outlet. The desired split, which was achieved by trial and error, directed less than 1% of the column outlet to the detector. The rest of the column outlet gas, having a minute concentration pulse of hydrogen sulphide, was vented into the laboratory.

The high sensitivity of the detector to hydrogen sulphide suggests a potential for very accurate analysis of more concentrated mixtures. This potential was occasionally realised on such analyses but in general the response of the FPD was seen to drift badly. The very high gain amplifier on the detector was found to be

very sensitive to small changes in the laboratory temperature, as were the original brass pressure regulators on the instrument which were later replaced with stainless steel regulators. Both the jet tip and the glass liner which shields the photomultiplier tube from the flame built up substantial deposits of sulphur. The growth of these deposits might reasonably be expected to cause a gradual change in the detector response.

We concluded that the instability and temperature sensitivity of the instrument rendered it inappropriate for very accurate analysis over periods of several hours.

3.1.4 Gas Analysis (Katharometer)

The second detector to be critically evaluated for the gas analysis duty was a katharometer or Hot Wire Detector (HWD), the response of which is proportional to the difference in thermal conductivity between the sample gas and the reference carrier gas. This detector is not, of course, sulphur specific, nor has it the detection sensitivity for hydrogen sulphide of the FPD thus precluding the possibility of studying the surface reaction. It has the advantage, however, of providing simultaneous analysis of the process stream water content although the water response is also the reason for the longer cycle time - 4.5 minutes compared to 1.8 minutes for the FPD. The detector stability was tested over a period of 12 hours during which no significant drift was observed (<.1% per hour).

The operating conditions of the gas chromatograph are given in Table 3.1. The helium cylinder is connected to the chromatograph with copper lines rather than nylon in order to avoid diffusion of water into the carrier gas. Water vapour is removed from the helium in a bed of Type

Table 3.1: The operating conditions of the Perkin Elmer 8410 Gas Chromatograph.

Detector	Katharometer
Detector Temperature	150°C
Carrier	Helium
Carrier flowrate	25 ml/min
Column Packing	HayeSep Q, 80-100 mesh
Oven Temperature	80°C
Peak Retention Times/mins :	
Nitrogen	0.6
Hydrogen Sulphide	1.8
Water	3.6
Sample Injection Temperature	110°C
Sample Loop Size	500µl

5A molecular sieve (C1) with added protection provided by Chrompak moisture and oxygen filters (C2 and C3 respectively). A HayeSep packing has been used in the column as this was found to give a slightly greater retention time for hydrogen sulphide. Thus the separation of the nitrogen and hydrogen sulphide peaks is improved compared to that achieved using the Phasesep packing with no loss of resolution of the hydrogen sulphide and water peaks which are well separated.

In order to carry out integration of the chromatogram peaks, the GC software requires the operator to set values for a number of parameters. Important amongst these are the base and area sensitivities. The value of the base sensitivity is related to the degree of slope and rate of change of slope of the GC signal which is interpreted as being either baseline or the leading or tailing edge of a peak. Thus an over-large value of this parameter will cause small peaks to be regarded as baseline, while too small a value may result in the software failing to locate the baseline if the signal is noisy. The area sensitivity sets the criteria by which the start of a peak and the peak crest are confirmed after detection of a significant rise in slope, and a significant decrease in signal slope after a maximum, respectively.[2] Both of these parameters may be selected automatically by the GC by examination of the signal noise and drift over a two minute period. Initial values were selected in this way. These proved to be unsatisfactory, however, because noise on the long tail of the water peak led to an apparently haphazard location of the peak end-point, resulting in an exaggerated standard deviation. In order to improve the accuracy of the integration the value of the base sensitivity parameter was changed to zero. As the software is no longer able to locate the baseline, it is necessary to force basepoints at the beginning and end

of each peak for which a facility exists in the programming of the GC method. Thus the peaks are integrated during 'windows' of time specified in the method. It is clear that this could lead to nonlinearity in the GC response for very small peaks where the residence time may be slightly increased. This method of integration was found not to affect the integrated area of the hydrogen sulphide peak nor the mean water signal, but it leads to a reduction in the standard deviation of the water signal of about 35%. With the method thus set up, the ratio (expressed as a percentage) of the standard deviation to the mean for a group of analyses is still an order of magnitude lower for the hydrogen sulphide analyses compared to the water analyses. These are respectively about 0.4% and 3.5% for a gas sample containing 0.19% hydrogen sulphide and 0.15% water.

The very large nitrogen peak has not been integrated due to the tendency of the GC software to cut the maximum off it in most analyses, drawing only a flat-topped peak. Where this does not happen, the signal is well on-scale, so that the cause of it is not apparent.

The GC has been calibrated for water and hydrogen sulphide by means of a minor modification to the sulphiding equipment as indicated in Figure 3.3. (With the needle valve, NV1, closed, the 3-way solenoid valve, SV2, switches the reactor outlet gas alternately to the gas sample valve (GSV) of the GC and to waste via the needle valve NV2. In either configuration, the gas stream subsequently passes over the detachable absorption bed (C10) through the soap film meter (C12) to vent.) Each point on the calibration curves (Appendix B) represents a run of several hours duration where the gas stream was analysed repeatedly by the GC. For the water calibration, all of the water content of the

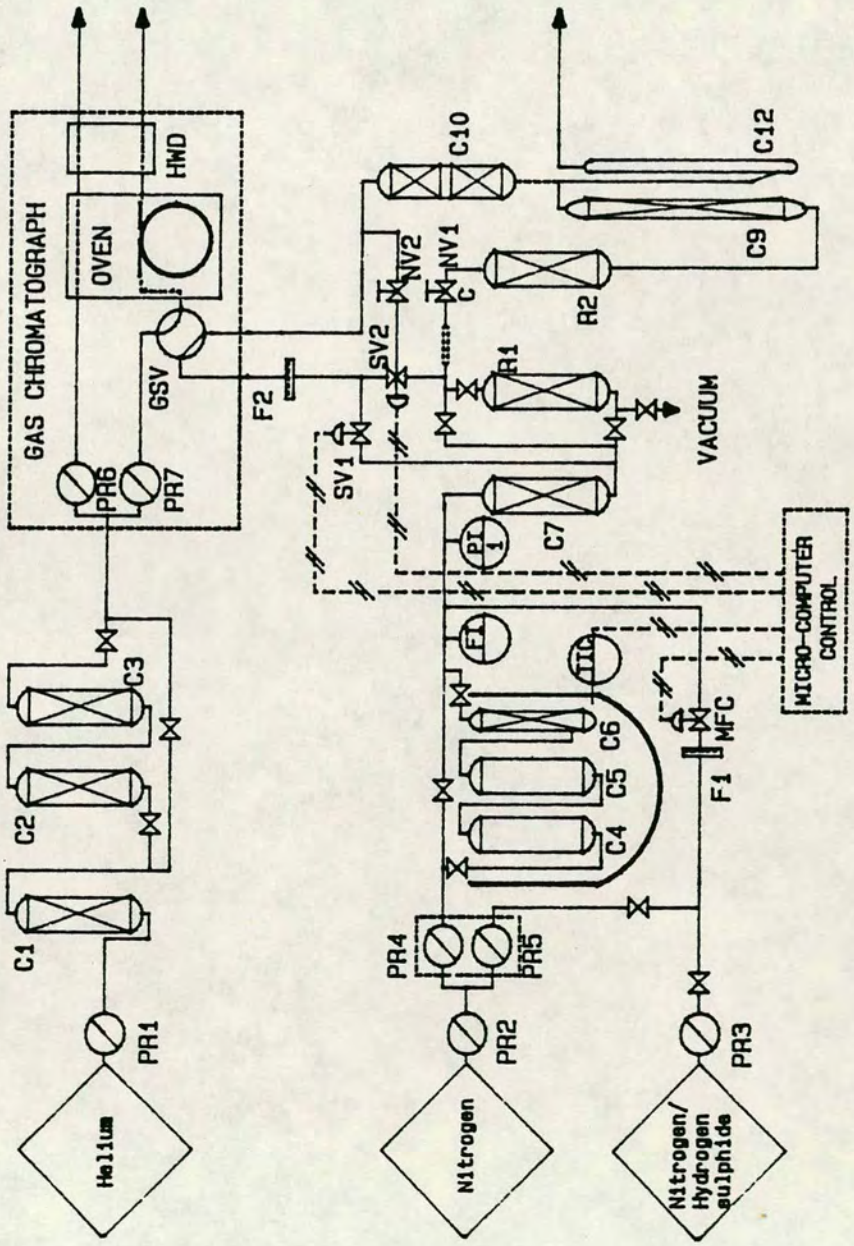

Figure 3.3: Experimental set-up for calibration of the gas chromatograph.

stream is adsorbed by the molecular sieve in the absorption bed (C10), and thus the molar flowrate of water is determined from the weight increase of the bed and the measured gas flowrate.[6] For the hydrogen sulphide calibration the upstream section of the absorption bed is filled with the zinc oxide absorbent and the downstream section with molecular sieve. All the hydrogen sulphide present in the stream is absorbed by the zinc oxide and any water produced in the reaction will be adsorbed either on the zinc oxide or on the molecular sieve.

3.1.5 Materials

The equipment has been constructed entirely in glass except for the various valves. The 6-port injection valve on the gas chromatograph is of Hastelloy C. The original stainless steel valve gave a slight gas leakage on return of the valve to the filling position after relatively few analyses. When it was removed for replacement dark corroded rings were apparent on its

---

[6]The molecular sieve (Type 5A) used in the absorption bed is one which is used for nitrogen/oxygen separations where it has been observed that water vapour present in the entering gas stream reduces the capacity of the bed to adsorb nitrogen. This would appear to be evidence for the competitive adsorption of water and of nitrogen onto surface sites. However, experiments done in the Chemical Engineering Department at Edinburgh University under Dr C.L. Pritchard's guidance,[3] while supporting this observation, have not been sufficiently quantitative to permit a conclusion to be drawn as to whether the water vapour occupies exclusively 'nitrogen sites' or whether there are some sites onto which water adsorbs but nitrogen does not. The water calibration results of the present work strongly suggest that the latter is the case as the measured weight increase of the absorption bed was consistent with the estimated weight increase based upon the assumption that the water bubbler operates at atmospheric pressure (the pressure was not monitored), and that the nitrogen stream leaving the bubbler is saturated with water at the bubbler temperature. If water vapour were displacing adsorbed nitrogen from the sieve to any extent then the measured weight increase should have been consistently less than the estimate.

surfaces. The solenoid valves (SV1 and SV2), mass flow controller (MFC) and rotaflow valves (NV1 and NV2) are all teflon. The two needle valves are stainless steel. As both are exposed to the hydrogen sulphide-containing gas, they are likely to have been corroded to some extent. Neither of the valves is in a critical position, however, being downstream of the reactor and analysis sections of the apparatus. It would have been possible to place the needle valve on the main line, NV1 in Figure 3.3, downstream of the absorbent dump bed (C9) thus not exposing it to the corrosive gas. The positioning of NV1 upstream of the bed is convenient, however, in that it allows the main soap film meter to be used for flow measurements during calibration runs by the simple expedient of a temporary connection of rubber tubing between the absorption bed and the top of the main dump bed. The mixture cylinder itself is aluminium and has shown no tendency for irreversible adsorption of hydrogen sulphide.

3.1.6 Automation and Control

The gas chromatograph, which is equipped with a pneumatically operated automatic gas sample valve, is set up to cycle indefinitely. A BBC microcomputer controls this cycling, allowing the user to interrupt the run. The computer also controls the switching of the solenoid valves and the setting of the mass flow controller. In order to vary the water content of the feed, the bath in which the water bubbler is contained is held at temperatures in the range 0-20°C. A temperature of about 0°C is achieved by filling the Dewar in which the bubbler is mounted with an ice/water mixture. For temperatures above 0°C a mercury contact thermometer is used as a switch to operate a peristaltic pump which circulates cold water from a second Dewar containing an ice/water mixture (Figure 3.4). The

Figure 3.4: Temperature control of the water bubbler bath.

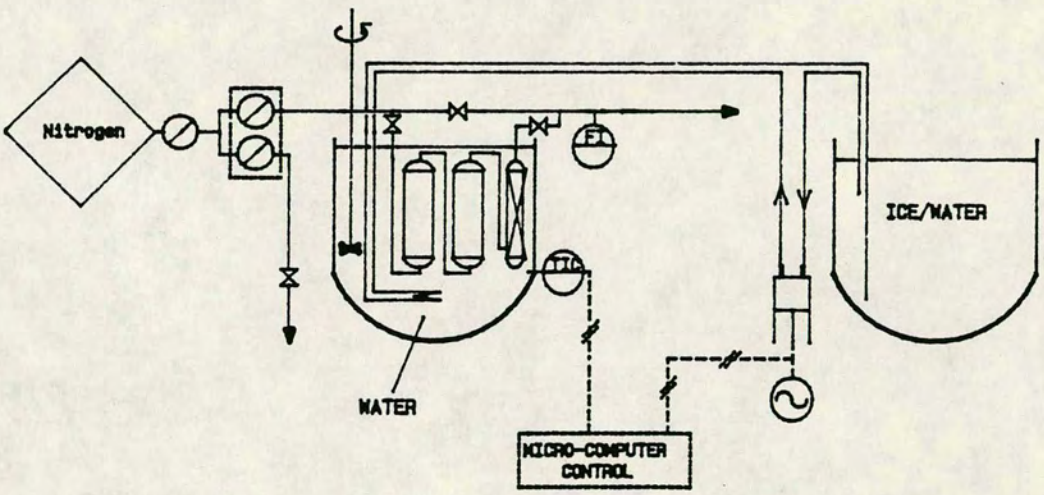

microcomputer controls the timing of this switching.

3.1.7 Experimental Procedures

The system is first flushed with nitrogen with the reactor by-passed in order to clear the lines of any traces of hydrogen sulphide from the previous run. The reactor is then put on-line and flushed with nitrogen to sweep out the air present from the loading of the reactor. This also serves the purpose of reducing the water partial pressure and absorbent water content below the levels to be used in the experimental run. The decline in the water concentration is generally not monitored by the GC except where a "dry run" is to be performed, in which case the nitrogen flushing serves as the water equilibration pretreatment, and it must therefore be ensured that the absorbent is in equilibrium with the gas phase. In most of the experimental runs the feed gas contains water vapour. The purpose of this is two-fold; the water content of the feed is a parameter of interest in studying the reaction rate, while feeding water to the reactor allows a closer approximation to the assumptions of differential analysis, that is that the changes of concentrations in the system are very small. Thus if a wet gas is to be used for the sulphiding experiment, a water equilibration treatment follows the nitrogen flushing. With the reactor by-passed, several analyses are made by the GC of the water/nitrogen feed stream, which contains the same partial pressure of water as is to be used in the sulphiding run. When the water signal is steady, the reactor is put on-line and the reactor outlet gas is analysed until the water signal has risen

to its level in the feed.[7] During most of this period of water adsorption, no water was present in the reactor outlet gas. When water was detected, however, the signal rose very slowly to its level in the feed. Such behaviour is not characteristic of physisorption, which is non-activated, and suggests the occurrence of some other process. Chemisorption of water may be important. Calculations based on the Kelvin equation,

$$p/p_s = \exp(-2\sigma_s V_m \cos\theta / r_p RT) \qquad (67)$$

(where r_p is the maximal radius of pores in which capillary condensation will occur at pressure p) indicate that at the highest relative pressure used of 0.15 corresponding to a water content in the feed of 0.5%, capillary condensation will only occur in pores having radii less than 5.5Å.

The procedure for the sulphiding experiment is similar to that for the water pretreatment. The feed stream is analysed for several hours while the reactor is by-passed. The duration of this initial period of feed analysis is decided by the operator. Each cycle of the GC, comprising sample injection, separation and analysis, and data transfer to the microcomputer, takes about 4.5 minutes at the end of which the computer program offers the operator a short menu of options before prompting the GC to continue. The option to put the reactor on-line can therefore be selected at any time. After the reactor has been put on-line, the program follows the pattern of feed and product sampling requested by the operator at the start of the run. This

---

[7]The time apparently taken to equilibrate the sample with the gas stream is increased by the adsorption of water on all exposed surfaces of the equipment between the water bubbler and the gas sample valve.

sampling pattern may, however, be altered or the run extended by means of appropriate intervention by the operator. Other options include allowing the setting of the mass flow controller to be changed, and causing the program to pause, for example to allow flow measurement, until re-started by the operator.

The timing of the solenoid switching is such that the gas stream is sampled at atmospheric pressure by the gas sample valve of the GC. The equilibration of the pressure of the gas in the sample loop with atmospheric pressure was monitored with a pressure transducer during the construction of the rig and found to be very rapid. The laboratory temperature is measured by a thermistor which is monitored by the microcomputer. The barometric pressure is read manually. Program listings and flowsheets are given in Appendix C.

3.1.8 Statistical Analysis

The chromatographic data on the feed and product stream concentrations of hydrogen sulphide have been analysed in terms of a differential flow reactor. Such an approach assumes the rate to be constant at all points within the reactor.[4] Validity of this assumption in a gas-solid non-catalytic reaction system is likely to entail very low conversions of both gaseous and solid reactants. As, in this reaction, the gaseous product, water, is also expected to affect the rate, it is necessary that the partial pressure of water in the gas stream should undergo only a small change as a result of the reaction. It is then possible to simplify the performance equation of the plug flow reactor thus,

$$\int_0^W dW/Q = c_{Ai}\int_0^x dx/(-r_A) \simeq c_{Ai}x/(-r_A) \qquad (68)$$

(where W is the weight of absorbent used in the run, Q is the total gas flowrate, c_{Ai} is the concentration of

the gaseous reactant in the feed stream, x is the conversion and $(-r_A)$ is the rate of consumption of the gaseous reactant) so that each experimental run yields a rate for a particular set of component concentrations in the reactor. The chief difficulty in differential analysis is that of achieving sufficient precision in the determination of concentrations that the error associated with the calculated rate may be reduced to an acceptable level. In the present work this difficulty has been overcome by the use of repetitive analysis of the feed and product streams.

In order to calculate the pseudo-steady state (pss) rate, it is necessary first to identify at what point it may be considered to begin, the end of the pss period being defined for all runs by the time, t_2, of the last product analysis. This is done with reference to any time-dependent drift observed in the feed analyses. Where a trend exists in the feed line, it is always very small.

Thus, having discarded some of the initial feed analyses where curvature or drift is apparent in the plotted data, a curve of the form

$$y_F = \alpha_F + \beta_F . t \qquad (69)$$

is fitted to the feed data where α_F and β_F are constants. Similarly, having estimated t_1, the time at which the pss period may be considered to start, a curve of the form

$$y_P = \alpha_P + \beta_P . t \qquad (70)$$

is fitted to the product data thus selected, where α_P and β_P are constants. In practice the rejection of the initial analyses of both feed and product may be done automatically and it has been found convenient to discard sufficient data pairs to leave n_F feed analyses and n_P product analyses where $n_F=32$ and $n_P=27$. These values allow easy use of F-tables and are generally

found to provide data which satisfy the definition of a pss. An F-test[5] provides a significance test of the hypothesis that the gradient, β, of a line of the general form

$$y = \alpha+\beta.t \tag{71}$$

is non-zero. The F-value which is defined as the ratio

(ms due to regression) / (ms deviations) (72)

(ms=mean square) is referred to F-tables on (1,n-2) degrees of freedom where n is the number of data pairs. If the calculated F-value is less than the 95% point of the F-distribution,

$$F < F_{95\%}(1,n-2) \tag{73}$$

then there is no evidence at the 5% level that $\beta<>0$. If,

$$F_F < F_{95\%}(1,n_F-2) \tag{74}$$

and

$$F_P < F_{95\%}(1,n_P-2) \tag{75}$$

then the pss rate is proportional to the mean difference, $\bar{r}$, between the feed and product signals,

$$\bar{r} = \bar{y}_F-\bar{y}_P \tag{76}$$

and

$$Var(r) = Var(y_F)+Var(y_P) \tag{77}$$

The standard deviation of the mean difference, known as the standard error, is given by

$$s(\bar{r}) = \{Var(y_F)/(n_F-1)+Var(y_P)/(n_P-1)\}^{\frac{1}{2}} \tag{78}$$

Where the F-value of either the feed or product data is found to be significant the difference, r, between the feed and product signals, will be linearly dependent on time and the mean difference must be calculated at the mean time of the interval, $\bar{t}_p$, where

$$\bar{t}_p = (t_1+t_2)/2 \tag{79}$$

and t_1 and t_2 delimit the pss period. The estimated feed and product signals, $\tilde{y}_F$ and $\tilde{y}_P$, may be obtained from equations (69) and (70) respectively for $t=\bar{t}_P$. In this case, equation (76) becomes

$$\bar{r} = \tilde{y}_F - \tilde{y}_P \tag{80}$$

The standard error of r is no longer given by equation (78) because some of the total variance is now accounted for by the regression on t. Thus,

$$\mathrm{Var}(\tilde{y}_F) < \mathrm{Var}(y_F)/n_F \tag{81}$$

and the variance of $\tilde{y}_F$ is given by

$$\mathrm{Var}(\tilde{y}_F) = \sigma^2\left[1/n_F+(\bar{t}_P-\bar{t}_F)/\Sigma(t-\bar{t}_F)\right] \tag{82}$$

Any significant trend observed in the feed analyses must arise either out of a drift in detector performance or from a real change in feed composition due to poor performance of the mass flow controller or of the nitrogen regulator (PR4) on the stream to the bubbler or from changing conditions in the bubbler itself eg. due to water build-up in the disentrainment section (C6). Whatever the cause, the drift should also be present in the product analyses. If the feed trend is subtracted from the fitted product trend, the difference should be statistically insignificant - as determined by an F-test - thus justifying the description of the process as a 'pseudo-steady state'. In this case, the standard error of the rate, $s(\bar{r})$, is given by

$$s(\bar{r}) = \{\mathrm{Var}(\tilde{y}_F)+\mathrm{Var}(\tilde{y}_P)\}^{\frac{1}{2}} \tag{83}$$

where the mean value of the explanatory variable, t, in the pss interval is equal to the mean value of t for the product analyses selected. In fact, the trends observed in the feed and product analyses were not found to be statistically significant.

3.2 Microbalance

Most of the experiments to investigate the rate of absorbent sulphiding and the factors affecting that rate have used a commercial ICI absorbent. This has an important practical advantage in that preparation of the material consists only of crushing and screening the particles to obtain the required particle size fraction. Apart from the variable composition of individual granules and the range of physical strength and structure they exhibit (section 4.12) the most serious disadvantage of this material is probably its poorly defined history. Were zinc oxide to be prepared in the laboratory there would clearly be a case for carrying out the preparation within a dry box and storing the material under nitrogen thereby excluding water and carbon dioxide. The granules of the commercial absorbent were, however, stored in a polythene bag prior to crushing and sorting by size. The size fraction selected was subsequently stored in screw-topped glass jars. Thus the material was effectively exposed to the atmosphere and both water and carbon dioxide are readily adsorbed on such material as heat treatment of the stored absorbent reveals (Table 4.1). The absorbent samples accurately weighed out for use in sulphiding runs therefore contain an unquantified amount of water. The absorbent is subsequently dosed with water to equilibrate it with the partial pressure of water to be used in the sulphiding run itself. The amount of water which is adsorbed during this period could be determined by numerical integration of the water analyses, however, because of the inferior accuracy of the GC analysis for water compared to that for hydrogen sulphide and because the amount of water on the absorbent prior to the water pre-treatment is unknown, it was decided to carry out experiments to study water adsorption quite separately using a microbalance.

3.2.1 Equipment Configuration

A Stanton Redcroft TG 761 thermobalance was used for this purpose. A diagram of the essential features of the balance and of the ancillary glassware required for the experiments is given in Figure 3.5. Absorbent samples of the same particle size range as was used for the sulphiding runs were used for the balance experiments. The low packing density of the material and the size of the crucible in which it is contained restrict the sample weight to about 20mg. In order to maximise the sensitivity of the weight measurement, a counter-weight of nominal weight 20mg was put in the counter-balance pan thus allowing changes in the sample weight to be measured on the 0-1mg scale of the balance. The digital weight display gives the sample weight to the nearest microgram. A low flowrate of dry nitrogen through the balance housing (about 25mlmin^{-1}) prevents any water adsorption on the balance mechanism which might produce errors in the registered sample weight. The temperature of the furnace in which the crucible containing the sample is suspended is controlled by electrical heating and by a continuous flow of cooling water, the temperature of which is independently controlled by the operator. With the tank of cooling water held at ice temperature, it is possible to attain a minimal temperature of 6°C in the furnace. The maximal furnace temperature of the balance is 1000°C.

The gas which sweeps the furnace is a mixture of two streams: a stream of pure nitrogen which has passed over a molecular sieve bed (C13) and a stream of wet nitrogen from the water bubbler. The water content of the stream may therefore be varied between zero and that water content equivalent to the vapour pressure of water at the bubbler temperature. The two streams mix in a short section packed with glass ballotini (C14). A soap film

Figure 3.5: Equipment for microbalance experiments.

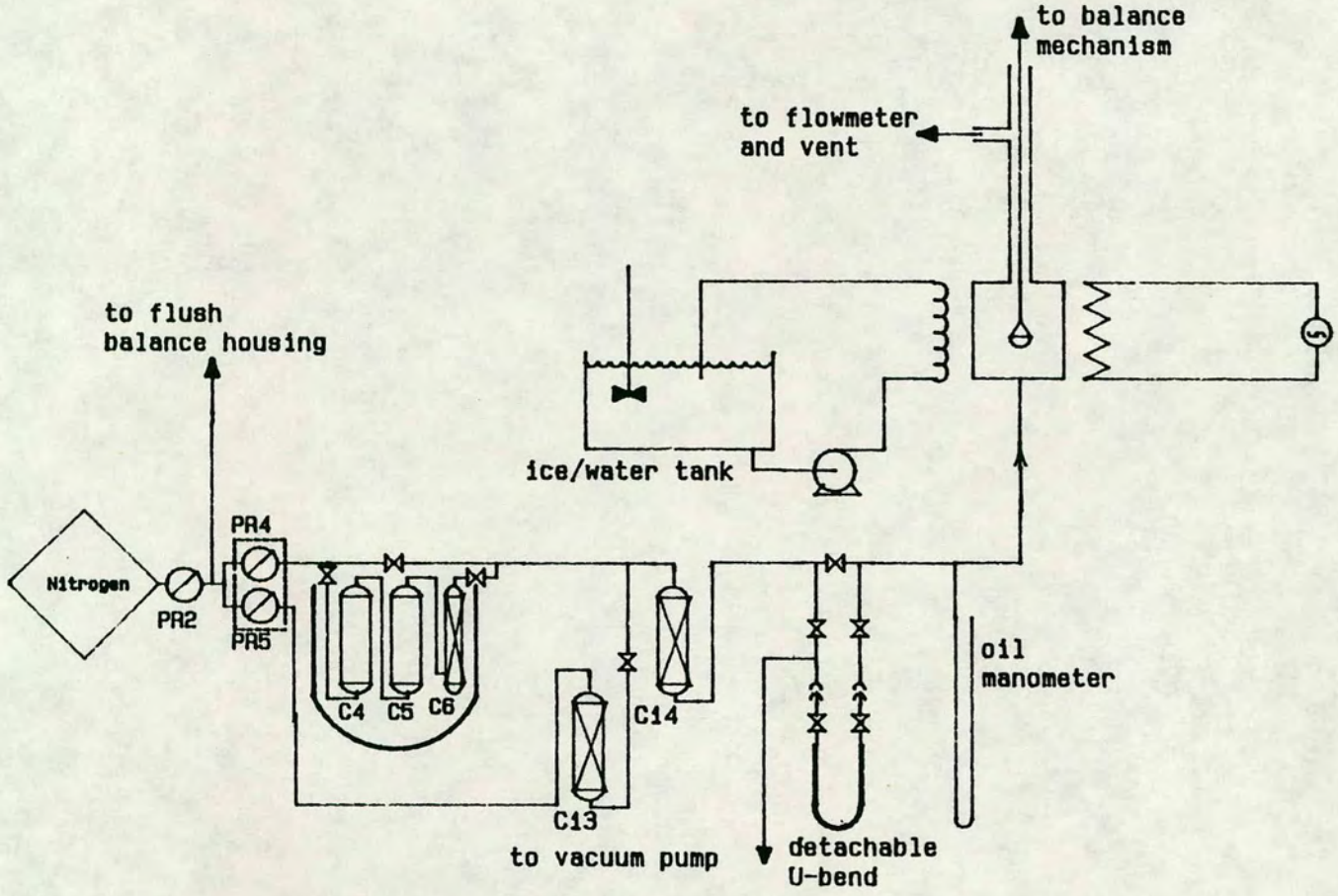

meter attached to the gas outlet from the microbalance and a detachable U-bend which may be isolated and by-passed allow the measurement of the gas flowrate and water content. The latter is measured by applying a liquid nitrogen bath to the U-bend for a given time to condense all the water vapour in the gas stream and then removing and weighing the U-bend after pumping out the nitrogen.

3.2.2 Calibration and Operation of the Microbalance

The microbalance must be calibrated for the particular flowrate used in the experiment. As the flow is upward through the furnace buoyancy forces decrease the apparent sample weight. The balance controls are therefore adjusted to give 0.000mg and 1.000mg for respectively no weight and the 1.000mg calibration weight on the balance pan under flow conditions. At this level of sensitivity the displayed weight tends to fluctuate with any small changes in background light or temperature or with static build-up, and the accuracy of any weight reading is therefore about ±2μg.

Experiments were performed to investigate the variation of the amount of water adsorbed on the sample with both temperature and water partial pressure. The total weight loss from a sample of stored 75-1 resulting from equilibration with a dry nitrogen stream at ambient temperature was also determined, as was the weight loss on heating the sample to 400°C. No analysis of evolved gases was performed so that it is not possible to say definitively what proportions of the weight loss during temperature programming are attributable to loss of water and loss of carbon dioxide respectively.

3.3 Surface Area Determination

Surface area measurements have been made on a number of materials using nitrogen adsorption at -195.8°C. Figure 3.6 shows the equipment used. It was originally intended that the measurements would be made in situ in the reactor in order to allow ready measurement of the effect on the specific surface area of water treatment and of sulphiding while avoiding handling and exposure to the atmosphere between treatments. Because of the large void space in the reactor (about 14ml), surface area determination using nitrogen at -195.8°C would have been very inaccurate. It was therefore proposed to use butane as the adsorptive gas at 0°C. A substantial range of values is cited[6] as being used for the area occupied by a butane molecule on the surfaces of different adsorbents. Reservoirs for both nitrogen and butane were provided, therefore, in order to calibrate the butane area on an absorbent sample for which the surface area had been determined by nitrogen adsorption. A small sample tube was therefore provided on the equipment for this calibration. Butane adsorption was not found to be amenable to analysis, however, as the resulting isotherm was of Type III (Figure 3.7) in the BET classification, and it is not possible to calculate surface areas from such an isotherm. This problem has been reported before,[6] when adsorption of butane at 25°C on calcium carbonate outgassed at 25°C led to a Type III isotherm while butane adsorption on the same material outgassed at 150°C gave a well defined Type II isotherm. The explanation proffered for this anomaly was the presence of adsorbed water in the first case. The outgassing procedure followed for the zinc oxides studied in this work was to outgas firstly at room temperature and then at 110-115°C for one hour. Further investigation of whether degassing at a higher temperature would have led to a Type II isotherm was not

Figure 3.6: Equipment for surface area determinations.

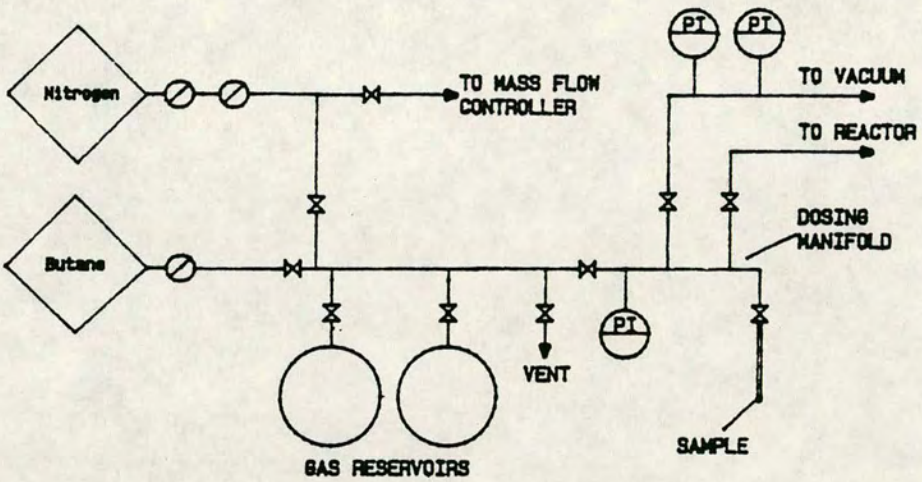

Figure 3.7: Brunauer classification of isotherms.

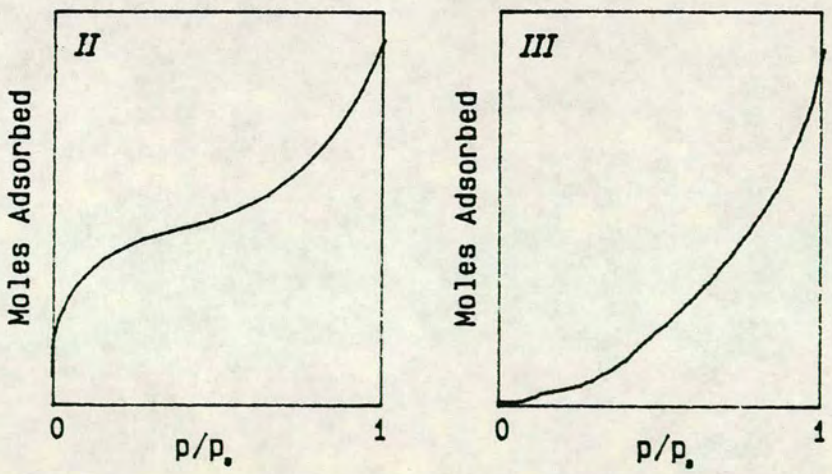

done, and subsequent surface area determinations were performed using nitrogen adsorption.

The use of nitrogen as the adsorptive gas for in situ measurements was judged to be impractical because of the large void volume of the reactor, as mentioned above. All surface area measurements were therefore made in the small sample tube. In order to minimise the quantity of nitrogen present within the tube which was not adsorbed on the adsorbent surface, the tube was filled with glass ballotini after loading the adsorbent. A scratch mark halfway down the tube indicating the level to which a Dewar of liquid nitrogen should be raised served both to further reduce the inventory of unadsorbed nitrogen in the tube, and to avoid icing up of the tube valve. The volumes above and below the scratch mark were determined by filling with mercury and weighing. All other volumes in the apparatus were found by nitrogen expansion at room temperature.

The samples were dosed with nitrogen up to a relative pressure ($p/p_{saturation}$) of about 0.1. Ruthven[7] has noted that determination of specific surface area from the BET equilibrium isotherm is applicable only in the reduced pressure range - $0.05 < p/p_s < 0.35$. As insufficient data points were available in this region, the surface area has been calculated from the location of 'Point B'[6] at the 'knee-point' of the isotherm. The error associated with this estimate is clearly related to the sharpness of the 'knee', being smaller for more rectangular isotherms. Very similarly shaped isotherms were obtained for zinc oxide, hydrozincite and partially sulphided zinc oxide, and the specific surface areas given for these materials are accurate to about ±4%.

3.4 Thermal Decomposition

Most of the sulphiding experiments have been done on absorbent materials which were already calcined when received. However, a number of runs have been performed on materials which were prepared from the precursor materials in the laboratory. The absorbent precursor is a basic zinc carbonate which must be calcined to give zinc oxide with loss of water and carbon dioxide. A diagram of the equipment used for these thermal decompositions is given in Figure 3.8. The equipment was also used to determine the water and carbonate contents of absorbents which had been stored open to the atmosphere.

In order to minimise exposure of the calcined materials to the atmosphere, the precursor materials were prepared in the desired particle size range prior to calcination. The material was then loaded into a silica tube contained within a temperature programmable oven. A linear heating rate of $10°Cmin^{-1}$ was used, except for some of the cement-free basic carbonates which had a tendency to fluidise where heating rates of $4-5°Cmin^{-1}$ were used. Fluidisation is very undesirable as it necessarily leads to non-uniform treatment of the material and to attrition resulting in fines. Calcination was continued for an hour once the desired maximum temperature had been reached.

The decomposition was performed under a vacuum of about 0.1mmHg with the evolved water and carbon dioxide being separated by fractional condensation at -78.5°C and -195.8°C. On completion of the calcination the gas volume of carbon dioxide was measured.

Figure 3.8: Thermal decomposition equipment.

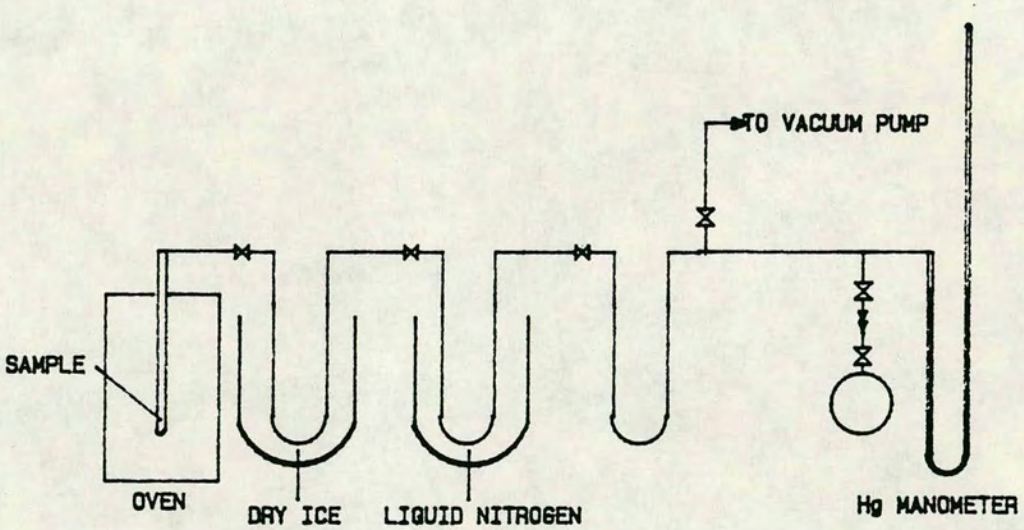

3.5 Electron Microprobe

The electron microprobe has been used to investigate the distribution of sulphur in sulphided absorbent granules. Of particular interest is whether the sulphur is uniformly distributed through the granule or whether there is any nonuniformity or zoning indicative of a mass transfer limited reaction. A uniform distribution of sulphur, or macroscopic homogeneity, would provide confirmation of the existence during reaction of very flat profiles of both hydrogen sulphide and water through the granule. It is likely, however, that at the level of the crystallites there are distinct zones of zinc oxide and zinc sulphide, but it is not anticipated that the microprobe could identify such inhomogeneity given that its resolution is limited to about 1 micron (10^4Å).[8] Although most of the sulphiding experiments have been done on absorbent particles in the size range 300-710 microns, all of the microprobe analyses have been done on whole granules of 3-4mm diameter. Granules have been used in order to test the claim[8] that the reaction rate is not limited by gaseous diffusion, as well as for the easier interpretation of information for a particle with a high degree of symmetry.

3.5.1 Theory of the Technique

The bombardment of a sample surface with electrons generates X-rays which are characteristic of the elements contained in the sample. The concentrations of

---

[8]Making certain simplifying assumptions about the nature of zinc oxide crystallites in a granule, ie. that they are spherical and of uniform size, it is possible to estimate the crystallite size based on measurements of specific surface area and Helium density. Using average values of the specific surface area and Helium density of nine different samples of the absorbent '75-1' measured at ICI[8] of $67 m^2 g^{-1}$ and $4.75 gml^{-1}$ respectively gives a crystallite radius of 96Å.

the individual elements may be calculated by considering the intensity of the emitted X-rays relative to the intensity of X-rays from a standard sample of known composition.[9]

The X-ray emission lines result from transitions between inner atomic energy levels. In order for such a transition to take place, an inner electron must first be ejected - by electron bombardment - thus creating a vacancy. The X-ray lines are labelled according to the source of the radiation. Thus the K spectrum arises due to an initial ionisation in the innermost electron 'shell', the K shell, which corresponds to a value of 1 of the principal quantum number, n. The L and M shells, corresponding respectively to n=2 and n=3, consist of a number of subshells, L_{I-III} and M_{I-V}, of decreasing energy, distinguished by different values of the orbital and magnetic quantum numbers. The principal X-ray lines observed in the K spectrum are the $K_{\alpha 1}$, produced by a L_{III}-K transition, the $K_{\alpha 2}$, produced by a L_{II}-K transition, and the $K_{\beta 1}$, produced by a M_{III}-K transition. The energy of a particular line increases with the atomic number of the emitting atom due to the increasing binding energy of the inner levels.

3.5.2 Energy Dispersive System

The Cameca electron microprobe which was used for this work is fitted with an energy dispersion system. This is useful for initial exploratory analysis of a sample as it effectively scans the whole spectrum of X-ray wavelengths, sorting these by energy and thus indicating all the elements present in the sample with some indication of their relative abundances. The rastered energy dispersion image which can be viewed over a wide range of magnifications reflects the variation of the mean atomic number over the surface. Thus areas with a

high mean atomic number appear brighter than those with a lower mean atomic number. The following elements, listed in order of increasing wavelength by which they were detected, are present in the sulphided absorbent: potassium, sodium, aluminium, silicon, calcium, magnesium, sulphur, titanium, iron and zinc. As carbon is used as a conductive coating on the samples, this prevents its quantitative analysis in the sample. Although light elements are more difficult to detect, it is surprising that oxygen is not identified as being present given its significant concentration. The explanation of this, however, is that the only strong oxygen line, the oxygen $K_{\alpha 1}$ line, lies virtually identically on top of the zinc $L_{\beta 1}$ line. Moreover, both of these lie on the leading edge of the much larger zinc $L_{\alpha 1}$ line. The impossibility of oxygen analysis with the electron microprobe was the reason for attempting ion probe analysis which is detailed in section 3.6.

3.5.3 Configuration of Equipment

The microprobe system includes four spectrometers located at a viewing angle of 40° to the normal to the stage on which the samples are mounted. This permits the simultaneous detection of four different elements. Each of the spectrometers is fitted with two different crystals mounted on a rotating shaft. The in-phase scattering, by the parallel planes of atoms in the crystal, of X-rays incident upon it is described by Bragg's law. For first order 'reflection',

$$\lambda = 2d \sin\theta_i \qquad (84)$$

where λ is the X-ray wavelength, d the interplanar spacing of the crystal and θ_i the angle of incidence. Different crystals are therefore suitable for particular ranges of wavelength, which correspond to particular atomic weight ranges. The crystals fitted to this

instrument are ODPB (lead stearate), TAP (thallium acid phthalate), PET (penta erythritol) and LiF (lithium fluoride) which are used for increasing atomic weight ranges.

The response of the microprobe depends on several factors: the accelerating voltage, probe current, surface roughness (section 3.5.4), element, spectrometer crystal type, temperature etc. In order to excite X-rays from a given line the accelerating voltage must exceed the excitation potential of the line, but to get a satisfactory count rate it should be about three times the excitation potential. The count rate is roughly proportional to the probe current but the relationship is not strictly linear so the probe was calibrated using the current to be used for the actual analyses - 10nA in this case. In fact the response increases more than linearly with probe current. The X-ray photons emitted from the sample are 'reflected' through different angles by the spectrometer crystal depending on the crystal d-spacing (itself temperature dependent) and the wavelength of the radiation which is characteristic of the elemental line, as indicated in equation (84). In order to analyse a particular element, the crystal is positioned so as to allow only X-rays from that elemental line to pass through the window of the counting chamber. There each photon generates a cascade of argon ions (the gas mixture is 90% Ar 10% CH_4) which generate a pulse due to the high voltage between the cylindrical walls and the central wire of the chamber. The background radiation must also be accounted for in any quantitative analysis. This arises due to the emission of photons by electrons which collide with atoms and decelerate. During calibration or analysis the count rate is measured at the crystal angle of interest. The crystal is then deflected slightly to measure the background count - the extent of the

deflection being as small as possible to count the relevant background signal consistent with the need to find a 'clean' area, ie. a crystal position where no lines are expected from any of the other elements present in the sample.

3.5.4 Sample Surface Preparation and Quantitative Analysis

For quantitative analysis it is essential to have as highly polished a surface as possible. A description follows of the procedure for mounting the samples and preparing the sample surface.

The granules were rubbed down on very fine sand paper before being sealed with araldite into short threaded brass tubes of about 4mm internal diameter. The samples were then further rubbed down on dry carborundum (silicon carbide). Although a carborundum slurry is more abrasive than dry carborundum, the former was not used because preliminary investigation found the absorbent to be very prone to 'plucking' in the presence of water. ('Plucking' is the name given to the removal of solid particles from the surface leaving small craters. It is thus highly undesirable if a uniformly smooth surface is to be achieved.) A coarse carborundum (grade 180) was used to accelerate the process of rubbing down to the desired level. The sample was then cleaned with petroleum ether. Further rubbing on finer grades of carborundum (grades 400 and/or 600) produced a flatter surface. Prolonged rubbing, however, led to a deterioration in the quality of the surface. This is probably a result of the large difference in hardness between the absorbent and the araldite and brass, which tends to lead to a retraction of the absorbent surface below the level of the araldite and brass. The absorbent surface itself develops significant relief as

the zinc oxide is rubbed down more readily than the small grains of cement distributed through it. These differences in hardness greatly restrict the quality of surface which can be achieved and this has implications for the precision of any quantitative analysis as discussed below. Therefore, after only a brief rubbing down on the finer carborundum, the sample is polished for 10-20 seconds using diamond pastes having particle sizes of 14, 6, 1 and 0.25 microns. Geological samples for microprobe study are usually cleaned in an ultrasonic bath to remove any impurities resulting from the preparation process. This treatment was found to be unsuitable for the absorbent samples, however, as it led to destruction of the carefully prepared surface and to substantial structural damage to the granule. It is very likely therefore that traces of the fine carborundum and diamond paste remain on the sample surface.

A very flat and highly polished surface is desirable because any surface irregularities will affect the accuracy of the calculated matrix corrections. These corrections allow the calculation of elemental concentrations from specimen/standard intensity ratios, and depend on

- the absorption of characteristic X-rays by material in the path of the X-rays,
- the enhancement of the X-ray lines due to fluorescence by other lines and by the continuum,
- the loss of X-ray intensity due to electron backscattering
- the variation in the efficiency of X-ray production which is a function of atomic number.

The extents of X-ray absorption and electron backscattering are particularly affected by surface irregularities. (In fact, an electron detector in front of the specimen is often used to pick-up the variation in the backscattered electrons, and a rastered image

obtained from this signal gives topographical information which can be useful in selecting a point for analysis.) In order to prevent charge build-up on the surface, samples must be coated with a fine layer of carbon. Carbon is commonly used because its low atomic number means that the coating does not contribute significantly to the absorption of generated X-rays. A small quantity of colloidal graphite ensures a conducting path from the sample to the holder.

3.5.5 Analytical Methods

Two different but complementary methods of analysis have been used. The first is to dedicate each spectrometer to the collection of X-rays of a particular wavelength, corresponding to an element of interest. A line scan is then set up by selecting the start and end points of the scan, the count time and the number of steps up to a maximum of 1024. The scan then proceeds by alternately moving the stage on which the samples sit, and analysing for the specified count time on each of the four spectrometers. The data recorded are just the four count rates for each step along the scan line. Thus information is obtained about the distribution along the scan of the elements studied, and correlation of the data for the different elements may indicate the presence of inclusions of different composition from the bulk material or of the presence of pores and large scratches in the surface. The drawback with this kind of analysis is that it is not quantitative because no measurement of the background radiation is made.

The second kind of analysis is point analysis. This is quantitative and any number of elements may be examined for. For the present work spectrometer 1 was used to analyse for aluminium and silicon, spectrometer 2 for sulphur, spectrometer 3 for calcium and titanium and

spectrometer 4 for zinc and iron. The choice of the distribution of the elements amongst the spectrometers is determined by the crystals in place, which is itself dependent on the variety of elements being monitored. The choice of analysis points located close to the line of a scan allows some quantifying of the profiles of the elements obtained from the scan. The count time used for a point analysis was 30 seconds for each element (except sulphur for which the count time was 60 seconds). This compares very favourably with the count time used for each point of a line scan, generally 0.5-5 seconds. One means of analysis which combines the merits of both the line and point analyses is the automatic point analysis which can be set up to do point analyses at fixed increments along a specified line. The disadvantages of this are that it is very time-consuming and, for a sample with a poor surface, an analysis may be done on a very poorly polished part of the surface which would not have been selected if the analysis had been manually controlled.

Electron bombardment of a specimen can cause surface damage due to the large temperature rise at the point of impact of the beam. To minimise such damage, which hinders quantitative analysis through its destruction of the flat surface and possible selective removal of material components such as water and carbon dioxide, a fairly low probe current of 10nA has been used in this work.

3.6 Ion Microprobe

Secondary ion mass spectrometry (SIMS) has been used to analyse the distribution of oxygen and sulphur in samples of sulphided absorbent. In this technique a beam of ions impinges on the sample surface causing a sputtering process to occur. Most of the sputtered

particles are neutral atoms, but a minority are ions and these may be focused into a secondary ion beam and analysed using a mass spectrometer.

The sputtering yield is a function of the composition of the sample, the primary ion source material, the energy of the incident ions as well as the angle of incidence of the primary beam and the orientation of crystalline samples. The variation of the yield with atomic number correlates well with the extent of the d-orbital occupancies, increasing with increasing filling of the orbitals. This has been explained[10] in terms of the more open structure of elements with low d-level filling, which is likely to increase the penetration depth of the primary ions, thus reducing the probability that surface particles will be etched.

The secondary ion emission process is complex as each component in the sample yields both singly and multiply-charged ions as well as molecular ions.[11] The mass spectrometer sorts the ions by mass-to-charge ratio and this can lead to difficulties in identification in samples where a large number of elements are present, and to a requirement for a high mass resolving power. This is a measure of the instrument's ability to resolve adjacent masses. These problems can also arise where the number of elements present in the sample is quite small, provided their respective masses are related by simple multiples. Thus, for the system of interest, where the principal elements present are oxygen, sulphur and zinc, which have atomic masses of 16, 32 and 65 respectively, reasonable resolving power is required to distinguish the singly charged sulphur and the singly charged molecular oxygen species. Improved resolution of mass peaks, achieved by narrowing the slits of the mass spectrometer, is, however, attained at the expense of sensitivity.

It is possible to use either positively or negatively charged primary ions and to select the polarity of the ions which are accelerated into the mass spectrometer chamber. A caesium positive ion (Cs^+) source has been used in this study with acceleration of negatively charged secondary ions. A reported comparison of such a system with one having an oxygen negative ion (O^-) source with acceleration of positive ions,[12] found that the caesium source gave preferential yields of electronegative species. Zinc was found to be barely detectable. The reverse is the position where O- bombardment is used. The Cs^+ source was selected for this study in order to investigate any correlation between the distributions of oxygen and of sulphur.

A method of analysis using the ion microprobe which finds wide applicability in the fields of semiconductivity and thin films is that of depth profiling. Where the erosion rate is accurately known, this gives depth concentration profiles of the species of interest. The present work has been done on the polished flat surfaces of hemispherical sections of granules precisely in order to investigate any concentration gradients through the granules. These are, however, much more easily and rapidly investigated by performing automatic point analysis scans along a diameter or radius on the surface.

The ion microprobe is still at a developmental stage, and although calibration and quantitative analysis are possible, these require both very highly polished surfaces and significant computing resources. Only semi-quantitative data, indicating the variation of component concentrations, are therefore presented with no estimation of absolute concentrations.

3.7 Scanning Electron Microscope

In a scanning electron microscope (SEM) a focused beam of high energy electrons is scanned over the surface of a solid sample. The interactions of the beam with the sample are complex and result in a number of physical interactions any of which may be used as a means of studying the sample.[13] The uses of the characteristic and continuum (background) X-rays in the analysis of chemical composition have already been mentioned (section 3.5). The collision of primary electrons with loosely bound outer electrons in the sample may cause the ejection of a secondary electron. If this secondary electron recombines with a hole formed during the scattering process, a photon having a wavelength in the visible or near infra red spectrum is generated. This phenomenon is known as cathodoluminescence and may also be used to investigate the sample composition. If, however, the secondary electron has sufficient energy and is produced within about 100Å[14] of the surface, it may escape from the sample and can be collected, together with any backscattered primary electrons, and used to give topographical information about the sample. This last is the use to which the SEM has been put in this work. As for the ion probe analysis, the sample must be coated with a thin film of gold of about 100Å in thickness to prevent charging of the sample.

3.8 Zinc Analysis

Zinc analyses were performed on two basic zinc carbonates. The carbonate sample was dissolved in dilute nitric acid and the pH of the solution adjusted to 10.5 by addition of ammonia and ammonium chloride, which act as auxiliary complexing agents to prevent the precipitation of zinc hydroxide during titration.[15] The solution is titrated with EDTA using eriochrome black T

as indicator.

3.9 Sulphur Analysis

Quantitative sulphur analyses on sulphided absorbent samples have been performed by the iodimetric method[15] in order to determine the sulphide content of pre-sulphided samples, and as an independent check on sulphide contents calculated by numerical integration of the data on the hydrogen sulphide content of the reactor product gas. The sulphided absorbent is added to a flask containing excess iodine solution acidified with dilute hydrochloric acid. The flask is immediately stoppered. Hydrogen sulphide is liberated rapidly according to the equation,

$$ZnS_{(s)} + 2HCl_{(aq)} \rightleftharpoons ZnCl_{2(aq)} + H_2S_{(g)} \qquad (85)$$

The iodine reduces the hydrogen sulphide to elemental sulphur-

$$I_2 + H_2S \rightleftharpoons S + 2I^- + 2H^+ \qquad (86)$$

The iodine remaining in the solution is determined by titration with sodium thiosulphate using a starch solution as indicator. The conversion of iodine to iodide gives the weight of sulphur in the sample.

A 0.1N sodium thiosulphate solution was prepared and a 25ml sample of the iodine solution (KI_3) was standardised against this. Sulphided absorbent samples added to 25ml of this standardised iodine solution acidified with hydrochloric acid were also titrated with sodium thiosulphate. The difference between the two titres is directly proportional to the number of moles of sulphide ions in the sample. Measurement errors arise from the reading of the burette but more significant is likely to be the judgement of the end-point which is indicated by the loss of colour of the solution. Additional error is introduced if there is any loss of hydrogen sulphide

between addition of the sulphided sample to the acidified iodine solution and stoppering of the glass flask. Finally, for samples of the commercial absorbent, which contains cement, a residue remains after the titration which was sometimes observed still to be coloured when the solution itself had lost all trace of colour. It is therefore difficult to estimate the total error associated with the sulphur analyses and this is probably most readily done by comparison with the results of numerical integration.

3.10 Sodium Analysis

The sodium contents of two basic carbonates were determined by dissolution of the carbonate in sulphuric acid, and aspiration of the solution into a flame photometer.

REFERENCES

[1] Dressler M., in
"Detectors in Gas Chromatography", ch.5
Sevcik J. (ed)
Journal of Chromatography Library, vol.4
Elsevier, Amsterdam (1975)

[2] Perkin Elmer Model 8400 Gas Chromatograph
Operator's Manual

[3] Pritchard C.L.
Personal communication

[4] Levenspiel O.
"Chemical reaction engineering"
John Wiley & Sons, New York (1972)

[5] Wetherill G.B.
"Intermediate statistical methods"
Chapman and Hall, London (1981)

[6] Gregg S.J., Sing K.S.W.
"Adsorption, surface area and porosity",ch.2
Academic Press, London (1967)

[7] Ruthven D.M.
"Principles of Adsorption & Adsorption
Processes", ch.2
John Wiley & Sons, New York (1984)

[8] Denny P.J.
Personal Communication

[9] Reed S.J.B.
"Electron microprobe analysis"
Cambridge University Press, Cambridge (1975)

[10] Colby J.W., in
"Practical scanning electron microscopy", ch.14
Goldstein J.I., Yakowitz H. (eds)
Plenum, New York (1976)

[11] Castaing R., Slodzian G., in
"Electron and Ion Beam Science and Technology,
Sixth International Conference"
Bakish R. (ed)
Electrochem. Soc., Inc., Princeton N.J.

[12] Storms H.A., Brown K.F., Stein J.D.
"Evaluation of a caesium positive ion source for
secondary ion mass spectrometry"
Anal. Chem. 49(13), 2023-30 (1977)

[13] Hearle J.W.S., Sparrow J.T., Cross P.M.
"The use of the scanning electron microscope"
Pergamon Press, Oxford (1972)

[14] Goldstein J.I., in
"Practical scanning electron microscopy",ch.3
Goldstein J.I., Yakowitz H. (eds)
Plenum, New York (1976)

[15] Skoog D.A., West D.M.
"Fundamentals of analytical chemistry"
Holt, Rinehart & Winston, London (1970)

CHAPTER 4

EXPERIMENTAL RESULTS

The results of sulphiding experiments - performed to investigate the influence of a number of factors on the rate of sulphiding of zinc oxide-based absorbents - are detailed herein. Results of electron and ion microprobe analyses to determine the sulphur distribution in sulphided particles, and information from physical and chemical analyses of the absorbents on specific surface area and absorbent composition are also presented.

4.1 Characterisation of Absorbents

Most of the experimental runs have been performed on the ICI low temperature absorbent '75-1'. This material is prepared commercially from a precursor by calcination at about 250°C for about 10 minutes. The composition of the precursor is approximately 82% of a commercial Basic Zinc Carbonate (BZC) and 18% binder. The BZC was thought to consist of two basic carbonates with the molecular formulae, $Zn_5(OH)_6(CO_3)_2$ (hydrozincite) and $Zn_4CO_3(OH)_6H_2O$ in roughly equal proportions, however, re-examination of thermal desorption and X-ray diffraction spectra suggests that it may only consist of poorly crystalline hydrozincite.[1] The binder used is a calcium aluminate cement. If the basic carbonates of the precursor are fully decomposed on calcination, then the composition of 75-1 by weight is: 76.8% high surface area zinc oxide (derived from the BZC) and 23.2% binder. In fact, not all of the carbonate is decomposed and the bulk of the residual carbonate is known to be present as calcium carbonate.[1] A batch of 75-1 thus prepared was obtained from ICI. The majority of the sulphiding runs have been done on 300-710μ 75-1 particles, this size range being selected as a result of preliminary

experiments on the effect of particle size on the reaction rates (section 4.3).

There will of course be some variation in composition and structural properties such as porosity and strength between individual granules. Screened material is therefore prepared in batches sufficient for 10-15 experimental runs, with the objective of minimising the differences in physical and chemical properties between reactor samples by using a large number of granules in a single preparation.

Sulphiding runs have been performed on a number of other absorbents. The absorbents used and the purpose of the various studies are detailed below.

1. The BZC was pelleted, crushed and screened to give the desired particle size fraction. It was then calcined under vacuum at 250°C for one hour and the resulting zinc oxide used as an absorbent to provide an indication of the effect of the added cement and low surface area zinc oxide in 75-1.
2. Sodium-free zinc oxide was prepared in order to determine whether sodium ions present in the BZC influence the rate of sulphiding. Zinc basic acetate ($Zn_4O(OAc)_6$) was hydrolysed to give zinc hydroxide which was then carbonated to give basic zinc carbonate. The zinc oxide was obtained by following the same calcination procedure as was used for the BZC.
3. Uncalcined BZC which had been pelleted, crushed and screened was used as an absorbent to compare the characteristics of the oxide and basic carbonate as absorbents.
4. Samples of 75-1 were heat-treated under vacuum at either 250 or 350°C and the resulting materials compared with each other and with the untreated 75-1 as absorbents.
5. Samples of the 75-1 precursor were calcined under vacuum at either 250 or 350°C for one hour. The calcination temperature is known to affect the specific surface area of the material thus prepared, with the specific surface area being maximised at a calcination temperature of 250°C. These materials were used to investigate the effect of the specific surface area on the rate.
6. 75-1 of the particle size range of interest was pre-sulphided during the course of either two or four

days sulphiding experiments in the sulphiding bed (R2) downstream of the reactor (Figure 3.1). These materials were then used as absorbents in order to study the rate behaviour at relatively high sulphur levels.

Table 4.1 gives some compositional and physical information about the absorbents.

4.2 Rate Behaviour during a Sulphiding Run

Figure 4.1 illustrates the typical variation of hydrogen sulphide content in the reactor outlet stream as a function of time.[9] The reactor feed stream analyses are also plotted to give an indication of the stability of the detector during the experimental period. The corresponding plot of the water content of the reactor outlet stream for the same experimental run is given in Figure 4.2.

The reaction rate[10] is initially very high but falls off rapidly giving an approximately constant rate after some time. Experimental run 68, illustrated in Figures 4.1 and 4.2, was performed on the commercial ICI absorbent '75-1' which contains about 77% high surface area zinc oxide by weight. Using this figure for the mean zinc oxide content of the absorbent allows the calculation of the absorbent zinc oxide conversion by numerical integration. (Verification of the validity of information derived from numerical integration is achieved by sulphur analysis of the discharged absorbent (section 4.9).) During the initial unsteady state rate period the rate of conversion of the solid absorbent is high but falling rapidly. At this stage of the reaction

---

[9]Sample output for experimental run 68 is given in Appendix D.

[10]Note that all reaction rates, except where explicitly stated to be otherwise, are specific rates calculated on the basis of the initial weight of sulphur-free absorbent used in the run.

Table 4.1: Summary of physical and compositional information for the absorbents studied.

Absorbents	Composition (*1)	Form	SSA/ m^2g^{-1}	Comments
(0) 75-1 precursor	81.8% BZC 18.2% binder	NA	NM	No sulphiding experiments performed on this material
(1) 75-1	Composition deduced from 0: 76.9% high SA ZnO 23.1% binder By analysis: 2% carbonate	300-710μ size fraction selected by crushing and screening whole granules	55	Prepared commercially by calcination of the precursor at about 250°C for a few minutes
(2) Sulphided 75-1	9.3-9.5% sulphur by weight	As for 1	30	Sulphided after particle screening
(3) Commercial Basic Zinc Carbonate	1:1 ratio of $ZnCO_3.3Zn(OH)_2.H_2O$ & $2ZnCO_3.3Zn(OH)_2$	Pelleted, crushed and screened	31	
(4) Absorbent prepared by calcination of 75-1(*2)	4.9% weight loss, of which 3.9% H_2O 1.0% CO_2 Precursor: 1.3% CO_3	Size fraction selected prior to calcination	45	Samples calcined at 250°C or 350°C
(5)(*3) Absorbent prepared by calcination of the 75-1 precursor	i)20.1% weight loss, of which 11.3% H_2O 8.8% CO_2 ii)23.0% weight loss, of which 13.3% H_2O 9.7% CO_2 Precursor: 13.3% CO_3	As for 4	i)100 ii)71	Samples calcined at i)250°C ii)350°C

Table 4.1 cont'd

Absorbents	Composition (*1)	Form	SSA m^2g^{-1}	Comments
(6) Calcined Basic Zinc Carbonate	25.5% weight loss, of which 11.9% H_2O 13.6% CO_2 Precursor: 18.5% CO_3	Size fraction selected, calcined then screened to remove fines	90-110	
(7) Na-free zinc oxide prepared from zinc basic acetate	26.6% weight loss, of which 13.0% H_2O 13.6% CO_2 Precursor: 18.5% CO_3	As for 6	35	Prepared by hydrolysis of $Zn_4O(OAc)_6$ to $Zn(OH)_2$, followed by carbonation and calcination

Note:

(*1) For absorbents 5,6 and 7 details of the weight losses which accompanied calcination of the basic carbonate precursors are given. This is to allow comparison of the basic carbonate precursors. Clearly the presence of inerts in the '75-1' precursor (absorbent 0) reduces the percentage weight loss during calcination. From the amount of carbon dioxide evolved, the minimal carbonate content of the precursor is calculated. Note that carbonate represents 21.9% w/w of hydrozincite and that complete decomposition of pure hydrozincite to zinc oxide will occur with a weight loss of 25.9% of which 9.8% is water and 16.1% carbon dioxide. Where the measured weight loss differs significantly from this, the cause may be any one or a combination of (a) incomplete decomposition, (b) the presence of adsorbed water on the precursor, or (c) the presence of some other basic carbonate. A sample of '75-1' (absorbent 1) was subjected to the same calcination procedure to obtain absorbent 4, and the corresponding small weight loss is given.

(*2) All laboratory calcinations were done in vacuo by ramping the temperature from ambient at around 10°C/min to the maximal temperature, which was maintained for one hour.

(*3) Absorbents 1 and 5 were both prepared by calcination of the 75-1 precursor. They differ only in the timing and conditions of the calcination.

Figure 4.1: Variation with time of the flowrate of hydrogen sulphide from the reactor during Run 68.

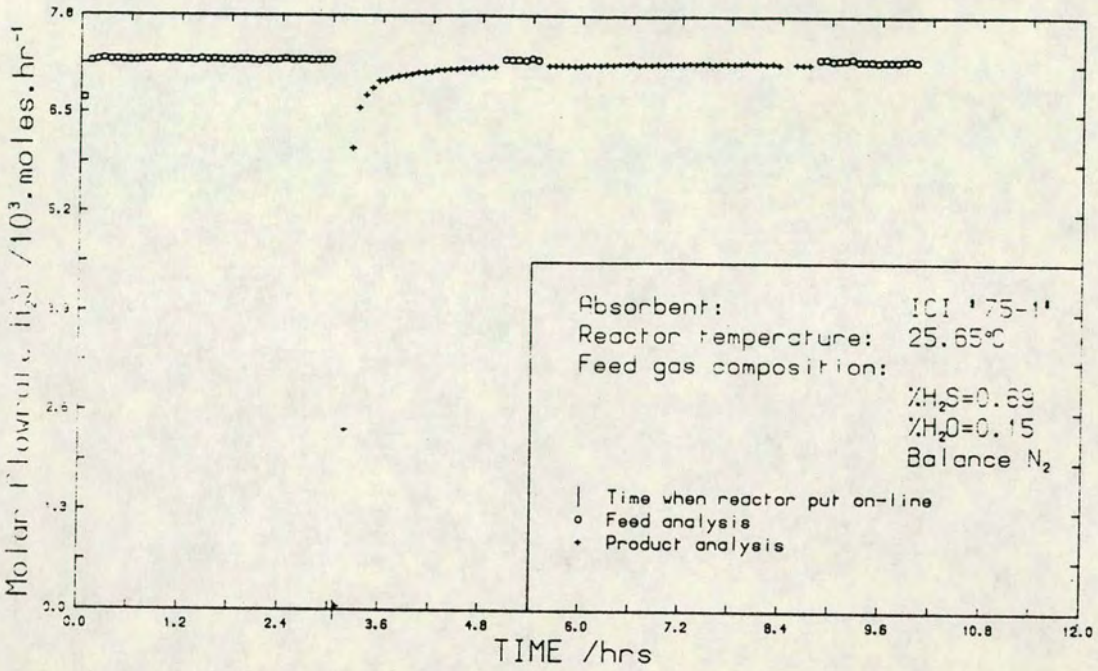

Figure 4.2: Variation with time of the flowrate of water from the reactor during Run 68.

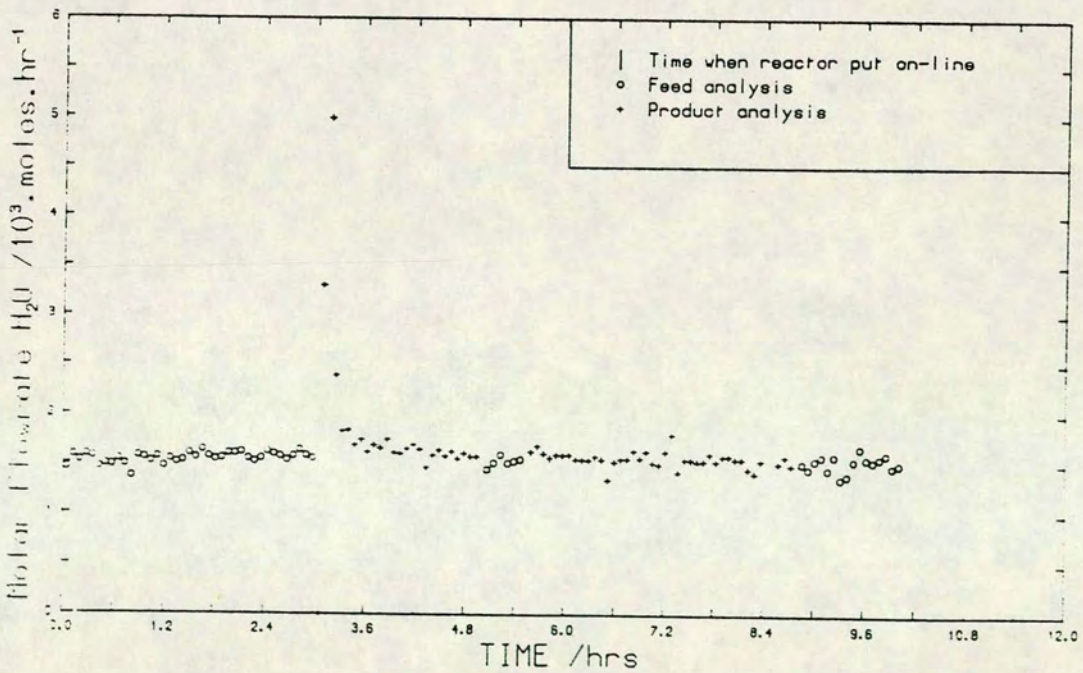

the absorbent composition is changing most rapidly. Table 4.2 summarises the decaying rate behaviour in terms of conversion-time data. The rate of absorbent conversion is observed to be very high during the first hour after the reactor is put on-line while the subsequent marginal increases in conversion in succeeding hours are an order of magnitude smaller. In particular, if the absorbent has a surface site density of 10^{19}sites.m^{-2}, then for the measured specific surface area of $55m^2g^{-1}$, 3.72% of the zinc oxide anions are exposed on the surface. If there is no pore diffusion limitation on the reaction rate, more than 98% of these surface oxygens will have reacted by the time the first product sample is injected into the gas chromatograph. If, however, the absorbent surface exposes a distribution of the different crystallite faces and if the chemical reactivity of these different crystallite faces to hydrogen sulphide varies appreciably then reaction of the bulk zinc oxide will already be underway by the time of the first product analysis. Thus the very rapid but decreasing rate observed during the first hour of reaction corresponds to a reaction which is not confined to the absorbent surface but extends beneath the surface to a depth of several atomic layers.

The latter, constant rate period may be regarded as a pseudo-steady state (pss) period. For several hours the conversion of hydrogen sulphide is approximately constant and very small, being less than 5%. The solid absorbent undergoes very slow conversion as calculated by numerical integration of the hydrogen sulphide data (Table 4.2). Thus, during the period of about 2-3 hours during which the pss is monitored, the conversion of the absorbent is generally less than 2%. This low conversion is the justification for the use of the term 'pss' to denote the reaction behaviour at this stage. Clearly the situation is not that of a true steady state

Table 4.2: Conversion-time data for Run 68. (Feed gas composition: .69% H_2S, .15% H_2O, balance nitrogen. Reactor temperature: 25.6°C. Absorbent: 75-1)

time/ hrs (*1)	absorbent conversion (*2)	absorbent %sulphur w/w	time/ hrs	absorbent conversion	absorbent %sulphur w/w
0.03	3.67	1.10	3.00	21.28	6.23
0.11	10.62	3.16	3.08	21.36	6.25
0.19	14.10	4.17	3.16	21.43	6.28
0.26	15.15	4.48	3.23	21.51	6.30
0.34	15.79	4.66	3.31	21.58	6.32
0.42	16.28	4.80	3.39	21.64	6.34
0.50	16.66	4.91	3.46	21.70	6.35
0.57	16.98	5.01	3.54	21.76	6.37
0.65	17.28	5.09	3.62	21.82	6.39
0.73	17.54	5.17	3.69	21.89	6.41
0.81	17.81	5.24	3.77	21.96	6.42
0.89	18.04	5.31	3.85	22.02	6.44
0.97	18.24	5.37	3.93	22.08	6.46
1.04	18.43	5.42	4.00	22.14	6.48
1.12	18.62	5.47	4.08	22.20	6.49
1.20	18.78	5.52	4.16	22.25	6.51
1.27	18.94	5.57	4.23	22.30	6.52
1.35	19.09	5.61	4.31	22.36	6.54
1.43	19.23	5.65	4.39	22.40	6.55
1.51	19.36	5.69	4.47	22.45	6.56
1.58	19.49	5.72	4.54	22.50	6.58
1.66	19.61	5.76	4.62	22.55	6.59
1.74	19.72	5.79	4.70	22.60	6.61
1.81	19.84	5.82	4.77	22.65	6.62
1.89	19.95	5.85	4.85	22.70	6.64
2.54	20.76	6.09	4.93	22.74	6.65
2.62	20.85	6.11	5.00	22.79	6.66
2.69	20.94	6.14	5.08	22.83	6.67
2.77	21.02	6.16	5.16	22.88	6.69
2.85	21.11	6.18	5.23	22.93	6.70
2.92	21.20	6.21			

Note:

(*1) The time given is the time elapsed since putting the reactor on-line.

(*2) Absorbent conversion is calculated on the basis of zinc oxide accounting for 77% by weight of the unsulphided absorbent.

because of the continuous consumption of the absorbent. Differential analysis of the rate data is valid for the pss period. It is interesting to note, however, that the sulphide content of the absorbent at pss is about 6.6% by weight (from numerical integration) which corresponds to an absorbent conversion of 22.5%. It is immediately apparent therefore that it is not possible to pre-select the absorbent conversion at which the pss rate will be measured and that it is unlikely to be possible to obtain pss behaviour on unsulphided zinc oxide. This subject is discussed more fully in relation to the effects of the water and hydrogen sulphide partial pressures (section 4.6).

Numerical integration of the water analyses provides an estimate of the amount of water evolved during the run. Given the stoichiometry of the reaction, this quantity might be expected to be approximately equal to the number of moles of hydrogen sulphide absorbed by the sample in the same period as calculated by numerical integration. The calculated number of moles of water evolved is expressed as a percentage of the number of moles of hydrogen sulphide absorbed in Table 4.3 for several experimental runs. This percentage is less than 100% for all of the runs but varies widely between runs. There is, however, no apparent correlation between the percentage of the amount of water which should theoretically be evolved and either the feed composition[11] or the initial state of the absorbent - whether pre-sulphided or not. It is noteworthy, however, that the accuracy of the GC analyses for water is greatly inferior to that for hydrogen sulphide

[11] A scatter plot of the hydrogen sulphide content of the feed versus its water content with 100(y/x)% as parameter indicates no trend of this quantity with either water content or hydrogen sulphide content of the feed.

Table 4.3: A comparison of the quantity of water evolved during reaction with the quantity of hydrogen sulphide absorbed, both calculated by numerical integration of the GC data.

Experimental Run no.	18	47	48	50
Absorbent	75-1	75-1	75-1	sulphided 75-1
Feed $\%H_2O$	.17	.47	.16	.49
Feed $\%H_2S$	.43	.51	.06	.06
Moles H_2S absorbed (x)	1.27×10^{-3}	1.71×10^{-3}	9.26×10^{-4}	2.63×10^{-4}
Moles H_2O evolved (y)	5.54×10^{-4}	5.63×10^{-4}	5.58×10^{-4}	1.89×10^{-4}
100(y/x)%	43.8	33.0	60.3	71.8

Experimental Run no.	52	53	63	69
Absorbent	75-1	sulphided 75-1	calcined 75-1	75-1
Feed $\%H_2O$	.48	.49	.14	.27
Feed $\%H_2S$	.06	.06	.22	.69
Moles H_2S absorbed (x)	8.14×10^{-4}	2.35×10^{-4}	1.43×10^{-3}	1.72×10^{-3}
Moles H_2O evolved (y)	3.30×10^{-4}	6.88×10^{-5}	3.77×10^{-4}	5.06×10^{-4}
100(y/x)%	40.6	36.5	26.4	29.4

Note:

The number of moles of hydrogen sulphide absorbed and of water evolved are calculated by numerical integration of the peak area data from the gas chromatograph up to the time of the last product analysis in each run.

analyses (section 3.1.4).

4.3 Particle Size Effect

In solid-catalysed reactions, experiments to investigate the variation of the observed reaction rate with size of the catalyst particles provide information on the rate controlling resistance.[2] For first order reactions under conditions where pore diffusion is rate controlling, the effectiveness factor, η, which is defined as the ratio of the observed rate to the rate for the situation where there is no pore diffusion limitation, is given by

$$\eta = [\tanh(mL)]/mL \qquad (87)$$

where

$$\phi = mL = L\sqrt{(k_v/D_e)} \qquad (88)$$

and ϕ is the Thiele modulus, k_v and D_e are the kinetic rate constant (s^{-1}) and the effective diffusivity respectively. L is a measure of the particle size being, for any particle shape, the ratio of the particle volume to its external surface area. Thus, in the regime of 'strong pore diffusion control', η is proportional to 1/mL and the reaction rate is inversely proportional to the particle size. Such a test of the effect of particle size on the reaction rate is also applicable to gas-solid noncatalytic reactions. Experiments were performed therefore with the objective of determining how small a particle size was required to avoid operating in a regime of pore diffusion control. The results indicate that a size effect is important both during the initial unsteady state and the later pseudo-steady state period.

During the unsteady state period of the reaction the effect of pore diffusion in limiting the reaction rate over large particles is observed, as has been described

for catalytic reactions. Shortly after the start of the reaction, however, the rate is observed to be higher on the larger particles as Figure 4.3 indicates. At this stage, the conversion of the bed of large particles is necessarily less than that of the bed of small particles. More interesting, however, is the observation that the intrinsic rate of reaction of the large particles exceeds that of the small particles even when the conversion of the former is equal to or greater than that of the latter. These results are considered in more detail below and in the next chapter (section 5.3).

Figure 4.3 is a plot of the unsteady state rate behaviour for the five particle sizes tested. Beds of the different sizes of particles were exposed to gas of the same composition and flowrate at the same reactor temperature. Evidently the pore diffusional resistances of the whole granules and of the 1.20-1.40 mm particles restrict the initial rate to some extent, with the effect being particularly pronounced for the whole granules where the rate is significantly reduced initially. After about 20 minutes, however, the granules show a higher reaction rate than the smaller particles and the time taken to achieve a pss rate is much increased as Figure 4.4 indicates.

Two groups of experiments were performed to investigate the effect of particle size on the rate behaviour. The experimental conditions and the reaction rates and absorbent sulphur contents at pss are presented in Table 4.4.

4.4 Comparison of Rates over 75-1 and Calcined BZC

A pair of experiments was performed in order to compare the rate of sulphur absorption of 75-1 with that of calcined BZC which is the principal constituent of 75-1.

Figure 4.3: The effect of particle size upon the flowrate of hydrogen sulphide from the reactor during the unsteady state period of the absorption reaction.

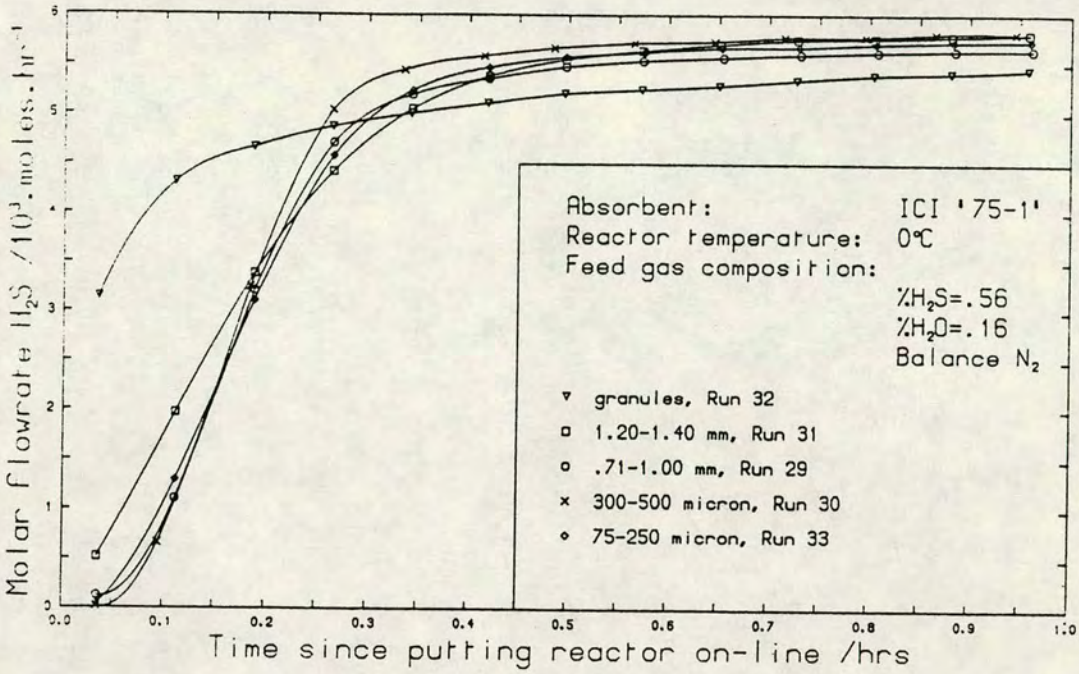

Figure 4.4: The effect of particle size on the rate of approach to a pseudo-steady state.

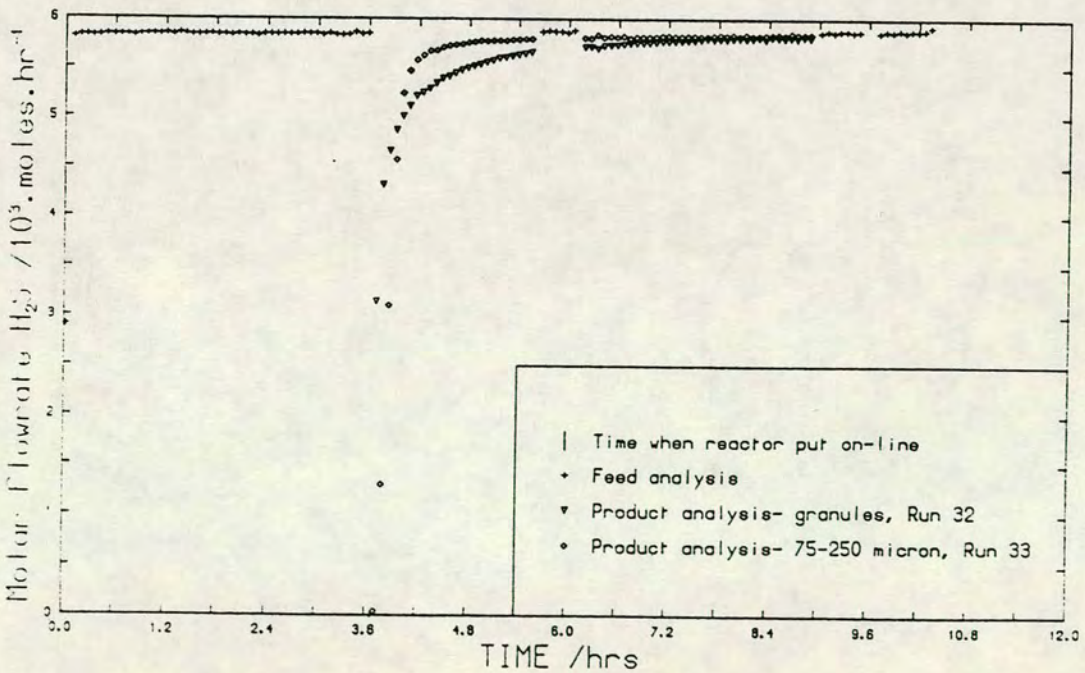

Table 4.4: The influence of absorbent particle size on the pss rate.

Experimental Run no.	15	19A	17	18
Absorbent	75-1	75-1	75-1	75-1
Particle Size /mm	granules 3-5 dia.	1.0-1.4	0.5-1.0	0.25-0.5
Reactor Temperature/°C	0	0	0	0
Feed $\%H_2O$	.19	.17	.18	.17
Feed $\%H_2S$	.43	.43	.42	.43
Pss Rate/ $mol(g_{abs})^{-1}s^{-1}$	NM(*1)	2.0×10^{-8}	2.1×10^{-8}	1.7×10^{-8}
Absorbent %S w/w at pss	7.20	6.63	6.69	6.53
Absorbent %conversion at pss	24.7	22.7	22.9	22.3

Table 4.4 cont'd

Experimental Run no.	32	31	29	30	33
Absorbent	75-1	75-1	75-1	75-1	75-1
Particle Size/mm	granules 3-5 dia.	1.2-1.4	0.71-1.0	0.3-0.5	0.075 -0.25
Reactor Temperature/°C	0	0	0	0	0
Feed $\%H_2O$	.16	.16	.17	.16	.16
Feed $\%H_2S$	.57	.56	.56	.56	.57
Pss Rate/ $mol(g_{abs})^{-1}s^{-1}$	2.3×10^{-8}	2.2×10^{-8}	1.7×10^{-8}	1.9×10^{-8}	1.9×10^{-8}
Absorbent %S w/w at pss	6.70	6.94	6.47	6.43	6.49
Absorbent %conversion at pss	22.9	23.8	22.1	22.0	22.2

Note:

(*1) Due to the fact that the reaction with larger absorbent particles takes longer to achieve a pseudo-steady state, experiment 15 was finished before the system reached pss. The measured rate at the end of the run was $2.9\times10^{-8}mol(g_{abs})^{-1}s^{-1}$. The absorbent sulphur content and conversion given describe the state of the absorbent at the time of calculating this rate.

The purpose of the runs was to discover whether the rates expressed per gram of high surface area zinc oxide were similar for the two materials. Such a test should ideally be performed on materials which have been prepared identically in other respects. This comparison, however, is complicated by the fact that the 75-1 is prepared by granulation whereas the BZC-derived particles of zinc oxide were prepared by pelleting powdered BZC, crushing the pellet formed and screening out the desired particle size fraction which was then calcined. The structural differences between the two absorbents may therefore be considerable, indeed the specific surface areas are very different as Table 4.5 shows. The pss rates for the two experiments were very similar although the conversion of the calcined BZC at pss was slightly higher. The specific surface areas of both materials were reduced by sulphiding with the calcined BZC showing a loss of specific surface area of more than 50%.

4.5 Comparison of Zinc Oxide and Basic Zinc Carbonate as Absorbents

A single run, run 28, was performed using uncalcined BZC as the absorbent in order to compare the efficacy of zinc oxide and basic zinc carbonate as absorbents for hydrogen sulphide. Table 4.6 details the experimental conditions and results of this run together with the results of a sulphiding experiment on 75-1, run 25, carried out under the same conditions of feed composition and reaction temperature. It is interesting to observe that while the conversion of the basic zinc carbonate is significantly higher than that of the commercial absorbent by the time a pseudo-steady state has been achieved, the pss rate over the basic carbonate is much lower whether it is expressed per gram of absorbent or per gram zinc. (Note that expressing the

Table 4.5: A comparison of rates of absorption of hydrogen sulphide by zinc oxide and by a zinc oxide based commercial absorbent, 75-1.

Experimental Run no.	13	14
Absorbent	calcined BZC	75-1
Absorbent SSA/m^2g^{-1}	89	55
Reactor Temperature/°C	0	0
Feed %H_2O	.34	.31
Feed %H_2S	.44	.43
Pss Rate/ $mol(g_{absorbent})^{-1}s^{-1}$	$2.90x10^{-8}$	$2.30x10^{-8}$
Pss Rate/ $mol(g_{ZnO})^{-1}s^{-1}$	$2.90x10^{-8}$	$2.99x10^{-8}$
Absorbent %sulphur w/w at pss	12.40	8.62
Absorbent %conversion at pss	33.6	29.8
Sulphided Absorbent SSA/m^2g^{-1}	41	41

Table 4.6: A comparison of the zinc oxide-based absorbent 75-1 and a basic zinc carbonate as absorbents for hydrogen sulphide.

Experimental Run no.	25	28
Absorbent	75-1	BZC(*1)
Particle size range/mm	0.5-1.0	0.5-1.4
Reactor Temperature/°C	0	0
Feed $\%H_2O$	.17	.18
Feed $\%H_2S$	.19	.19
Pss Rate/ $mol(g_{absorbent})^{-1}s^{-1}$	2.16×10^{-8}	0.67×10^{-8}
Pss Rate/(*2) $mol(g_{zinc})^{-1}s^{-1}$	3.50×10^{-8}	1.12×10^{-8}
Absorbent %sulphur w/w at pss	6.29	8.83
Absorbent(*2) %conversion at pss	21.5	29.3

Note:

(*1) BZC is a commercially available Basic Zinc Carbonate

(*2) The zinc-based reaction rates and the conversions of 75-1 and BZC are calculated on the basis that they are composed of 76.9% zinc oxide and pure hydrozincite respectively (Table 4.1).

rate per gram zinc indicates the relative effectiveness of zinc utilisation in different zinc-containing compounds used as absorbents.) However, the relatively negligible contribution of the pss conversion compared to the unsteady state conversion is amply demonstrated by Figure 4.5.

Whilst it might be expected that the reaction of hydrogen sulphide with basic zinc carbonate would produce carbon dioxide, as the following stoichiometry suggests,

$$5H_2S + 2ZnCO_3.3Zn(OH)_2 \rightleftharpoons 5ZnS + 8H_2O + 2CO_2 \qquad (89)$$

no carbon dioxide was in fact seen as the initial attenuation of the GC signal was set fairly high in order to reduce the size of the nitrogen peak, and the attenuation was reduced only immediately prior to the hydrogen sulphide peak. (Carbon dioxide elutes after nitrogen and before hydrogen sulphide on the Hayesep packed column.) Khalid Sohail[3], a postgraduate student in the Chemical Engineering Department at Edinburgh University, has, however, repeated the experiment and observed carbon dioxide in the product stream from the reactor.

4.6 Influence of Water and Hydrogen Sulphide Partial Pressures

In order to maintain equilibrium with respect to the adsorbed water on the absorbent, the reaction is always preceded by a period during which the reactor bed is exposed to a stream of the carrier gas containing the same partial pressure of water as is to be used in the subsequent run. The duration of this pre-treatment is determined by the time required for equilibration of the sample, indicated by the GC water analyses.

Increasing the partial pressure of water in the feed

Figure 4.5: A comparison of the pattern of solid conversion with time for a basic zinc carbonate and a zinc oxide-based absorbent.

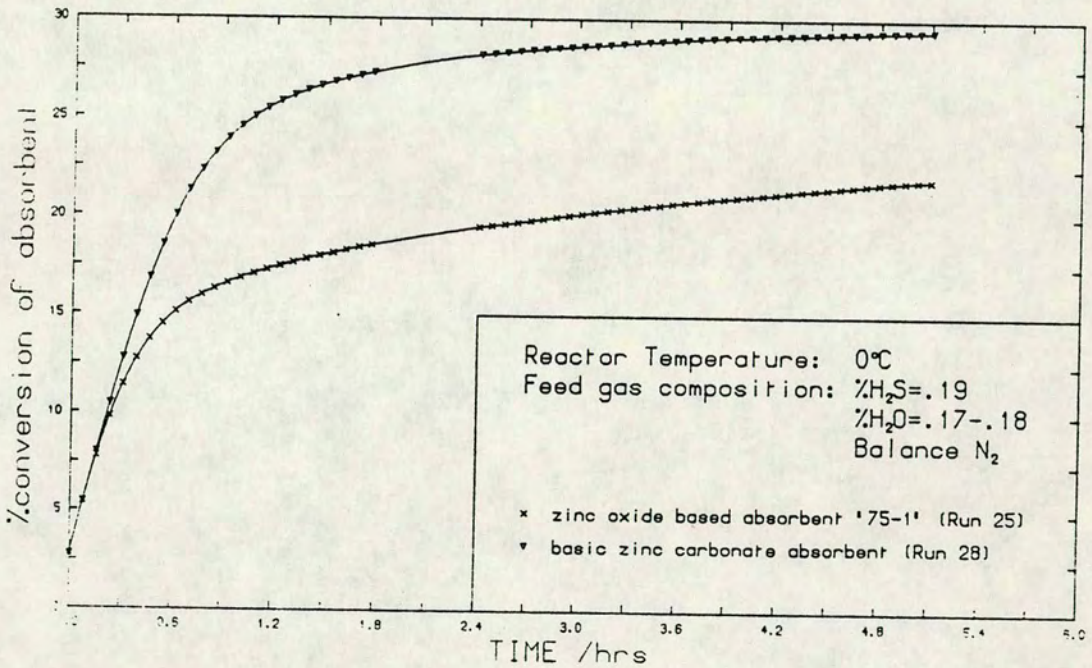

stream is observed to increase both the unsteady state and the pss rates. Figure 4.6 illustrates the effect of the water partial pressure on the unsteady state rate. The analyses for the three different runs may be superimposed because the weights of absorbent, the feed gas flowrates and the hydrogen sulphide content of the feeds are the same for the three runs. The apparent scatter of the data is greater than for the run of Figure 4.1 but this effect is due simply to the change of scale to accommodate the much lower partial pressure of hydrogen sulphide. Initially complete conversion of the hydrogen sulphide occurs on all three runs but after about 20 minutes the rates begin to decrease, this decrease being most rapid for the dry stream so that at any time, the reaction rates of the three runs decrease in the order of decreasing water content of the feed gas, viz.

$$(\text{rate})_{\text{Run 51}} > (\text{rate})_{\text{Run 48}} > (\text{rate})_{\text{Run 49}}$$

Note that Run 51 was extended in order to allow the conversion of hydrogen sulphide to drop to fulfill the conditions for differential analysis of the pss period. A fourth run, Run 52, was performed with a water content of the feed gas of .48%. In order to reduce the time taken for attainment of a pss, however, the quantity of absorbent used in the run was reduced and the analysis cannot therefore be compared graphically as in Figure 4.6.

A set of 16 runs were performed in order to investigate the effects of the partial pressures of water and hydrogen sulphide on the rate of sulphiding of 75-1. The data for these experiments are presented in Table 4.7 and the pss rates for these experimental runs are plotted in Figure 4.7 as a function of the water content of the feed. The same data are plotted in Figure 4.8 as

Figure 4.6: The effect of the partial pressure of water in the reactor feed upon the flowrate of hydrogen sulphide from the reactor.

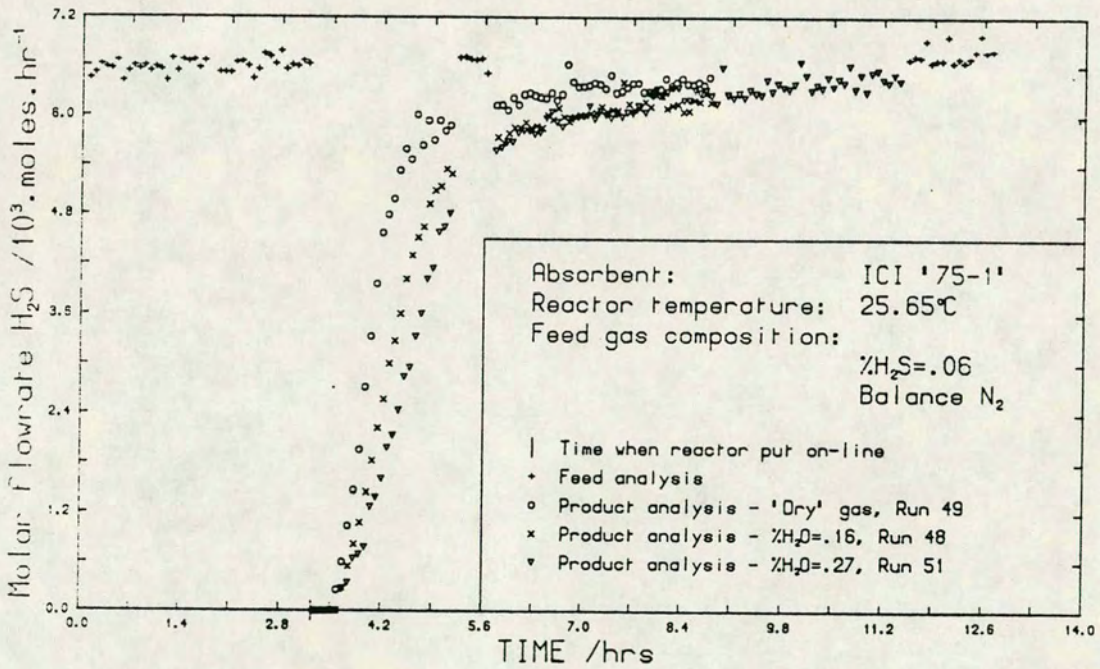

Table 4.7: Variation of the reaction rate and absorbent sulphur content at pseudo-steady state with changes in the partial pressures of hydrogen sulphide and water in the feed gas stream.

Experimental Run no.	49	48	51	52
Absorbent	75-1	75-1	75-1	75-1
Reactor Temperature/°C	25.6	25.6	25.6	25.6
Feed $\%H_2O$	0	.16	.27	.48
Feed $\%H_2S$	.06	.06	.06	.06
Pss Rate/ $mol(g_{absorbent})^{-1}s^{-1}$	1.07×10^{-8}	1.44×10^{-8}	1.55×10^{-8}	2.26×10^{-8}
Absorbent %sulphur w/w at pss	3.65	4.81	6.64	7.50
Absorbent %conversion at pss	12.3	16.3	22.7	25.8

Experimental Run no.	37	34	35	36
Absorbent	75-1	75-1	75-1	75-1
Reactor Temperature/°C	25.6	25.6	25.6	25.6
Feed $\%H_2O$	0	.15	.28	.51
Feed $\%H_2S$	.20	.20	.20	.20
Pss Rate/ $mol(g_{absorbent})^{-1}s^{-1}$	1.01×10^{-8}	1.95×10^{-8}	2.64×10^{-8}	2.68×10^{-8}
Absorbent %sulphur w/w at pss	4.55	5.65	6.60	8.55
Absorbent %conversion at pss	15.4	19.2	22.6	29.2

Table 4.7 cont'd

Experimental Run no.	44	41	42	47
Absorbent	75-1	75-1	75-1	75-1
Reactor Temperature/°C	25.6	25.6	25.6	25.6
Feed $\%H_2O$	0	.15	.27	.47
Feed $\%H_2S$	.51	.51	.51	.51
Pss Rate/ $mol(g_{absorbent})^{-1}s^{-1}$	0.56×10^{-8}	1.60×10^{-8}	1.64×10^{-8}	2.73×10^{-8}
Absorbent %sulphur w/w at pss	4.70	6.40	7.21	8.68
Absorbent %conversion at pss	15.9	21.9	24.7	30.0

Experimental Run no.	67	68	69	66
Absorbent	75-1	75-1	75-1	75-1
Reactor Temperature/°C	25.6	25.6	25.6	25.6
Feed $\%H_2O$	0	.15	.27	.47
Feed $\%H_2S$	.70	.69	.69	.68
Pss Rate/ $mol(g_{absorbent})^{-1}s^{-1}$	0.63×10^{-8}	1.84×10^{-8}	2.10×10^{-8}	2.20×10^{-8}
Absorbent %sulphur w/w at pss	5.05	6.58	7.35	8.74
Absorbent %conversion at pss	17.1	22.5	25.2	30.2

Figure 4.7: Variation of the pseudo-steady state rate with the water content of the reactor feed.

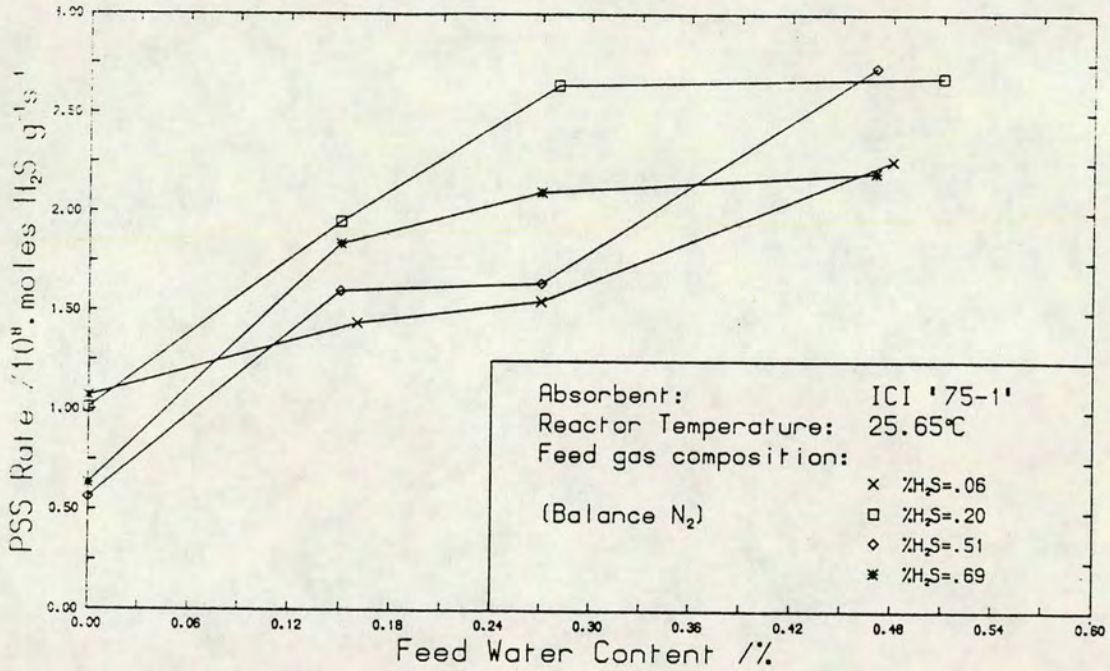

Figure 4.8: Variation of the pseudo-steady state rate with the hydrogen sulphide content of the reactor feed.

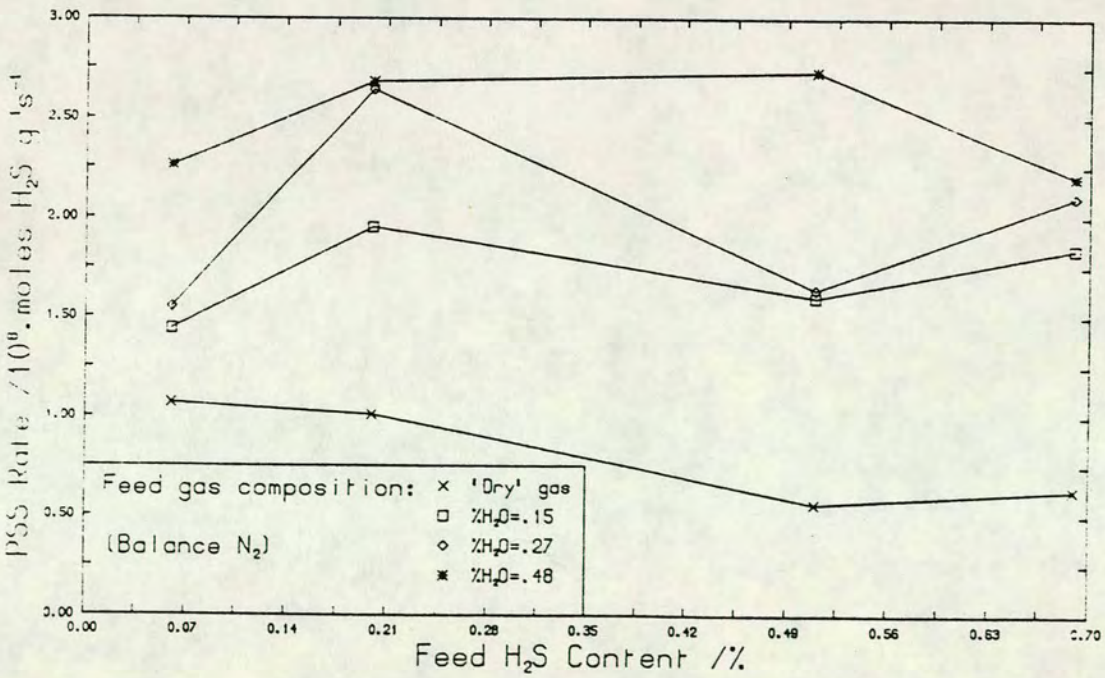

a function of the hydrogen sulphide content of the feed with the water content as parameter. It is evident that the pss rate increases with increasing water content of the feed but the precise nature of the rate dependence is not clear. In contrast, the pss rate appears almost independent of the partial pressure of hydrogen sulphide in the feed within the range considered although there may be shallow maxima in the data of Figure 4.8. The sulphide contents of the absorbents at pss have been calculated for each of these runs and are given in Table 4.7. It is observed that the absorbent sulphide content or, equivalently, the absorbent conversion at pss increases with increasing partial pressures of both water and hydrogen sulphide in the feed. It would be desirable to measure the effect on the reaction rate of changes in the feed gas composition at a constant level of absorbent conversion. As any single run indicates, however, the reaction rate decreases with progressive sulphiding of the absorbent and thus the qualitative effect of increased absorbent conversion on the reaction rate is known.[12] The observed rate increase with increased water content of the feed is therefore modified. In the case of the influence of the hydrogen sulphide partial pressure where no strong effect on the rate is seen, the interference of the absorbent sulphide content being non-constant between comparable runs is more unsatisfactory and may mask some real effect of the hydrogen sulphide partial pressure.

---

[12]Note, however, that this does not imply that the intrinsic chemical rate is proportional to the concentration of solid reactant. If the rate determining process is one of mass transfer, either of the gaseous or solid reactant, then the increase in the mean diffusional path length, which inevitably accompanies increased conversion, will result in a decreasing rate of reaction. In fact, it is widely assumed that the rate of a gas-solid noncatalytic reaction is independent of the concentration of the solid reactant, as discussed in section 2.3.2.

Results are presented in Table 4.8 of the effect of changes in the water partial pressure on the amount of adsorbed water on the absorbent as determined by microbalance experiments. The water content of the gas stream was determined using two slightly different experimental set-ups. The first is illustrated in Figure 3.5. With the by-pass valve on the U-bend closed and the U-bend immersed in a Dewar of liquid nitrogen, the water containing stream sweeps through the U-bend and any water present in the stream is condensed out. A constant and measured flowrate is passed for a fixed period of time after which the flow is stopped, the U-bend is isolated and pumped out to remove gaseous nitrogen. The U-bend is then detached and weighed. For an undiluted stream from the bubbler which was contained in a Dewar filled with an ice/water mixture, this measurement procedure gave a water content for the stream of 0.80%. Assuming that the nitrogen stream is saturated with water at the bubbler temperature, this water content corresponds to a bubbler temperature of 3.75°C. While water contents of only 0.52-0.58% were obtained in a similar system used in calibrating the gas chromatograph (Appendix B), in that case the operating pressure of the bubbler was significantly higher due to the downstream pressure drops across the capillary flowmeter and the gas sample valve of the GC. There were no significant pressure drops in the gas handling system for the microbalance. Because of occasional problems of leakage at the isolation valve upstream of the detachable U-bend which necessitated the U-bend being in place although not in use, it was decided to replace the detachable U-bend with an integral one which was removed by sealing glass constrictions. The water content of a mixed stream of 'dry' and 'wet' gas (where 'wet' gas denotes the gas stream from the bubbler) combined in the volumetric ratio 3:1 was determined

Table 4.8: Microbalance experiments to investigate the effect of temperature and water partial pressure on the amount of adsorbed water on the absorbent 75-1.

Experiment no.	1		
	Sample weight /mg	Weight gain(*1) /mg	/%
Initial sample	20.020	0.162	0.82
Temperature & composition of gas flushing sample			
0.80% H_2O in N_2 at 25°C	20.013	0.155	0.78
N_2 at 25°C	19.858	0.000	0.00
N_2 at 150°C	19.524	-0.334	-1.68
0.80% H_2O in N_2 at 25°C	19.782	-0.076	-0.38

Experiment no.	2		
	Sample weight /mg	Weight gain(*1) /mg	/%
Initial sample	20.283	0.292	1.46
Temperature & composition of gas flushing sample			
0.19% H_2O in N_2 at 9°C	20.190	0.199	0.99
0.19% H_2O in N_2 at 16°C	20.149	0.158	0.79
0.19% H_2O in N_2 at 25°C	20.109	0.118	0.59
0.19% H_2O in N_2 at 35°C	20.066	0.075	0.38
0.19% H_2O in N_2 at 45°C	20.027	0.036	0.18
N_2 at 25°C	19.991	0.000	0.00
0.19% H_2O in N_2 at 25°C	20.073	0.082	0.41

Table 4.8 cont'd

Experiment no.	3		
	Sample weight /mg	Weight gain[*1] /mg	/%
Initial sample	20.236	0.253	1.27
Temperature & composition of gas flushing sample			
N_2 at 25°C	19.983	0.000	0.00
0.80% H_2O in N_2 at 25°C	20.137	0.154	0.77
0.19% H_2O in N_2 at 25°C	20.079	0.096	0.48
N_2 at 25°C	19.983	0.000	0.00
N_2 at 400°C	19.153	-0.830	-4.15
N_2 at 25°C	19.173	-0.810	-4.05

Note:

(*1) The weight gain is expressed relative to the weight of the absorbent sample in equilibrium with a nitrogen stream at 25°C in order to give a constant standard. Note, however, that in Experiment 2 this equilibrium is only measured after temperature treatment of the absorbent - the effects of which appear to be irreversible as oppose to the reversible effects of changes in water partial pressure (section 4.6).

using this modified equipment and found to be 0.19%. This is consistent with the first measurement.

It should be noted that the initial sample weights for the three experiments, while likely to be a function of the ambient temperature and humidity, are only approximate due to the starting procedure whereby the samples are loaded with the furnace being flushed with gas rather than containing a stagnant atmosphere. The sample weight immediately begins to change rapidly (a slower weight change would be seen in a stagnant atmosphere unless the water partial pressure were in equilibrium with the sample in which case no weight change would occur) as water adsorbs or desorbs in order to achieve equilibrium between the surface concentration and the water partial pressure. In all three experiments this initial weight change is a loss and is most likely due principally to the lower humidity of the gas flushing the sample relative to the ambient atmosphere of the laboratory. In order, therefore, to allow comparison between the three experiments, the weight gains have been given relative to the weight of the sample in equilibrium with a pure nitrogen stream at 25°C.

It is clear from experiments 1 and 3 that reducing the partial pressure of water in the gas flushing the absorbent has the expected effect of causing desorption of water from the sample. These adsorption/desorption processes appear to be reversible at 25°C and are attributed to physisorbed water on the absorbent surface. Thus, the sample in experiment 3 has an initial physisorbed water content of 100(20.236-19.983)/20.236% = 1.25% by weight and that of experiment 1 a physisorbed water content of 0.81%, in addition to any sorbed water which is not removed by equilibration with a pure nitrogen stream at

25°C. Heating the sample of experiment 1 at 150°C gives a further weight loss of 1.68% relative to the initial sample weight. Earlier analysis by mass spectrometer of the gases evolved during temperature programmed decomposition of hydrozincite indicated that carbon dioxide evolution begins at around 150°C. It is known from calcination experiments on 75-1 (as used in the preparation of absorbent (4) of Table 4.1) that the absorbent contains carbonate species. These may originate from incomplete decomposition of basic zinc carbonate during the absorbent preparation or from the adsorption of atmospheric carbon dioxide onto the absorbent surface. Although the nature of the carbonate species is not well-defined, it is probable that some of the 1.67% weight loss at 150°C is due to the evolution of carbon dioxide. The more severe heat treatment of the absorbent in experiment 3 at 400°C is likely to remove all traces of chemisorbed water and carbon dioxide from the absorbent surface. The measured weight loss is 4.1% of the initial sample weight.

In the context of these figures for weight losses corresponding to various sample treatments, it is of interest to consider the number of surface sites exposed by the absorbent. For a specific surface area of $55 m^2 g^{-1}$ (Table 4.1) and an assumed surface site density of $10^{19} sites.m^{-2}$, 5.5×10^{20} sites are exposed on the surface per gram of material. Of these, half will be oxygen and half zinc ions for a sample of zinc oxide. If the surface were fully hydroxylated, the adsorbed water would represent 0.82% by weight of the sample. Mattmann's and Nagao's figures of 8.4 and 7.5 $OH^-/100Å^2$ (section 2.2.3) for the surface hydroxyl density on fully hydroxylated zinc oxide correspond respectively to sorbed water contents of 0.69% and 0.62%. Similarly, if carbon dioxide adsorbed to form a surface layer of zinc carbonate ($ZnCO_3$), the carbonate would represent 2.69% by

weight of the sample. If, however, water and carbon dioxide are adsorbed so as to form a monomolecular layer of hydrozincite ($2ZnCO_3.3Zn(OH)_2$) then the water and carbonate species present in the surface layer would represent 0.49% and 1.08% of the total sample weight respectively.

4.7 Reactor Temperature

The experiments performed to investigate the effect on the reaction rate of changes in the feed composition were carried out at a reaction temperature of 25.65°C. Further experiments have been performed at constant feed composition to study the effect of reaction temperature upon the rate. Experiments were performed at several temperatures in the range 0-45°C, the data for which are given in Table 4.9. An inverse effect of temperature on the pss rate is observed in the temperature range studied. The rate falls as the reactor temperature is raised from 0 to 25.65°C but appears to be approximately constant and independent of temperature between 25.65 and 44.8°C. The increased reaction rate at lower temperatures is also observed during the unsteady state period as reflected by the calculated absorbent sulphur contents at pss which decrease with increasing temperature. The results are presented in Table 4.8 of complementary experiments performed on a microbalance to measure the amount of water adsorbed at equilibrium on a sample of the same particle size range as was used in the rate studies. Because of the physical arrangements for control of the temperature of the balance furnace within which the sample is situated, the minimum temperature that can be maintained conveniently is about 8°C. As the absorbent sample temperature is raised, the amount of water adsorbed on the absorbent at equilibrium decreases for a given partial pressure of water in the gas sweeping the

Table 4.9: The effect of reaction temperature on the rate of hydrogen sulphide absorption by 75-1.

Experimental Run no.	54	56	55	57	58
Reactor Temperature/°C	0	16.4	25.6	35.0	44.8
Feed $\%H_2O$	.16	.15	.16	.16	.16
Feed $\%H_2S$	.21	.21	.21	.21	.21
Pss Rate/ $mol(g_{absorbent})^{-1}s^{-1}$	2.00×10^{-8}	1.83×10^{-8}	1.50×10^{-8}	1.61×10^{-8}	1.55×10^{-8}
Absorbent %sulphur w/w at pss	7.03	5.99	6.04	5.84	5.80
Absorbent %conversion at pss	24.0	20.4	20.6	19.9	19.7

furnace as experiment 2 indicates.

The physisorbed water content of the initial sample, calculated as in the previous section, is 1.46%. It is likely, however, that this figure includes some more strongly adsorbed water molecules which are removed when the sample is heated to 45°C. Such an explanation is proposed because of the observed lower sample weight after equilibration with the water/nitrogen stream at 25°C after the higher temperature dosing compared with the sample weight for the same treatment prior to the higher temperature treatment. If the difference, 0.036mg, represents more strongly bound surface water then the physisorbed water content of the initial sample is estimated to be 1.26%.

4.8 Interrupted Experimental Runs

A number of experiments have been done to investigate the effect of isolating the reactor at the end of a sulphiding run and then re-exposing the partially sulphided absorbent to the feed gas after re-equilibration with a water/carrier stream. Table 4.10 tabulates the experimental conditions and results of these runs.

Two pairs of runs were performed with the first run in each pair (runs 20 and 23) being performed under identical conditions. At the end of run 20, the reactor was isolated and the absorbent left overnight exposed to the feed gas atmosphere in the vapour space of the reactor. In order to obtain information both on the effect of interrupting a run and also on any effect of the gaseous atmosphere during the period of isolation, the reactor was pumped out after its being isolated at the end of run 23. The second experiment of each pair was very brief and the data collected insufficient for calculation of pss rates. However, numerical

Table 4.10: The effect of interrupting a sulphiding run on the rate of absorption of hydrogen sulphide upon resuming the run.

Experimental Run no.	20	21	23	24	73	74
Experiment Order	1^{st}	2^{nd}	1^{st}	2^{nd}	1^{st}	2^{nd}
State of Reactor During Isolation	Under 1 atm. pressure of gas		Evacuated		Under 1 atm. pressure of gas	
Absorbent	75-1	sulph'd 75-1 from Run 20	75-1	sulph'd 75-1 from Run 23	75-1	sulph'd 75-1 from Run 73
Reactor Temperature /°C	0	0	0	0	0	0
Feed $\%H_2O$	.19	.18	.18	.17	.15	.15
Feed $\%H_2S$	.38	.38	.38	.38	.19	.19
Pss Rate/ $mol(g_{abs})^{-1}s^{-1}$	$1.9x10^{-8}$	NA	$1.9x10^{-8}$	NA	$2.61x10^{-8}$	$0.49x10^{-8}$
Absorbent %sulphur w/w at pss	6.73	NA	6.69	NA	8.04	9.79
Absorbent %conversion at pss	23.0	NA	22.9	NA	27.7	34.0
Absorbent %sulphur w/w at end of run	6.90	7.09	6.87	7.07	-	-
Absorbent %conversion at end of run	23.6	24.3	23.6	24.3	-	-

integration of the data indicates the additional conversion of the solid absorbent. In both runs 21 and 24 the absorbent adsorbed additional water during the water equilibration treatment which preceded the sulphiding run. No difference in sulphiding rate between these two runs was observed.

A third interrupted pair of runs on the same absorbent was performed with the second run being of sufficient duration to allow calculation of the pss rate. The molar flowrates of hydrogen sulphide for these two runs, run 73 and 74, are plotted in Figures 4.9 and 4.10 respectively. As for the previous pairs of experiments, additional water was adsorbed during the water equilibration pre-treatment of Run 74. Although the absorbent conversion has only increased marginally between measurement of the pss rates for the first and the second run of the pair, from 27.5% to 33.5%, the pss rate for the second run is only 20% of that for the first. For all of these experiments it was observed that the initial reaction rate of the second run of the pair greatly exceeded the measured pss rate for the first run.

4.9 Effect of Pre-sulphiding of Absorbent

The pss rates of sulphiding calculated for the experiments using pre-sulphided 75-1 are given in Table 4.11. Alongside these data are presented the pss rates for unsulphided absorbent exposed to the same flowrate and composition of feed. While pre-sulphided absorbent shows the same pattern of reaction as unsulphided absorbent, that is an initial unsteady state period where the rate is falling rapidly followed by a pseudo-steady state, the duration of the unsteady state period is much less for the pre-sulphided absorbent and the measured pss rate much lower.

Figure 4.9: Variation with time of the flowrate of hydrogen sulphide from a reactor containing the unsulphided absorbent 75-1.

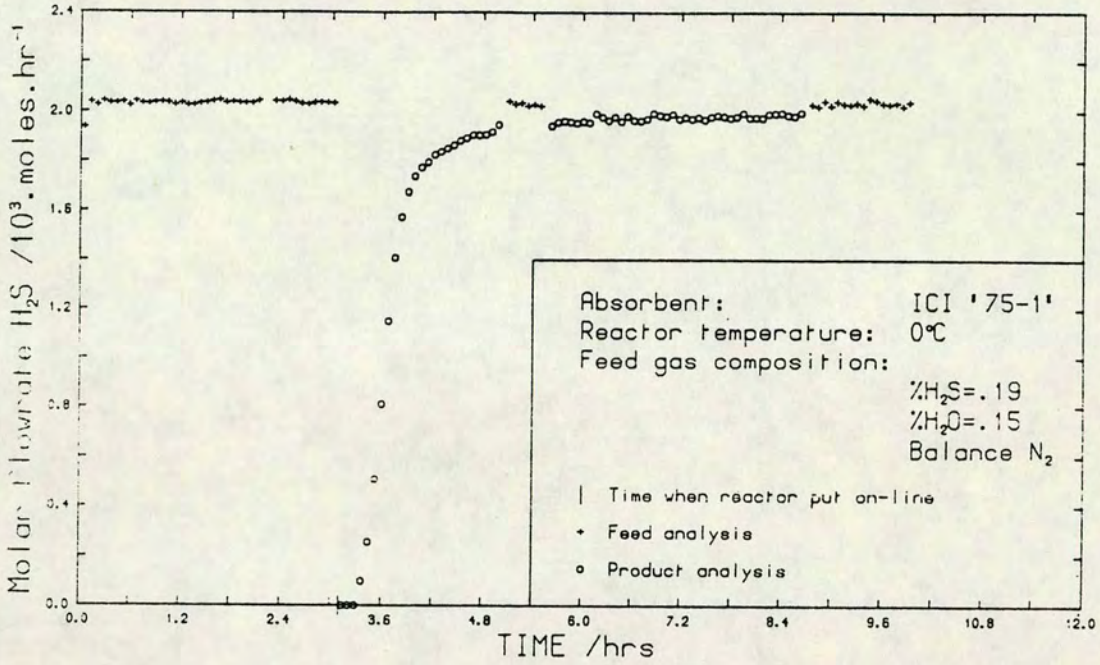

Figure 4.10: Variation with time of the flowrate of hydrogen sulphide from a reactor containing partially sulphided 75-1.

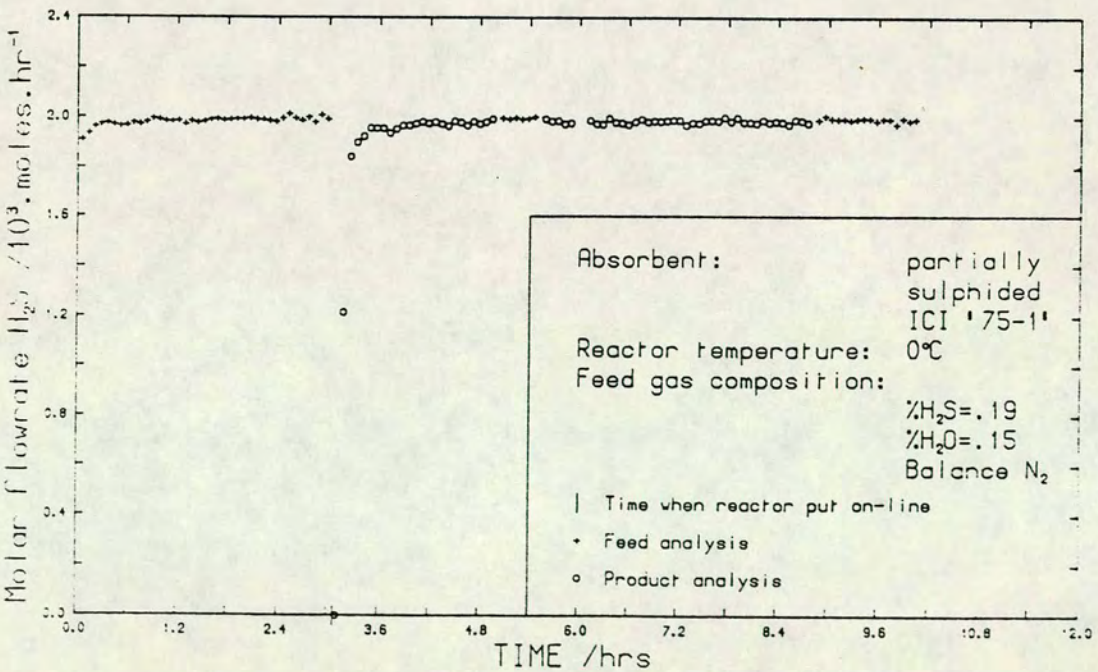

Table 4.11: The effect of pre-sulphiding on the measured rate of absorption of hydrogen sulphide.

Experimental Run no.	50	53	52	38	39	36
Absorbent	pre-sulph'd 75-1	pre-sulph'd 75-1	75-1	pre-sulph'd 75-1	pre-sulph'd 75-1	75-1
Absorbent SSA/m^2g^{-1}	30	30	55	30	30	55
Absorbent initial weight %S	9.3	9.5(*1)	0(*2)	9.3	9.5	0
Reactor Temperature /°C	25.6	25.6	25.6	25.6	25.6	25.6
Feed $\%H_2O$	.49	.49	.48	.50	.49	.51
Feed $\%H_2S$	.06	.06	.06	.19	.20	.20
Pss Rate(*3) /$mol(g_{abs})^{-1}s^{-1}$	$0.60x10^{-8}$	$0.42x10^{-8}$	$2.26x10^{-8}$	$0.63x10^{-8}$	$0.54x10^{-8}$	$2.68x10^{-8}$
Absorbent %sulphur w/w at pss	10.51	10.66	7.50	9.95	9.81	8.55
Absorbent %conversion at pss	36.7	37.2	25.8	34.6	34.1	29.1
Absorbent %sulphur at end of run (calculated)	10.62	11.04	8.04	-	-	-
(measured)	10.2	9.8	7.9	NM	NM	NM

Table 4.11 cont'd

Experimental Run no.	45	46	47
Absorbent	pre-sulphided 75-1	pre-sulphided 75-1	75-1
Absorbent SSA/m^2g^{-1}	30	30	55
Absorbent initial weight %S	9.3	9.5	0
Reactor Temperature /°C	25.6	25.6	25.6
Feed $\%H_2O$	.48	.48	.47
Feed $\%H_2S$	.50	.50	.51
Pss Rate(*3)/ $mol(g_{abs})^{-1}s^{-1}$	$0.39x10^{-8}$	$0.43x10^{-8}$	$2.73x10^{-8}$
Absorbent %sulphur w/w at pss	11.26	11.44	8.68
Absorbent %conversion at pss	39.5	40.1	30.0

Note:

(*1) The pre-sulphided material was prepared in two beds separated by a layer of ballotini in the second reactor (Figure 3.1). The gas flow through the bed was downward. After two days sulphiding the upper bed was removed. The lower bed was removed after a further two days sulphiding. The purpose of this preparation was to produce two batches of sulphided absorbent with different sulphur contents. Sulphur analyses indicate, however, that the sulphur contents of the two materials are very similar.

(*2) Electron microprobe analysis indicates the presence of trace quantities of sulphur in the absorbent 75-1.

(*3) Pseudo-steady state rates are expressed as moles of hydrogen sulphide absorbed per gram of absorbent per second. Thus the rates for the sulphided materials are not directly comparable with those over initially fresh absorbent.

Measurements of the specific surface areas of the absorbents indicate that sulphiding leads to a decrease in the specific surface area. This conclusion is confirmed by pre- and post-run surface area measurements on both 75-1 and BZC. Both absorbents show a decrease in specific surface area after sulphiding.

For the experimental runs 48 to 53, which were performed under the same conditions of temperature and feed gas hydrogen sulphide content, the numerical integration of the hydrogen sulphide product analyses was extrapolated beyond the last product analysis to the end of the run in order to calculate the final sulphur content of the absorbent. For each of these six runs a sample of the sulphided absorbent removed from the reactor was analysed to determine its sulphur content by weight. Both the measured and calculated sulphur contents for runs 50, 52 and 53 (all of which were exposed to a feed gas containing 0.49% water) are given in Table 4.11. The experimental runs 49, 48 and 51 (exposed to feed gases containing 0, 0.16 and 0.27% water respectively) gave measured and calculated sulphur contents of 3.9% and 3.95%, 5.5% and 5.15%, and 7.9% and 8.04% respectively.

4.10 Heat treatment

The heat treatment of 75-1 under vacuum at 250 or 350°C was found to enhance the pss rate measured over the absorbent. This result was duplicated for samples of material separately heat treated. The information concerning these six runs, including two control experiments on untreated material, is given in Table 4.12. The reactivity of the heat treated absorbents does not appear to depend upon the temperature of the heat treatment. The heat treatment caused a loss of carbon dioxide from the absorbent (reported in Table

Table 4.12: The effect on the reaction rate of heat-treating the absorbent prior to reaction.

Experimental Run no.	59	60	61	62	63	64
Absorbent	75-1	75-1	75-1	75-1	75-1	75-1
Pre-run Treatment of the Absorbent	none	heated to 250°C	heated to 350°C	none	heated to 250°C	heated to 350°C
Specific Surface Area/m^2g^{-1}	49	41	46	NM	NM	NM
Reactor Temperature /°C	0	0	0	0	0	0
Feed $\%H_2O$	.15	.15	.15	.15	.14	.14
Feed $\%H_2S$	.22	.22	.22	.22	.22	.22
Pss Rate/ $mol(g_{abs})^{-1}s^{-1}$	1.54×10^{-8}	2.16×10^{-8}	2.32×10^{-8}	1.72×10^{-8}	2.22×10^{-8}	2.19×10^{-8}
Absorbent %sulphur w/w at pss	6.38	6.75	6.90	6.64	7.24	6.70
Absorbent %conversion at pss	21.5	22.8	23.3	22.4	24.5	22.6

4.1) but did not affect the measured specific surface area. As no further experiments were performed on the heat treated material after storage for some time, no information is available on whether the observed rate enhancement decays with time.

4.11 Effect on the Reaction Rate of the Temperature of Calcination of the 75-1 Precursor

Samples of the 75-1 precursor were calcined at either 250 or 365°C for an hour yielding absorbents with specific surface areas of 100 and 71 m^2g^{-1} respectively. Sulphiding experiments performed on these two absorbents resulted in sulphided absorbents with very similar conversions at pss. The initial rates were identical on the two materials, but the unsteady state rate began to drop more rapidly on the lower surface area material (run 73) than on the higher surface area material (run 72) after about 35 minutes. The pss rate, however, was found to be higher on the lower surface area material (run 73) as Figure 4.11 and Table 4.13 demonstrate. A second pair of experiments on the two absorbents confirmed these results qualitatively but the data are not presented here due to an error in the measurement of the gas flowrate.

4.12 Results of Electron Microprobe Analyses

Electron microprobe analysis was used on the sulphided absorbent granules to check the validity of the claim that the sulphiding reaction is chemically controlled. If the reaction is chemically controlled, the distribution of sulphur should be uniform through the granule. The analysis also provides information on the distribution of cement in the granule.

Figure 4.11: The effect of the absorbent calcination temperature upon its sulphiding performance.

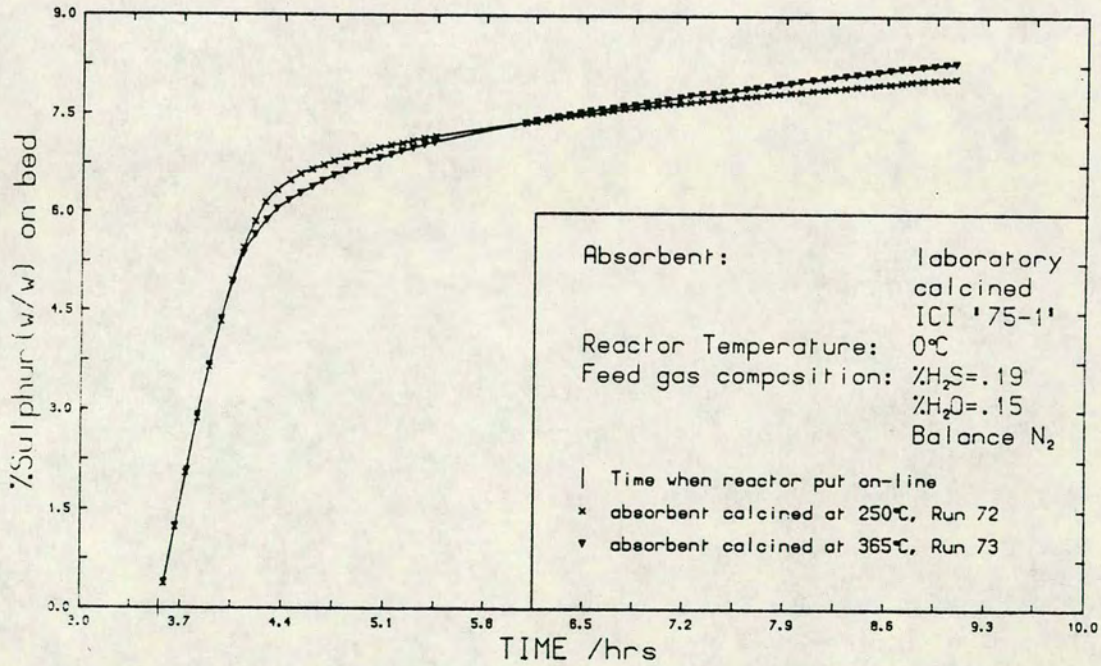

Table 4.13: The effect of the calcination temperature of the absorbent precursor on the rate of absorption of hydrogen sulphide.

Experimental Run no.	72	73
Absorbent	75-1(*)	75-1(*)
Calcination Temperature/°C	250	365
Specific Surface Area/m^2g^{-1}	100	71
Reactor Temperature/°C	0	0
Feed $\%H_2O$	.15	.15
Feed $\%H_2S$	.19	.19
Pss Rate/ $mol(g_{absorbent})^{-1}s^{-1}$	1.89×10^{-8}	2.61×10^{-8}
Absorbent %sulphur w/w at pss	7.88	8.04
Absorbent %conversion at pss	26.8	27.7

Note:

(*) This material was prepared by the author by calcination of the 75-1 precursor in the laboratory ie. it is absorbent **(5)** of Table 4.1.

4.12.1 Structure and Sulphur Distribution of Sulphided Absorbent Granules

Figures 4.12 are plots of the variation of the count rates for sulphur, aluminium, zinc and calcium along a radius of a polished cross-section of a heavily sulphided granule, scanning from the circumference into the centre of the granule. The granule was taken from the inlet of the main dump bed (C9 in Figure 3.1) and has therefore been exposed to various streams having different hydrogen sulphide and water contents. The count rates for the different elements are not comparable but are proportional to the weight percentages of the respective elements in the sample. Most of the noise on the count rates may be attributed to the relatively poor quality of the sample surface. Clearly this will be reflected in a significant standard deviation between quantitative point analyses on the sample. Distinct from the noise on the count rates are the sharp peaks and troughs which correspond to inclusions of material of different composition from the rest of the surface, or to pores. Thus, the troughs in the zinc plot labelled B_{1-10} are seen to correspond with troughs in the sulphur plot and with peaks in the calcium and aluminium plots. These therefore indicate the presence of small particles of cement. The peaks in the calcium and aluminium plots do not correspond exactly, however, with the trough B_6 in the zinc plot matching up with a peak in the calcium but not the aluminium plot, and there being no peaks in the calcium plot corresponding to the pair labelled C_1 in the aluminium plot. It appears therefore that inclusions of calcium and of aluminium compounds besides calcium aluminate are present in the absorbent. The zinc troughs at A_1 and A_2 most probably result from pores intersecting the surface at these locations. Since no measurement of the background radiation is made during a

Figure 4.12: Radial scans of a heavily sulphided absorbent granule using an electron microprobe.

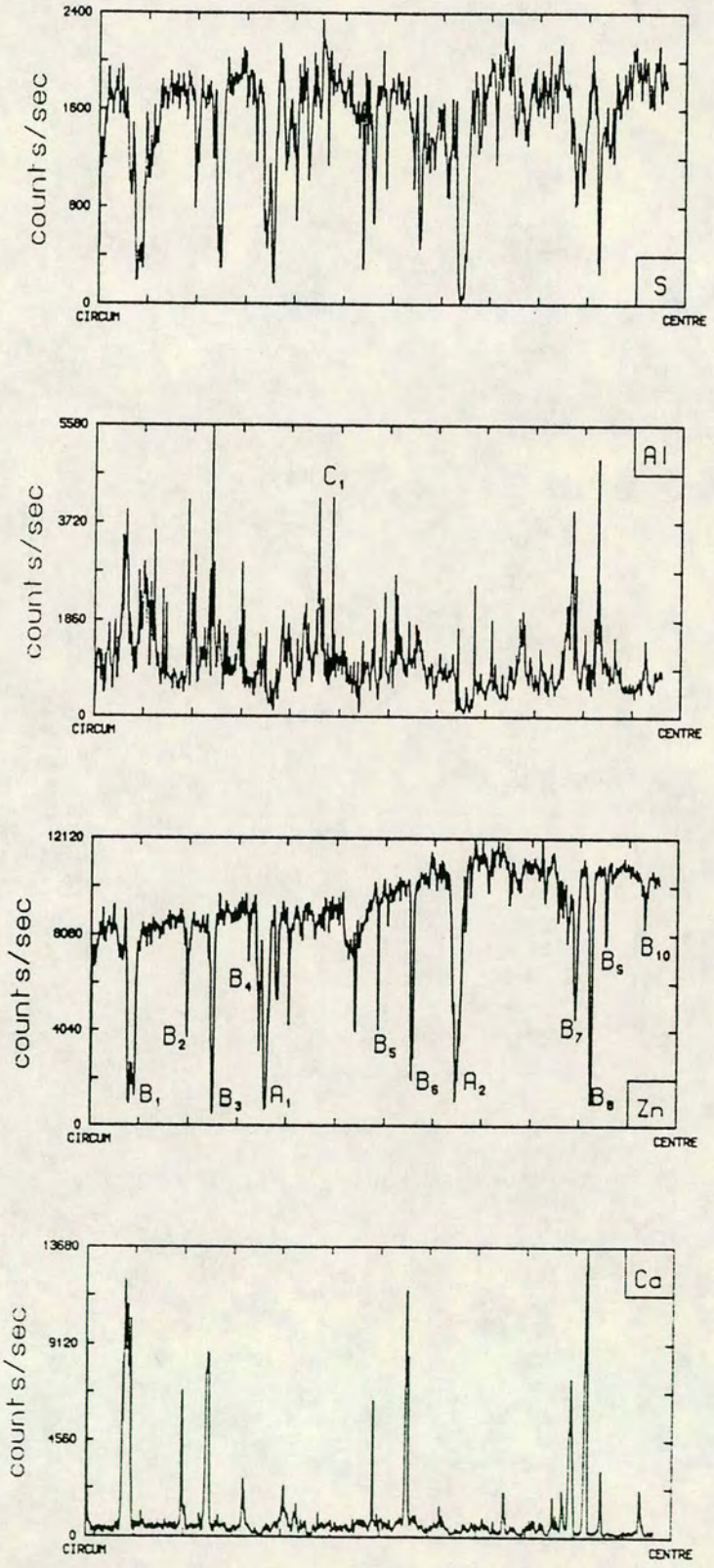

line scan, it is not possible to say definitively without further information whether the low 'background' count rates for aluminium and calcium upon which the sharp peaks appear superimposed are indicative of the presence throughout the sample of calcium and aluminium at low levels or whether they simply represent the radiation of the continuum.

One interesting feature of the zinc plot is the apparent increasing zinc concentration towards the centre of the granule. At first sight there would appear to be two possible explanations for this. The first is that the sample surface has a better finish towards the centre of the circular cross-section. This is improbable as the reverse trend is generally observed with a narrow outer annulus of the sample having a much smoother surface due to the proximity of the araldite support. Moreover, if the quality of the surface were better towards the centre of the sample, this should be reflected in a higher sulphur count rate, provided no other factors affect the sulphur distribution. Alternatively, the higher zinc content towards the centre of the sample surface might be attributed to a lower conversion of zinc oxide to zinc sulphide towards the centre - zinc representing 80.3% and 67.1% by weight of zinc oxide and zinc sulphide respectively. However, the uniformity of the sulphur content casts doubt on this explanation.

Crushing of a number of granules between the fingers reveals two distinct typical structures. While some of the granules are readily crushed to small particles, others crack revealing a much denser and harder core. Thus a third feasible explanation of the nonuniform zinc content of the sample is that the granule analysed has the core structure described and that the nonuniformity results from a nonuniform density of the granule. If this explanation is indeed correct then it suggests that

the apparently fairly uniform sulphur distribution may result from the combination of a sulphur content which falls towards the centre of the granule and a nonuniform density as described above.

A number of point analyses were made on the heavily sulphided granule. These gave weight percentages of sulphur in the range 9.1-12.4% with a mean sulphur content of 11.1%. In these analyses, however, the sum of the weight percentages of the components of the absorbent, after calculation of the weight percentage of oxygen by consideration of the likely form in which the components identified are present, fell significantly short of 100% being around 73-78%. It is proposed that the shortfall may arise due to the porous nature of the material. In particular, the development of cracks during the sulphiding process due to the larger size of the sulphide anion compared to the oxide anion may be responsible for this effect. It is possible to eliminate the porosity in the surface layer of the sectioned granule by impregnation of the absorbent under vacuum with araldite. This strengthens the material and allows a much better polish to be obtained over the entire surface. The loss of information on the absorbent composition is substantial, however, as a large proportion of the surface may be made up by 'islands' of araldite. Alternatively, it may be the case that the reason for the low value of the sum of weight percentages is due to a fault with the zinc analysis. As zinc represents most of the mass of the absorbent, any error in its measurement would significantly affect the value of the summed weights. Moreover, on two other analyses on the same sample, very low values of the zinc content were obtained, although the sulphur content (sulphur is the second most abundant component) was normal. This suggests that the problem may indeed have been instrumental.

4.12.2 Analysis of Unsulphided Absorbent Granules

The variation of the zinc count rate across a diameter of an unsulphided granule of 75-1 is indicated in Figure 4.13. As in the analysis of sulphided 75-1, the zinc content appears to be higher towards the centre of the granule. SEM pictures of the surface showed no distinctive features, however, with the surface appearing to be of uniform brightness. The cement particles are not identifiable using the SEM but are clearly seen with a microscope and appear to be randomly distributed through the granule. A number of point analyses were done on the unsulphided 75-1 and these are tabulated in Table 4.14. Analyses 1, 2, 4 and 5 give broadly similar point compositions although the aluminium content in analysis 1 is significantly higher than in the other analyses. The very low zinc content and very high calcium content of analysis 3 indicate that the sample area is located on a particle of cement. If the calcium is assumed to exist as calcium carbonate then the sum of the weight percentages including the contribution from iron oxide in the sample is about 95%.

4.12.3 Analyses of Granules from a Sulphiding Experiment (Run 32)

Experimental run 32 was performed on whole granules of 75-1 as part of a group of runs to investigate the effect of particle size on the rate of absorption of hydrogen sulphide (see section 4.3). A number of sulphided granules from this run were mounted and analysed using the electron microprobe. Figure 4.14 shows the variation of the sulphur and zinc count rates along a radial scan. The concentration of zinc is clearly higher towards the centre of the granule. The sulphur count rate also appears to be higher at the centre of the granule than at the circumference but the

Figure 4.13: Diameter scans of an unsulphided absorbent granule using an electron microprobe.

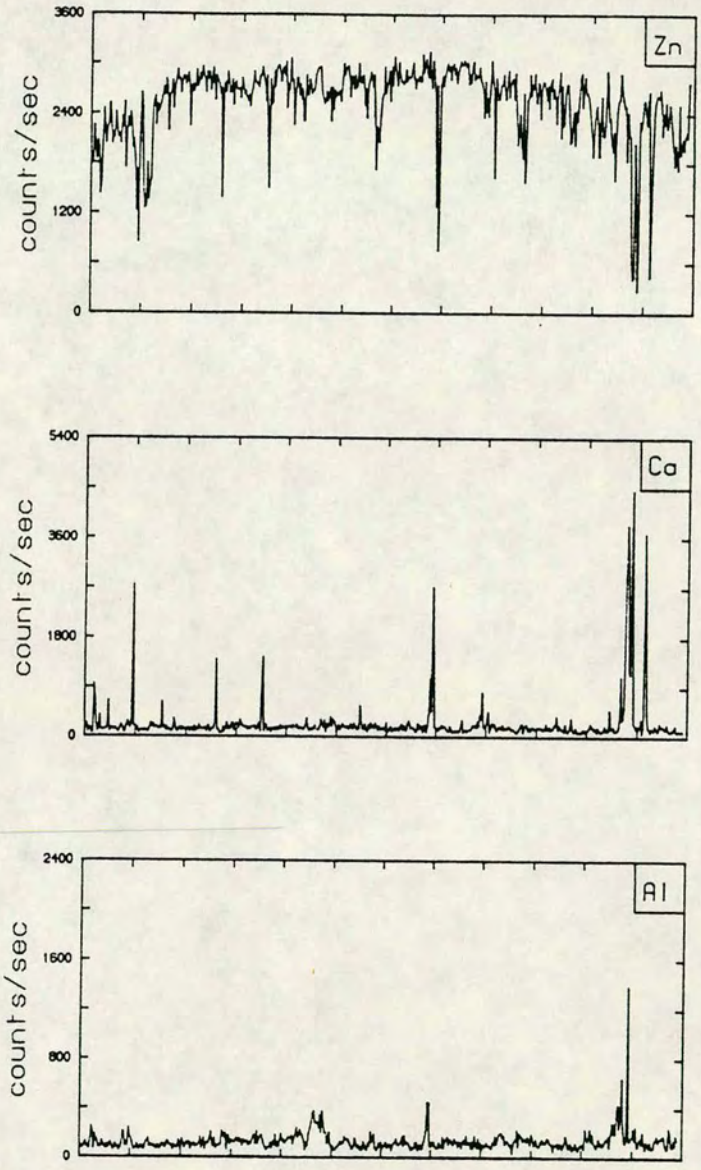

Table 4.14: Electron microprobe point analyses on unsulphided 75-1

	Weight %ages (w_i)				
Analysis no.	Zn	Al	Ca	O(*1)	$\sum_i w_i$(*2)
1	69.8	5.2	0.8	22.7	98.7
2	73.6	0.2	0.1	18.4	92.3
3	3.1	0.3	34.2	42.1	90.0
4	68.0	1.6	1.1	19.4	90.4
5	65.3	1.0	0.4	17.4	84.2

Note:

(*1) The electron microprobe cannot detect oxygen in these samples because of the zinc interference (section 3.5.2). The values given therefore for the oxygen content in each analysis are calculated on the basis that zinc, aluminium and calcium exist in the sample as zinc oxide, aluminium oxide and calcium carbonate respectively.

(*2) The summed weight percentages given for the five analyses exclude the trace elements sulphur, silicon and iron detected in the sample. These are in all cases present at the level of a fraction of a percent except for iron in analysis number 3 which represents 4% by weight of the sample and is likely to be present as an oxide.

Figure 4.14: Radial scans for sulphur and zinc on a granule from experimental run 32.

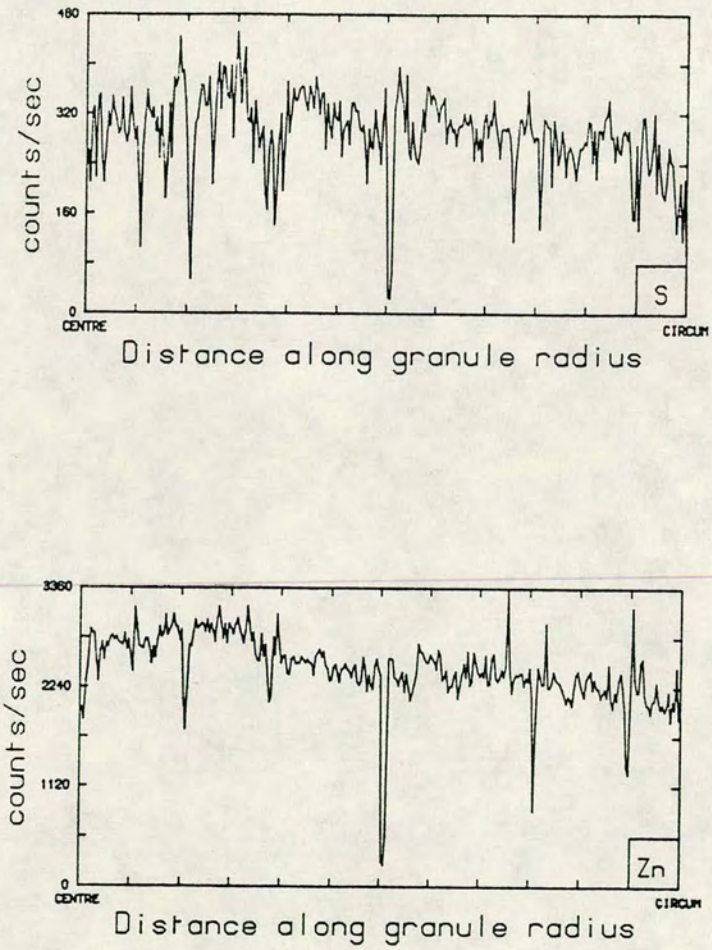

trend is statistically less significant than that of the zinc count rate due to the higher noise level on the signal. An energy dispersion image of the granule cross-section showed two distinct zones - a central bright area surrounded by a darker annulus. Scanning electron microscope photographs also reveal this zoned structure as Plates 4.1 and 4.2, taken on two different granules, indicate. The darkest outer band in each photograph is the araldite, and beyond that the brass tube in which the sample is mounted. (The brass tube is only just visible in Plate 4.2 at the bottom lefthand corner.) The two zones of the granule are clearly visible and examination at higher magnification reveals them to be separated by a very fine crack which runs right round the central brighter zone. Note that the absence of such cracks in partially or fully reacted granules has been interpreted[4] as indicating the validity of modelling the reacting system using the constant radius grain model. In the present case, the presence of cracks is unsurprising in view of the larger size of the sulphide compared to the oxide anion.

Two automatic point scans each of 30 point analyses were performed. The end-points of the two scans were selected so that the scans traversed the interface between the brighter and darker zones. The variation of the weight percentages of sulphur and zinc in the sample thus determined are plotted in Figure 4.15. For both scans, the direction of the scan was from the central brighter zone outwards across the outer darker zone. The decrease in the zinc content in moving from the brighter to the darker zone is again apparent with the zinc content dropping from about 65% to 60%. The trend is obscured to some extent, however, by the scatter in the point analyses. This probably arises principally from the poor surface evident in Plates 4.1 and 4.2, so that an inaccurate analysis may result from the

Plate 4.1: Scanning electron micrograph of a polished sulphided granule from experimental run 32 - sample 1.

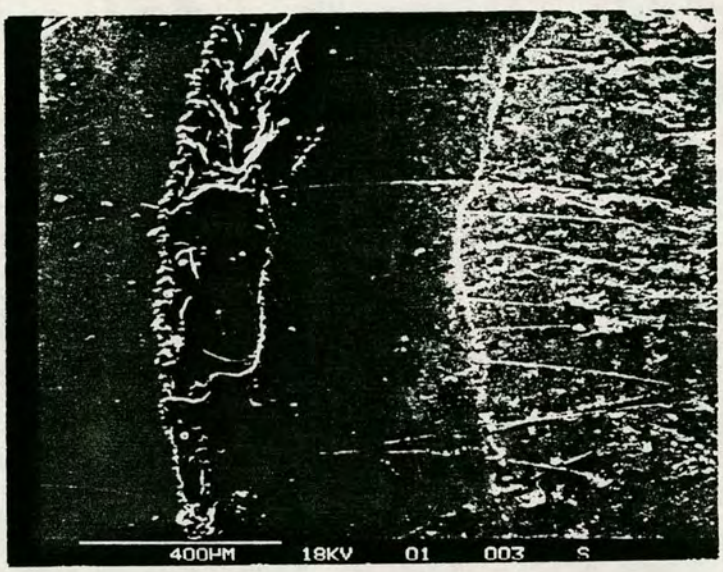

Plate 4.2: Scanning electron micrograph of a polished sulphided granule from experimental run 32 - sample 2.

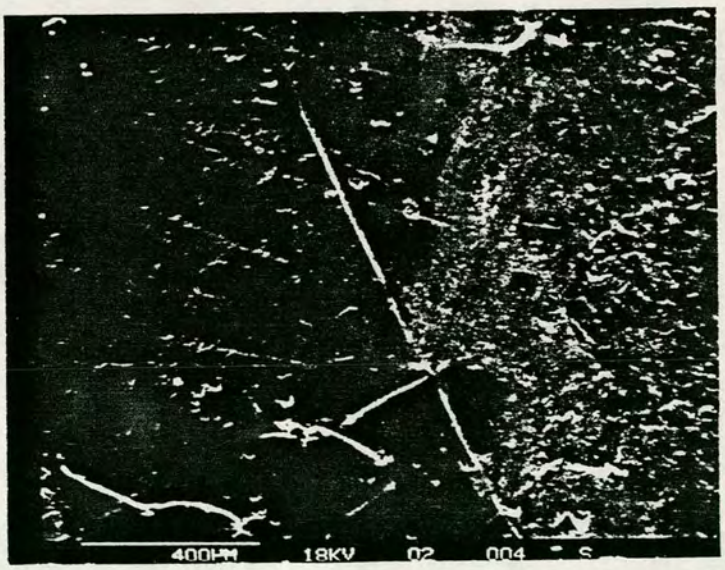

Figure 4.15: Automatic scans of point analyses of a sulphided granule from run 32.

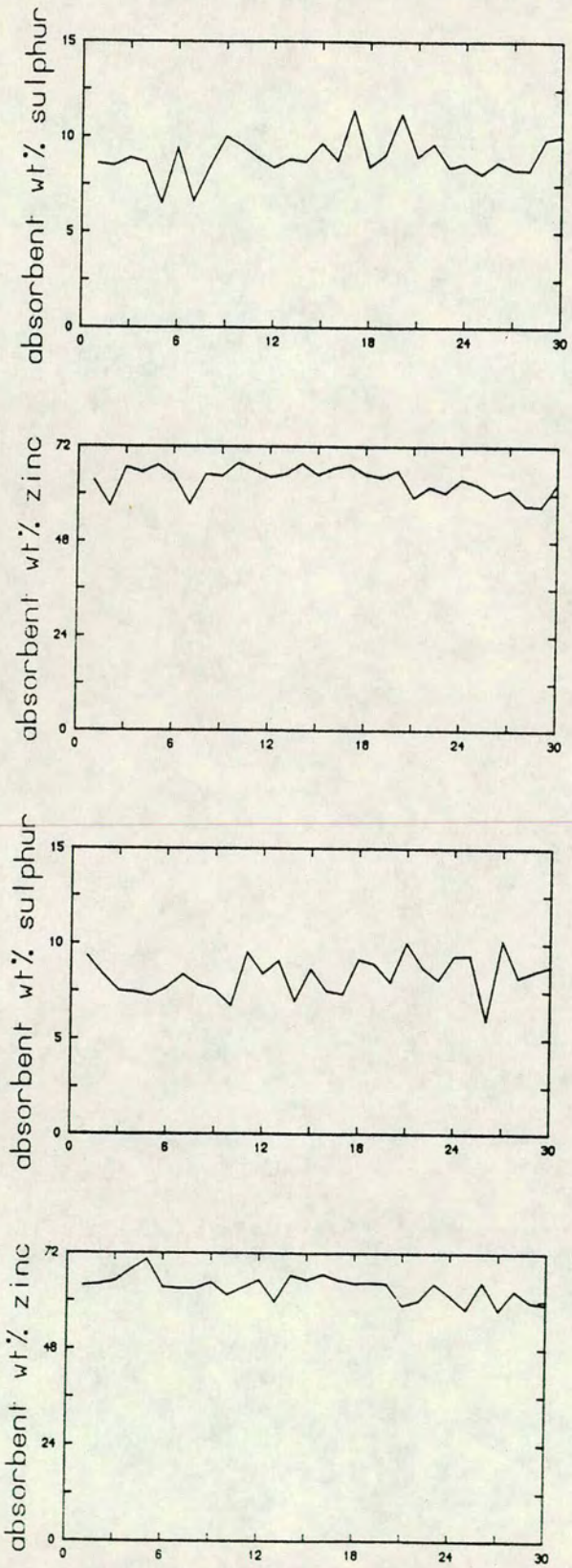

selection of a patch of surface which is badly pitted or scratched due to the inadequate polishing procedure.

4.12.4 Results of Ion Probe Analyses (Run 32)

In analysing samples of sulphided absorbent using the electron microprobe, the oxygen content of the sample cannot be measured and must therefore be calculated on the basis of a number of assumptions. These concern the form in which the various elements detected are present and include some assumption about the degree of stoichiometry of the unreacted zinc oxide. In view of the observed variation of the zinc count rate across a radial scan of a sulphided granule it is useful to be able to make an independent measurement of the variation of sulphur and oxygen through the granule using the ion probe. With this instrument, however, the measurement of zinc is very difficult and was found to be particularly unsatisfactory in the present work because of the poor quality of the sample surface. The analysis was limited therefore to sulphur, oxygen and carbon. As calibration of the ion probe was not possible, the levels of these components cannot be quantified.

Two perpendicular radial scans of point analyses were made on a sample from experimental run 32 using a step length of 25 microns. The boundary between the granule and the araldite is easily identifiable by the abrupt fall in the sulphur and oxygen signals and the corresponding step increase in the carbon signal. The two scans are of very similar appearance and clearly show a uniform distribution of oxygen and sulphur along the radii except for the outermost 150-200 microns where the oxygen content falls and the sulphur content rises. Thus it appears that at pseudo-steady state the conversion of the absorbent is essentially uniform except for a thin outer shell or skin of the granule

which has a slightly higher conversion. There is some indication of an increase in carbon content in a thick outer shell of the sample but the much poorer signal-to-noise ratio of the carbon signal compared to the signals for sulphur and oxygen prevents any definite conclusion on this point.

4.12.5 Analysis of a Granule from the Absorption Front

The absorption front in a packed bed of granules of the absorbent '75-1' exposed to a hydrogen sulphide containing gas is detectable by the faint yellow colour imparted to the granules at the front. As these granules become more sulphided, they lose their yellow colour, turning a slightly darker shade of gray than the original unsulphided granules. The yellow front meanwhile moves on through the bed and thus provides a visual warning of slippage or 'breakthrough' of hydrogen sulphide. A number of yellow-tinged granules were taken from the absorption front of the dump bed and analysed using the electron microprobe. The observed sulphur distribution is plotted in Figure 4.16. It is evident that the hydrogen sulphide has not penetrated to the centre of the granule which remains unsulphided while a thick outer shell of the absorbent contains between 2.3 and 5.3% w/w sulphur as determined by point analyses. It is further observed that the unreacted absorbent is not located exactly centrally within the granule but displaced slightly. This may be caused by the large changes in hydrogen sulphide partial pressure in the vicinity of the absorption front or may be a function of the nonuniform density of the absorbent.

4.13 Effect of Sodium Ions in the Absorbent

In order to determine whether the sodium ions present in basic zinc carbonate might affect the rate of sulphiding of the zinc oxide prepared from it, basic zinc carbonate

Figure 4.16: Diameter scan of an absorbent granule taken from the absorption front of the dump bed.

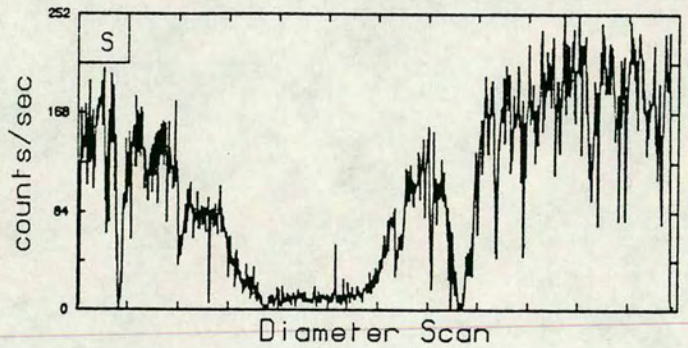

was prepared by a different route avoiding the use of alkali metal salts. The route selected was the hydrolysis of basic zinc acetate to zinc hydroxide followed by carbonation to basic zinc carbonate. The basic zinc carbonate was calcined according to the same procedure used for BZC. The equations describing these reactions are given below.

$$Zn_4O(OAc)_6 + H_2O \rightleftharpoons 3Zn(OAc)_2 + Zn(OH)_2 \quad (90)$$

$$5Zn(OH)_2 + 2CO_2 \rightleftharpoons Zn_5(OH)_6(CO_3)_2 + 2H_2O \quad (91)$$

$$Zn_5(OH)_6(CO_3)_2 \rightleftharpoons 5ZnO + 2CO_2 + 3H_2O \quad (92)$$

As with the basic zinc carbonate, the sodium-free hydrozincite was pelleted, crushed and sieved prior to calcination. The sodium contents of solutions of the two basic carbonates were determined, and the sodium content of the basic zinc carbonate found to be 75 times that of the 'sodium-free' hydrozincite.[13]

Because of the lengthy and difficult preparation required for the Na-free zinc oxide and the limited size of the sample prepared, a thorough investigation of its sulphiding characteristics has not been performed. Nevertheless, some interesting properties of the material have been observed. Two preparations of sodium-free hydrozincite were made of which the first was much smaller. Together, this material was sufficient after calcination for three sulphiding runs and a sample for surface area measurement. Two sulphiding runs were performed on BZC-derived zinc oxide for comparison. The two samples for these runs came from two different calcinations and a surface area

[13]Unfortunately, the record of the molarities of the basic carbonate solutions was lost so that the absolute sodium contents of the materials is unknown.

measurement was therefore made on each. The rates measured for these five sulphiding runs are given in Table 4.15.

As the experimental run 75 on BZC-derived zinc oxide and runs 76 and 77 on Na-free zinc oxide were all performed on the same weight of absorbent bed, it is possible to compare the reactor outlet molar flowrates of hydrogen sulphide for these three runs directly. Figure 4.17 is a plot of this data. The figure clearly shows the decay in sulphiding activity of the Na-free zinc oxide between runs 76 and 77 which were performed on consecutive days. This decline in performance is quantified in Table 4.15 by the much lower sulphur content of the absorbent in Run 77 at pss compared to that of Run 76. Although Run 79, performed 5 days after Run 77, was stopped prematurely, numerical integration allows an assessment of whether a further decline in activity has occurred. This analysis reveals that for a time on-stream of about 3 hours and 8 minutes, for which the measured rate and absorbent sulphur content of Run 79 were 2.35 $x10^{-8}$ $mol(g_{absorbent}{}^{-1}s^{-1}$ and 3.81% w/w as given in Table 4.15, the sulphur content of the absorbent sample in Run 77 was 4.60% w/w. This is a significant difference and indicates that the activity of the Na-free zinc oxide has continued to decline. In this context it is pertinent to note that only a single measurement of the specific surface area of the Na-free zinc oxide was made. The surface area of the sample, measured 3 days after the calcination process, was found to be 35 m^2g^{-1}. It is therefore not possible to say whether the declining activity of the material corresponds to a declining surface area or to some quite separate

Table 4.15: The effect on sulphiding performance of residual sodium ions in the absorbent.

Experimental Run no.	75	78	76	77	79
Date of Run	12.5.89	18.5.89	13.5.89	14.5.89	19.5.89
Absorbent	calcined BZC	calcined BZC	Na-free zinc oxide	Na-free zinc oxide	Na-free zinc oxide
Date of Calcination	11.5.89	17.5.89	12.5.89	12.5.89	12.5.89
Absorbent SSA/m^2g^{-1}	96	108	35 (*1)	35 (*1)	35 (*1)
Reactor Temperature/°C	0	0	0	0	0
Feed $\%H_2O$	.16	.15	.15	.15	.17
Feed $\%H_2S$	.087	.087	.087	.087	.087
Pss Rate/ $mol(g_{abs})^{-1}s^{-1}$	$2.71x10^{-8}$	$2.84x10^{-8}$	$4.64x10^{-8}$ (*2)	$2.78x10^{-8}$	$2.35x10^{-8}$ (*3)
Absorbent %sulphur w/w at pss	8.87	9.59	8.22	5.06	3.81
Absorbent %conversion at pss	23.6	25.6	21.8	13.2	9.9

Note:

(*1) A single measurement of the specific surface area of the Na-free zinc oxide was made on 15.5.89.

(*2) The rate given for Run 76 is not in fact a pss rate as inspection of Figure 4.17 reveals. As the reaction had not reached a pss the rate given is merely the rate calculated for the latter part of the process.

(*3) Run 79 was stopped prematurely due to exhaustion of the supply of the hydrogen sulphide/nitrogen mixture. The rate given is thus, as for Run 76, just the latter slow rate.

Figure 4.17: The effect of the presence of residual sodium ions in the absorbent on the variation with time of the flowrate of hydrogen sulphide from the reactor.

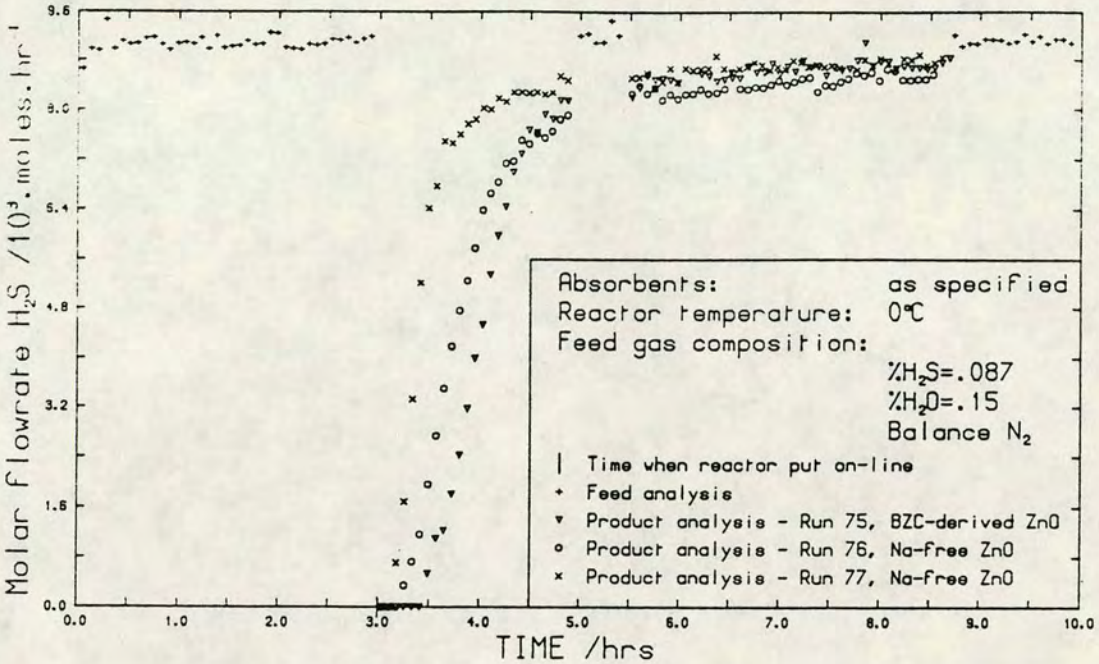

Figure 4.18: The effect of the presence of residual sodium ions in the absorbent upon the increase in solid conversion with time.

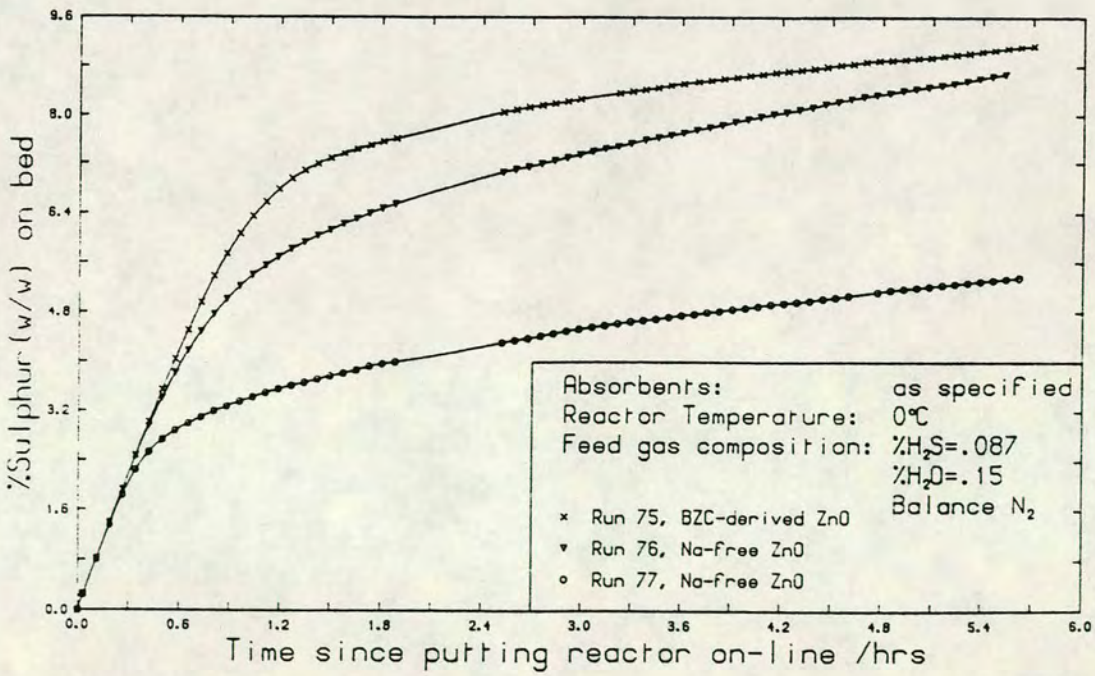

phenomenon.[14]

Figure 4.17 reveals an interesting difference in the sulphiding performance of the Na-free and BZC-derived zinc oxide samples. Initially the decline in reaction rate of Run 75 is delayed relative to that of Run 76. After about an hour, however, the position is reversed and a higher rate is observed on the Na-free material. If this material could be satisfactorily stabilised at its initial level of sulphiding activity, then breakthrough runs on these two materials might indeed show the Na-free zinc oxide to give superior performance. Figure 4.18 represents the differences in sulphiding activity more vividly in terms of the rise in absorbent sulphur content with time.

---

[14]In noting the apparent instability of the Na-free zinc oxide, the question naturally arises as to the stability of BZC-derived zinc oxide and of the commercial absorbent '75-1'. The performance of the commercial absorbent has been remarkably consistent over the long period during which experiments have been conducted. No replicate experiments have been performed on BZC-derived zinc oxide from the same calcination batch, however, the results of experimental runs 75 and 78 of Table 4.15 are in reasonable agreement given the difference in specific surface area measured. Moreover, there is no evidence for any gross changes in surface area with time as the surface areas of the samples for Runs 13 (Table 4.5), 75 and 78 were measured 22 days, 4 days and 1 day respectively after the calcination process. (The error in the calculation of specific surface areas from nitrogen adsorption experiments is difficult to estimate but may be up to ± 5 m^2g^{-1}.)

REFERENCES

[1] Denny P.J.
Personal communication

[2] Levenspiel O.
"Chemical Reaction Engineering", ch.14
John Wiley & Sons, New York (1972)

[3] Sohail K.
Personal communication

[4] Rajeswara Rao T., Gunn D.J., Bowen J.H.
"Kinetics of calcium carbonate decomposition"
Chem. Eng. Res. Des. 67, 38-47 (1989)

CHAPTER 5

DISCUSSION OF RESULTS

In this chapter, the experimental results are analysed and possible mechanisms by which the zinc oxide granules react are discussed. The optimal performance of a commercial absorption unit is considered in the light of the experimental results. An attempt is made to identify those properties of the commercial material which make it a good absorbent for hydrogen sulphide and directions for future research are indicated.

5.1 Time Dependence of the Reaction and Possible Mechanisms

One common feature of the sulphiding experiments performed is the observation of a rate of reaction which decays with time. Numerical integration of the area between the curves of molar flowrate of hydrogen sulphide versus time for the feed and product streams allows the calculation of the cumulative number of moles of hydrogen sulphide absorbed at any time. Thus, although it may be difficult to define the distribution of zinc sulphide in a partially reacted bed corresponding to a particular measured rate and set of experimental conditions, it is possible to calculate the average sulphur content of the bed.

Regardless of the mode of propagation of the reaction into the bulk of any zinc oxide particle, the initial reaction is bound to occur at a surface. The commercial absorbent used has a high internal surface area, and whether the initial reaction takes place here or whether it is restricted to the external surface depends on the relative rates of the surface reaction and of pore diffusion. The energies of atoms located on a surface differ from those of the same atoms in a bulk structure,

as do the atomic separations. Moreover these properties are also different on the different crystal planes viz. the (0001), (000$\bar{1}$) and (10$\bar{1}$0). Thus, if one face of the crystal were much more reactive, for example, than the others, the progress of the reaction through the crystal would tend to be anisotropic and the distribution of crystal faces exposed on the surfaces of the particle could strongly affect its measured reactivity. There is strong evidence of a relationship between the distribution of crystal faces on zinc oxide and its specific surface area.[1] This suggests that zinc oxide which has been prepared with a low surface area exposes predominantly prism faces while for high surface area zinc oxides the polar faces represent a substantial fraction of the surface.

The experimental data available can only be used indirectly as a guide to possible mechanisms for the surface reaction because so few data points on any single run relate to this stage of the reaction.

Most of the data relate to stages of the reaction where various kinds of diffusion are important. A number of experiments were performed to determine whether the resistance to gaseous diffusion in the pores of the absorbent granules limited the observed rate of reaction. This situation is easily tested for because the time for the reactant gas to diffuse into the centre of a particle increases with increasing particle size (Appendix E) and thus pore diffusion is more likely to be rate-limiting for larger particles. Figure 4.3 illustrates this phenomenon. Run 32, which was performed on whole absorbent granules (2.5-3.5mm) shows a markedly lower initial rate compared with those runs performed on smaller particles. Some slight effect of pore diffusion limiting the initial reaction rate over particles of size 1.20-1.40mm is also evident.

This explanation of the observed lower initial rates of reaction being caused by the effect of pore diffusion in limiting access of the gaseous reactant to the internal surfaces is supported by the results of electron microprobe analysis of partially sulphided granules. Figure 4.16 shows the variation of the sulphur count along a diameter scan of a sectioned granule taken from the absorption front of the dump bed. The granule clearly consists of a thick outer partially sulphided shell enclosing an unreacted core. This unreacted core is not concentric with the outer surface of the granule but somewhat off-centre. If the hardness of the material, which was observed to be non-uniform, is inversely related to its porosity then this lack of symmetry in sulphiding is unsurprising. Further evidence for the role of pore diffusion comes from Denny's measurements of the porosities and specific surface areas of sulphided absorbents.[2] Higher values for both these properties were found when the granules were split in half to expose the core, indicating that pore blockage had occurred in the outer shells of the granules. In contrast to these findings are the results of diffusion experiments on unsulphided and partially sulphided zinc oxide prepared from BZC.[3] The diffusivity of ethane through a disc of zinc oxide was measured before and after in situ treatment with hydrogen sulphide. While the extent of sulphiding of the zinc oxide sample was not quantifiable, the penetration of hydrogen sulphide into the disc and its reaction there was evident by the discoloration of the sample. No effect of the sulphiding upon the measured diffusivity was observed.

The distribution of sulphur in an absorbent granule differs greatly after several hours of sulphiding ie. at that stage where the reaction appears to be in a pseudo-steady state, from its initial highly non-uniform

distribution. A number of granules from Run 32 were analysed by electron microprobe and found to have a fairly uniform sulphur content within the accuracy of the method as Figures 4.14 and 4.15 indicate. Thus, after the initial stage of the reaction where the reaction is localised by pore diffusion to an outer shell, there is an intermediate stage prior to pss where the reaction is proceeding faster in the interior of the granule than it is in the outer shell.

The mode of reaction of smaller particles - Runs 29, 30 and 33 of Figure 4.3 - is somewhat simpler, being uncomplicated by pore diffusion resistance in the initial stages. Thus, on the macroscopic level, the reaction is evidently homogeneous in these smaller particles and if the rate could be measured it would indicate the rate of the surface reaction. Note that the initial rate of reaction on larger particles is also a surface rate but in this case the apparent surface rate underestimates the true rate because the extent of reacting surface is limited by pore diffusion and therefore unknown. To eliminate this effect of pore diffusion, subsequent experiments were performed on small particles in the size range 300-710 microns. The effect of particle size upon the reaction rate is discussed in more detail in section 5.3.

Given the absorbent's measured specific surface area of about 55 m^2g^{-1}, only 3.7% of the zinc oxide in any granule is present on its internal or external surfaces. As conversions in the range 12-34% have been measured it is clear that zinc oxide present initially in the bulk of crystallites has reacted to form zinc sulphide. A number of mechanisms by which this could occur are postulated. Contacting of the reactant gas, hydrogen sulphide, with the solid reactant, zinc oxide, which is not exposed on the surface of a crystallite involves the

movement of one or other of the reactants. If the zinc sulphide which forms on the surfaces of the zinc oxide crystallites is porous, then hydrogen sulphide may diffuse through this product layer to the interface between sulphide and oxide and there react with the zinc oxide. In considering this transport mechanism it is of relevance to note the larger size of the sulphide as compared with the oxide ion and the observed reduction in porosity and surface area which accompany sulphiding.[2] The larger anion, through its effect in increasing molar volume, may reduce the effective diffusivity of hydrogen sulphide in the pore structure. It may also, however, create such stress at the zinc oxide/zinc sulphide interface that distortion and minute cracks result allowing the ingress of water and/or hydrogen sulphide.

If, however, the zinc sulphide which forms on the zinc oxide crystallites is not porous then diffusion of hydrogen sulphide to the reaction surface is prevented and the reaction can only proceed by diffusion of the solid reactant through the product matrix to the gas-solid interface. This could be achieved very slowly by the lattice diffusion of sulphur and oxygen ions respectively away from and towards the gas-solid interface. A mechanism for this transport of ions is

provided by the defects present in the solid lattice.[15] Gour et al.[5] have proposed that solid state diffusion is the mechanism by which hydrogen sulphide reacts with the bulk zinc oxide. The observation that zinc oxide sulphided for several hours contains only α-ZnS (Wurtzite)[6] whereas sulphided absorbent examined after much longer periods of sulphiding contains both α-ZnS and β-ZnS (Sphalerite),[7] is consistent with this mechanism of solid state diffusion. Thus, it seems probable that diffusion of oxide and sulphide ions through a Wurtzite structure which consists of phases of zinc oxide and zinc sulphide separated by a solid solution would be easier than transport of ions between zinc oxide and the zinc blende structure (Sphalerite). If lattice diffusion is important, it is also possible that the mechanism might involve the transport of cations through a relatively immobile anionic structure. Thus sulphur atoms might add on to the zinc oxide surfaces and the diffusion in opposite directions of zinc ions and protons (hydrogen) would allow the loss of water molecules. This mechanism appears more plausible than anionic diffusion with respect to steric effects if the zinc oxide may be considered as an oxygen sublattice

---

[15] M.W. Roberts[4] has mentioned the difficulty of distinguishing defect zinc oxide and zinc hydride in a zinc oxide/water system. Thus, where non-stoichiometric zinc oxide has been formed by heat treatment of the zinc oxide and oxygen vacancies exist at or very close to the surface, the addition of water to a zinc ion which is adjacent to an oxygen vacancy and in a low oxidation state, Zn^{+}, may result in the formation of zinc hydroxy-hydride. The oxygen of the hydroxyl group may then occupy the vacancy and loss of hydrogen may occur leaving zinc oxide. (see section 2.2.3) Alternatively, the surface hydride may be retained. In the experimental system used in the current work hydrogen would not have been detected due to the low sensitivity to hydrogen of a thermal conductivity detector using helium as carrier and because of the swamping effect of the large nitrogen peak which would elute almost coincidentally. Figure 5.1 (a) indicates a slightly different mechanism whereby oxygen vacancies may be lost by the absorption of water without loss of hydrogen.

with zinc occupying half of the tetrahedral holes as represented in Figure 2.2. In such a case, the transport of the smaller cation should be favoured while diffusion of protons should have a significantly lower activation energy than either zinc or anion diffusion. The high temperatures at which diffusivites in the solid state are measured and the high activation energies required for solid state diffusion (section 2.1.3) suggest, however, the implausibility of such mechanisms for the pss reaction of hydrogen sulphide with zinc oxide. If, however, solid state diffusion is indeed the mechanism by which bulk zinc oxide reacts then it is likely that the process is chemically rather than physically driven, that low levels of impurities in the absorbent have an effect on the measured rate disproportionate with their concentration, and that dislocations and grain boundaries within and between crystallites affect the rate of diffusion.

A third possible mechanism is that of surface diffusion. This is more difficult to visualise in terms of what the driving force for diffusion would be and how the structure would change with progress of the reaction and the development of a new pore structure. Some comparison of the relative likelihood of these three mechanisms can be made on the basis of the following dicussion of the experimental results.

5.2 Autocatalysis - The Water Effect

The presence of water in the gas stream at the levels studied (up to 0.5% ie. 5000ppm) increases the reaction rate at all solid conversions. This is clearly seen in Figure 4.6 where the partial pressure of hydrogen sulphide in the stream leaving the reactor rises most rapidly when no water is present in the feed stream. As the partial pressure of water in the feed increases, the

rate at which the reaction rate decays with time decreases.

The simplest reaction scheme consistent with the observations is thus:

$$H_2S + ZnO \rightleftharpoons H_2O + ZnS \quad (93)$$

$$H_2O + ZnO \rightleftharpoons Zn(OH)_2 \quad (94)$$

$$H_2S + Zn(OH)_2 \rightleftharpoons ZnS + 2H_2O \quad (95)$$

where equation (93) is necessary in view of the finite initial rate of reaction observed using a "dry" feed gas.

The effect of water in increasing the pss rate is illustrated in Figure 4.7 for four different inlet partial pressures of hydrogen sulphide. Thus the rate of the diffusional process which enables the reaction of zinc oxide present in the interior of crystallites is also enhanced by the presence of water vapour in the feed. This would seem to provide evidence against the mechanism of gaseous diffusion of hydrogen sulphide through a layer of zinc sulphide which should be largely unaffected by changes in the concentration of such a minor component.

The role of water in influencing the rate of solid state diffusion is most easily visualised for a system exhibiting Frenkel disorder in the oxygen sublattice and possibly also non-stoichiometry in the form of a zinc excess arising from oxygen vacancies rather than zinc interstitials. For such a crystal defect type, water adsorbed on the crystallite surfaces might act as a sink for oxygen vacancies providing a driving force for the movement of defects and thus also for the transport of anions through the structure. Figure 5.1 illustrates this possible mechanism. The first mechanism illustrated, whereby an oxygen vacancy is consumed by

Figure 5.1: Mechanism of solid state diffusion.

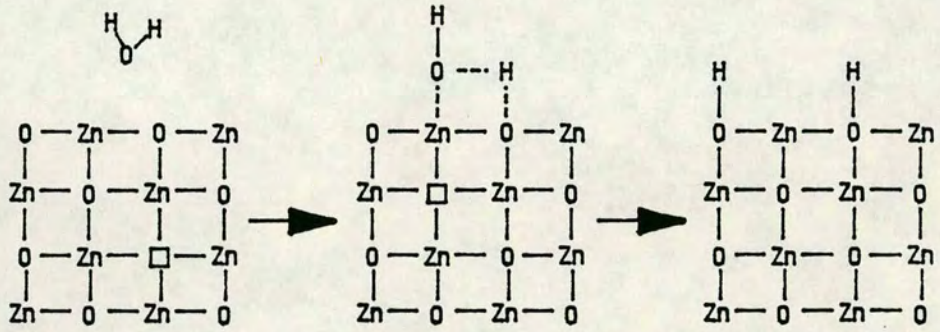

(a) Absorption of water via a vacancy mechanism - ie. consumption of the vacancy at the surface.

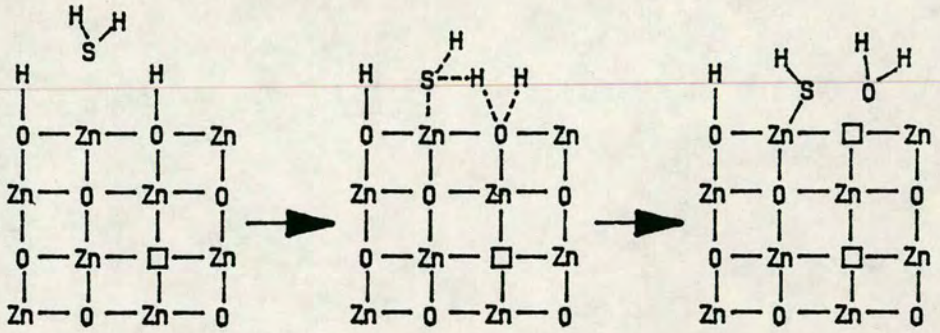

(b) Reaction of hydrogen sulphide with hydroxylated zinc oxide with loss of water, followed by

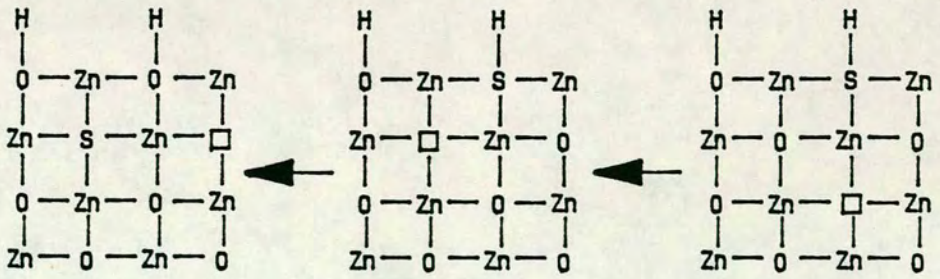

(c) diffusion of anions through the crystal structure.

the absorption of a molecule of water, probably represents an irreversible reaction. In fact, adsorption of water is observed to be reversible (section 4.6) and is likely to involve only the breaking of an O-H bond and formation of Zn-O and O-H surface bonds. The second mechanism indicated by (b) and (c) shows how hydrogen sulphide might be adsorbed with the release of water and how the presence of oxygen vacancies in the zinc oxide might permit the diffusion of anions through the structure. Note that this representation of the zinc oxide structure is in fact incorrect in terms of bonding as a comparison with the 3-dimensional Wurtzite structure of Figure 2.1 immediately reveals. It is a valid representation of zinc oxide only in so far as the zinc and oxygen are both 4-coordinate. Clearly the evaluation of a potential mechanism of diffusion or reaction in spatial terms must be based on consideration of the 3-dimensional structure. Because of the limited usefulness of a 2-dimensional representation, no attempt has been made to consider the mechanism of anion diffusion along dislocations.

As far as surface diffusion is concerned, it is likely that a hydroxylated surface would facilitate proton transfer reactions and that such a surface would be energetically more uniform than an unhydroxylated zinc oxide surface and therefore permit greater mobility of ions over the surface. Clearly, if the product layer is porous, then with respect to the mechanism whereby the reaction of zinc oxide in the bulk of the crystallites is due to the transport of hydrogen sulphide to the reaction surface, the hydroxylated surface may permit a higher rate of surface diffusion of hydrogen sulphide. Whether this has a significant effect on the pss rate will depend upon the relative contributions of surface diffusion and bulk diffusion to the rate of transport of

hydrogen sulphide through the product layer. This in turn depends upon the pore structure of the absorbent, with surface diffusion being more important in fine pores where the mechanism of gaseous diffusion is Knudsen diffusion. In such pores and particularly at low temperatures surface diffusion may account for more than 50% of the mass flux.[8] Water may also tend to occupy the distorted regions or gaps - of the order of Angstroms in width - at the zinc oxide/zinc sulphide interfaces which are created by the accommodation of the larger sulphur anion into the Wurtzite structure. If multilayers of adsorbed water exist, the relatively high solubility of hydrogen sulphide in water[16] could be important in feeding hydrogen sulphide to the reaction surface.

The inverse effect of temperature upon the rate of reaction in the range 0-25°C (Table 4.9) confirms the importance of adsorbed water in the reaction mechanism. The observed loss of adsorbed water from an absorbent sample with increasing temperature under a constant partial pressure of water is tabulated in Table 4.8 (Experiment 2). Thus, at temperatures around and below ambient, the beneficial effect of increasing temperature upon the kinetic rate constant, diffusivities and defect concentrations is far outweighed by the deleterious effect on the quantity of water adsorbed on the absorbent surfaces. Above ambient there is a range of temperature where these two opposing effects are of similar magnitude and the reaction rate is relatively insensitive to temperature eg. experimental runs 55, 57 and 58 in Table 4.9. At elevated temperatures, there will be very little adsorbed water. The reaction

---

[16]Solubility of hydrogen sulphide in cold water is 437cm^3 in 100cm^3 water.

mechanism may be quite different and the effect of temperature on the reaction rate is governed by kinetic rather than equilibrium considerations so that increasing the reaction temperature enhances the rate.[9]

Although the use of a partial pressure of water to improve the utilisation of absorbent beds of zinc oxide appears very attractive, there are other considerations which may be of much greater importance. In the North Sea, where zinc oxide beds are used to sweeten Natural Gas, the gas is dried prior to the sweetening process. This is essential because of the risk of methane hydrate formation which can rapidly result in pipe blockage. At gas pressures of more than 1000psig (about 70barg) and with average sea bed temperatures of 4°C, the water content of the gas must be kept below 100ppm (0.01%) to avoid methane hydrate formation[10] and will generally be reduced to 20-50ppm to allow some margin for error. Low pressure applications look more promising, however, as the water content at which methane hydrate formation becomes possible is much higher (eg. about 6000ppm or 0.6% at atmospheric pressure and 0°C).

In contrast to the marked dependence of the reaction rate upon the partial pressure of water, Figure 4.8 indicates that the pss rate shows no strong trend with partial pressure of hydrogen sulphide in the range studied. There is a slight suggestion of a maximum in the curves which might arise from competitive adsorption of water and hydrogen sulphide if the reaction proceeds faster in the presence of adsorbed water and a high partial pressure of hydrogen sulphide has the effect of excluding water from the surface. Equally, at very low partial pressures of hydrogen sulphide in the feed, the surface might be starved of the gaseous reactant. An examination of Table 4.7 reveals, however, that the absorbent conversion at pseudo-steady state, or,

equivalently, its sulphur content, increases with increasing partial pressure of hydrogen sulphide in the feed. If the rates were to be plotted at constant solid conversion then this would have the effect of relatively increasing the rates at higher hydrogen sulphide pressures. Thus the maxima referred to are probably only indicative of the variation in solid conversion between experiments.[17]

One of the surprising experimental observations made is that although prior to a sulphiding experiment absorbent samples were pre-treated by equilibration with a nitrogen stream containing a partial pressure of water equal to that in the reactor feed, there still appears to be a nett consumption of water by the absorbent during the sulphiding runs. Table 4.3 illustrates this phenomenon for a number of experimental runs.

The relatively poor accuracy of the water analyses compared to the hydrogen sulphide analyses has been mentioned (section 3.1.4). A further source of error in the numerical integration, however, which will lead to an underestimate of the amount of water evolved is a feature of the discrete nature of the analysis. Thus the amount of water evolved is likely to be underestimated if a sample of product gas is not taken just at that time at which the partial pressure of water in the outlet stream is maximal. However, except where the curve of molar flowrate versus time is highly

---

[17]Note, that the interference of solid conversion observed here does not conflict with the experimental result of Mantri et al. reported in section 2.3.2 of the validity of the assumption that gas-solid reactions are zero order with respect to the solid reactant. In that case, a chemical dependence was investigated. In the current work, where the zinc sulphide is not intimately and homogeneously mixed with the zinc oxide, a mass transfer effect is assumed to exist.

peaked, this error is unlikely to account for much of the water apparently irreversibly adsorbed. Further evidence for this nett consumption of water by the absorbent comes from 're-start' experiments. These are runs which have been interrupted and then left for several hours (usually overnight) with the reactor isolated and held at reaction temperature so that the absorbent is exposed to stagnant gas of the composition of the reactor outlet gas. When the run is re-started, it is firstly equilibrated with a nitrogen stream containing the same partial pressure of water as was used in the run prior to interruption. During this second equilibration treatment further adsorption of water has been observed indicating that the partial pressure of water in the reactor has dropped during the period of isolation. This is unlikely to be due to leaks in the system as no odour of hydrogen sulphide was detected, and as the reactor is at atmospheric pressure, being isolated after the flow has been turned off. Inward leaks are therefore as likely as outward leaks and these would be expected to lead to a rise in the water partial pressure given the low water contents of the feeds used in these experiments (see Table 4.10). Moreover, the system has been thoroughly tested at all stages of development and modification to ensure its integrity. It is therefore concluded that the fall in the water partial pressure is due to continued adsorption of water by the partially sulphided absorbent during the period of isolation.

It is clear that the partially sulphided absorbent isolated under an atmosphere of stagnant gas as described above continues to undergo physical change. The strongest evidence for this claim is the high reaction rate which is observed upon re-exposing the absorbent to hydrogen sulphide containing gas. The sulphiding experiment performed after isolation shows

the same time-decaying rate behaviour as the experiment on the unsulphided absorbent, suggesting that some solid rearrangement has taken place during the period of isolation. The initial period of high reaction rate is, however, short-lived and a pss is established much more rapidly than in the first run of the pair. This could be indicative of solid rearrangement exposing fresh zinc oxide on some small fraction of the surface area. In only one pair of experiments (runs 73 and 74) was the second experiment of sufficient duration to allow a pss rate to be measured. The pss rate of the second run of the pair was only 20% of the pss rate of the first, and corresponded to an increase in the absorbent conversion from 31.7% to 38.6%. From a commercial standpoint it would be interesting to know whether a temporary interruption of the feed to an absorption bed affects the ultimate sulphur pick-up by the bed. Such a comparison - between the pss rates achieved at the same solid conversion by running a bed continuously or subjecting it to a single or multiple interruptions - is difficult and impracticable to make accurately on the apparatus described in chapter 3 which was developed for differential analysis on a much shorter time-scale. The calculated solid conversion of the continuously operated bed will be subject to substantial error because of the significant contribution to the absorbent conversion made by the inevitably very long pss process. Here, the incremental conversion is directly proportional to the small difference (1-5%) between the hydrogen sulphide contents of the feed and product streams. An assessment of the relative performances of the two absorbent samples under the different operating regimes should therefore be made by analysing the sulphur contents of the discharged samples.

Further evidence for solid rearrangement of the partially sulphided absorbent bathed in stagnant gas

comes from colour changes evident at the absorption front of the dump bed. During an experiment the position of the reaction front is easily located, being identified by a yellow tinge to the absorbent granules. Behind the front, the partially sulphided granules are a slightly darker shade of grey than the unsulphided granules downstream of the front. Several hours after the hydrogen sulphide containing stream has been switched off, however, it is much more difficult to locate the absorption front as the yellow tinge appears to have faded or to have become more dispersed. If this colour arises due to distortion in the crystallite close to the external surface of the granule caused by mechanical stress around the large sulphide ion (section 2.1.1), its disappearance may be understood in terms of crystal rearrangement to reduce stress around the dislocations caused by the moving reaction front within individual crystallites. Clearly, at later stages of the reaction the yellow colour will not be seen as the reaction front will have progressed further into the granule and the colour associated with it will be masked by the greyness of both oxide and sulphide, which colour is imparted by the cement added during granulation of the absorbent.[18]

The drastic reduction in pss rate observed between the first and second runs of an interrupted experiment has been referred to. A very low pss rate was also measured on absorbent particles which had been pre-sulphided in batches. These rates are given in Table 4.11 together with the rates measured over initially unsulphided absorbent. Once again, the pss rate over the

[18]Early qualitative examination of some sectioned sulphided granules with a binocular microscope revealed a very faint yellow ring concentric with the surface but at some distance from it which may have indicated the position of the reaction front.

pre-sulphided material is only 20% of that over the absorbent which was not pretreated although the absorbent conversion at pss is only 5-12% higher than the 30% conversion of the initially fresh material.

5.3 Absorbent Particle Size - Is there an optimum ?

With regard to the operation of a commercial packed bed, whether it be an absorber unit or catalytic reactor, there is always an optimal particle size. This optimum arises due to the conflicting demands to minimise pressure drop across the bed and to maximise the utilisation or effectiveness of the absorbent or catalyst. The former aim is achieved by increasing the average particle size whereas the latter is achieved by decreasing the particle size and thereby decreasing the effect of pore diffusion resistance. In the present case the possibility is investigated that the complexity of the effect of pore diffusion on the reaction rate may suggest an optimal particle size even when pressure drop considerations are neglected.

It is clear that during the early stages of the reaction of a granule of zinc oxide the concentration of hydrogen sulphide falls sharply in the outer shell of the granule corresponding to the reaction zone (Figure 4.16). Where pore diffusion is not observed to limit the initial rate, as in small particles, the reaction zone extends to the centre of the particle at all stages of the reaction. In whole granules, however, the width of the reaction zone increases with time as the slowing reaction rate in the outer shell allows the reaction front to penetrate further into the granule. Just as the effect of pore diffusional resistance is to reduce the concentration of hydrogen sulphide in the interior pores of a granule, so it must also moderate the concentration profile of the gaseous product water,

tending to increase the water concentration in the interior of the granule. Thus, pore diffusional resistance combined with a large particle size results in less uniform concentration profiles of both gaseous reactant and product. Initially, this results in a lower reaction rate in larger particles as has been observed but it is conceivable that due to the autocatalytic nature of the reaction, the beneficial effect of the higher water concentration in larger particles could reverse the effect of particle size on the rate. Thus, if a higher partial pressure of water were generated within a larger particle due to the effects of pore diffusion, the rate of reaction would be greater in the larger particle. In comparing the rates of reaction of a small and a large particle, therefore, four stages of reaction may be envisaged. In the first stage, the reaction rate is greater for the small particle due to the rate of pore diffusion limiting access of hydrogen sulphide to the interior of the large granule. In the second stage, the rate over the small particle has dropped considerably due to the build-up of zinc sulphide. The reaction rate is now higher in the large particle, the core of which still has a lower sulphide content than the outer shell. The third stage is reached when the conversions of the two particles are similar. The larger particle continues to show a higher rate due to the now favourable effects of the combination of pore diffusion resistance and autocatalysis. The proposed fourth and final stage corresponds to a time such that the rate of the controlling diffusion process is sufficiently slow that the influence of pore diffusion is negligible and similar rates are observed on both systems. Only the first 3 stages are evident in Figures 5.2 and 5.3. One of the interesting aspects of this description of the progress of reaction in particles of different size is

Figure 5.2: The effect of particle size on the growth of solid conversion (Runs 29-33)

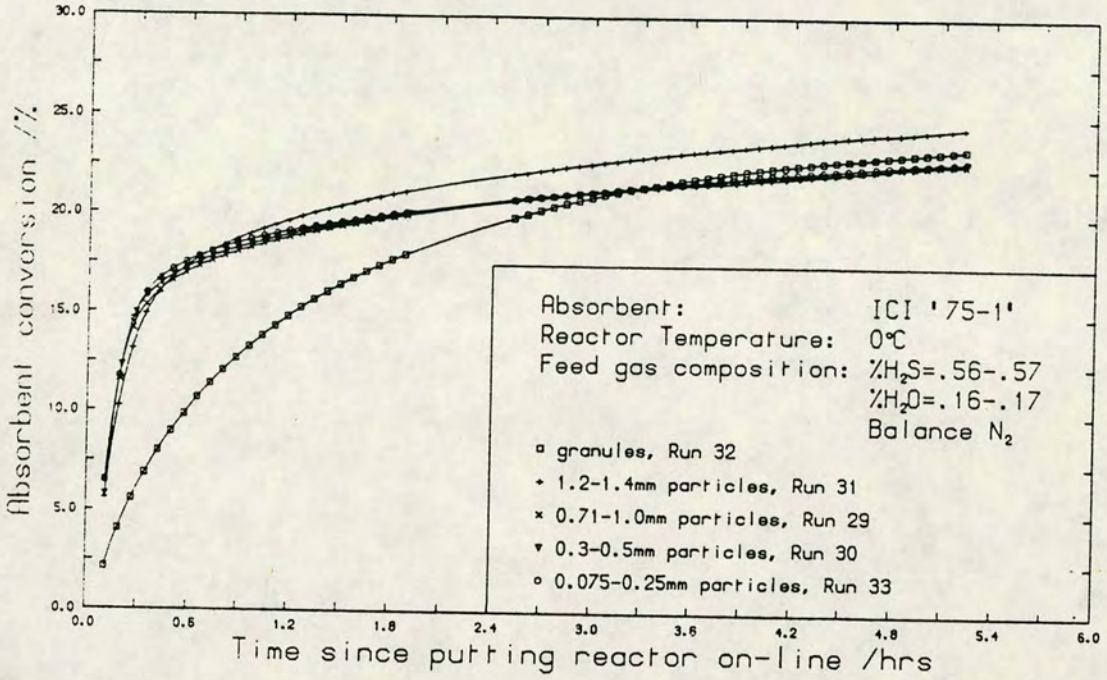

Figure 5.3: The effect of particle size on the growth of solid conversion (Runs 15,17,18 and 19)

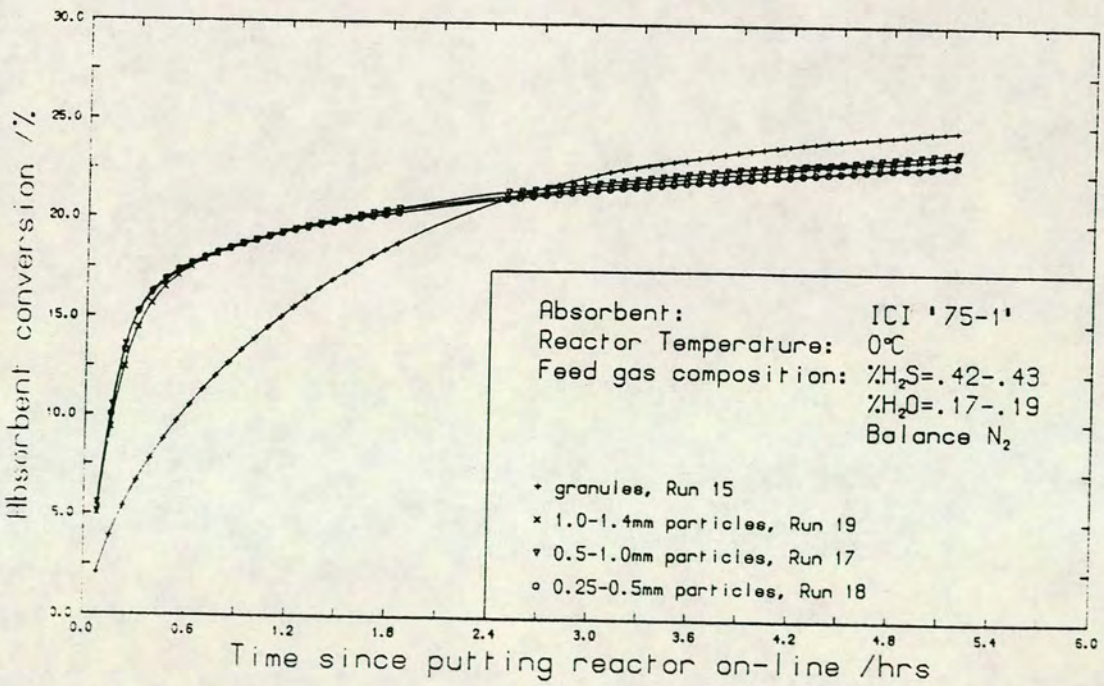

that initially pore diffusion restricts the rate in the larger particle whereas latterly it enhances it. Thus, at high rates of reaction the effect of the pore diffusion limitation on hydrogen sulphide penetration is dominant over its effect on the 'trapping' of water within the particle whereas at low rates of reaction the reverse is the case.

Sapre[11] has shown theoretically that such diffusional enhancement of autocatalytic reactions in catalyst particles occurs. He considers the situation where the reactant may react according to the following scheme:

$$A_{(g)} \rightleftharpoons B_{(g)} \tag{96}$$

$$A_{(g)} + B_{(g)} \rightleftharpoons 2B_{(g)} \tag{97}$$

The reactions are respectively first and second order with rate constants k_1 and k_2. Note that without the first reaction, the conversion of A would not proceed unless some of the product were initially present. Sapre has analysed the system in terms of the dimensionless constant, β, which is the ratio of the Thiele moduli for the two reactions and is given by

$$\beta = (k_1/k_2 c_{A0})^{\frac{1}{2}} \tag{98}$$

where c_{A0} is the initial concentration of A. For $\beta=1$, no diffusional enhancement is observed, but for β much less than 1, the effectiveness factor, η, for the system increases with the Thiele modulus contrary to the behaviour for a non-autocatalytic reaction in a catalyst particle. The effectiveness factor passes through a maximum because at very high values of the Thiele modulus the effect of the poor use of the catalyst interior is more significant than the diffusional enhancement of the rate. The value of the effectiveness factor may reach several hundred. Thus, for a given system, an optimal particle size exists for a particular set of operating conditions. It has further been shown

that the optimal particle size decreases along the length of a fixed bed reactor.

For the hydrogen sulphide/zinc oxide system the equivalent equations to (96) and (97) which Sapre has considered are equations (93)-(95). Equations (94) and (95) represent qualitatively the observed autocatalytic effect but may have no mechanistic significance. This would be the case, for example, if the role of water in enhancing the sulphiding rate arises solely from its ability to increase the rate of anion diffusion through the product layer or of self-diffusion on the crystallites' surfaces while the rates of the reactions represented by equations (93) and (95) are very similar.

Figures 5.2 and 5.3 are plots of the growth of the solid conversion with time for the different particle size fractions for which results are presented in Table 4.4 and Figures 4.3 and 4.4. By considering the slopes of the conversion curves for the different particle sizes in Figure 5.2, it is apparent that the reaction rate over the granular material is lower than that over the smaller particles up to a conversion of about 17%. This corresponds to between 4 and 5 monolayers depth on the basis of a specific surface area of $55 m^2 g^{-1}$. No pore diffusion limitation is evident for the 1.2-1.4mm particles, however, although these show a significantly enhanced rate compared to the smaller particles after about an hour on-stream (corresponding to a conversion of about 18%). The set of runs presented in Figure 5.3 show similar behaviour. Without a model of the reaction system it is difficult to interpret what the effect of particle size is in the later stages of the reaction but the size of the effect is fairly small, representing a difference in solid conversion of less than 2% with the maximum ultimate conversion of just over 24% being shown by the 1.2-1.4mm particles.

5.4 Modelling of the Hydrogen Sulphide/Zinc Oxide Reaction

To the author's knowledge, only the grain model, developed by Szekely et al.,[12] has been used to model the reaction of zinc oxide with hydrogen sulphide at ambient temperature. Gibson and Harrison[13], in analysing rate data over a broad range of temperature, used independent determination of all model parameters except the grain or product layer diffusivity to see how well the model described the experimental data (section 2.4.3). The grain diffusivity was assumed to be high such that diffusion through the product layer was not rate-limiting. The reaction was assumed to be first order in hydrogen sulphide concentration as found by Westmoreland et al.[9] and the intrinsic rate constant determined by these workers was used. The particle diffusivity was estimated using the random pore model based on correlations for the contributions from Knudsen and molecular diffusion. The remaining physical properties of the system were either measured directly or calculated from directly measured properties. The model was found to provide a reasonable fit to the experimental data for reaction temperatures in the range 600-700°C where the most significant resistance to reaction is provided by internal diffusion. Where internal diffusion is rate controlling, the grain model reduces to the shrinking core model. Thus a plot of $[1 + 2(1-\bar{x}) - 3(1-\bar{x})^{2/3}]$ versus time should be linear.[14] This is indeed found to be the case except at high conversions ($\bar{x}>0.8$) where the shrinking core model overpredicts the reaction rate. At lower temperatures, 375-500°C, the grain model greatly overpredicts the reaction rate at all but very low conversions. Moreover, the rate was found to drop rapidly and the reaction effectively to stop long before complete conversion had been achieved. Gibson and Harrison

attribute these deviations of the model predictions from the experimental results to the greater importance of the grain diffusion resistance at higher conversion and at lower temperature. Interpreting the grain diffusion process as one of solid state diffusion, the dependence of the resistance upon temperature and conversion is readily explained in terms of the high activation energy[19] of the process and the increasing path length for diffusion associated with increasing solid conversion.

While the use of the grain model to describe these results is interesting as is the assignation of the product layer diffusional process as one of solid state diffusion, it is highly probable that the mechanism of the sulphiding reaction at these elevated temperatures is quite different from that at ambient temperature. In particular, the autocatalytic effect may be entirely absent due to the unfavourable equilibrium between water vapour and adsorbed water at these temperatures. The position of the adsorption equilibrium suggests that surface diffusion of an adsorbed species is likely to contribute negligibly to the diffusion or reaction processes although self-diffusion - of atoms, ions or clusters on the crystallite surfaces - will be enhanced. The rate-limiting effect of the pore diffusion resistance will be relatively greater than at ambient temperature because the dependence of diffusivity upon temperature is much weaker than the temperature dependence of the intrinsic kinetic rate.

Cresswell[15] has used the same model to analyse the rate

---

[19]Gibson and Harrison found optimal values of the grain diffusivity to fit their experimental data at 375 and 500°C. These values are not given, however, so that no preliminary estimate of the activation energy of the solid state diffusion process is available.

controlling processes of the hydrogen sulphide/zinc oxide reaction at ambient temperature as measured by the 'breakthrough' experiments performed at ICI. Considering in turn the three limiting cases of the grain model[14], namely chemical rate control, pore diffusion control and film mass transfer control, he has calculated the time required for complete conversion. The film mass transfer coefficient and particle diffusivity were calculated from correlations, while the kinetic rate constant was estimated from the measured sulphur profile through the bed assuming the reaction to be first order in hydrogen sulphide concentration and using the relationship between the effectiveness factor and the Thiele modulus to correct the rate constant for the effect of pore diffusion. In this way, Cresswell showed that pore diffusion is much the slowest of these three processes. Using the extension of the grain model to a fixed bed system, developed by Evans and Song[16], Cresswell has compared the plot of solid conversion against distance along a packed bed as predicted by the model with the actual profile measured on a commercial bed operating at 100 bar. The agreement between the two is very poor, with the model greatly overpredicting the conversion towards the bed inlet and underpredicting it towards the exit. Thus hydrogen sulphide breaks through much earlier than the model predicts with consequently much poorer utilisation of the bed capacity. Cresswell attributes the inadequacy of the model to its failure to account for the growing resistance with conversion of the solid product layer. He concludes, however, that extension of the model to account for this resistance and for the observed beneficial effect of water on the reaction rate and upon the ultimate conversion of the solid would render it unuseable.

5.5 The Chemical, Physical and Structural Nature of the Absorbent

In this section the effect of the absorbent's physical structure upon its sulphur pick-up characteristics and the preparative method which determines that structure are considered. The presence of impurities in the commercial absorbent is also discussed as is their likely impact on surface and bulk structures and thereby on the rates of physical and chemical processes. In the light of this discussion, some suggestions are made as to how zinc oxide might be modified to improve its hydrogen sulphide absorption characteristics.

In the commercial process for the manufacture of the zinc oxide absorbent, '75-1', the basic carbonate is granulated using a binder. The granules thus produced are calcined at about 250°C for about 10 minutes. The calcination temperature is selected to maximise the specific surface of the absorbent produced.

Calcination experiments performed at 250°C and 365°C confirmed that a higher specific surface area is obtained at the lower temperature - 100 m^2g^{-1} compared with 71 m^2g^{-1}. Under otherwise identical experimental conditions the weight losses for the samples calcined at 250°C and 365°C were 20.1% and 23.0% respectively (Table 4.1). The standard sulphiding experiment performed on each of these two materials yielded surprising results, however, as Figure 4.11 and Table 4.13 indicate. In spite of the difference in specific surface area between the two materials, the initial reaction rates are identical up to a sulphur pick-up of about 5% w/w which is equivalent to an absorbent conversion of almost 20%.

Beyond this point the rate over the lower[20] surface area material begins to drop more rapidly. The position is rapidly reversed, however, by the later but more rapid fall in reaction rate over the higher surface area material which shows a significantly lower pss rate of 1.9×10^{-8} moles per gram absorbent per second compared with the pss rate of 2.6×10^{-8} moles per gram absorbent per second for the lower surface area material.

A number of interesting observations can be made about this result. Firstly, the identity of the initial rates, although real, is probably somewhat deceptive resulting as it does from complete conversion of the hydrogen sulphide fed. The experiments do not thus allow us either to confirm or to challenge with regard to the surface rate the assumption implicit in the ICI calcination procedure that a high specific surface area has a beneficial effect on the rate. The fact, however, that at an early stage of the reaction a higher rate is observed on the higher surface area material suggests that the rate at low absorbent conversion (less than 20%) may be dependent upon the absorbent's surface area. In order to test whether this is indeed the case it would be necessary to repeat the experimental runs using either less absorbent or a higher gas flowrate to ensure that the conversion of hydrogen sulphide is less than 100%.

At higher conversions the pss rate is clearly higher on the material with lower measured surface area. Measurements of the specific surface areas of absorbents before and after sulphiding (eg. Table 4.5) suggest that at this stage of the reaction, the specific surface

---

[20]Note that this refers to the specific surface areas as measured prior to sulphiding. No measurements of surface area are available corresponding to intermediate points during the experimental runs.

areas of the differently calcined materials are unlikely to differ significantly. The cause of the difference in rates is therefore likely to be some other property of the absorbent which was affected by the calcination process. This might be the concentration or nature of crystal defects or the distribution of crystal faces exposed on the particle surfaces. However, at such low calcination temperatures, the concentration of thermally created point defects is likely to be very low and insignificant compared to the levels of non-equilibium defects and dislocations, while the presence of impurities - such as sodium cations - will be more important in determining surface structure.[17] As a test of the hypothesis that the property of the absorbent which most strongly influences the rate changes during the course of the reaction, it would be interesting to do a sulphiding experiment on a sample of the absorbent which had been calcined at a temperature below 250°C but which yielded a specific surface area similar to that of the material calcined at 365°C. A sample so prepared would clearly retain a higher carbonate content.

With regard to the dependence of the absorbent activity upon the calcination temperature of the precursor, two pieces of experimental work with zinc oxide by other researchers are pertinent. Students working with Dr J.M. Davidson[3] in the Chemical Engineering Department at Edinburgh University prepared samples of zinc oxide from basic zinc carbonate by calcining at 250°C or 350°C. The samples were then pressed to form discs of diameter 16mm and thickness 10mm which were mounted in a diffusion cell. The diffusion of ethane from a mixture with nitrogen into a pure nitrogen stream through these discs was measured at ambient temperature and the diffusivity in the zinc oxide prepared at 350°C found to be 50% higher than that in the zinc oxide prepared at 250°C (2.25×10^{-6} and 1.51×10^{-6} $m^2 s^{-1}$

respectively). While no measurements were made to check the reproducibility of the pressing procedure, the magnitude of the difference in diffusivities is sufficient to suggest that a real difference may exist. Plyasova et al.[18] have observed the distortion of the zinc oxide structure (section 2.1.4) prepared at low calcination temperatures (300°C) and attributed this to the effect of residual carbonate and hydroxide in the structure. It is likely therefore that the extent of distortion in the samples calcined at 250°C and 350°C differs.

Zarkanitis and Sotirchos[19], in studying the capacity of limestones for removal of sulphur dioxide, have considered the effect of the temperature at which the limestone is calcined to form calcium oxide. They observed that material calcined at 850°C had a lower specific surface area but higher ultimate capacity than material calcined at 750°C although the initial sulphiding rates were similar. They measured pore size distributions and attributed the higher surface areas of the materials calcined at the lower temperature to the lower mean pore diameter. In view of the large increase in solid volume associated with the reaction, it was concluded that the lower capacities of the higher surface area materials were due to the combination of higher local reactivities and greater intraparticle diffusional limitations leading to earlier pore blocking at the external surface of the particle.

While such an explanation for the differences in sulphiding of zinc oxide samples calcined at different temperatures is supported by the observed differences in surface area and diffusivity, it should be noted that these experiments were performed on particles of a size (300-710 microns) selected specifically to exclude pore diffusion effects. Blockage of small pores may still

occur but these pores will be distributed randomly through a particle rather than being located at the external surface. This does not, however, preclude the result of pore blockage being a reduction in ultimate sulphur capacity. This is a function, as Zarkanitis and Sotirchos have discussed, of the extent of interconnectedness of the pore space. Thus, where large pores or cavities are accessed via a smaller pore, the large pore may become inaccessible by the blockage of the small feeder pore. As such 'dead-ended' pores do not contribute to gas diffusivity as measured in a diffusion cell, their closure as a result of sulphiding should not affect the measured diffusivity. This explanation is therefore not inconsistent with Halcrow and Dickson's observations[3].

The use of cement in the commercial absorbent gives the granules strength. The effect of the cement on the progress of the reaction could most readily be studied by comparing the sulphiding rates over granules prepared with and without cement, or, as the latter would be difficult to prepare, by comparing the rates over material pelleted with and without cement. Alternatively, a blank run could be done on the cement to see whether any reaction took place. This last experiment is less satisfactory as a negative result would not exclude the possibility that some interaction between the zinc oxide and the cement might influence the reaction rate. A comparison of the sulphiding rates over absorbent samples prepared with and without cement has been done at ICI.[20] It was concluded that the presence of cement did not affect the rate except in so far as it acted as an inert diluent.

A comparison between sulphiding runs performed on the commercial absorbent, '75-1', and zinc oxide prepared by calcining the commercial basic zinc carbonate (BZC) is

provided by Table 4.5. The materials are clearly very different although BZC is the principal component of the absorbent precursor (see Table 4.1). The pure zinc oxide (Run 13) has a much higher specific surface area but it is of interest that after sulphiding the specific surface areas of both materials are much less and are the same within experimental error at 41 m^2g^{-1}. If the pss rates are expressed per mole of zinc oxide initially present in each of the two materials then they are found to be very similar although the conversion of the pure zinc oxide is slightly higher, being 33.6% compared to 29.8% for the 75-1. Note, however, that the value of the conversion calculated for the commercial absorbent is subject to error in proportion to the standard deviation of the estimated cement content.[21] The similarity of the rates on a zinc oxide basis suggests a lack of interference by the cement in the reaction process. This conclusion is further supported by optical microscope and electron microprobe scans which indicate that the cement is present as small inclusions apparently distributed randomly through the granules.

The non-uniform hardness and structure of granules which has been observed (section 4.12.1) appears not to be related to a maldistribution of cement. It may arise due to other causes deriving from the variability in the granulation process itself.

Impurities are also present in the commercial absorbent but these, unlike cement, are not added deliberately for their beneficial properties but arise due to the preparative or storage and handling procedures.

---

[21]This is, of course, the case for all sulphiding runs using '75-1'. The high degree of repeatability between runs, however, suggests that no significant difference in cement content exists in samples of the size used.

Significant among these is the carbonate species. Atmospheric carbon dioxide is readily adsorbed on the surfaces of the absorbent as IR spectra of high surface area zinc oxide samples have shown. Heat treatment of the previously calcined absorbent at 250°C or 350°C in vacuo[22] causes evolution of carbon dioxide and this heat treated absorbent appears to be more active for hydrogen sulphide removal than is the untreated absorbent (Table 4.12). Interestingly, however, it is the pss rate which is 30-40% higher for the heat treated material, that is, the rate of reaction of zinc oxide in the bulk of the crystallites is enhanced by the treatment. The fact that the result of heat treatment of the absorbent is not merely a surface effect is not readily explained without further experimentation. If the rate enhancement is due in any part to the removal of the carbonate species then it might be expected that the extent of the rate enhancement should be less for materials which have been stored for longer between treatment and sulphiding because of the re-adsorption of carbon dioxide. If, however, the loss of carbonate species is the sole cause of the increased rate then no decline in sulphiding performance should be observed if the heat treated absorbent is stored under nitrogen. While loss of carbonate during heat treatment of 75-1 might be expected to improve the activity of the absorbent so produced, it is noteworthy that the bulk of the weight loss (80%) is due to loss of water (see absorbent (4) in Table 4.1).

---

[22] Tanabe et al.[21] note that calcination in vacuo of hydroxides or carbonates of magnesium, calcium and barium results in a higher surface area than calcination under atmosphere because of the absence of water vapour which can facilitate sintering. It seems plausible that the same may be true with respect to the calcination of hydrozincite to form zinc oxide.

In view of the likely presence on the surfaces of the commercial absorbent of carbonate species due to adsorption, and of the possible presence of small pockets of carbonate in the crystallite bulk due to incomplete calcination, it is interesting to consider the properties of basic zinc carbonate as an absorbent. A single sulphiding run was performed on basic zinc carbonate (BZC), the principal component of the precursor to the commercial absorbent. The results of this run are given in Table 4.6 together with those of a run performed on 75-1 under identical conditions. The initial specific surface area of the BZC is significantly less than that of the 75-1, being 31 m^2g^{-1} compared with 55 m^2g^{-1}. The surface area of the BZC was not re-measured after sulphiding.

The pss rates for the two runs have been expressed per mole of absorbent and per mole zinc to allow comparison of the efficiencies of the materials both on a weight basis and as far as zinc utilisation is concerned. The performance of the two materials is strikingly different. Compared to the commercial absorbent, the basic zinc carbonate shows a much higher initial reactivity which is sustained for a longer period. The pss rate once achieved, however, is very low, being less than one third of the pss rate on the 75-1 on a zinc basis. While such runs illustrate the differences in the reaction patterns between the two materials, they do not necessarily allow selection of the better absorbent for a given duty. Such information is best obtained by breakthrough runs designed to mimic the commercial application.

Sodium ions are known to be present in the basic zinc carbonate from which the absorbent 75-1 is derived (section 4.13). It appears that these affect the stability of the zinc oxide formed. The presence of

sodium in the zinc oxide structure should lead to a decrease in conductivity (which might provide a means of determining its concentration) analogous to the effect of lithium (section 2.1.2, equations (11) and (12)). It results, however, in an increase in point defects. With regard to the sulphiding reaction it is of interest too that sodium is known to interact with hydroxyl groups in the structure, indicating a potential link between the presence of sodium and the autocatalytic effect.

5.6 Conclusions

The following conclusions may be drawn from the afore-going experimental results and discussion:

1. The specific rate of reaction of a particle decays with time on-stream due to the formation of zinc sulphide, and possibly due also to concomitant structural changes.
2. The presence of water vapour in the feed stream enhances the rate of reaction at all stages of reaction and therefore delays the onset of the pseudo-steady state reaction.
3. In the ambient temperature range, lowering the reaction temperature increases the rate because of its effect of increasing the quantity of water adsorbed on the absorbent surfaces.
4. The dependence of the specific rate of reaction upon the partial pressure of hydrogen sulphide is weak but at equivalent solid conversions the relationship between the rate and the hydrogen sulphide partial pressure is apparently one of direct proportionality.
5. The calcination temperature of the absorbent precursor which maximises the specific surface area of the absorbent is non-optimal with respect to the absorbent's ultimate sulphiding performance. Thus improved absorption performance but reduced surface area are observed at a higher calcination temperature.
6. The effect of impurites, probably residual sodium ions, in the absorbent is favourable in that it appears to stabilise the absorbent. A zinc oxide absorbent prepared in the absence of sodium ions showed a deteriorating activity over a period of several days. Whether or not this was associated with a change in specific surface area and/or pore structure was not established.
7. The effect of 're-calcining' zinc oxide suggests that the presence of small quantities of carbonate in zinc

oxide which has been prepared by calcination of basic zinc carbonate is deleterious. This may be due to its effect on Lewis acidity although it may also disrupt the zinc oxide structure in such a way as to impede the transport of ions between and through solid phases.

8. An optimal particle size exists for a given absorption duty but the effect of particle size upon absorption activity although measurable is small.

5.7 Proposed Directions for Future Research

Given the autocatalytic nature of the reaction between zinc oxide and hydrogen sulphide, it would be particularly interesting to study the surface reaction in order to elucidate the role of water in enhancing the rate. In commercial units it may be impracticable to alter significantly the partial pressure of water in the feed to an absorption unit. There may also be considerable variation in the stream's water content over which the operator has little or no control. It is potentially therefore of great interest to know whether a different operating procedure could enhance the performance of the bed ie. whether periodic interruption of the bed usage in order to treat the absorbent in situ with water would be advantageous or whether its effect would be very short-lived. Alternatively it might be sufficient to interrupt the absorption, switching to another column, to allow time for the process of crystal rearrangement. The merits of such an operating procedure can only be investigated experimentally. While it may be possible to extrapolate the pseudo-steady state rate of the first run of a pair for an interruption period of several hours and thereby estimate the absorbent conversion which would have been achieved if an absorption run had been continued rather than interrupted, this procedure is unlikely to be valid where the period of interruption extends to several days. Thus in the case of runs 73 and 74 (Table 4.10),

where the length of time between the end of the first run and the end of the second is 12 days, the assumption that the pss rate of run 73 remains constant over this extended period implies complete conversion of the absorbent in just under 4 days. In fact, it is probable that the pss rate will slowly decline, however, the calculation suggests that while interruption may benefit ultimate conversion and mean reaction rate (no evidence is presented here either to justify or refute such a proposition), there is likely to be an optimal interruption time.

Clearly an improved understanding of the process by which the bulk zinc oxide reacts would be invaluable. If the role of water in this process were understood, it might suggest a direction for new more active absorbents incorporating within their structure an effectively catalytic component mimicking the observed role of water in the present process. In view of evidence for the interaction of sodium ions with hydroxyl groups, it would be useful to prepare zinc oxide doped to different extents with sodium in order to determine both the criterion for absorbent stability and whether the sodium concentration interferes with the autocatalytic effect. The presence of sodium ions in the absorbent may, however, be disadvantageous in some circumstances. It has been observed,[20] for example, that a partial pressure of carbon dioxide in the feed to an absorber bed leads to a lower sulphur capacity, and it is possible that the increased basicity caused by sodium ions in the zinc oxide may exacerbate this problem.

Essential to the gaining of an understanding of how the absorbent 75-1 reacts, and to the development of improved absorbents must be the use of well-characterised absorbents. Thus, where impurities are present either by intention or as a result of

contamination during preparation or storage and handling, analytical techniques should be available to determine not only their concentration but also their location - on surfaces or within the bulk structure - and distribution. Thus, for example, with respect to cations, their presence as separate oxide phases or in solid solution is likely to be critical in determining their effect. X-ray photo-electron spectroscopy (XPES) can be used to identify the existence of separate phases in the absorbent, while for paramagnetic impurities the use of electron paramagnetic resonance (EPR) might provide additional information about, for example, whether cation impurities occupy tetrahedral or octahedral sites in the oxygen lattice.

Although specific surface areas were determined in this study, no attempt was made to characterise the pore structure of the absorbents. Given the importance of the pore diffusional resistance to the rate of reaction over granular material and the possibility that the influence of calcination temperature upon absorption activity may derive from its effect on the pore structure of the absorbent, it would be useful to combine measurements of pore size distribution (eg. from nitrogen adsorption and desorption experiments) and of diffusivities in order to give a preliminary description of the pore structure of different absorbents.

As further absorbent tests will be performed on material pelleted in the laboratory - as opposed to the work reported here which was mostly performed on commercially granulated material - it is essential that the repeatability of the pelleting procedure is well-defined.

Finally, as a tool for studying the effect of water on

the reaction, in order to establish whether a nett consumption of water occurs during the course of a reaction and for determining what poisoning effect, if any, carbon dioxide has, it could be very instructive to operate a pulse reactor system. Such a reactor would allow the examination of the effect of very small doses of the various gases. In order to interpret such experiments the absorbent bed would have to be precisely defined in terms of the pore volumes of the bed and of the absorbent particles. Its operability, moreover, would be dependent upon a much more sensitive detector for hydrogen sulphide. For such a reactor mode, however, the Flame Photometric Detector (FPD) could well prove useful as the experimental set-up could readily incorporate the regular injection of calibration mixtures into the detector, and the very different mode of study of the reaction would not require the long-term detector stability essential to differential analysis. Subject to the use of the same carrier gas for the gas chromatograph and for the experiment and to the outcome of a test to determine any interference effect of water on the analysis of hydrogen sulphide, it might be possible to analyse continuously with the FPD. Alternatively, a continuous flow system could be used with an infra-red drift cell and UV analyser which would permit the examination of surface and gaseous water and carbon dioxide and the analysis of hydrogen sulphide down to about 250ppm.[23] The use of hydrogen/deuterium exchange in combination with solid state NMR might give an insight into the location of water in the system and thereby into the mechanism by which it enhances the rate of hydrogen sulphide absorption.

---

[23]This corresponds to a time of 41 minutes to react all the surface zinc oxide of a 0.5g sample (see Appendix A) if the surface zinc oxide is reacted before any of the bulk material.

REFERENCES

[1] Bowker M., Houghton H., Waugh K.C., Giddings T., Green M.
"Crystal plane dependence of adsorption and reaction on zinc oxide"
J. Catal. 84, 252-255 (1983)

[2] Carnell P.J.H., Denny P.J.
"Techniques for investigating sulphur removal by zinc oxide absorbents"
AIChE Ammonia Safety Symp. (1984)

[3] Halcrow M.
"Investigation of diffusion through zinc oxide"
Department of Chemical Engineering
University of Edinburgh
Laboratory Week Report (1990)

[4] Roberts M.W.
Personal communication

[5] Gour P.K., Upadhyay S.N., Pande S., Chatterjee R., Bhattacharyya N.B., Sen S.P.
"Effect of precipitating agents on activity and physical parameters of zinc oxide"
Proc. Symp. Sci. Catal. Its Appl. Ind.
Sindri, India (1979)

[6] Furmer Yu.V., Beskov V.S., Brui O.I., Yudina V.V., Dantsig M.L.
"Kinetics of the chemisorption of hydrogen sulphide by zinc oxide adsorbents"
The Soviet Chem. Ind. 14(12), 1499-1507 (1982)

[7] Carnell P.J.H., in
"Catalyst Handbook", ch.4
ed. Twigg M.V.
Wolfe Scientific (1988)

[8] Kapoor A., Yang R.T., Wong C.
"Surface Diffusion"
Catal. Rev. 31(1&2), 129-214 (1989)

[9] Westmoreland P.R., Gibson J.B., Harrison D.P.
"Comparative kinetics of high-temperature reactions between H_2S and selected metal oxides"
Environ. Sci. Technol. 11, 488-491 (1977)

[10] Kohl A.L., Riesenfeld F.C.
"Gas purification", p582-585
McGraw-Hill, New York (1960)

[11] Sapre A.V.
"Diffusional enhancement of autocatalytic reactions in catalyst particles"
AIChE J., 35(4), 655-657 (1989)

[12] Szekely J., Evans J.W., Sohn H.Y.
"Gas-solid reactions"
Academic Press, New York (1976)

[13] Gibson J.B., Harrison D.P.
"The reaction between hydrogen sulphide and spherical pellets of zinc oxide"
Ind. Eng. Chem. Process Des. Dev. 19, 231-237 (1980)

[14] Levenspiel O.
"Chemical reaction engineering", ch.12
Wiley International (1972)

[15] Cresswell D.L.
"Rate-controlling mechanisms in the low temperature reaction between ZnO and H_2S - order of magnitude estimates"
ICI internal report

[16] Evans J.W., Song S.
"Application of a porous pellet model to fixed, moving and fluidised bed gas-solid reactors"
Ind. Eng. Chem. Process Des. Dev. 13(2), 146-152 (1974)

[17] Mackrodt W.C.
Personal Communication

[18] Plyasova L.M., Yurieva T.M., Solovieva L.P., Ketchik S.V., Khadzhiev D.I., Minyukova T.P.
"Distribution peculiarities of zinc ions in oxides"
React. Kinet. Catal. Lett. 22(3-4), 315-318 (1983)

[19] Zarkanitis S., Sotirchos S.V.
"Pore structure and particle size effects on limestone capacity for SO_2 removal"
AIChE J. 35(5), 821-830 (1989)

[20] Denny P.J.
Personal communication

[21] Tanabe K., Misono M., Ono Y., Hattori H.
"New solid acids and bases", vol.51 of Studies in Surface Science and Catalysis
Elsevier

APPENDIX A

Timescale of an Experiment to Study the Surface Reaction of Zinc Oxide with Hydrogen Sulphide.

For an absorbent with a surface site density, ρ_s, and a specific surface area, S_{abs}, m_{abs} grams of the absorbent expose ($\rho_s S_{abs} m_{abs}/2$) surface oxygens, where it is assumed that half of the surface sites are zincs and half oxygens. For a process gas flowrate, q, containing x% hydrogen sulphide, the maximum rate, (-r), of replacement of surface oxygens by sulphurs is given by

$$(-r) = \left(xPqN\right)/\left(100RT\right) \qquad (99)$$

where R is the Universal gas constant, N is Avogadro's number and P and T are the pressure and temperature of the process stream. The minimal time, t_{min}, for replacement of all surface oxygens by sulphurs is thus given by,

$$t_{min} = \left(100\rho_s S_{abs} m_{abs} RT\right)/\left(2xPqN\right) \qquad (100)$$

The specific surface area of the absorbent 75-1 is around $55 m^2 g_{-1}$. For a typical surface site density of 10^{19}sites.m^{-2}, the minimum time for reaction of all the surface zinc oxide may be calculated for a given absorbent and gas flowrate for either detector.

Absorbent beds of about 0.5g have typically been used with feed gas flowrates of about 0.5 $l.min^{-1}$ at STP. For a feed gas containing 0.01% (100 ppm) hydrogen sulphide, t_{min}=102 minutes. The cycle time for the FPD is 1.8 minutes, thus allowing about 56 analyses of the reactor outlet gas to be made before complete conversion of the surface zinc oxide is achieved.

The lowest hydrogen sulphide content which has been accurately analysed by the HWD is 0.06% (600 ppm) and

this is thought to be close to the limit for reasonable repeatability of analysis. For the same flow conditions as above, the minimum time for complete conversion of the surface zinc oxide of a 0.5g sample is, t_{min}=17 minutes. The possibility of studying the surface reaction using the HWD is further reduced by the longer cycle time of 4.5 minutes, allowing only 3 analyses to be made. There are practical difficulties with regard to adequate and reasonably rapid flushing of gas lines which arise if the gas flowrate, q, is reduced in order to increase t_{min}. Equally, increasing the size of the absorbent bed is unsatisfactory because the bed may no longer be considered shallow and the movement of the absorption front through the bed is then clearly evident.

Although the times calculated for 100% conversion of the surface zinc oxide are described as minimal times, experimental runs using the Hot Wire Detector (HWD) suggest that these correspond to the actual times for complete reaction of the surface. It is concluded that of the two detectors, only the Flame Photometric Detector (FPD) is suitable for the study of the surface reaction of zinc oxide with hydrogen sulphide.

APPENDIX B

Calibration of the Gas Chromatograph for Hydrogen Sulphide and Water.

(1) Calibration for Hydrogen Sulphide

Calibration runs were performed at nine different hydrogen sulphide concentrations in the range 0.02-1.11% (200-11100 ppm). The hydrogen sulphide concentration in the gas stream was calculated by measuring the gas flowrate and the weight increase of an absorption bed downstream of the gas chromatograph (Figure 3.3). A typical weight increase of 60-100mg is measured with an accuracy of ±0.2mg, that is a relative error of 0.2-0.4%. Gas flowrates used are in the range 100-300mlmin^{-1} and are measured using a soap film meter with a relative error of about 2%. As the gas samples are injected at atmospheric pressure, the hydrogen sulphide concentrations are adjusted to a standard pressure of 760mmHg. The atmospheric pressure is not monitored continuously, and thus a small error is introduced by the assumption of a constant pressure. The variation of the atmospheric pressure during a calibration run of about 4 hours is, however, generally less than 0.3%. Repetitive analysis of the gas stream allows the use of the mean GC signal, the standard deviation of which is smaller than that of any single analysis by a factor $n^{-\frac{1}{2}}$ where n is the number of analyses used to compute the mean.

A curve of the general form,

$$y = \alpha.x \qquad (101)$$

has been fitted to the data, where α is a constant, and y and x are the percentage hydrogen sulphide content of the gas and the mean GC signal respectively. Thus the trivial assumption is made that there is no GC signal

for hydrogen sulphide when no hydrogen sulphide is present in the gas analysed. It is also assumed that over this range of hydrogen sulphide concentration the GC response is linear. The determination of the constant α in equation (101) by the method of least squares is based on the assumption that only the dependent variable, y, is subject to error. For this reason, and because the calibration is used to predict hydrogen sulphide concentrations corresponding to values of the GC signal, the mean GC signal was selected as the explanatory or independent variable. The data and calibration line are plotted in Figure B.1. The coefficient, α, of the best fitting straight line is 0.119 with a standard deviation of 0.002.

(2) Calibration for water

Five calibration runs were performed on gas streams with water contents in the range 0.18-0.58%. All but one of these showed a negative trend in the GC response with time, representing drifts of 0.03-1.53% of the mean signal per hour. This compares with drifts in the hydrogen sulphide signals of 0.08-0.26% of the mean signal per hour. All but one of these drifts were positive. The calibration of the GC for water was done at an early stage of the experimental program. The bubbler disentrainment section was subsequently re-filled with a packing having a much lower pressure drop and this was found to reduce the problem of the negative drift in the GC signal. The falling mole fraction of water in the stream is explicable in terms of the rising pressure in the bubbler due to the build-up of water downstream in the disentrainment section. The water vapour pressure is unchanged, being fixed by the bubbler temperature, but the total flowrate of the water-saturated stream falls while the flowrate of the dry make-up nitrogen stream remains constant and

Figure B.1: Gas chromatograph calibration plot for hydrogen sulphide.

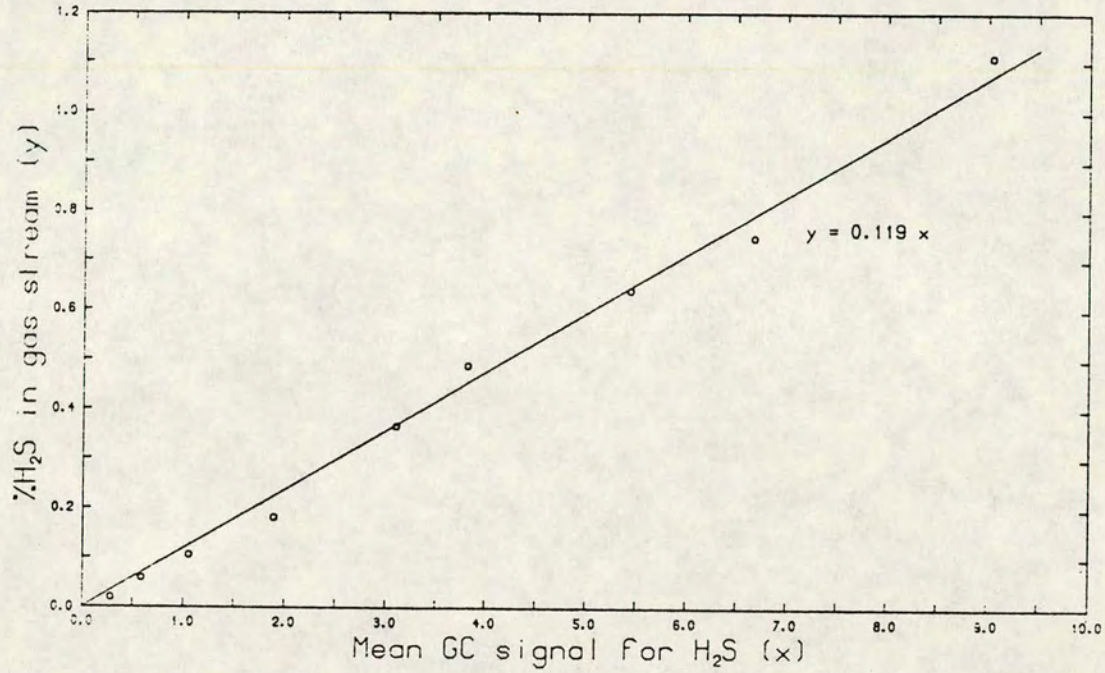

Figure B.2: Gas chromatograph calibration plot for water.

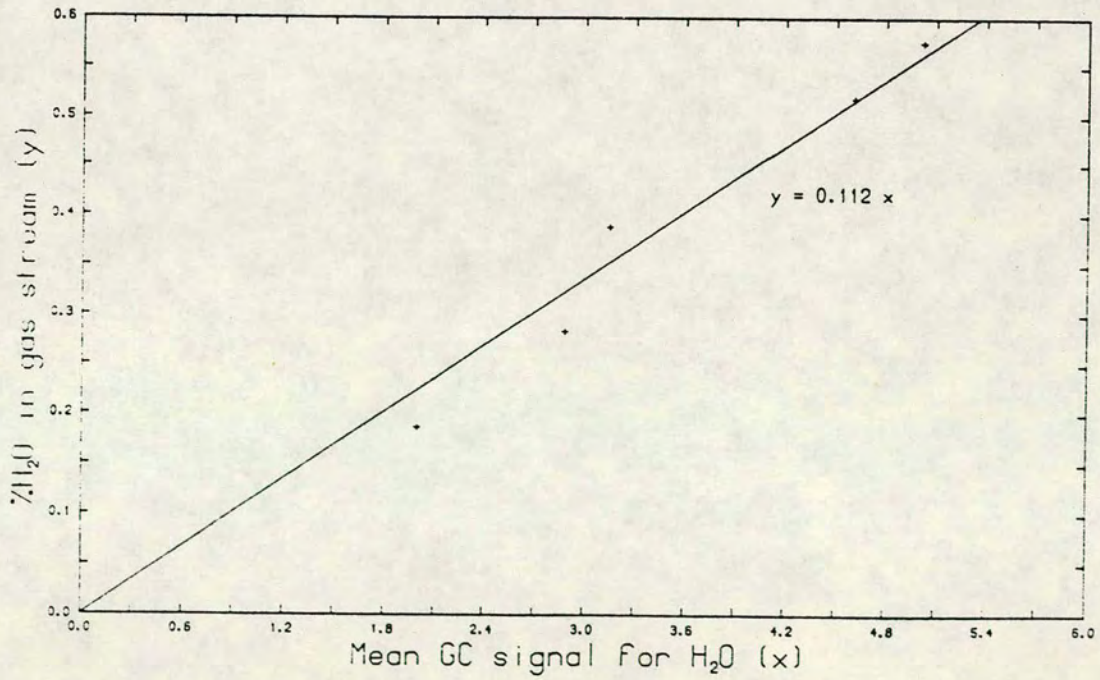

thus the water content of the mixed stream drops. The very slight positive drift observed in the signal for hydrogen sulphide is most likely to be a column effect as the column has been observed to irreversibly adsorb hydrogen sulphide initially for very low loadings (section 3.1.3).

A curve of the same form as equation (101) was fitted to the data which is plotted in Figure B.2. The coefficient, α, of the best fitting line is 0.112 with a standard deviation of 0.004.

APPENDIX C

Program Listings and Flowsheets

This appendix contains listings of 4 computer programs. These are:

1. the control program for the sulphiding experiment (written in BASIC);
2. the program used to analyse nitrogen adsorption data (written in IMP);
3. the program used to numerically integrate the hydrogen sulphide analyses, in order to calculate absorbent conversion (written in IMP); and
4. the program to compute pseudo-steady state rates (written in BASIC).

A simplified flowsheet for the control program for the BBC microcomputer is also given, and a brief summary of the function of its various 'procedures' or routines follows. Note that not all of the routines are indicated on the flowsheet.

PROCINITIALISE defines the filenames for the storage of data on disc and opens the feed data file.

PROCSAMPLING1 defines the pattern of sampling of the feed and product streams which is to be followed after the reactor is put on-line. Additional changes may be made at the end of any analysis by means of the routine PROCOPTIONS.

PROCFLOW1 defines the carrier gas in use and the level of hydrogen sulphide in the mixture cylinder.

PROCFLOW2 sets the gas flowrate through the mass flow controller (MFC).

PROCEQUILIBRATE is used to ensure that the bubbler bath is at the set-point temperature before the gas chromatograph link to the microcomputer is enabled.

This is important because of the finite time taken to start the run during which no monitoring or control of the bubbler temperature is performed. The routine calls PROCBUBBLER.

PROCBUBBLER monitors the temperature of the bath in which the water bubbler is contained and switches the cooling water pump on and off to maintain it within the specified tolerance about the set-point.

PROCSAMPLE closes the 2-way solenoid or diverts the 3-way solenoid to waste according to whether the stream being sampled is the feed to, or the product from, the reactor.

PROCT monitors the thermistor reading the laboratory temperature.

PROCFLUSH switches the positions of the solenoid valves in order to flush the gas sample valve (GSV) of the GC with either feed or product.

PROCBSWITCH(TCYCL) calls PROCBUBBLER for a period of time controlled by the parameter TCYCL. This is used during the GC analysis to ensure that the microcomputer is expecting input from the GC when an analysis finishes.

PROCREPORT reads data from the GC from the RS423 port and calls PROCSTAT to decipher it. If the conditions are met, as specified in PROCSAMPLING1, for changing the stream to be analysed then PROCSWITCH is called. Otherwise, PROCOPTIONS is called.

PROCSTAT picks out the data required from the GC report and stores it on disc.

PROCSWITCH changes the stream being analysed from feed to product or vice versa.

PROCOPTIONS is called after every GC analysis. It allows the operator to change the stream to be analysed, to alter the flowrate through the MFC, to cause the program to pause for an indefinite length of time or to stop the run. If the option to stop the run is selected then the variable ZZ is set equal to 78 and so, as the flowsheet indicates, this prevents another cycle of analysis. Finally, during the initial period when the reactor is still isolated and the feed stream is being analysed, the option is available to put the reactor on-line. If this option is selected the routine PROCREACTOR is called.

PROCREACTOR controls the procedure by which the reactor is put on-line (which is done manually) to ensure that the procedure is identical for every experimental run.

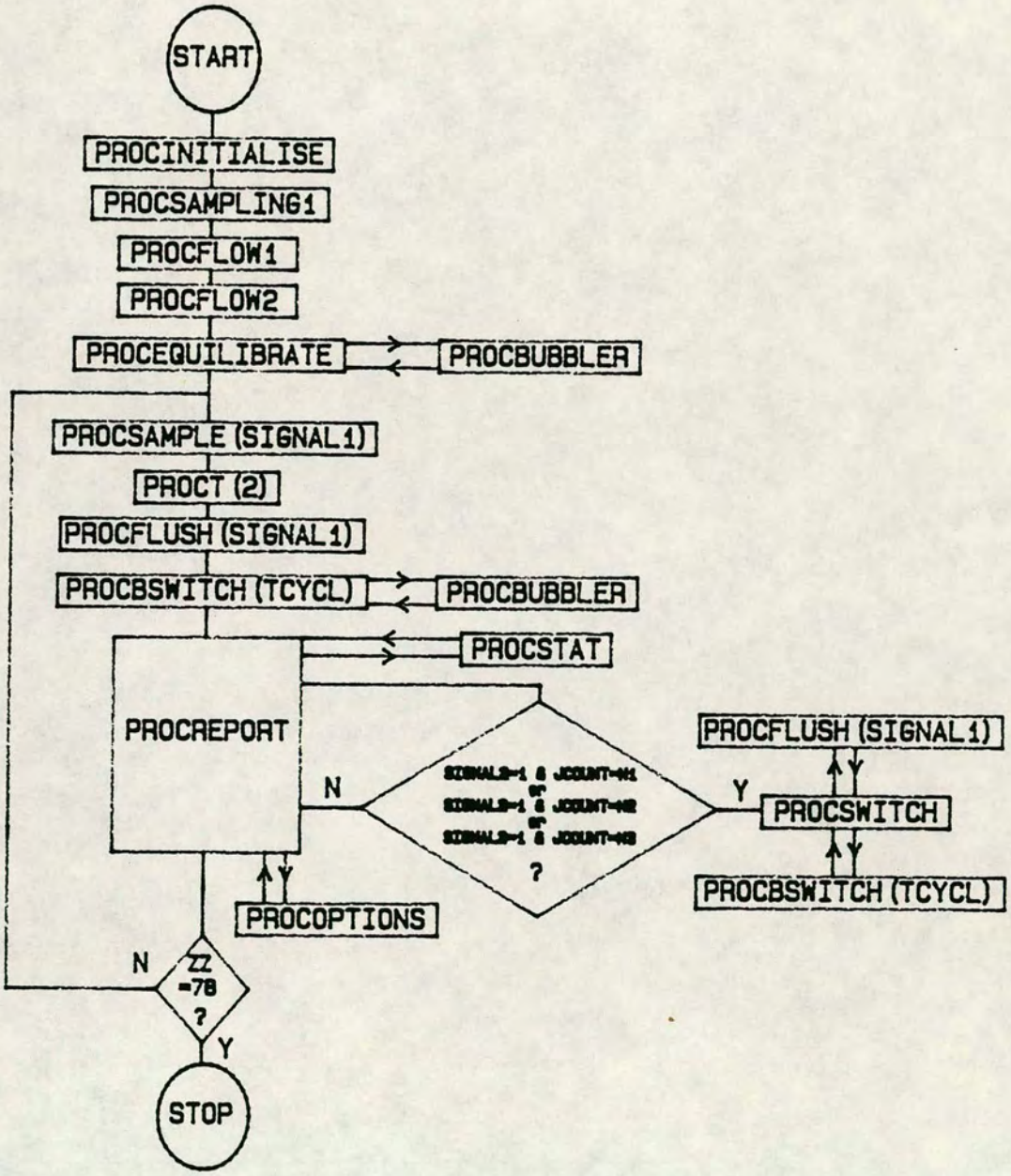
START
PROCINITIALISE
PROCSAMPLING1
PROCFLOW1
PROCFLOW2
PROCEQUILIBRATE
PROCBUBBLER
PROCSAMPLE (SIGNAL1)
PROCT (2)
PROCFLUSH (SIGNAL1)
PROCBSWITCH (TCYCL)
PROCBUBBLER
PROCSTAT
PROCREPORT
N
Y
PROCFLUSH (SIGNAL1)
PROCSWITCH
PROCBSWITCH (TCYCL)
?
PROCOPTIONS
N
ZZ =78 ?
Y
STOP

```
   10 MODE131
   20 PRINT "  "
   30 *KEY 10 ?&FE62=255 |M ?&FE60=63 |M LISTO 7 |M MODE131 |M OLD |M CLS |M PRI
NT"PROGRAM RETAINED AND MFC FLOW = 284" |M
   40 *FX7,4
   50 *FX8,4
   60 @%=10
   70 PRINT " ":PRINT " "
   80 PRINT "** WARNING! **"
   90 PRINT " ":PRINT "In case of failure, pressing 'BREAK' will cause the MFC f
low to be set"
  100 PRINT "to 284 ml/min (ie. ?&FE60=63). This is to avoid flow disturbances."
:PRINT " "
  110 PRINT "If a different flowrate is required, press 'ESCAPE' and alter the '
BREAK'"
  120 PRINT "key definition at line 30"
  130 PRINT " ":PRINT " "
  140 PRINT "Otherwise, press any key to proceed":Z10=GET:*FX21,0
  150 PROCINITIALISE
  160 PROCSAMPLING1 : CLS
  170 PRINT "IF THE CAPILLARY FLOWMETER IS TO BE USED FOR A SECOND GAS FLOW,"
  180 PRINT "OR FOR THE ONLY FLOW, IT SHOULD NOW BE SET UP"
  190 PROCFLOW1
  200 PROCFLOW2
  210 PRINT "DO YOU WISH TO SET THE BBC CLOCK TO ZERO (Y/N) ?  ";:Z9=GET:*FX21,0
  220 IF Z9=89 THEN TIME=0:PRINT "TIME=0"
  230 SIGNAL1=0:SIGNAL2=0:RONSTREAM=0:IW=0:JCOUNT=0:Z4=0
  240 S=&FE42
  250 PRINT"SOLENOID SWITCHED TO FLUSH GSV"
  260 ?S=?S OR 16
  270 PRINT" "
  280 INPUT "ENTER ISOTHERMAL/RUN TIME IN MINUTES  "TISO : TISO=TISO*6000
  290 PRINT "ENTER EFFECTIVE EQUILIBRATION TIME IN MINUTES  "
  300 INPUT "  ie. equilibration time plus time for negative timed events  "TEQ
  310 TEQ=TEQ*6000
  320 PRINT" "
  330 PRINT "IF COMMUNICATIONS CORRECTLY SET UP, AND GSV ADEQUATELY FLUSHED, "
  340 PRINT "THEN PRESS ANY KEY TO START"
  350 Z7=GET
  360 *FX21,0
  370 PROCEQUILIBRATE
  380 CLS:PRINT "ENABLE INPUT FROM RS423 PORT"
  390 *FX2,1
  400 PRINT" "
  410 STARTTIME=600+TEQ
  420 REPEAT
  430   T=TIME
  440   REPEAT:UNTIL TIME>=STARTTIME+T
  450   PROCSAMPLE(SIGNAL1)
  460   REPEAT:UNTIL TIME>=STARTTIME+500+T
  470   CLS:PRINT "START OF GC RUN"
  480   XTIME=TIME : XTIM=XTIME/360000 : XTIM=INT(XTIM*1000)/1000
  490   XTIM$=STR$(XTIM)
  500   IF SIGNAL1=0 THEN PRINT£X, XTIM$ ELSE PRINT£Y, XTIM$
  510   PROCT(2):TLAB=SY:K4$=STR$(TLAB)
  520   IF LEN(K4$)=2 THEN K4$=K4$+".00"
  530   IF LEN(K4$)=4 THEN K4$=K4$+"0"
  540   K4$="      "+K4$
  550   PROCFLUSH(SIGNAL1)
  560   IF SIGNAL1=0 THEN K3$="    F  " ELSE K3$="    P  "
```

```
  570   JJ=JCOUNT/35
  580   IF INT(JJ)<>JJ THEN GOTO 620
  590   *FX3,10
  600   PRINT " ":PRINT "RUN   TIME   STREAM   LAB TEMP   H2S AREA   AMT.      WA
TER AREA   AMT.":PRINT " "
  610   *FX3,4
  620   PRINT TAB(10,8) "MONITORING BUBBLER TEMPERATURE            "
  630   TCYCL=XTIME+TISO : PROCBSWITCH(TCYCL)
  640   PROCREPORT
  650   UNTIL ZZ=78
  660 PRINT CHR$(7) : PRINT "TO SHUT OFF GAS FLOW FROM MFC, TYPE 'S'"
  670 Z5=INKEY(500) : *FX21,0
  680 IF Z5=83 THEN ?&FE60=0:PRINT "FLOW THRO' MFC OFF"
  690 ENDTIME=TIME
  700 @%=10
  710 SEC1=(ENDTIME DIV 100) MOD 60:MIN1=(ENDTIME DIV 6000) MOD 60:HR1=ENDTIME D
IV 360000
  720 REACTORTIME=ENDTIME-RONSTREAM
  730 SEC2=(REACTORTIME DIV 100) MOD 60:MIN2=(REACTORTIME DIV 6000) MOD 60:HR2=R
EACTORTIME DIV 360000
  740 VDU2
  750 PRINT " ":PRINT "LENGTH OF RUN =  ";HR1;" HRS  ";MIN1;" MINS  ";SEC1;" SEC
S"
  760 IF SIGNAL2=1 THEN PRINT "REACTOR ONSTREAM FOR ";HR2;" HRS  ";MIN2;" MINS
";SEC2;" SECS"
  770 VDU3
  780 CLOSE£X
  790 IF SIGNAL2=1 THEN CLOSE£Y
  800 END
  810
  820 DEF PROCT(X)
  830 LOCAL I
  840 SY=0
  850 FOR I= 1 TO 5000 : SY=SY+ADVAL(X) : NEXT I
  860 SY=SY/5000 : SY=FNTHERMISTOR(SY) : SY=INT(SY*100)/100
  870 ENDPROC
  880
  890 DEF FNTHERMISTOR(A)
  900 RI=100 : VREF=1.8 : V=A*VREF/65520
  910 IF V>=VREF THEN V=VR-1E-8
  920 RT=V*RI/(VREF-V)
  930 IF RT<=0 THEN RT=1E-10
  940 T=1825.625/(LOG(RT)+4.128)
  950 =T-273.1
  960
  970 DEF PROCREPORT
  980 PRINT " " : PRINT "WAITING FOR DATA FROM RS423 PORT"
  990 I=0:N=0:M=0
 1000 REPEAT
 1010   B$=""
 1020   REPEAT:C$=GET$:B$=B$+C$:UNTIL C$=CHR$(13)
 1030   IF LEN(B$)=1 THEN M=M+1:N=N+1 ELSE N=0
 1040   IF M=1 AND N=0 THEN B$=LEFT$(B$,26):K1$=MID$(B$,5,6):K2$=MID$(B$,11,6):K
$=K1$+K2$+K3$+K4$:PRINT B$ ELSE GOTO 1080
 1050   *FX3,10
 1060   PRINT K$;
 1070   *FX3,4
 1080   IF M=2 AND N=0 THEN PRINT B$
 1090   IF M=4 AND N=0 THEN PROCSTAT
 1100   UNTIL N=6
 1110 JCOUNT=JCOUNT+1
 1120 *FX3,10
 1130 PRINT " "
 1140 *FX3,0
 1150 *FX2,0
 1160 WAIT=TIME:REPEAT:UNTIL TIME>=WAIT+500
```

```
1170 IF SIGNAL2=1 AND JCOUNT=N1 THEN PROCSWITCH
1180 IF SIGNAL2=1 AND JCOUNT=N2 THEN PROCSWITCH
1190 IF SIGNAL2=1 AND JCOUNT=N3 THEN PROCSWITCH
1200 IF SIGNAL2=1 AND JCOUNT=N4 THEN PROCEXIT
1210 IF IW=0 THEN PROCOPTIONS
1220 IW=0
1230 ENDPROC
1240
1250 DEF PROCSTAT
1260 LOCAL Y$,Z$
1270 Y$=MID$(B$,12,10):K5$="     "+MID$(B$,14,8):K6$="    "+MID$(B$,53,6)
1280 IF VAL(Y$) > 0.05 AND SIGNAL1=0 THEN PRINT£X,Y$
1290 IF VAL(Y$) > 0.05 AND SIGNAL1=1 THEN PRINT£Y,Y$
1300 *FX3,10
1310 @%=&20209
1320 IF VAL(Y$) > 0.01 THEN PRINT K5$;:PRINT K6$;
1330 *FX3,0
1340 PRINT B$
1350 ENDPROC
1360
1370 DEF PROCEXIT
1380 CLS : SOUND 1,-15,100,30
1390 PRINT "** WARNING ** - TO PREVENT AUTOMATIC SHUTDOWN, TYPE 'S' " : Z1=INKE
Y(500) : *FX21,0
1400 IF Z1=83 THEN PROCOPTIONS ELSE IW=1 : ZZ=78 : PRINT "RUN COMPLETE"
1410 ENDPROC
1420
1430 DEF PROCFLOW1
1440 DIM FACT(4)
1450 A1=6.9304 : A2=4.3977
1460 FACT(1)=1.00 : FACT(2)=1.39 : FACT(3)=0.81 : FACT(4)=0.00 : FACTH2S=0.85
1470 PRINT "ENTER NUMBER TO INDICATE CARRIER GAS, ie"
1480 INPUT "Nitrogen (=1), Helium (=2), Methane (=3), other(=4)  "CARR
1490 IF CARR=4 THEN INPUT "ENTER THE MFC FLOW CALIBRATION FACTOR FOR THE CARRIE
R GAS USED  "FACT(4)
1500 INPUT "ENTER THE NOMINAL % CONCENTRATION OF H2S IN THE GAS  "CONC
1510 FACTOR=((CONC*FACTH2S) + ((100-CONC)*FACT(CARR)))/100
1520 FLOWMAX=FACTOR*(A1 + A2*255) : FLOWMIN=FACTOR*(A1 + A2*20)
1530 FLOWMAX=INT(FLOWMAX*10)/10 : FLOWMIN=INT(FLOWMIN*10)/10
1540 ?&FE62=255
1550 ENDPROC
1560
1570 DEF PROCFLOW2
1580 INPUT "ENTER THE GAS FLOW REQUIRED THROUGH THE MASS FLOW CONTROLLER (ml/mi
n)  "FLOW
1590 F=(FLOW-A1)/A2
1600 F=INT(F/FACTOR)
1610 IF F>255 THEN F=255 : PRINT "WARNING ! FLOWRATE REQUESTED EXCEEDS MAXIMUM
OF ";FLOWMAX;" ml/min; FLOW SET TO MAXIMUM"
1620 IF F<20 THEN F=20 : PRINT "WARNING ! FLOWRATE REQUESTED IS LESS THAN MINIM
UM OF ";FLOWMIN;" ml/min; FLOW SET TO MINIMUM"
1630 ?&FE60=F
1640 FLOW=FACTOR*(A1 + A2*F) : FLOW=INT(FLOW*10)/10
1650 PRINT "FLOWRATE IS ";FLOW;" ml/min"
1660 ENDPROC
1670
1680 DEF PROCOPTIONS
1690 CLS
1700 IF SIGNAL2=0 THEN PRINT "TYPE 'P' TO BEGIN SAMPLING PRODUCT STREAM"
1710 IF SIGNAL2=1 AND SIGNAL1=0 THEN PRINT "TYPE 'C' TO ANALYSE PRODUCT STREAM"
1720 IF SIGNAL2=1 AND SIGNAL1=1 THEN PRINT "TYPE 'C' TO ANALYSE FEED STREAM"
1730 PRINT "      'F' TO CHANGE FLOWRATE"
1740 PRINT "      'N' TO STOP EXPERIMENTAL RUN"
1750 PRINT "      'W' TO CAUSE PROGRAM TO PAUSE"
1760 PRINT " ":PRINT " "
1770 ZZ=INKEY(600) : *FX21,0
```

```
 1780 IF ZZ<>-1 THEN PRINT "KEY PRESSED - ";:PRINT CHR$(ZZ):PRINT "TYPE 'C' TO C
ONFIRM":Z4=INKEY(400)
 1790 IF ZZ<>-1 AND Z4<>67 THEN GOTO 1690
 1800 *FX21,0
 1810 IF ZZ=80 THEN PROCREACTOR
 1820 IF ZZ=67 THEN SIGNAL1=1-SIGNAL1:PROCFLUSH(SIGNAL1):WAIT=TIME:TCYCL=WAIT+18
000:PROCBSWITCH(TCYCL):REPEAT:UNTIL TIME>=TCYCL
 1830 IF ZZ=70 THEN PROCFLOW2
 1840 IF ZZ=87 THEN PRINT "PRESS ANY KEY TO CONTINUE":Z2=GET
 1850 IF ZZ=78 THEN PRINT "RUN COMPLETE" ELSE PRINT " ":PRINT "RUN CONTINUED":*F
X2,1
 1860 ENDPROC
 1870
 1880 DEF PROCFLUSH(Y)
 1890 IF Y=0 THEN ?S=?S AND (NOT 32):?S=?S OR 16:PRINT "FLUSH GSV WITH REACTOR F
EED"
 1900 IF Y=1 THEN ?S=?S AND (NOT 16):?S=?S OR 32:PRINT "FLUSH GSV WITH REACTOR O
UTLET STREAM"
 1910 ENDPROC
 1920
 1930 DEF PROCSAMPLE(W)
 1940 IF W=0 THEN ?S=?S AND (NOT 16):PRINT "CLOSE 2-WAY VALVE TO SAMPLE FEED"
 1950 IF W=1 THEN ?S=?S AND (NOT 32):PRINT "DIVERT 3-WAY VALVE TO SAMPLE PRODUCT
"
 1960 ENDPROC
 1970
 1980 DEF PROCINITIALISE
 1990 CLS
 2000 D0$="R" : D4$="F" : D5$="P"
 2010 INPUT "Enter today's date (in form 01/06/88)  "DATE$
 2020 INPUT "Enter experimental run number  "NUM$
 2030 INPUT "Enter RF value in method for H2S  "RFH$
 2040 INPUT "          and RF value for water  "RFW$
 2050 D1$=LEFT$(DATE$,2) : D2$=MID$(DATE$,4,2)
 2060 INPUT "Enter number of day's run eg. 1 for first, 2 for second etc  "D3$
 2070 FILE1$ = D0$ + D1$ + D2$ + D3$ + D4$ : FILE2$ = D0$ + D1$ + D2$ + D3$ + D5
$
 2080 PRINT "Feed data will be stored under the filename - "FILE1$
 2090 PRINT "Any product data collected will be stored under the filename - "FIL
E2$
 2100 X=OPENOUT FILE1$
 2110 PRINT£X,FILE1$
 2120 *FX3,10
 2130 PRINT "  ":PRINT DATE$;:PRINT "    EXPERIMENTAL RUN ";:PRINT NUM$
 2140 PRINT "  ":PRINT "RF(H2S)= ";:PRINT RFH$;:PRINT "     RF(WATER)= ";:PRINT
RFW$:PRINT "  "
 2150 *FX3,4
 2160 ENDPROC
 2170
 2180 DEF PROCREACTOR
 2190 SIGNAL2=1 : SIGNAL1=1
 2200 Y=OPENOUT FILE2$ : PRINT£Y,FILE2$
 2210 WAIT=TIME : REPEAT : UNTIL TIME>=WAIT+500
 2220 CLS
 2230 PRINT "TO STANDARDISE THE PROCEDURE FOR PUTTING THE REACTOR ON-LINE, PLEAS
E"
 2240 PRINT "READ ALL THE INSTRUCTIONS BELOW BEFORE PROCEEDING AS INDICATED"
 2250 PRINT " " : PRINT " " : PRINT " "
 2260 PRINT "(1) **IMPORTANT** ENSURE THAT THE VALVE ON THE VACUUM LINE IS CLOSE
D" : PRINT " "
 2270 PRINT "(2) Loosen the screw which secures the large rotaflow valve" : PRIN
T " "
 2280 PRINT "(3) Press 'C' to continue" : PRINT " "
 2290 PRINT "(4) When instructed, OPEN ROTAFLOW VALVE UPSTREAM OF REACTOR" : PRI
NT " "
 2300 PRINT "(5) When instructed, OPEN ROTAFLOW VALVE DOWNSTREAM OF REACTOR" : P
```

```
RINT " "
 2310 PRINT "(6) When instructed, CLOSE REACTOR BY-PASS VALVE"
 2320 PRINT " " : PRINT " " : PRINT " "
 2330 PRINT "THE PROGRAM WILL THEN WAIT 1 MINUTE TO ALLOW THE PRODUCT GAS TO FLU
SH THROUGH"
 2340 PRINT "TO THE GAS SAMPLE VALVE" : PRINT " "
 2350 Z3=GET
 2360 WAIT=TIME : REPEAT : UNTIL TIME>=WAIT+200 : CLS
 2365 REPEAT : UNTIL TIME>=WAIT+500
 2370 PRINT TAB(10,10) "OPEN ROTAFLOW VALVE UPSTREAM OF REACTOR"
 2380 WAIT=TIME : REPEAT : UNTIL TIME>=WAIT+900 : CLS
 2385 REPEAT : UNTIL TIME>=WAIT+1200
 2390 PRINT TAB(10,10) "OPEN ROTAFLOW VALVE DOWNSTREAM OF REACTOR"
 2400 XTIME=TIME : XTIME=XTIME/360000 : XTIME=INT(XTIME*1000)/1000
 2410 XTIM$=STR$(XTIME) : PRINT£Y, XTIM$
 2420 BLANK$="0.0000"
 2430 PRINT£Y, BLANK$ : PRINT£Y, BLANK$
 2440 WAIT=TIME : REPEAT : UNTIL TIME>=WAIT+900 : CLS
 2445 REPEAT : UNTIL TIME>=WAIT+1200
 2450 PRINT TAB(10,10) "CLOSE REACTOR BY-PASS VALVE"
 2460 WAIT=TIME : REPEAT : UNTIL TIME>=WAIT+1200
 2470 RONSTREAM=TIME : CLS : PROCFLUSH(SIGNAL1)
 2480 WAIT=TIME:TCYCL=WAIT+6000:PROCBSWITCH(TCYCL):REPEAT:UNTIL TIME>=WAIT+6000
 2490 JCOUNT=0
 2500 ENDPROC
 2510
 2520 DEF PROCSAMPLING1
 2530 CLS : M1=25 : M2=6 : M3=36 : M4=16
 2540 PRINT "After the reactor is put on-line, the default pattern of sampling o
f the feed"
 2550 PRINT "and product streams is as follows : " : PRINT " "
 2560 PRINT "25 product analyses followed by"
 2570 PRINT " 6  feed       ''        ''     ''"
 2580 PRINT "36 product      ''        ''     ''"
 2590 PRINT "16  feed    analyses" : PRINT " "
 2600 PRINT "Do you wish to accept this sampling sequence ? (Y/N)  "
 2610 Z2=GET : *FX21,0
 2620 IF Z2=78 THEN PROCSAMPLING2 ELSE PRINT "DEFAULT SAMPLING PATTERN ACCEPTED"
 2630 N1=M1 : N2=M1+M2 : N3=N2+M3 : N4=N3+M4
 2640 WAIT=TIME : REPEAT : UNTIL TIME>= WAIT+300
 2650 ENDPROC
 2660
 2670 DEF PROCSAMPLING2
 2680 CLS : PRINT "DEFAULT SAMPLING PATTERN IS, "
 2690 PRINT "25 (=M1) PRODUCT ANALYSES"
 2700 PRINT " 6 (=M2)  FEED       ''"
 2710 PRINT "36 (=M3) PRODUCT     ''"
 2720 PRINT "16 (=M4)  FEED       ''" : PRINT " "
 2730 PRINT "ENTER NEW VALUES FOR THE NUMBER OF CONSECUTIVE ANALYSES IN EACH OF
THE"
 2740 PRINT "FOUR SEQUENCES"
 2750 INPUT "M1= "M1 : INPUT "M2= "M2 : INPUT "M3= "M3 : INPUT "M4= "M4
 2760 PRINT " " : PRINT "NEW VALUES ACCEPTED"
 2770 ENDPROC
 2780
 2790 DEF PROCSWITCH
 2800 CLS : SOUND 1,-15,100,30
 2810 PRINT "** WARNING ** - TO PREVENT AUTOMATIC SWITCHING OF ANALYSIS BETWEEN
FEED AND"
 2820 PRINT "PRODUCT STREAM, TYPE 'S' " : Z6=INKEY(500) : *FX21,0
 2830 IF Z6=83 THEN PROCOPTIONS ELSE IW=1:SIGNAL1=1-SIGNAL1:PROCFLUSH(SIGNAL1):W
AIT=TIME:TCYCL=WAIT+18000:PROCBSWITCH(TCYCL):REPEAT:UNTIL TIME>=TCYCL:*FX2,1
 2840 ENDPROC
 2850
 2860 DEF PROCEQUILIBRATE
 2870 CLS : PRINT" " : PRINT"EQUILIBRATION OF BUBBLER TEMPERATURE"
```

```
2880 LOCAL I
2890 ACR=&FE6B : PCR=ACR+1
2900 BSIGN=1000 : LO=0 : HI=0 : BUB1=3 : BUB2=3 : VHI=224 : VLO=192
2910 ?ACR=?ACR AND 227
2920 VOLT=VHI
2930 ?PCR=?PCR AND 31 OR VOLT
2940 CRITERION=0
2950 REPEAT
2960   PROCBUBBLER
2970   IF CRITERION=0 AND VOLT=VLO THEN CRITERION=1
2980   IF CRITERION=1 AND VOLT=VHI THEN CRITERION=2
2990   UNTIL CRITERION=2
3000 WAIT=TIME:REPEAT:UNTIL TIME>=WAIT+400
3010 ENDPROC
3020
3030 DEF PROCBUBBLER
3040 BTEMP=0
3050 FOR I=1 TO 1000 : BTEMP=BTEMP+ADVAL(1) : NEXT I
3060 BTEMP=BTEMP/1000
3070 IF BTEMP<BSIGN THEN HI=HI+1 ELSE HI=0
3080 IF BTEMP>BSIGN THEN LO=LO+1 ELSE LO=0
3090 IF HI=BUB1 THEN VOLT=VLO:PRINT TAB(10,10)"BUBBLER TEMP HIGH - CIRCULATE CW
     "
3100 IF HI>BUB1 THEN VOLT=VLO
3110 IF LO=BUB2 THEN VOLT=VHI:PRINT TAB(10,10)"BUBBLER TEMP AT OR BELOW SETPOIN
T - CW OFF"
3120 IF LO>BUB2 THEN VOLT=VHI
3130 ?PCR=?PCR AND 31 OR VOLT
3140 ENDPROC
3150
3160 DEF PROCBSWITCH(T)
3170 REPEAT : PROCBUBBLER : UNTIL TIME>=T-1500
3180 ENDPROC
```

```
%begin
!*************************************************************************
!
!     PROGRAM TO CALCULATE THE GROWTH OF ABSORBENT CONVERSION WITH
!     TIME USING:
!                (a) TRAPEZOIDAL RULE
!                (b) SIMPSON'S RULE
!     FOR NUMERICAL INTEGRATION.
!
!*************************************************************************
!
! This program uses the file of hydrogen sulphide product analyses and the
! line fitted to the feed analyses to calculate the growth of the amount
! of hydrogen sulphide absorbed with time during a sulphiding run.
!
   %long %real %function quad(%long %real x1,x2,x3)
      %result = x3**3/3-(x1+x2)*x3**2/2+x1*x2*x3
   %end
!
   %routine setup(%long %real %array %name x, %long %real %name d1,d2,d3,
      %integer %name k)
!
      d1 = x(k-1)
      d2 = x(k)
      d3 = x(k+1)
      %return
   %end
!
   %external %routine %spec emas3 prompt(%string %name text)
   %integer i,j,m,n,signal,signal1,signal2,signal3,nsim,ik,nf
   %long %real a,b,SA,Qtot,pbar,Tlab,Z,ZZ,SWt,ZT,MW,correction,h1,h2,const1,
      const2,const3,d1,d2,d3,msdev,xmean,cssx,svaryp,totsd
   %long %real %array x,y,Area,Acum,sum,conv,svaryf(0:120),percentS,p,rate,
      rate1,time,solid,s2(1:120)
   %constant %real rho=1@19, L=6.023@23, MWZnO=81.4, MWHZ=548.91
! rho=surface site density, L=Avogadro's no., MWZnO=MW(ZnO), MWHZ=MW(HZ)
!
! Initialisation of variables
!
   Area(0) = 0; Acum(0) = 0; signal = 0; MW = MWZnO; correction = 1
   totsd = 0
! Keyboard input of experimental conditions:
   EMAS3prompt("Enter the number of data pairs in file :   ")
   read(m)
   n = m-1 { n is number of intervals, or trapezoids summed }
   EMAS3prompt("Enter parameters of line fitted to feed data : constant ?   ")
   read(a)
   EMAS3prompt("                                              coefficient ?   ")
   read(b)
   EMAS3prompt("Enter the pre-run surface area in m2/gm of the absorbent :   ")
   read(SA)
```

```
    EMAS3prompt("Enter the total gas flowrate (ml/min) :   ")
    read(Qtot)
    EMAS3prompt("Enter the barometric pressure (mmHg)   "); read(pbar)
    EMAS3prompt("      and the lab temperature (degrees C)   ")
    read(Tlab)
    Tlab = Tlab+273.15
    EMAS3prompt("If absorbent is '75-1', type '0'  "); read(correction)
    %if correction=0 %then correction = .769
    EMAS3prompt("If absorbent is essentially ZnO type '0', if HZ, type '1'  ")
    read(signal2)
    %if signal2=1 %then MW = MWHZ
    EMAS3prompt("Weight of (unsulphided) absorbent used for the run (mg) ?  ")
    read(SWt)
    EMAS3prompt( %c
       "Initial state absorbent sulphided (type '0') or not (type '1')?  ")
    read(signal1)
    %if signal1=0 %then %start
       EMAS3prompt( %c
          "Enter cumulative moles H2S absorbed at end previous run :  ")
       read(Acum(0))
    %finish
    EMAS3prompt("Enter variables associated with fitted feed line: nf  ")
    read(nf)
    EMAS3prompt(".....mean square of deviations  "); read(msdev)
    EMAS3prompt(".....mean time  "); read(xmean)
    EMAS3prompt("Enter corrected sum of squares of t ie. CS(t,t)  ")
    read(cssx)
    EMAS3prompt("Enter sample variance of product analyses  ")
    read(svaryp)
!
!
! Read datafile of time-analysis pairs
!
   selectinput(1)
   %for i = 0,1,n %cycle
      read(x(i)); read(y(i))
   %repeat
!
! If absorbent was pre-sulphided, check 1st product analysis to decide how to
! calculate amount H2S absorbed between opening reactor and 1st analysis, ie.
! about 90 secs.
!
! Revert to keyboard input
!
   selectinput(0)
   printstring("First H2S analysis =  "); printfl(y(1),3)
   newline
   printstring("Last H2S analysis =  "); printfl(y(n),3)
   newline
   EMAS3prompt( %c
      "To set H2S concn at time zero equal to first analysis, type '0'  ")
   read(signal3)
   %if signal3=0 %then y(0) = y(1)
```

```
!
! Calculate standard deviation of estimated feed analyses
   %for i = 0,1,n %cycle
      svaryf(i) = msdev*((1/nf)+(x(i)-xmean)**2/cssx)
   %repeat
!
   Z = 100*rho*SA*MW/(2*L) { %age oxygen ions exposed on surface }
   ZZ = rho*SA*SWt/(2*L*1@3) {mols surf. O2- exposed by absorbent sample}
! If sample is '75-1' then only 76.9% of absorbent weight is high SA ZnO
   ZT = correction*SWt*1@-3/MW { mols of absorbent used }
   newlines(2); printstring( %c
      "Oxygen ions exposed on surface as %age total oxygen")
   printstring(" ions = "); print(Z,2,2); printstring(" %")
   newlines(2)
!
! Calculation of initial solid conversion
!
   %if signal2=0 %then %start
      conv(0) = 100*Acum(0)/ZT
   %else
      conv(0) = 100*Acum(0)/(5*ZT)
   %finish
!
!
! Calculation of number of moles of hydrogen sulphide absorbed using the
! Trapezoidal rule.
!
   %for i = 1,1,n %cycle
! 'Area(i)' is the area under the feed curve from x(i-1) to x(i) minus the
! area of the ith trapezoid
      Area(i) = a*(x(i)-x(i-1))+(x(i)**2-x(i-1)**2)*b/2-0.5*(y(i-1)+y(i))*(x %c
         (i)-x(i-1))
! standard deviation of the area
      s2(i) = 0.25*(x(i)-x(i-1))**2*(svaryf(i)+svaryf(i-1)+2*svaryp)
! conversion of area to units of moles
      Area(i) = Area(i)*Qtot*60*pbar*133.32*1@-6/(8.4*100*8.314*Tlab)
      Acum(i) = Acum(i-1)+Area(i)
      totsd = totsd+s2(i)
!
! Calculate instantaneous rates (moles H2S absorbed/gram absorbent.sec)
      rate(i) = Area(i)/((x(i)-x(i-1))*3600*SWt*1@-3)
!
      %if signal2=0 %then %start
         percentS(i) = 100*Acum(i)*32/(SWt*1@-3+Acum(i)*16)
         conv(i) = 100*Acum(i)/ZT
      %else
! assuming reaction is,
! 5H2S + HZ = 5ZnS + 2CO2 + 8H2O
! ie. weight loss on sulphiding
         percentS(i) = 100*Acum(i)*32/(SWt*1@-3-Acum(i)*12.4)
         conv(i) = 100*Acum(i)/(5*ZT)
      %finish
      {conv(i) is the absorbent %age conversion at time x(i)}
```

```
!
! Calculate time and moles unreacted solid corresponding to above
! instantaneous rate.
!
      time(i) = (x(i)+x(i-1))/2-x(0)
      solid(i) = (100-(conv(i)+conv(i-1))/2)/100
!
! Calculate instantaneous rate per mole active ZnO remaining
      rate1(i) = rate(i)*SWt*1@-3/(ZT*solid(i))
!
      %if signal=0 %then %start
         %if Acum(i)>ZZ %then signal = i+1
      %finish
   %repeat
!
! Take square root to find standard deviation from sample variance
   totsd = (totsd)**0.5
! Convert sd to units of moles
   totsd = totsd*Qtot*60*pbar*133.32*1@-6/(8.4*100*8.314*Tlab)
!
! Recalculate area using Simpson's Rule...
!
!
   nsim = int((m-1)/2)
   sum(0) = 0
!
   %for i = 1,1,nsim %cycle
      j = 2*i-1
      setup(x,d1,d2,d3,j)
!
! h1 and h2 are time intervals between analyses; their sum is the width
! of the integration interval
!
      h1 = x(j)-x(j-1)
      h2 = x(j+1)-x(j)
!
      const1 = y(j-1)/(h1*(h1+h2))
      const2 = -y(j)/(h1*h2)
      const3 = y(j+1)/(h2*(h1+h2))
!
      p(i) = 0
      p(i) = p(i)+const1*(quad(d2,d3,d3)-quad(d2,d3,d1))
      p(i) = p(i)+const2*(quad(d1,d3,d3)-quad(d1,d3,d1))
      p(i) = p(i)+const3*(quad(d1,d2,d3)-quad(d1,d2,d1))
!
! p(i) is area between feed and product curves...
      p(i) = a*(x(j+1)-x(j-1))+(x(j+1)**2-x(j-1)**2)*b/2-p(i)
!
! conversion of area to units of moles...
      p(i) = p(i)*Qtot*60*pbar*133.32*1@-6/(8.4*100*8.314*Tlab)
!
      sum(i) = sum(i-1)+p(i)
!
   %repeat
```

```
!
!
   %if signal>0 %then %start
      printstring("All surface oxygens reacted after product analysis ")
      write(signal,2)
   %finish
!
!
! Output of numerical integration data to file
!
   selectoutput(2)
   newline
   printstring( %c
      "analysis   time       moles       cumulative   %conversion  %sulphur")
   newline
   printstring( %c
      "                     absorbed     moles abs'd                 on bed")
   newlines(2)
   %for i = 1,1,n %cycle
      j = i+1
      write(j,4); spaces(4); print(x(i),2,3); spaces(3); printfl(Area(i),3)
      spaces(4); printfl(Acum(i),3); spaces(7); print(conv(i),2,2)
      spaces(6); print(percentS(i),2,2)
      newline
   %repeat
!
   printstring("Standard deviation of moles absorbed =  "); printfl(totsd,3)
!
!
! Output to file of comparison of numerical integration by Trapezoidal
! (piecewise linear approximation) and Simpson's (piecewise quadratic
! approximation) rules.
!
   selectoutput(3)
   closestream(2)
   printstring("CUMULATIVE MOLES H2S ABSORBED:")
   newlines(3)
   printstring( %c
      "time                  Trapezoidal                    Simpson's")
   newlines(2)
!
   %for i = 1,1,nsim %cycle
      j = 2*i
      Area(j) = Area(j)+Area(j-1)
      print(x(j),2,3); spaces(7); printfl(Area(j),3); spaces(7)
      printfl(Acum(j),3); spaces(7)
      printfl(p(i),3); spaces(7); printfl(sum(i),3)
      newline
   %repeat
!
```

```
!
! Output of instantaneous rates to file
!
   selectoutput(4)
   closestream(3)
   printstring("time       fractn unreacted      g rate       rate per mol")
   newline
   printstring( %c
      "                                                  unreacted absorbent")
   newlines(2)
   %for i = 1,1,n %cycle
      print(time(i),2,3); spaces(7); printfl(solid(i),3); spaces(7)
      printfl(rate(i),3); spaces(6); printfl(rate1(i),3)
      newline
   %repeat
!
!
%end %of %program
```

```
%begin
!*************************************************************************
!
!         CALCULATIONS FOR BET PLOT FROM NITROGEN ADSORPTION DATA
!
!*************************************************************************
!
! This program reads dosing and equilibrated pressures for a SA measurement
! experiment from a datafile defined as channel 1. It outputs to the screen a
! table of pressures converted to mmHg and moles dosed and adsorbed. The (x,y)
! pairs for a BET plot are sent to the file defined by the user as channel 2,
! and the (equilibrated pressure, cumulative moles adsorbed) pairs required for
! the EASYGRAPH isotherm plot to the file defined as channel 3.
!
   %external %routine %spec emas3 prompt(%string %name text)
!
   %real Tlab,TlabK,a1,a2,Tcold,p0,Vvu,Vvl,Vv
   %real %array pdosmv,peqmv,pdos,peq,ndos,nunads,nads,x,y(1:30)
   %real %array ndoscum,nadscum(0:30)
   %constant %real R=8.314, Vman=13.692, AntA=14.9542, AntB=588.72, AntC=-6.60
   %integer i,n,n1,n2,m,signal,signv
!
   newlines(2)
   emas3prompt("What is the liquid nitrogen temperature (degrees Kelvin) ?  ")
   read(Tcold)
! calculation of nitrogen vapour pressure
   p0 = exp(AntA-AntB/(Tcold+AntC))
   emas3prompt( %c
      "Type '1' if expansion expts done to calc. voidage, else '0':  ")
   read(signv)
   %if signv=1 %then %start
emas3prompt("Enter total voids volume of sample tube :  ")
read(Vv)
      emas3prompt("Enter voids volume in lower section of sample tube :  ")
read(Vvl)
Vvu = Vv-Vvl
   %finish %else %start
      Vvu = .472; Vvl = .728
   %finish
!
   emas3prompt("What is the lab temperature (degrees Centigrade) ?  ")
   read(Tlab)
   TlabK = Tlab+273.15
!
   emas3prompt("How many data pairs are there in the file ?  ")
   read(n)
! PT calibration constants
   a1 = -9.6401; a2 = 25.3686
   nadscum(0) = 0; m = n; signal = 0; ndoscum(0) = 0
!
```

```
! read dosing and equilibrium pressures from file
!
   selectinput(1)
   %for i = 1,1,n %cycle
      read(pdosmv(i))
      read(peqmv(i))
   %repeat
!
   %for i = 1,1,n %cycle
! convert pressures to mmHg
      pdos(i) = a1+a2*pdosmv(i)
      %if pdos(i)<0 %then pdos(i) = 0
      peq(i) = a1+a2*peqmv(i)
      %if peq(i)<0 %then peq(i) = 0
! calculate number of moles dosed
      ndos(i) = pdos(i)*133.32*1@-6*Vman/(R*TlabK)
! total moles dosed
      ndoscum(i) = ndoscum(i-1)+ndos(i)
! moles left unadsorbed
      nunads(i) = peq(i)*133.32*1@-6*((Vman/TlabK)+(Vvu/TlabK)+(Vvl/Tcold))/R
! hence cumulative moles adsorbed
      nadscum(i) = ndoscum(i)-nunads(i)
! moles adsorbed in ith dose
      nads(i) = nadscum(i)-nadscum(i-1)
      %if nads(i)<0 %and signal=0 %then %start
         signal = 1; m = i-1
      %finish
! calculate expressions for BET plot
      x(i) = peq(i)/p0
      y(i) = peq(i)/(nadscum(i)*(p0-peq(i)))
   %repeat
!
   newlines(3)
   printstring( %c
      "Dose Dosing pressure   Equil'd pressure   Moles   Moles   Moles ")
   printstring(" Total")
   newline
   printstring( %c
      " no.                                     dosed  unads'd  ads'd ")
   printstring(" moles")
   newline
   printstring( %c
      "       /mV    /mmHg       /mV    /mmHg     x1E6    x1E6    x1E6 ")
   printstring(" ads'd")
   newlines(2)
   %for i = 1,1,n %cycle
      write(i,2)
      print(pdosmv(i),4,2); print(pdos(i),5,1); print(peqmv(i),7,2)
      print(peq(i),5,1)
      ndos(i) = ndos(i)*1@6; nunads(i) = nunads(i)*1@6; nads(i) = nads(i)*1@6
      print(ndos(i),5,1); print(nunads(i),5,1); print(nads(i),5,1)
      nadscum(i) = nadscum(i)*1@6; print(nadscum(i),4,1)
      newline
   %repeat
   newlines(2)
!
```

```
    selectinput(0)
    closestream(1)
!
    emas3prompt("For data for the BET plot, start at which dose number ?  ")
    read(n1)
    emas3prompt( %c
       "For data for the isotherm plot, start at which dose number ?  ")
    read(n2)
!
    selectoutput(2)
    %for i = n1,1,m %cycle
       printfl(x(i),3); spaces(2); printfl(y(i),3); newline
    %repeat
    selectoutput(3)
    closestream(2)
    %for i = n2,1,m %cycle
       print(peq(i),3,1); spaces(2); print(nadscum(i),4,1); newline
    %repeat
!
    selectoutput(0)
    closestream(3)
    newlines(2)
    printstring("BET and isotherm data sent to files defined as channels ")
    printstring("2 & 3 respectively"); newline
    printstring("Data taken up to dose number"); write(m,3)
!
%end %of %program
```

```
>
  10 CLS
  20 PRINT "PROGRAM TO CALCULATE PSEUDO-STEADY STATE RATE":PRINT " ":PRINT " "
  30 INPUT "FLOWRATE (ml/min)          "FLOW
  40 INPUT "PRESSURE (mmHg)            "P
  50 INPUT "TEMPERATURE (degrees C)    "T
  60 INPUT "SAMPLE WEIGHT (mg)         "WT
  70 T=T+273.1
  80 PRINT " "
  90 INPUT "NO. OF DATA POINTS TO CALCULATE FEED LINE  ?  "NF
 100 INPUT "   CONSTANT OF FITTED FEED LINE  ?  "ALPHAF
 105 INPUT "COEFFICIENT OF FITTED FEED LINE  ?  "BETAF
 110 INPUT "MEAN VALUE OF TIME FOR FITTED FEED LINE  ?  "TFBAR
 120 INPUT "         SD OF TIME FOR FITTED FEED LINE  ?  "SDTF
 130 INPUT "MS DEVIATIONS (FEED)  ?  "MSDEV
 140 PRINT " "
 150 INPUT "MEAN H2S PRODUCT SIGNAL  ?  "YP
 160 INPUT "SD OF MEAN PRODUCT SIGNAL  ?  "SDYP
 170 INPUT "NO. OF DATA POINTS TO CALC. MEAN PRODUCT SIGNAL  ?  "NP
 180 INPUT "MEAN VALUE OF TIME FOR FITTED PRODUCT LINE  ?  "TPBAR
 190 REM PREDICTED FEED SIGNAL AT T=TPBAR
 200 YF=ALPHAF + BETAF*TPBAR
 210 REM CALCULATE PSS RATE ...
 220 REM ESTIMATED VARIANCE OF YF
 230 SSDYF=MSDEV*(1/NF + (TPBAR-TFBAR)^2/((NF-1)*SDTF^2))
 240 REM SD OF (YF-YP)
 242 XF=SSDYF/NF : XP=(SDYP^2)/NP
 250 SD=SQR(XF + XP)
 260 REM CALCULATE PSS RATE ...
 270 RATE=FLOW*(YF-YP)*P*3.182E-7/(WT*T)
 280 REM SD OF RATE ...
 290 SDRATE=RATE*SD/(YF-YP)
 300 PRINT " ":PRINT " "
 310 PRINT "CALCULATIONS ASSUME ONLY SOURCE OF ERROR IS GC SIGNALS"
 320 PRINT " ":PRINT " "
 330 PRINT "         RATE = ";:PRINT RATE
 340 SDRATE=RATE*SD/((YF-YP)*SQR(NP))
 350 PRINT "     SD(RATE) = ";:PRINT SDRATE
 360 CONV=100*(YF-YP)/YF : CONV=INT(CONV*100)/100
 370 PRINT "% CONVERSION = ";:PRINT CONV;:PRINT " %"
 372 PRINT " ":PRINT " "
 374 FRACT=XP/(XF+XP) : FRACT=INT(FRACT*100)/100
 376 PRINT "FRACTION OF VARIANCE ARISING FROM PRODUCT ANALYSES = ";:PRINT FRACT
 380 END
```

APPENDIX D

Sample GC Output with Analysis and Rate Calculations

At the end of this appendix are given the original record sheet of the experimental conditions for run number 68 and the printer output. While continuous temperature measurement is made by means of a thermistor (averaged readings from which are given in the printer output), a more accurate reading is taken from a thermometer several times during the course of a run. The barometric pressure is also noted at intervals but is indicated as being unchanged during run 68.

The first 8 analyses on the printer output relate to the "water equilibration" pretreatment of the absorbent. The first two columns give the peak retention time and area. The time of sampling and the area of the water peak are recorded on disc. A calibration of the GC may be programmed into the data handling section of the method to give an immediate visual indication of the amount of water in the stream. This has not been done so columns 3-5 have no meaning.

The second section of the printer output relates to the sulphiding run itself. The column titles are self-explanatory, however, as for the pretreatment no calibration has been programmed so that the amounts of hydrogen sulphide and water indicated have no significance. For each sample only the sample time and the two peak areas are recorded on disc.

No significant drift was apparent in either feed of product analyses of hydrogen sulphide (after excluding the first 39 product analyses). The rate of the pss reaction is therefore directly proportional to the difference between the mean feed and mean product analyses (see section 3.1.8).

The intrinsic pss reaction rate is given by the expression:

$$\text{rate} = Q(\bar{y}_F - \bar{y}_P)P \;/\; m_{abs} f_{calib} RT \qquad (102)$$

where f_{calib} is the calibration factor of the GC which relates the hydrogen sulphide peak area to its mole fraction in the gas stream analysed (see Appendix B), and the gas flowrate, pressure, temperature, absorbent mass and universal gas constant are in consistent units. The pss rate of run 68 thus defined is 1.84×10^{-8}moles per gram absorbent per second.

SULPHIDING EXPERIMENT

DATE 16/4/89 RUN NO. 68
SAMPLE DESCRIPTION 300-710 μ 7S-1
SAMPLE WEIGHT 704.5 mg.
PRE-SULPHIDING SA MEASUREMENT SS
INITIAL REACTOR STATE: ~~EVACUATED~~ / FLUSHED WITH CARRIER
GC LEFT RUNNING AT TEMPERATURE ON NIGHT BEFORE RUN? Y/~~N~~

EXPERIMENTAL CONDITIONS: WATER EQUILIBRATION

WATER EQUILIBRATION? Y/~~N~~
CAPILLARY PRESSURE DROP 49 mm Hg.
CAPILLARY FLOWRATE
MFC FLOWRATE ~248 ml/min"
MFC OUTPUT SIGNAL VOLTAGE 1.261 V.

EXPERIMENTAL CONDITIONS: SULPHIDING

SAMPLING PATTERN 2SP 6F 40P 16F
CARRIER GAS nitrogen.
CAPILLARY PRESSURE DROP 49 mm Hg.
PRESSURE AT PCM. 10 psi.
CAPILLARY FLOWRATE
WET GAS STREAM? Y/~~N~~
TEMPERATURE OF BUBBLER COLD BATH ~ 0°C.
NOMINAL CONCN OF H_2S IN CYLINDER ~ 1.08%.
MFC FLOWRATE 284 ml/min.
MFC OUTPUT SIGNAL VOLTAGE

REACTOR TEMPERATURE m/ R112.
TOTAL FLOWRATE 426.2 ml/min.
EFFECTIVE H_2S CONCN IN MIXED STREAM
EFFECTIVE WATER CONCN IN MIXED STREAM
ATMOSPHERIC PRESSURE 758.00 (10.45) w/c (21.08). $\bar{p}$ = 758.0
LAB TEMPERATURE 23.85 (10.44) 24.25 (13.50) 24.45 (21.08). $\bar{T}$ = 24.2
CHART RECORDING TAKEN? Y/~~N~~ partial.
DATAFILES: R1604IF/P (WE) R1604ZF/P (S)

m_f = 61

POST-SULPHIDING SA MEASUREMENT

m_p = 66

COMMENTS 7.43 flush with ~ 3m N_2. 10.00 start WE run.
10.43 start sulphiding run.

3.72% O^{2-} species in surf.

LAB TEMP = 24.68 deg C FEED RUN 1 9:59 89/04/16

2.765 0.8114 0.276 36.0907 29.2844 WATER

LAB TEMP = 24.61 deg C FEED RUN 2 10:04 89/04/16

2.738 1.2712 0.273 36.0907 45.8800 WATER

LAB TEMP = 24.65 deg C FEED RUN 3 10:08 89/04/16

2.726 1.2858 0.272 36.0907 46.4076 WATER

LAB TEMP = 24.70 deg C PRODUCT RUN 4 10:15 89/04/16

2.770 0.8312 0.277 36.0907 29.9990 WATER

LAB TEMP = 24.69 deg C PRODUCT RUN 5 10:20 89/04/16

2.793 0.6278 0.279 36.0907 22.6590 WATER

LAB TEMP = 24.67 deg C PRODUCT RUN 6 10:25 89/04/16

2.744 1.0057 0.274 36.0907 36.2988 WATER

LAB TEMP = 24.66 deg C PRODUCT RUN 7 10:29 89/04/16

2.721 1.2472 T 0.272 36.0907 45.0150 WATER

LAB TEMP = 24.71 deg C PRODUCT RUN 8 10:34 89/04/16

2.749 1.3234 0.274 36.0907 47.7655 WATER

LENGTH OF RUN = 0 HRS 41 MINS 24 SECS
REACTOR ONSTREAM FOR 0 HRS 24 MINS 10 SECS

16/04/89 EXPERIMENTAL RUN 68

RF(H2S)= 55.4692 RF(WATER)= 36.0907

RUN	TIME	STREAM	LAB TEMP	H2S AREA	AMT.	WATER AREA	AMT.
1	10:45	F	24.88	5.3746	298.12	1.2252	44.21
2	10:50	F	24.82	5.7700	320.06	1.3307	48.02
3	10:54	F	24.78	5.7825	320.75	1.2845	46.36
4	10:59	F	24.81	5.7971	321.56	1.3379	48.28
5	11:04	F	24.72	5.7814	320.69	1.3195	47.62
6	11:08	F	24.74	5.7861	320.95	1.2309	44.42
7	11:13	F	24.74	5.7791	320.56	1.2589	45.43
8	11:17	F	24.73	5.7744	320.30	1.2507	45.13
9	11:22	F	24.76	5.7761	320.39	1.3005	46.93
10	11:27	F	24.82	5.7840	320.83	1.2565	45.34

11	11:31	F	24.80	5.7900	321.16	1.1544	41.66	
12	11:36	F	24.82	5.7843	320.85	1.3304	48.01	
13	11:41	F	24.81	5.7955	321.47	1.3140	47.42	
14	11:45	F	24.80	5.7854	320.91	1.2805	46.21	
15	11:50	F	24.81	5.7912	321.23	1.3220	47.71	
16	11:54	F	24.83	5.7781	320.50	1.2406	44.77	
17	11:59	F	24.85	5.7860	320.94	1.3030	47.02	
18	12:04	F	24.83	5.7750	320.33	1.2741	45.98	
19	12:08	F	24.85	5.7947	321.42	1.2909	46.59	
20	12:13	F	24.85	5.7821	320.73	1.3539	48.86	
21	12:18	F	24.87	5.7882	321.07	1.3165	47.51	
22	12:22	F	24.92	5.7842	320.84	0.0159	0.57	1.3
845	49.96							
23	12:27	F	24.90	5.7821	320.73	1.3265	47.87	
24	12:31	F	24.91	5.7799	320.60	1.3011	46.96	
25	12:36	F	24.91	5.7867	320.98	1.3118	47.34	
26	12:41	F	24.94	5.7892	321.12	1.3522	48.80	
27	12:45	F	24.94	5.7813	320.68	1.3521	48.79	
28	12:50	F	25.00	5.7746	320.31	1.3651	49.26	
29	12:55	F	24.97	5.7905	321.19	1.3066	47.15	
30	12:59	F	25.00	5.7795	320.58	1.2821	46.27	
31	13:04	F	24.99	5.7865	320.97	1.3093	47.25	
32	13:09	F	25.00	5.7965	321.53	1.3692	49.41	
33	13:13	F	25.00	5.7843	320.85	1.3468	48.61	
34	13:18	F	25.03	5.7850	320.89	1.3271	47.89	
35	13:22	F	25.03	5.7926	321.31	1.2946	46.72	

RUN	TIME	STREAM	LAB TEMP	H2S AREA	AMT.	WATER AREA	AMT.
36	13:27	F	25.03	5.7822	320.73	1.3291	47.97
37	13:32	F	25.02	5.7822	320.73	1.3820	49.87
38	13:36	F	25.03	5.7867	320.98	1.3317	48.06
39	13:41	F	25.04	5.7879	321.05	1.3066	47.15

RUN	TIME	STREAM	LAB TEMP	H2S AREA	AMT.	WATER AREA	AMT.	
40	13:48	P	25.20	0.0377	2.09	2.7796	100.32	
41	13:52	P	25.18	1.8844	104.52	4.1954	151.41	
42	13:57	P	25.13	4.8472	268.87	2.0056	72.38	
43	14:02	P	25.12	5.2730	292.49	1.5359	55.43	
44	14:06	P	25.10	5.4104	300.11	0.0152	0.55	1.5
0	55.83							
45	14:11	P	25.12	5.4894	304.49	1.4184	51.19	
46	14:15	P	25.15	5.5643	308.65	1.4653	52.88	
47	14:20	P	25.12	5.5695	308.94	1.3584	49.02	
48	14:25	P	25.14	5.5969	310.45	1.4175	51.16	
49	14:29	P	25.15	5.6148	311.45	1.3925	50.25	
50	14:34	P	25.17	5.6248	312.00	1.4675	52.96	
51	14:39	P	25.18	5.6375	312.71	1.3538	48.86	
52	14:44	P	25.16	5.6573	313.80	1.3451	48.54	
53	14:48	P	25.20	5.6544	313.64	1.3882	50.10	
54	14:53	P	25.17	5.6638	314.17	1.4232	51.36	
55	14:57	P	25.13	5.6805	315.09	1.3821	49.88	
56	15:02	P	25.18	5.6829	315.23	1.2301	44.39	
57	15:07	P	25.21	5.6922	315.74	1.3325	48.09	
58	15:11	P	25.22	5.6891	315.57	1.3761	49.66	
59	15:16	P	25.19	5.7031	316.34	1.3252	47.82	
60	15:21	P	25.17	5.7030	316.34	1.3664	49.31	
61	15:25	P	25.21	5.7042	316.41	1.3023	47.00	
62	15:30	P	25.22	5.7138	316.94	1.3497	48.71	
63	15:34	P	25.21	5.7096	316.70	1.3214	47.69	
64	15:39	P	25.25	5.7146	316.98	1.3240	47.78	
65	15:47	F	25.22	5.7910	321.22	1.2148	43.84	
66	15:51	F	25.23	5.7896	321.14	1.2700	45.83	
67	15:56	F	25.26	5.7900	321.17	1.3408	48.39	
68	16:01	F	25.22	5.7834	320.80	1.2683	45.77	

69	16:06	F	25.25	5.8058	322.04	1.2847	46.36
70	16:10	F	25.25	5.7856	320.92	1.2996	46.90
71	16:18	P	25.25	5.7302	317.85	1.3670	49.33
72	16:23	P	25.23	5.7309	317.89	1.4162	51.11
73	16:27	P	25.27	5.7308	317.88	1.3494	48.70
74	16:32	P	25.30	5.7308	317.88	1.3115	47.33

RUN	TIME	STREAM	LAB TEMP	H2S AREA	AMT.	WATER AREA	AMT.
75	16:36	P	25.28	5.7256	317.59	1.3394	48.34
76	16:41	P	25.30	5.7288	317.77	1.3352	48.18
77	16:46	P	25.27	5.7411	318.45	1.3411	48.40
78	16:50	P	25.30	5.7391	318.34	1.2998	46.91
79	16:55	P	25.33	5.7359	318.17	1.2999	46.91
80	17:00	P	25.30	5.7446	318.65	1.2952	46.74
81	17:04	P	25.32	5.7392	318.35	1.3278	47.92
82	17:09	P	25.34	5.7503	318.97	1.3007	46.94
83	17:13	P	25.36	5.7459	318.72	1.1300	40.78
84	17:18	P	25.33	5.7606	319.53	1.2823	46.28
85	17:23	P	25.33	5.7361	318.18	1.3085	47.22
86	17:27	P	25.37	5.7466	318.76	1.3091	47.24
87	17:32	P	25.35	5.7430	318.56	1.3775	49.71
88	17:37	P	25.33	5.7519	319.05	1.3117	47.34
89	17:41	P	25.37	5.7436	318.59	1.3696	49.43
90	17:46	P	25.43	5.7550	319.22	1.2733	45.95
91	17:50	P	25.43	5.7545	319.20	1.2590	45.43
92	17:55	P	25.48	5.7518	319.05	1.3686	49.39
93	18:00	P	25.52	5.7594	319.47	1.5155	54.69
94	18:04	P	25.54	5.7539	319.16	1.1969	43.19
95	18:09	P	25.55	5.7642	319.73	1.3050	47.10
96	18:14	P	25.57	5.7571	319.34	1.3031	47.03
97	18:18	P	25.57	5.7507	318.98	1.2840	46.34
98	18:23	P	25.58	5.7605	319.53	1.2906	46.58
99	18:27	P	25.64	5.7582	319.40	1.3508	48.75
100	18:32	P	25.62	5.7575	319.36	1.2877	46.47
101	18:37	P	25.66	5.7565	319.30	1.3307	48.02
102	18:41	P	25.63	5.7713	320.13	1.3340	48.14
103	18:46	P	25.65	5.7533	319.13	1.3065	47.15
104	18:51	P	25.64	5.7662	319.84	1.3066	47.15
105	18:55	P	25.61	5.7524	319.08	1.2248	44.20
106	19:00	P	25.89	5.7620	319.61	1.1881	42.88
107	19:04	P	25.92	5.7459	318.72	1.2957	46.76
108	19:17	P	25.81	5.7547	319.20	1.2739	45.97
109	19:22	P	25.74	5.7490	318.89	1.3317	48.06

RUN	TIME	STREAM	LAB TEMP	H2S AREA	AMT.	WATER AREA	AMT.
110	19:26	P	25.94	5.7525	319.08	1.2564	45.34
111	19:34	F	25.70	5.8089	322.21	1.2733	45.95
112	19:38	F	25.64	5.8116	322.36	1.2268	44.27
113	19:43	F	25.63	5.7926	321.31	1.2984	46.86
114	19:48	F	25.63	5.7984	321.63	1.3320	48.07
115	19:52	F	25.61	5.8023	321.85	1.2207	44.05
116	19:57	F	25.60	5.8170	322.66	1.3346	48.16
117	20:02	F	25.61	5.7866	320.98	1.1440	41.28
118	20:06	F	25.57	5.7871	321.01	1.1721	42.30
119	20:11	F	25.58	5.7893	321.13	1.2953	46.74
120	20:15	F	25.55	5.7788	320.54	1.4043	50.68
121	20:20	F	25.57	5.7871	321.01	1.3100	47.27
122	20:25	F	25.53	5.7852	320.90	1.2879	46.48
123	20:29	F	25.59	5.7824	320.74	1.3149	47.45
124	20:34	F	25.54	5.7896	321.14	1.3480	48.65
125	20:39	F	25.51	5.7968	321.54	1.2404	44.76
126	20:43	F	25.51	5.7835	320.81	1.2636	45.60

LENGTH OF RUN = 10 HRS 4 MINS 45 SECS
REACTOR ONSTREAM FOR 7 HRS 1 MINS 3 SECS

APPENDIX E

Calculation of Time for Diffusion of a Gas Mixture into a Sphere

A mass balance of the diffusing species across a shell at radius r and of thickness Δr permits the calculation of the time taken for the mole fraction of gas B at the centre of a porous sphere (of radius a) to rise to 0.99 when the sphere is initially bathed in gas A and is exposed to gas B at its external surface at time t=0.

Thus,

$$-(r^2N_{Br})_{r+\Delta r} = -(r^2N_{Br})_r + r^2\Delta\partial c_B/\partial t \qquad (103)$$

where N_{Br} is the flux of gas B in the positive r direction. In the limit as $\Delta r \to 0$, equation (103) becomes

$$\partial(r^2N_{Br})/\partial r = -r^2\partial c_B/\partial t \qquad (104)$$

If the flux N_{Br} is given by Fick's equation,

$$N_{Br} = -D_{AB}\partial c_B/\partial r \qquad (105)$$

where D_{AB} is the diffusivity, then equation (104) becomes

$$D_{AB}\left[\partial^2 c_B/\partial r^2 + (2/r)\partial c_B/\partial r\right] = \partial c_B/\partial t \qquad (106)$$

Making the substitution $v=c_Br$, equation (106) reduces to

$$\partial v/\partial t = D_{AB}\partial^2 v/\partial r^2 \qquad (107)$$

The boundary conditions are:

$v=0$ at $r<a$, $t=0$

$v=ac_0$ at $r=a$, $t\geq 0$

$v=rf(r)$ at $0<r<a$, $t>0$

Crank[1] gives the solution to this problem as

$$(c-c_1)/(c_0-c_1) = 1 + 2\Sigma_{n=1}^{\infty}(-1)^n\exp\left[-D_{AB}n^2\pi^2t/a^2\right] \qquad (108)$$

where c_0 is the surface concentration and c_1 the initial

uniform concentration through the sphere of gas B; c is the concentration at the centre of the sphere.

The molecular diffusivity, D_M, of hydrogen sulphide in nitrogen at 25°C and atmospheric pressure, as estimated by the Wilke-Lee modification of the Hirschfelder-Bird-Spotz method,[2] is $1.76 \times 10^{-5} m^2 s^{-1}$. The mean pore radius of the absorbent 75-1 has been measured at ICI by mercury porosimetry as 200Å. This gives a Knudsen diffusivity,[3] D_K, of $5.74 \times 10^{-6} m^2 s^{-1}$. Given the distribution of pore size and the similar magnitudes of the diffusivities, it is likely that both molecular diffusion and Knudsen flow are important. A combined diffusivity, D, as given by

$$1/D = 1/D_M + 1/D_K \qquad (109)$$

is $4.3 \times 10^{-6} m^2 s^{-1}$. The effective diffusivity is given by

$$D^e = \varepsilon D/\tau_p \qquad (110)$$

where ε and τ_p are the particle porosity and the tortuosity of the pores respectively. For a porosity of 0.5 and an assumed tortuosity of the partially sulphided absorbent of 6[4], an effective diffusivity of $3.6 \times 10^{-7} m^2 s^{-1}$ is obtained.

For granules having radii of 1, 2 or 5mm and a diffusivity of $3.6 \times 10^{-7} m^2 s^{-1}$, the times corresponding to $(c-c_1)/(c_0-c_1)=0.99$ are about 1.5, 6 and 37.5 seconds respectively. Note that these estimates are only as good as the diffusivity estimate from which they are computed.

REFERENCES

[1] Crank J.
"The mathematics of diffusion", p85-87
Clarendon Press, Oxford (1956)

[2] Treybal R.E.
"Mass transfer operations", pp.25-27
McGraw Hill, New York (1968)

[3] Kennard E.H.
"Kinetic theory of gases", p.302
McGraw Hill, New York (1938)
(as cited in Ruthven D.M. "Principles
of adsorption and adsorption processes",
p.164, Wiley Interscience, New York (1984))

[4] Satterfield C.N.
"Mass transfer in heterogeneous catalysis"
M.I.T. Press, Cambridge Mass. (1970)

APPENDIX F

Error in Numerical Integration

Where numerical integration is used to approximate the integral of a given expression, bounds on the error involved in the method of numerical integration may be computed as a function of the smallest and largest values within the integration interval of the second derivative of the expression. Thus a definite integral,

$$J = \int_a^b f(x)dx \tag{111}$$

may be approximated by a piecewise linear function, J^*, given by

$$J^* = h[\tfrac{1}{2}f(a) + f(x_1) + f(x_2) + \ldots + f(x_{n-1}) + \tfrac{1}{2}f(b)] \tag{112}$$

where $h=(b-a)/n$, $a=x_0$, $b=x_n$ and $x_j=x_0+jh$ $(\forall j)$. This is known as the Trapezoidal rule and the error,

$$\varepsilon = J^*-J \tag{113}$$

in the method may be shown[1] to lie in the interval

$$KM_2^* \leqq \varepsilon \leqq KM_2 \tag{114}$$

where

$$K = (b-a)^3 / 12n^2 \tag{115}$$

and M_2^* and M_2 are the smallest and largest values respectively of the second derivative of the function, $f(x)$, in the integration interval.

In the present case, where the function (the reaction rate expression) which defines the variation of the flow of hydrogen sulphide with time, the $f(x)$ of equation (111), is both unknown and likely to be highly complex, another approach to estimation of the error intrinsic in the method must be used. Two sources of error contribute to the error associated with the estimation of the amount of hydrogen sulphide absorbed by the absorbent in a given time interval. The first is due to

the approximation of the smooth curve response, which would be observed if it were possible to monitor the hydrogen sulphide flow continuously, by a piecewise linear function. This error may be estimated rather accurately by the use of Simpson's rule for numerical integration. Simpson's rule, which is based on the integration of Lagrange's interpolation formula over an interval, uses a piecewise quadratic approximation for the function or data to be integrated which gives an approximate area for a pair of intervals from x_i to x_{i+2} viz..

$$\int_{x_i}^{x_{i+2}} f(x)dx \simeq h/3\left[f_i + 4f_{i+1} + f_{i+2}\right] \qquad (116)$$

where $f_i=f(x_i)$. The summation of the expression over the integration interval of equation (111) yields

$$\int_a^b f(x)dx \simeq h/3\left[f_0+4f_1+2f_2+4f_3+\ldots +2f_{2n-2}+4f_{2n-1}+f_{2n}\right] \qquad (117)$$

The expression for the integral is rather more complex in this case because the unequal size of the time intervals between analyses - a pair of which compose the integration interval - prevents simplification of the expression for the integral. It is possible to use higher order approximations but these are computationally more time consuming and sufficient accuracy is usually obtained with a quadratic approximation.

The second source of error is the measurement error itself. A good estimate for the error associated with any single data point is given by the standard deviation of an analysis as computed from GC calibration runs where multiple analyses were made on a stream of constant composition.

Because the product curve is convex to the y-axis,

whereas the application of linear regression to the feed analysis data confirms the suitability of a linear fit, if there is any systematic error in the numerical integration, its effect will be to overestimate the amount of hydrogen sulphide absorbed. This is due to the fact that a piecewise linear approximation to a convex curve - such as the product analyses form - will always lie beneath the curve between the end-points of the approximations. In the present case this leads to an underestimation of the molar flowrate of hydrogen sulphide in the reactor outlet stream, and as a piecewise linear approximation to a straight line - such as the feed analyses form - results in no error, the overall effect is to overestimate the extent of the absorbent conversion. The purpose of the following error analysis is to attempt to quantify that overestimation and to determine the standard deviation of the calculated absorbent conversion by reference to the known standard deviation of GC analyses.

Two sulphiding experiments, Run 48 on ICI '75-1' and Run 75 on calcined hydrozincite (ie. essentially pure zinc oxide), have been integrated numerically according to both the Trapezoidal and Simpson's rule. In each case, the difference in the calculated number of moles of hydrogen sulphide absorbed is about 1%.

Assuming that the measurement of time is exact, the sample variance of the area A_i which is bounded by the curves of feed and product analyses and by the lines $t=t_{i-1}$ and $t=t_i$ and defined as

$$A_i = \tfrac{1}{2}(t_i-t_{i-1})(\tilde{y}_{Fi}+\tilde{y}_{Fi-1}) - \tfrac{1}{2}(t_i-t_{i-1})(y_{Pi}+y_{Pi-1}) \qquad (118)$$

is given by[2],

$$s^2(A_i) = \tfrac{1}{4}(t_i-t_{i-1})^2\left[s^2(\tilde{y}_{Fi}) + s^2(\tilde{y}_{Fi-1}) + 2s^2(y_P)\right] \qquad (119)$$

The sample variance of the total area, (s^2(total area)), is given by

$$s^2(\text{total area}) = \Sigma_{i=1}^{n} s^2(A_i) \qquad (120)$$

For both Runs 48 and 75, the standard deviation of the number of moles absorbed is less than 1%. A total error of about 2% is therefore expected to result from these two sources.

A source of systematic error in the numerical integration arises because of the volume of the gas lines between the reactor and the gas sample valve (GSV) of the GC. Thus an analysis taken at time t corresponds to the gas composition in the reactor at time t-Δt where Δt is the time taken for gas to pass from the reactor to the gas sample valve. This time is estimated on the basis of the volume of the gas lines from the reactor to the T-piece and from the T-piece to the GSV and the corresponding gas flowrates to be about 25.4 seconds, and its omission will therefore result in an overestimation of the number of moles absorbed by about 0.4%.

REFERENCES

[1] Kreyszig, E.
"Advanced Engineering Mathematics", pps 784-792
John Wiley & Sons, 1979

[2] Barford, N.C.
"Experimental Measurements: Precision, Error and Truth", ch.2
John Wiley & Sons, 1985

ROYAL SOCIETY
OF
CHEMISTRY

Chemical Communications

Reprinted From

J. Chem. Soc., Chemical Communications.

Issue 21 1989

Autocatalysis by Water in the Reaction of Hydrogen Sulphide with Zinc Oxide

J. Michael Davidson,*[a] Patrick J. Denny,[b] and Catriona H. Lawrie[a]

Autocatalysis by Water in the Reaction of Hydrogen Sulphide with Zinc Oxide

J. Michael Davidson,*[a] Patrick J. Denny,[b] and Catriona H. Lawrie[a]

[a] *Department of Chemical Engineering, University of Edinburgh, Mayfield Road, Edinburgh EH9 3JL, U.K.*
[b] *ICI C&P Ltd., Catalysis Research Centre, PO Box 1, Billingham, Cleveland TS23 1LB, U.K.*

A study of the rate of the reaction of hydrogen sulphide with zinc oxide; the reaction is autocatalytic due to the effect of water.

Zinc oxide has a strong affinity for hydrogen sulphide and is used as an absorbent for sour gas streams. Its activity as an absorbent is dependent on the surface area and in the case of high surface area material,[1] the reaction, equation (1), proceeds near to completion and is not confined to the surface phase. The reaction proceeds even at sub-ambient temperatures and we have now studied its rate using commercial samples having nitrogen Brunauer–Emmett–Teller (B.E.T.) surface areas up to 110 $m^2\ g^{-1}$.

$$H_2S + ZnO \rightarrow H_2O + ZnS \qquad (1)$$

We find that the reaction is autocatalytic due to the effect of water, the general characteristics being as follows. Using H_2S in N_2 carrier (0.06—0.7% v/v) at 273—298 K/1.0 atm there is a rapid reaction starting in the surface layer of the particles which subsides to a much slower pseudo-steady state rate (pss) in a manner dependent on the particle size. Large particles demonstrated marked diffusional effects. The fast initial rate decreases with increasing particle size due to restricted access of H_2S to the internal surface area; in the pss the rate increases with particle size due to the increased concentration of product water towards the centre of the particles. With smaller particles (300 to 710 μ) gaseous diffusional effects are absent and the pss rate can be studied conveniently over several hours using the methods of differential analysis. Microprobe analyses across sections of the 3 mm granules show the sulphide to be deposited uniformly even at 20% conversion of the ZnO whereas at very low conversion it is concentrated in the outer shell with a central unreacted core.

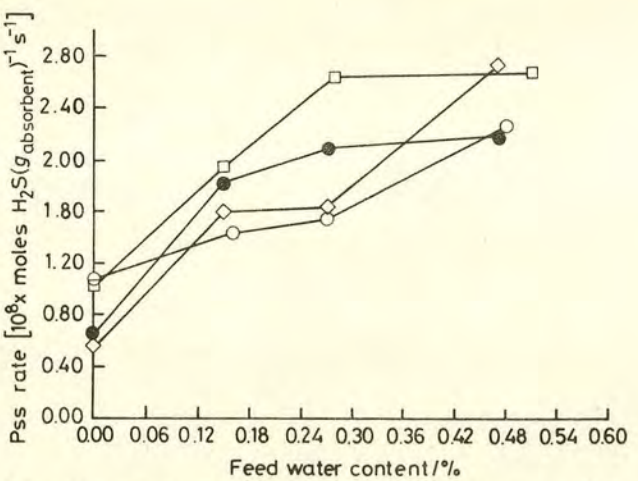

Figure 1. Pseudo-steady state rate (pss) *vs.* feed water content. □: % H_2S = 0.20; ◇: % H_2S = 0.51; ●: % H_2S = 0.69; ○: % H_2S = 0.06. Absorbent = ICI experimental low temperature absorbent 300—710 μ particles. T (reactor) = 25.6 °C.

Our pss rate data, summarised in Figure 1, were obtained using flow rates of 0.4—0.45 dm^3 min^{-1} over samples of 0.2—0.6 g of ZnO. Reactor inlet and outlet compositions were established by repetitive gas chromatographic analysis at 4.5 min intervals (Hayesep Q 80—100 mesh column with He carrier) in 10 h runs. The conversion of the ZnO at pss was in the range 9—23%, increasing with the levels of both H_2S and H_2O in the feed. Conversions of ZnO and H_2S over the full pss period of our experiments were less than 1 and 5%, respectively. Analysis of the gas composition with a standard deviation of 0.5% of the mean for H_2S and 4% for H_2O allowed calculation of the rate with standard deviation of about 2%. Figure 1 shows the marked catalytic effect of water, the lines being drawn to connect points derived from runs having identical H_2S concentration. If these pss data are re-plotted with water vapour concentration as the parameter, it becomes apparent that the rate is not markedly dependent on H_2S concentration, although there may be a shallow maximum indicative of competitive co-adsorption of H_2S and H_2O. For a set of experiments using 0.21% H_2S and 0.16% H_2O we found that the reaction rate decreases as temperature increases (2.00, 1.83, 1.50×10^{-8} mol g^{-1} s^{-1} at 273, 289, 298 K), levelling off in the temperature range 298—318 K.

We believe that our results are consistent with a mechanism whereby H_2S reacts rapidly with surface hydroxy groups on ZnO. The role of water is apparently to cause solid state rearrangement or diffusion bringing fresh absorbent to the surface of crystallites. Re-start experiments support this view; if the feed is discontinued for an interval and then re-admitted, the reaction proceeds through a renewed rapid phase and decline, the effect being more pronounced if residual H_2O is left in the reactor and is not removed by pumping after isolation. The general form of the dependence of the pss rate on H_2O vapour concentration together with the inverse temperature effect are consistent with reversible adsorption of H_2O on the ZnO surface. Further supporting evidence for the role of H_2O is given by the inverse particle size effect on the rate.

Received, 31st July 1989; Com. 9/03226F

Reference

1 A. Charpmael, Brit. Pat. 337,792 (1930), see M. C. Sneed and R. C. Brasted, 'Comprehensive Inorganic Chemistry,' vol. 4, van Nostrand, New York and London, 1955, p. 48.